Autophagy regulates neuronal excitability by controlling cAMP/Protein Kinase A signalling

Inaugural-Dissertation

zur

Erlangung des Doktorgrades

der Mathematisch-Naturwissenschaftlichen Fakultät

der Universität zu Köln

vorgelegt von

Melina Overhoff

aus Wesel

Köln, 2022

1. Gutachterin: Prof. Dr. Natalia Kononenko

2. Gutachter: Prof. Dr. Matthias Hammerschmidt

Tag der mündlichen Prüfung: 31.03.2022

Table of contents

1. List of figures

2. List of tables

3. Abbreviation

AAV9	Adeno-associated virus serotype 9
AD	Alzheimer's disease
AKAP	A-kinase anchoring proteins
ALS	Amyotrophic lateral sclerosis
AMPA	α-amino-3-hydroxy-5-methyl-4-isoxazolepropionic acid receptor
AMPK	AMP-activated protein kinase
ASD	Autism spectrum disorder
ATG	Autophagy-related protein/gene
ATP	Adenosine triphosphate
AVs	Autophagic vacuoles
BafA1	Bafilomycin A1
BDNF	Brain-derived neurotrophic factor
C-α	Catalytische subunit α
°C	Celsius
CA1	*Cornu Ammonis* area 1 (Hippocampus)
CALCOCO2	Nuclear dot protein 52
cAMP	3',5'-cyclic adenosine monophosphate
cDNA	Coding DNA
Co-IP	Protein complex immunoprecipitation
(p)CREB	(Phosphorylated) cAMP response element-binding protein
CX	Cortex
DNA	Deoxyribonucleic acid
DMEM	Dulbecco's modified eagle medium
EndoA	Endophilin A
(m)EPSP	(Miniature) excitatory postsynaptic potential
ER	Endoplasmic reticulum
FACS	Flourescence activated cell sorting
FBS	Fetal bovine serum
FC	Fold change
$GABA_A$	γ-aminobutyric acid
GABARAP	Gamma-aminobutyric acid receptor-associated protein
GABARAPL1	GABARAP-like 1, also termed as GEC1
GABARAPL2	GABARAP-like 2, also termed as GATE-16
GAPDH	Glyceraldehyde-3-Phosphate Dehydrogenase
GFP	Green fluorescent protein
GLUR1	Glutamate receptor 1
GO	Gene Ontology
GTP	Guanosine triphosphate
H89	H-89 dihydrochloride (N-[2-[[3-(4-Bromophenyl)-2-propenyl]amino]ethyl]-5-isoquinolinesulfonamide dihydrochloride)
HCS	High content screening microscopy
HEK	Human embryonic kidney cells
HTT	Huntingtin
mHTT	Mutated huntingtin
HD	Huntington's disease
hrs	Hours
HP	Hippocampus

ICC	Immunocytochemistry
IHC	Immunohistochemistry
(m)IPSP	(Miniature) inhibitory postsynaptic potential
kDa	Kilodalton
KO	Knockout
LBs	Lewy bodies
LC3	Microtubule-associated protein 1 light chain 3
LC3I	Non-lipidated LC3
LC3II	Phosphatidylethanolamine lipidated LC3
LIR	LC3-interacting regions
LRRK2	Leucine-rich repeat kinase 2
LTD	Long-term depression
LTP	Long-term potentiation
MAPK	Mitogen-activated protein kinase
MEFs	Mouse embryonic fibroblasts
min	Minutes
MS	Mass spectrometry
mTOR	Mammalian target of rapamycin
mTORC1/2	Mammalian target of rapamycin complex 1/2
Nes	Nestin
NBR1	Next to BRCA1 gene 1 protein
NDP52	Nuclear domain 10 protein, also termed CALCOCO2
NMDA	N-methyl-D-aspartate receptor
NSC34	Mouse motor neuron-like hybrid cell line
ON	Overnight
OPTN	Optineurin
P62	Sequestosome 1/ SQSTM1
PAS	Phagophore assembly sites
PCR	Polymerase chain reaction
PD	Parkinson's disease
PDE4	Phosphodiesterase isozyme 4
PE	Phosphatidylethanolamine
PI3K	Phosphatidylinositol 3-kinase
PI3P	Phosphatidylinositol 3-phosphate
PINK	PTEN-induced kinase
PKA	cAMP-dependent protein kinase A
pPKA	Phosphorylated PKA phosphorylation sites
pS6	S6 ribosomal protein
PSD	Postsynaptic density
PSD95	Postsynaptic density protein 95
P/S	Penicillin/Streptomycin
R1 / R2	Regulatory subunit type 1 / Regulatory subunit type 2
RFP	Red fluorescent protein
RNA	Ribonucleic acid
Rpm	Revolution per minute
RT	Room temperature
S	Serine
SDS	Sodium dodecyl sulfate

SHIRPA	**S**mithKline Beecham, **H**arwell, Imperial College, **R**oyal London Hospital, **p**henotype **a**ssessment
s.m.	Starvation media
SNARE	Soluble N-ethylmaleimide-sensitive-factor attachment receptor
SOD1	Superoxide dismutase 1
SYB2	Synaptobrevin 2
Synj1	Synaptojanin 1
T	Threonine
Tmx	Tamoxifen-inducible line
UPS	Ubiquitin-proteasome system
VAMP	Vesicle associated membrane proteins
WB	Western blotting
WT	Wild-type

4. Summary

Autophagy is an evolutionarily conserved process that serves to provide nutrients during starvation and to eliminate detrimental cellular components like dysfunctional organelles and damaged proteins. This role of autophagy might be critical in neurons because of their postmitotic nature. However, accumulating evidence indicates that autophagy is not merely a housekeeping process. Here, we show that the crucial AuTophaGy protein ATG5 functions in neurons to regulate the cAMP-dependent protein kinase A (PKA)-mediated phosphorylation of synapse-confined proteome. This function of ATG5 is independent of bulk degradation of synaptic proteins and requires the starvation-induced targeting of PKA regulatory subunit type 1 (R1) to neuronal autophagosomes. Loss of ATG5 in either excitatory or inhibitory neurons causes a drastic accumulation of PKA R1 at synapses, which sequesters the PKA catalytic subunit and causes cAMP-dependent remodelling of the synaptic phosphoproteome. Autophagy-deficient excitatory synapses are characterized by increased thickness of the postsynaptic density and alterations in AMPA receptor GLUR1 trafficking, a phenotype that results in augmented excitatory neurotransmission and appearance of seizures in mice with glutamatergic forebrain-confined ATG5 deletion. My work has identified a previously unknown role of neuronal autophagy in regulating PKA-dependent signalling at glutamatergic synapses and suggest PKA as a target for treating autophagy-associated neurodegenerative diseases.

5. Zusammenfassung

Die Autophagie ist ein evolutionär konservierter Prozess in Zellen, der dazu dient, in Perioden mit verringerter Nährstoffzufuhr, Nährstoffe bereitzustellen und schädliche Zellbestandteile wie dysfunktionale Organellen und beschädigte Proteine zu beseitigen. Diese Rolle der Autophagie könnte bei Neuronen aufgrund ihrer postmitotischen Natur besonders wichtig sein. Allerdings mehren sich die Studien, die der Autophagie vielseitigere Funktionen zusprechen als die reine Aufrechterhaltung der zellulären Homöostase. Die vorliegende Studie zeigt, dass das wichtige AuTophaGy-Protein ATG5 in Neuronen die Phosphorylierung von synaptischen Proteinen durch die cAMP-abhängige Proteinkinase A (PKA) reguliert. Diese Funktion von ATG5 ist unabhängig von der homöostatischen Beseitigung synaptischer Proteine und erfordert den durch Nährstoffmangel ausgelösten Abbau der regulatorischen Untereinheit Typ 1 (R1) von PKA. Der Verlust von ATG5 in exzitatorischen oder inhibitorischen Neuronen führt zu einer Anreicherung von PKA R1 in Synapsen, wodurch die katalytische Untereinheit der PKA sequestriert und eine cAMP-abhängige Umgestaltung des synaptischen Phosphoproteoms induziert wird. Autophagie-defiziente exzitatorische Synapsen zeichnen sich durch eine verdickte postsynaptische Dichte und Veränderungen im Transport der AMPA Rezeptor Untereinheit GLUR1 aus, ein Phänotyp, durch den es zu einer erhöhten Erregungstransmission und zum Auftreten von Krampfanfällen bei Mäusen führt, denen ATG5 in glutamatergen Neuronen des Vorderhirns fehlt. Meine Arbeit hat eine bisher unbekannte Rolle der neuronalen Autophagie bei der Regulierung der PKA-abhängigen Signalübertragung an glutamatergen Synapsen aufgezeigt und legt PKA als Ziel für die Behandlung von Autophagie-assoziierten neurodegenerativen Erkrankungen nahe.

6. Introduction

6.1 Autophagy

6.1.1 Physiological roles of autophagy

Autophagy is an evolutionarily conserved process in cells that provides nutrients during starvation and maintains cellular homeostasis. Therefore, parts of the cytoplasm and/or damaged proteins and organelles are sequestered in autophagosomes for degradation to supply amino acids for cell survival. However, it has been shown that autophagy is essential in various physiological processes besides starvation, such as development, differentiation, tumorigenesis, immunity, and neurodegeneration (Perrotta et al. 2020; Mizushima and Levine 2010; Li et al. 2020; Levine et al. 2011; Frake et al. 2015). Additionally, it was described that autophagy operates constitutively on a low baseline level, even under nutrient-rich environmental conditions, to maintain cellular homeostasis (Hara et al. 2006; Komatsu et al. 2006). Furthermore, autophagy was considered a non-selective degradation mechanism used under starvation (Ichimura et al. 2008; Tsukada and Ohsumi 1993) and in newborn mice (Kuma et al. 2004), but the discovery of autophagy receptors helped to identify several proteins and organelles that are specifically targeted by autophagy to maintain cellular homeostasis.

There are three types of autophagy to distinguish: 1) chaperone-mediated autophagy, 2) microautophagy, and 3) macroautophagy. Chaperone-mediated autophagy enables the degradation of cytosolic proteins with a particular pentapeptide consensus motif (Majeski and Dice 2004; Aman et al. 2021; Yorimitsu and Klionsky 2005). Micro- and Macroautophagy are both pathways that involve dynamic membrane rearrangement to engulf large portions of cytoplasmic material and whole organelles for degradation (Yang and Klionsky 2009). Microautophagy supports the degradation of cytoplasmic material directly at the surface of the lysosome by invagination of the limiting membrane (Yorimitsu and Klionsky 2005). In contrast, during macroautophagy, a de-novo double-membraned vesicle is formed that grows and engulfs detrimental proteins and whole organelles. The closed vesicles are termed autophagosomes, which become transported to the lysosomes for fusion and subsequent degradation of delivered contents. In this study, the focus is on macroautophagy, hereafter referred to as autophagy, in neurons.

The process of autophagy can be subdivided into four major steps: 1) initiation of the phagophore formation, 2) nucleation, 3) expansion of the phagophore, and 4) the fusion of the resulting autophagosome with a lysosome (Figure 1). A significant breakthrough for studying the molecular basis of autophagy was achieved by identifying the genes involved in this process, which can be grouped into several functional subunits, such as the ULK1 kinase complex for the induction of autophagy (ULK, ATG13, ATG101, and RB1CC1/FIP200), ATG9 for delivery of other ATG proteins and recycling of membranes, the class III phosphatidylinositol 3-kinase (PI3K) complex (VPS34-Beclin1-VPS15) for vesicle nucleation, and the ATG12-ATG5-ATG16L conjugation system for the MT-associated protein 1 light chain 3 (LC3) lipidation to phosphatidylethanolamine (LC3-PE or LC3II), which allows membrane expansion and enclosure of the autophagosome (Ariosa and Klionsky 2016; Hu et al. 2015). After the autophagosome closure, it matures and gets transported to the lysosomes for fusion. The resulting organelle is called autolysosome, a very acidic (pH=4.5-5) organelle aroused by the so-called V-ATPase complexes. After successfully degrading the content by hydrolases, the amino acids are released as an internal supply of nutrients. All in all, these steps require at least 18 core evolutionally conserved ATG-related proteins (Yang and Klionsky 2009), initially discovered in yeast (Nakatogawa et al. 2009).

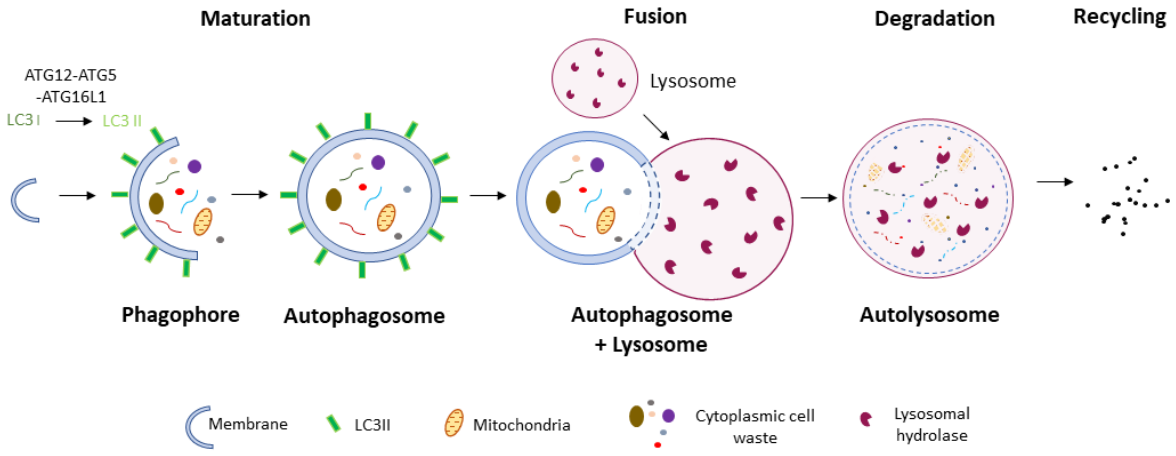

Figure 1: Macroautophagy.

During macroautophagy, harmful material is engulfed in double-membranes vesicles and transported to the lysosomes for degradation. This process can be subdivided into 4 main steps: 1) initiation of the phagophore formation, 2) nucleation, 3) expansion of the phagophore, and 4) the fusion of the resulting autophagosome with a lysosome. The degraded material is back released into the cytosol as an internal supply of nutrients during starvation or other stressful situations.

6.1.2 Initiation of phagophore formation

Autophagy is initiated by a complex composed of the serine/threonine kinase ATG1 (Unc-51-like kinase (ULK1) complex) and two accessory proteins, ATG13 and ATG17. The assembly of this complex is under the tight control of the mammalian target of rapamycin complex 1 (mTORC1), a serine/ threonine kinase that acts in response to amino acids and growth factors (Liu and Sabatini 2020). Under nutrient-rich conditions, mTORC1 is active, favours protein biosynthesis, and inhibits autophagy, whereas mTORC1 is inhibited upon nutrient deprivation, allowing an increase in autophagic activity (Noda et al. 2002). This regulation of autophagy by mTORC1 is controlled by inhibitory phosphorylation marks applied to ATG1 and ATG13 under nutrient-rich conditions leading to hyperphosphorylation of these proteins (Kim et al. 2011a; Hosokawa et al. 2009; Ganley et al. 2009). Upon the inactivation of mTORC1 by starvation, ATG13 is rapidly and partially dephosphorylated, leading to a higher binding affinity for ATG1 and ATG17. The interaction of ATG1 with hypophosphorylated ATG13 and ATG17 allows the activation of ATG1 kinase activity and promotes the activation of the ATG1-ATG13-ATG17 complex at phagophore assembly sites (PAS) (Hosokawa et al. 2009; Almeida et al. 2013; Hosokawa et al. 2009; Jung et al. 2009). Another pathway also controls autophagy is mediated through the AMP-activated protein kinase (AMPK). This energy-sensing kinase perceives reduced ATP levels and promotes autophagy by inducing ULK1 activation and inactivation of mTORC1 (Sarkar 2013). The activated ULK complex translocates from its former cytosolic localization to autophagy-specific exit sites of the endoplasmic reticulum (ER), which are specified by ATG9 vesicles, and with less extent to mitochondria and plasma membrane to recruit membranes for autophagosome formation (Mercer et al. 2018; Karanasios et al. 2013; Hamasaki et al. 2013).

6.1.3 Nucleation

This step of autophagy is driven by the PI3K complex that includes the lipid kinase vacuolar protein sorting 34 (VPS34, also called PIK3C3), 15 (VPS15/PIK3R4), Beclin-1 (BECN1), and ATG14, and that is a direct downstream target of the activated ULK1 complex. Once ULK1 activates the PI3K complex, it is recruited to the phagophore initiation site to generate phosphatidylinositol 3-phosphate (PI3P), the first membranous compartments called

omegasome. Additionally, it leads to the recruitment of tryptophan-aspartic acid (WD) repeat domain phosphoinositide-interacting (WIPI) proteins to the phagophore membrane, which, in turn, controls the recruitment of crucial downstream autophagic proteins (e.g., ATG16L1 by WIPI2) that dictate where the phagophores form (Menzies et al. 2017; Dooley et al. 2014).

6.1.4 Elongation and expansion of the phagophore and autophagosome closure

The expansion and elongation of the formed phagophore to an autophagosome mainly depends on two ubiquitin-like conjugation systems, the lipidation of LC3 (also known as ATG8) and the complex formation of ATG12-ATG5-ATG16L1 (Ichimura et al. 2000; Mizushima et al. 1998). Both are highly conserved and essential for autophagy.

LC3 can be subdivided into two forms, called LC3I and LC3II. LC3I is cytosolic, whereas LC3II is membrane-bound (Kabeya et al. 2000). The processing of LC3I to LC3II is mediated by a cysteine protease called ATG4 that cleaves LC3I to expose a glycine residue. The exposed glycine is subsequently activated by ATG7, in a reaction that requires ATP, to form a thioester intermediate with the active cysteine residue of ATG7. The glycine residue of LC3 is then transferred to ATG3, which allows the conjugation of LC3 to phosphatidylethanolamine (PE), leading to the formation of LC3II, which can be recruited to autophagosomal membranes and was shown to decorate the inside as well as the outside of autophagosomes (Fig. 2a) (Menzies et al. 2017; Nakatogawa et al. 2009; Mercer et al. 2018).

The ATG12-ATG5-ATG16L1 complex is formed in the second cascade involving ATG7 and ATG10, which support the covalent conjugation of ATG12 to ATG5. ATG16L1 directly interacts with ATG5, and the formed ATG12-ATG5-ATG16L1 complex is then recruited to the phagophore via WIPI2b (Dooley et al. 2014). In contrast to LC3II, the ATG12-ATG5-ATG16L1 complex localizes exclusively at the growing phagophore's outer membrane, recruiting LC3II to the phagophore for extension and elongation (Fig. 2b) (Mizushima et al. 2003; Saitsu et al. 2013; Mizushima et al. 2001). The two conjugation systems act in close crosstalk to each other, which could be shown in genetically modified organisms where mutations of the ATG12-ATG5-ATG16L1 complex significantly decreased the LC3II level (Suzuki et al. 2001). Furthermore, it was shown that purified ATG12-ATG5 conjugates promote LC3-II formation *in-vitro* (Hanada

et al. 2007). Thus, ATG12-ATG5 can be considered as a modulator of LC3II lipidation. The expansion of the autophagophore is assisted by ATG9, a transmembrane protein that localizes to the trans-Golgi network and the endocytic compartment to facilitate the supply of lipid bilayers (Bento et al. 2016). However, until today the source of membranes for autophagosome recruitment is unclear.

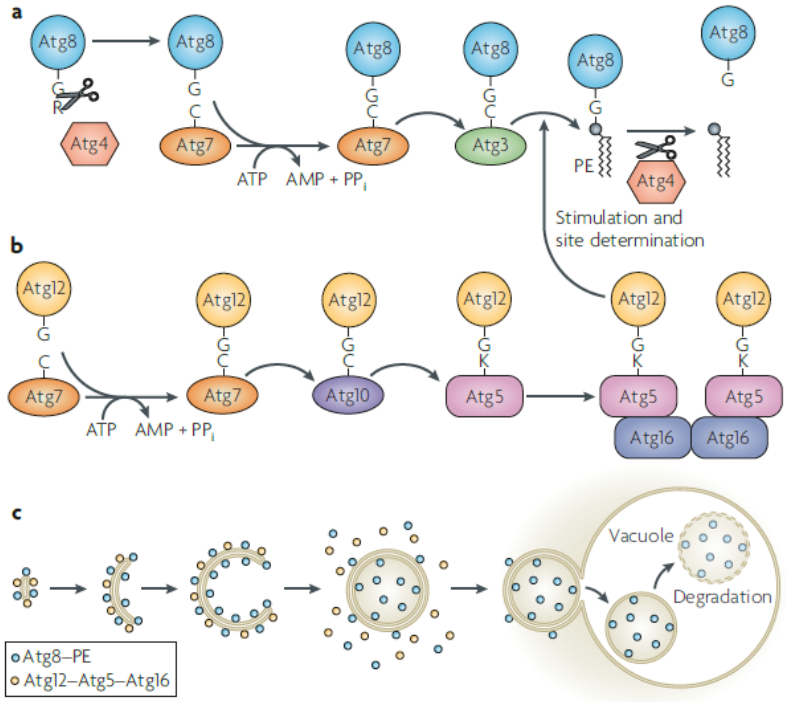

Figure 2: The two ubiquitin-like conjugation systems.

For successful elongation of the formed phagophore, it is essential that the two ubiquitin-like conjugation systems are formed, the lipidation of LC3/ ATG8 (a) and the complex formation of ATG12-ATG5-ATG16L1 (b). The ATG12-ATG5-ATG16L1 complex recruits lipidated LC3 to the growing phagophore for elongation and expansion of the double membraned organelle (figure taken from (Nakatogawa et al. 2009)).

6.1.5 Fusion of the autophagosome with the lysosome

Once the expanding phagophore matures and closes, the completed autophagosomes are transported along the microtubules via dynein motors to the cell soma to fuse with a lysosome (Monastyrska et al. 2009; Fass et al. 2006). Alternatively, the mature autophagosome can fuse with late endosomes before final fusion with a lysosome, forming an amphisome structure. Therefore, amphisomes contain cytosolic material derived from the autophagosome and

endocytic material. The fusion of autophagosomes/ amphisomes with lysosomes is supported by several protein classes, including small GTPases, tethering proteins and SNARE complex proteins (Lőrincz and Juhász 2020). The growing phagophore acquires GTPase proteins RAB2 and RAB7 and RF-like GTPase ARL8, which bind to the HOPS tethering complex, bringing autophagosomes and lysosomes closely together, and thus promoting the autophagosome-lysosome fusion (Boda et al. 2019; Lőrincz and Juhász 2020; Langemeyer et al. 2018). In the last fusion step, the mechanical force for the fusion event is applied by components of the SNARE machinery, such as VAMP7 and VAMP9 (Fader et al. 2009; Furuta et al. 2010), Syntaxin 17, SNAP29 and VAMP8 (Itakura et al. 2012). For sufficient fusion, the transport and subsequent re-localization of the autophagosomes/ amphisomes from the cell processes to the cell soma, where the lysosomes are located, is essential. Therefore, also motor proteins can be counted as mandatory in the fusion event. Those include various effectors of small GTPases RAB7 and ATL8, including FYCO1 (FYVE and coiled-coil domain-containing 1) and BORC (BLOC-one-related complex), which link autophagosomes and lysosomes to motor proteins and mediate both plus-end and minus-end transport of those vesicles along the microtubules (Pankiv et al. 2010; Guardia et al. 2016; Langemeyer and Ungermann 2015). Additionally, direct interactors of dynein-dynactin complex, such as ORP1L (oxysterol-binding protein-related protein 1L) and RILP (RAB-interacting lysosomal protein), mediate retrograde transport of autophagosomes to the cell body (Wijdeven et al. 2016; Khobrekar et al. 2020; Lőrincz and Juhász 2020). Once the autophagosome fuses with the lysosome, the material is degraded by hydrolases in the acidic environment of the lysosome. After successful degradation, the resulting amino acids are released into the cell's cytoplasm.

6.1.6 Autophagy in neurons and neurodegeneration

This study focuses on autophagy in neurons, in which autophagy function is implemented in development, physiology and ageing (Kulkarni et al. 2018; Azarnia Tehran et al. 2018; Liang and Sigrist 2018; Stavoe and Holzbaur 2019). Autophagy is essential for brain physiology since brain-specific depletion of autophagy, induced by the loss of ATG5 or ATG7 (under a *Nestin*-Cre promotor, affecting all neuronal precursors), in mice results in axon degeneration and intracellular protein aggregates culminating in neurodegeneration (Hara et al. 2006; Komatsu

et al. 2006; Komatsu et al. 2007b). However, currently, it is not clear if this phenotype is due to the cell-autonomous role of autophagy in neurons, since mouse models where ATG proteins were deleted under neuron-specific promotors did not reveal signs of neurodegeneration (Komatsu et al. 2007b; McMahon et al. 2012; Hernandez et al. 2012; Lieberman et al. 2020; Negrete-Hurtado, Overhoff et al. 2020). Autophagy might be especially crucial in postmitotic cells, like neurons, due to their highly polarized morphology with dendrites and long axons. Their complex morphology and postmitotic nature make neurons extremely dependent on a well-working clearance process and transport system to remove harmful material and constantly reorganize to maintain cellular homeostasis. Especially synapses, specialized structures to enable communication between different neurons, along the axons represent high energy demand and protein turn-over areas. Synapses contain a mean of circa 300000 proteins within a volume of 0.37 ± 0.0.4 μm^3 (Wilhelm et al. 2014). An electrical stimulus runs down the axon after a specific threshold is reached in the soma. It arrives at the presynapse, causing a neurotransmitter release into the synaptic cleft that triggers neuronal activity in the postsynaptic neuron. To facilitate the release of neurotransmitters, the neurotransmitter vesicle membrane must fuse with the presynaptic membrane, releasing the content, followed by the retrieval of fused vesicle membranes by endocytosis (Sudhof 2004). Depending on the neuronal subtype, the vesicle cycle needs to happen exceptionally rapidly and repeatedly at a frequency exceeding 100 Hz (Kock and Sakmann 2008). These conditions lead to increased wear and tear of proteins that become dysfunctional and accumulate in the presynaptic zone. The speciality of this area was likely the reason that studies examining synaptic autophagy have focused on autophagosomes in axons, but autophagy has been observed to occur also in neuronal somata and dendrites. The autophagosomes formed at distal processes of neurons are retrogradely transported along microtubules, in a dynein-dependent manner (Katsumata et al. 2010; Ravikumar et al. 2005), to the cell soma to fuse with the lysosomes for degradation (Lee et al. 2011; Soukup et al. 2016; Stavoe et al. 2016). During the retrograde transport, closed autophagosomes mature and undergo several fusion events with late endosomes and become increasingly acidified to allow efficient lysosomal degradation (Maday et al. 2012). Several neuronal events require autophagy induction in neurons, including neurotransmitter receptor turn-over (Rowland et al. 2006; Hui et al. 2019), synaptic development (Shen and Ganetzky 2009; Stavoe et al. 2016),

synaptic pruning (Tang et al. 2014) and synaptic plasticity (Glatigny et al. 2019; Nikoletopoulou et al. 2017; Kallergi et al. 2020). However, the signals inducing autophagy, the physiological roles for autophagy, and autophagy's subcellular distribution in neurons are distinct (Hill and Colón-Ramos 2020). In non-neuronal cells, autophagy is primarily induced by starvation, whereas neurons seemed to escape this effect, exhibiting no autophagy in the brain after starvation in a GFP-LC3 transgenic mouse model (Mizushima et al. 2008). In contrast, other studies could show that starvation induces autophagy in neurons, depending on mTOR (Alirezaei et al. 2010; Oliva Trejo et al. 2020; Young et al. 2009). Next to starvation, autophagy in neurons is induced as a response to neuronal signalling induced by N-methyl-D-aspartic acid (NMDA), an excitotoxin, or potassium chloride, which leads to neuronal depolarization (Shehata et al. 2012; Wang et al. 2015). Furthermore, high-frequency stimulation resulted in a rapid increase of autophagic flux in *Drosophila* neuromuscular junctions (Vanhauwaert et al. 2017; Soukup et al. 2016) and led to the formation of autophagosomes pre- and postsynaptically in rat hippocampal neurons (Shehata et al. 2012; Wang et al. 2015). These studies could show that prolonged neuronal stimulation impacts autophagy biogenesis, even though the formation of autophagosomes at distal processes of neurons was also observable under baseline conditions, without stimulus presentation (Maday et al. 2012; Soukup et al. 2016).

To maintain cellular homeostasis in the presynaptic zone and postsynaptic density, neurons utilize autophagy to remove and degrade damaged proteins and organelles and for activity-dependent restructuring of the synapse (reviewed in (Liang 2019; Nikoletopoulou and Tavernarakis 2018)). Studies focusing on the interplay between autophagy and presynaptic proteins could show that presynaptic active zone protein bassoon can sequester ATG5 locally by direct binding, thereby inhibiting autophagy, whereas a knockdown of Bassoon caused an accumulation of LC3-positive structures at presynaptic boutons (Okerlund et al. 2018). In contrast, presynaptic proteins Endophilin A and Synaptojanin induce/ promote synaptic autophagosome biogenesis (Soukup et al. 2016; Murdoch et al. 2016; Vanhauwaert et al. 2017). Another study suggested that autophagy is involved in neurotransmitter release through a direct interaction of ATG16L1 with RAB26, which is present on the membrane of synaptic vesicles facilitating the recruitment of the autophagy-machinery onto synaptic vesicles to induce their clearance (Binotti et al. 2015), thereby controlling the number of

synaptic vesicles available for release (Nikoletopoulou and Tavernarakis 2018). Furthermore, autophagy is not exclusively active in the presynaptic zone but also in dendrites and the postsynaptic density. It was shown that autophagy could facilitate the $GABA_A$ receptor clustering and trafficking at the postsynapse, demonstrating that autophagy regulation at synapses facilitates the cross-talk between the pre- and postsynaptic sides (Rowland et al. 2006). Moreover, $GABA_A$ receptor accumulated in autophagosomes targeted for degradation in the absence of presynaptic innervation, pointing to a role of autophagy in the induction of long-term synaptic depression (Vijayan and Verstreken 2017; Shehata et al. 2012; Rowland et al. 2006). However, not only $GABA_A$ receptor levels at the postsynaptic sites are controlled by autophagy but also AMPA receptor subunit GLUR1 level was shown to be regulated by autophagy (Shehata et al. 2012). Further studies could show that autophagy is involved in the degradation of several postsynaptic proteins, like PSD95, PICK1 and SHANK3, (Nikoletopoulou et al. 2017). Selective degradation of postsynaptic density protein PSD95, mediated by phosphorylation at position T19, allows lateral AMPA receptor shuffling and demonstrates that autophagy is indispensable for long term depression dependent shrinkage and elimination of dendritic spines (Kallergi et al. 2020) and is, therefore, an essential part of learning and memory formation.

6.1.7 Selective autophagy

Autophagy was initially considered a non-selective degradation pathway, but a growing list of cargos in neurons are turned over by selective autophagy. A specific cargo recognition step mediated by one or more autophagy receptors enhances targeted substrates' engulfment and degradation during selective autophagy. Selective and bulk autophagy share most molecular machinery, but selective autophagy generates specialized autophagosomes that selectively engulf specific cargoes. Selective autophagy is characterized by the receptor-mediated cargo recruitment to the autophagy machinery (Stavoe and Holzbaur 2019). Several autophagy receptors are already identified, such as Sequestosome 1 (SQSTM1)/ p62 (Bjørkøy et al. 2005), a neighbour of BRCA1 gene (NBR1) (Kirkin et al. 2009), optineurin (OPTN) (Wild et al. 2011), Tax1 binding protein 1 (TAX1BP1) (Newman et al. 2012), nuclear dot protein 52 (NDP52)/CALCOCO2, TOLL-interacting protein (TOLLIP) (Baines et al. 2014) and 26S

proteasome regulatory subunit (RPN10) (Stolz et al. 2014; Menzies et al. 2017). These receptors detect ubiquitin and the LC3-interacting region (LIR) motif, creating a bridge between the ubiquitinated cargo and autophagosomes and enhancing selective degradation via the autophagy system (Bjørkøy et al. 2005; Pankiv et al. 2007). Selective autophagy was reported to be responsible for the degradation of several cellular structures, for example, the degradation of aggregates (aggrephagy), mitochondria (mitophagy), the endoplasmic reticulon (ER) (reticulophagy) and lipid droplets (lipophagy) (Galluzzi et al. 2017a).

One of the best-described forms of selective autophagy is mitophagy, which preserves energy homeostasis by eliminating defective mitochondria and thereby preventing the release of harmful by-products. Mitochondria are typically localized at distal neuronal compartments with high energy demands far away from the cell body, like synapses and growth cones, turning mitophagy into a challenging cellular event that needs to be tightly controlled (reviewed in (Doxaki and Palikaras 2020)). Degradation of mitochondria is stimulated by multiple signalling pathways, with the PTEN-induced putative kinase 1 (PINK1)/ Parkin pathway being the best-described one. PINK1, a mitochondrial protein kinase, is inserted on the outer mitochondrial membrane upon potential membrane dissipation, leading to Parkin recruitment to the mitochondrial surface (Harper et al. 2018; Sekine and Youle 2018; Pickles et al. 2018). PINK1 and Parkin interact and facilitate a feed-forward mechanism generating poly-Ub chains, amplifying mitophagy signals (Pickles et al. 2018). However, mitophagy can also be mediated by various receptors as BNIP3, NIX and FUNDC1 that localize to the outer mitochondrial membrane surface and interact directly with LC3, mediating mitochondrial elimination (reviewed in (Palikaras et al. 2018)).

Another essential process of selective autophagy to maintain cellular homeostasis is reticulophagy. The ER forms an impressively complex network consisting of sheets, tubules and cisternae that extends throughout the neuron, including processes and the cell body. The ER underlies a permanent remodelling, restructuring and turn-over during regular homeostasis, which is increased due to cellular stress (Grumati et al. 2018; Wu et al. 2017b). Several transmembrane receptors mediating ER degradation that are localized at specific ER compartments were characterized in the past, for example, FAM134B (Khaminets et al. 2015), SEC62 (Fumagalli et al. 2016), RTN3 (Grumati et al. 2017), CCPG1 (Smith et al. 2018) and

TEX264 (Delorme-Axford et al. 2019). Most of the receptors contain an LIR motif, enabling them to interact with LC3 to mediate ER fragment degradation. Nevertheless, the crosstalk of the ER-luminal cargo and the transmembrane localized receptors is still enigmatic (Grumati et al. 2018).

A further important cargo of autophagy, often associated with neurodegenerative diseases, is the degradation of protein aggregates, aggrephagy. Cargo for aggrephagy is composed of misfolded proteins resulting from mutations, incomplete translation giving defective ribosomal products, misfolding after translation, aberrant protein modifications, oxidative damage, and failed assembly of protein complexes (Lamark and Johansen 2012). Protein inclusion bodies are highly positive for autophagy receptors p62, autophagy-linked FYVE protein (ALFY) and NBR1, which are believed to orchestrate inclusion body construction and degradation by autophagy (Pankiv et al. 2007; Kirkin et al. 2009; Johansen and Lamark 2011; Clausen et al. 2010). However, the appearance of protein aggregates in specific subtypes of neurons hallmarks several neurodegenerative diseases such as Alzheimer's (AD), Parkinson's (PD), Huntington's disease (HD) and amyotrophic lateral sclerosis (ALS). That led to the contradiction that toxic protein aggregates lead to degeneration of neurons in several diseases, whereas on the other hand, it could be demonstrated that adaptor protein p62 inclusion bodies are part of a cell surviving strategy (Komatsu et al. 2007a) and that neurons with p62 positive inclusion bodies do not undergo degeneration. Additionally, mutations in autophagy receptors impair neurotoxic aggregates' clearance (Maruyama and Kawakami 2013; Rea et al. 2014). However, autophagy is a crucial regulator of the levels of intracytoplasmic aggregate-prone proteins that cause neurodegenerative diseases, including polyglutamine-expanded huntingtin (Ravikumar et al. 2002), mutant α-synuclein (Webb et al. 2003), mutant TDP-43 (Barmada et al. 2014), and wild-type and mutant tau (Berger et al. 2006).

6.1.8 Autophagy and neurodegeneration

A few mutations in the autophagy core machinery proteins cause neurodegeneration. A mutation in the ATG5 gene (E122D) was described to lead to congenital ataxia, mental

retardation, and developmental delay in Turkish siblings. This mutation caused a decrease in autophagy flux and defects in the conjugation of ATG5 to ATG12 (Kim et al. 2016).

Another protein, WD-repeat domain 45 (WDR45 / WIPI4), a PIP3 sensor involved in the recruitment of autophagy proteins during autophagophore expansion, was found to cause static encephalopathy childhood with neurodegeneration in adulthood (SENDA/BPAN). The list of symptoms contains early childhood psychomotor retardation that remains static until adulthood with a sudden onset of progressive dystonia-parkinsonism and dementia in the twenties to early thirties of the patients (Kingwell 2013). Characteristic for the disease is the iron deposition in the globus pallidus and substantia nigra that is identifiable via brain magnetic resonance images (MRI). Impairment in the process of autophagy was characterized by impaired autophagy flux and accumulation of lipidated LC3-positive membranes (Saitsu et al. 2013). Another recent publication led to the assumption that BPAN could be caused by impaired macroautophagy machinery in neurons due to a WDR45 mutation that leads to impairment in organelle autophagy resulting in ER stress, among other things (Wan et al. 2020).

Neurodegenerative diseases affect people of both sexes worldwide. The minority of affected people carry a genetic predisposition, most of them are sporadic cases, and little is known about the cause of affection. Under debate are several intrinsic and extrinsic risk factors that are still under investigation. The correlation with ageing could be shown in different studies (Chang et al. 2017; Hansen et al. 2018; Stavoe et al. 2019) as the most prominent “risk factor”. The most common neurodegenerative diseases, AD and PD, have been under investigation for many years, but still, preventative therapeutics are unavailable, and patients are treated palliatively according to symptoms. Therefore, a deep understanding of autophagy impairment during neurodegeneration in neuronal cells could be a beneficial therapeutic intervention.

6.1.8.1 Alzheimer disease (AD)

A progressive cognitive decline is the primary symptom of AD patients. Affected are neurons all over the brain. The degeneration of neurons is caused by intracellular aggregated tau

protein and extracellular accumulation of amyloid-β (Aβ) plaques, generated by the cleavage of Amyloid precursor protein (APP) by β- and γ-secretase (Vassar et al. 1999). The first evidence that autophagy might be affected in AD was the detection of subcellular vesicles located in swollen processes of affected neurons, which could be identified as immature autophagic vacuoles (AVs) (Nixon et al. 2005). This phenotype was also found in PS-1/APP double transgenic mice (Yu et al. 2005) even before the appearance of Aβ plaques. These accumulations of AVs indicate an autophagy dysfunction. Over the years, two genes could be identified that cause the onset of familial AD. Mutations in the gene presenilin-1 (PS1) are within the best-described ones. In PS1 null blastocysts, neurons from mice hypomorphic for PS1 or conditionally depleted of PS1, autophagosome clearance was prevented due to selective impairment of lysosomal acidification and caused by failed PS1-dependent trafficking of the v-ATPase V0a1 subunit to the lysosomes. The observed phenotype mimicked the phenotype of AD patient fibroblasts (Lee et al. 2010; Coffey et al. 2014), leading to an accumulation of autophagosomes due to impaired clearance. Another gene that caught attention due to the reduced expression level in AD brains is Beclin-1 (BECN1), an initiation protein of autophagy (Pickford et al. 2008; Small et al. 2005). A reduction of Beclin-1 in mice resulted in decreased level of autophagy and the accumulation of Aβ peptides leading to neurodegeneration (Jaeger et al. 2010). On the other hand, overactive Beclin-1 and increased levels of Beclin-1 resulted in reduced cellular APP levels (Rocchi et al. 2017; Jaeger et al. 2010). Reduced levels of Beclin-1 could also be mediated by Caspase-3 cleavage, which is activated in AD patient brains (Rohn et al. 2011). The studies on Beclin-1 indicate that decreased levels of Beclin-1 lead to decreased clearance level of Aβ, pointing to Beclin-1 as a promising therapeutic target. Next to the genetic causes of AD, most patients are affected by a sporadic onset of AD. The onset of AD is usually influenced by an extensive range of environmental factors, lifestyle, and genetic elements. Several environmental factors are described to favour AD development, including exposure to heavy metals like lead, mercury, arsenic, cadmium and aluminium, and pesticides and nanoparticles. Exposure to heavy metals is believed to have the capacity to enhance Aβ peptide formation along with tau phosphorylation and to initiate amyloid plaques and neurofibrillary tangle formation (Rahman et al. 2020). Investigating lifestyle factors, most studies concentrated on physical activity and specific diets regarding AD development. Thereby, it could be revealed that higher adherence to the

Mediterranean-type diet and higher physical activity were independently associated with a reduced risk of developing AD (Singh et al. 2014; Scarmeas et al. 2009) as well as a higher intake of fish (Wu et al. 2015). Another interesting finding is that a higher intake of calories and fats may be associated with a higher risk of AD in individuals carrying the apolipoprotein E epsilon4 allele (Luchsinger et al. 2002). Taking all the described environmental factors influencing the risk of AD development into account, it seems beneficial to keep cellular baseline levels of autophagy high to clear harmful material before it becomes cell damaging.

6.1.8.2 Parkinson disease (PD)

PD is the second most common neurodegenerative disorder with characteristic symptoms of tremors, rigidity, akinesia, bradykinesia, and postural instability in PD patients. The phenotype is caused by neurodegeneration of dopaminergic neurons in the substantia nigra due to increased α-synuclein protein accumulation, the so-called Lewy bodies (LBs), a hallmark in PD. Several studies could show that α-synuclein protein is degraded via autophagy (Webb et al. 2003) and that increased level of α-synuclein mediated by gene duplication leads to PD (Singleton et al. 2003). Increased level of α-synuclein even counteracts autophagy by RAB1a mediated mislocalization of transmembrane protein ATG9, which is involved in membrane recruiting and omegasome formation (Winslow et al. 2010). Additionally, mutation in the α-synuclein (SNCA) gene per se could be observed to induce early-onset (A30P, A18T, A29S E46K, A53T, G51D) but also late-onset (H50Q) forms of PD (Fujioka et al. 2014; Krüger et al. 1998; Lesage et al. 2013; Polymeropoulos et al. 1997; Proukakis et al. 2013; Zarranz et al. 2004). All the mutations are associated with artificial aggregation leading to the formation of Lewy bodies. Next to gene mutations in α-synuclein several autosomal dominant and recessive ones could be identified in the last years that led to PD. One that also led to ATG9 delocalization and impaired autophagy was a mutation in the Vacuolar Protein Sorting-Associated Protein 35 (VPS35) (Zavodszky et al. 2014), causing a rare form of autosomal-dominant variation of PD. In familiar PD cases, two autosomal-recessive gene mutations of proteins acting in the same pathway were identified. Loss-of-function mutations of Parkin RBR E3 ubiquitin-protein ligase (PARK2 / Parkin) and PTEN-induced putative kinase 1 (PINK1 / PARK6) cause autosomal-recessive and sporadic juvenile-onset PD (Kitada et al. 1998; Valente et al. 2004). Both proteins

are involved in the clearance of non-functional mitochondria via mitophagy. PINK1 attaches to damaged mitochondria with low membrane potential, recruiting Parkin to mediate selective autosomal degradation (Matsuda et al. 2010) via p62 (Geisler et al. 2010). Loss-of-function studies in model organisms revealed that a loss of Parkin does not cause nigrostriatal neuronal loss but a reduction in synaptic excitability (Goldberg et al. 2003) and a shift in dopamine receptor levels and localization (Itier et al. 2003). Also, a change in signalling and altered network dynamics could be observed and could accompany symptomatic PD (Baaske et al. 2020). Another observed phenotype is the accumulation of fragmented mitochondria with abnormal internal structures in aged mice (Noda et al. 2019) and the increased sensitivity to oxidative stress (Kang et al. 2019), which is most likely generated by the impaired degradation of non-functional mitochondria. Another autosomal recessive form of PD is caused by a gene mutation in ATPase type 13A2 (ATP13A2 / PARK9). This protein acts on lysosomes functional in ion transport to enable acidification. In PD patient-derived fibroblast carrying an ATP13A2 mutation, lysosomal acidification was impaired, and the degradation of lysosomal substrates was reduced, leading to an accumulation of autophagosomes. Analysis of PD brain tissue showed decreased level of ATG13A2 protein in dopaminergic nigral neurons, colocalizing with Lewy bodies (Dehay et al. 2012). Next to the genetic causes for PD disease onset, several environmental factors were also identified to favour the development of PD, including the exposure to heavy metals, pesticides, and illicit substances that cause abnormal morphology in the substantia nigra (Ball et al. 2019). All in all, considering that several genetic mutations in genes involved in autophagy leading to the onset of PD draw a strong link for the importance of autophagy in PD development prevention.

6.1.8.3 Huntington's disease (HD)

Patients affected from HD show cognitive dysfunction, psychiatric disturbances, and severe motor dysfunction caused by the neurodegeneration of medium spiny neurons of the caudate-putamen. The disease is caused by a trinucleotide repeat expansion (>35 repeats) mutation of cysteine, adenine, and guanine (CAG) in the coding region of the ubiquitously expressed gene now known as the HD gene (A novel gene containing a trinucleotide repeat that is expanded and unstable on Huntington's disease chromosomes. The Huntington's

Disease Collaborative Research Group 1993). On the protein level that causes a long tract of polyglutamine (poly Q) repeats near the N-terminus of huntingtin (HTT). Surprisingly, autophagy seemed to have paradoxical effects in HD. Autophagy inhibitor mTOR is sequestered into HTT aggregates, resulting in impaired kinase activity and induction of autophagy (Ravikumar et al. 2004), accompanied by increased LC3-II and p62 levels (Heng et al. 2010). That would lead to the assumption that autophagy is induced/activated in HTT patients. However, it could be shown that autophagy activator protein Beclin-1 is recruited into the HTT aggregates reducing autophagy induction (Shibata et al. 2006). Additionally, it was found in HTT mouse models that autophagosome formation is enhanced and eliminated by the lysosomes. However, the cargo loading of autophagosomes fails, and the degradation is relatively inefficient (Martinez-Vicente et al. 2010). Next to the modulation of the two essential player proteins in autophagy initiation, HTT also affects Rab5 and Rhes, two positive regulators of autophagy interacting with Beclin-1 (Mealer et al. 2014; Ravikumar et al. 2008). Even after several years, the precise role of HTT in autophagy remains still enigmatic. A hypothesis could say that the increased formation of autophagosomes could be a compensatory mechanism to clear HTT aggregates, but over time the autophagic machinery becomes dysfunctional leading to neurodegeneration (Son et al. 2012).

6.1.9 Treatment options targeting autophagy

The accumulation of aggregated proteins in neurodegenerative diseases and the decline of autophagy in neurodegenerative disease progression brought up the idea that enhancing or inducing autophagy could efficiently treat neurodegenerative diseases. Promising drugs in the field can be categorized into two groups, mTOR-dependent or mTOR-independent (Menzies et al. 2017; Hansen et al. 2018). The mTOR pathway plays a vital role in regulating cellular homeostasis, with mTOR as a critical player. Activated mTOR suppresses autophagy induction and functions as an autophagy suppressor. One of the classical mTOR inhibitors is Rapamycin and other Rapalogs. Rapamycin is a direct inhibitor of the mTOR protein and could show beneficial effects in several studies using AD and PD model organisms. It was shown to extend life span (Harrison et al. 2009; Miller et al. 2011), increase the clearance of aggregated protein accumulations (Dehay et al. 2010; Jiang et al. 2014; Ozcelik et al. 2013) and delay or even

reverse nearly every age-related disease or decline in functionality in mice (Lin et al. 2013a). However, it could also be shown that treatment with Rapamycin can have severe side effects in a dose-dependent manner. Resveratrol is another compound that reduces cerebral Aβ levels and deposition in the cortex. This natural polyphenol promotes autophagy by operating as a caloric restriction mimetic, leading to increased intracellular calcium that promotes AMPK activation, mTOR inhibition and autophagy induction (Vingtdeux et al. 2010). Even though several autophagy-modulating compounds are identified (rapamycin, chloroquine, HCQ), their effects are well described in the literature and are licensed for use in humans; they are not used for therapeutical application. The first reason is that some molecules have an intrinsically low pharmacological specificity. Second, autophagy operates at the interface of multiple cellular processes and a blockage of mTOR to induce autophagy also causes a decrease in translation, cellular growth and proliferation (Galluzzi et al. 2017b). All in all, identifying downstream targets of autophagy that are misregulated in diseases would help to design a more specific therapy with possibly fewer side effects. Another crucial step in establishing a novel treatment therapy in neurodegenerative disease would be to find criteria that allow discovering earlier in life that a person will be affected by PD or AD before extensive neurological damage occurs.

6.1.10 Non-canonical functions of autophagy

Besides the housekeeping role, autophagy was shown to mediate other physiological roles important for neuronal function. Autophagy plays a major role in BDNF-TrkB neurotrophic signalling. Neurotrophins are released and have biological activity that involves regulating cell survival, and growth cone dynamics (Deinhardt et al. 2011; Teng et al. 2005; Nykjaer et al. 2004; Lee et al. 2001), but are also required for long-term synaptic plasticity (Kang et al. 1997; Korte et al. 1998; Messaoudi et al. 2002; Minichiello et al. 1999; Patterson et al. 1996; Ying et al. 2002). Autophagy contributes to neurotrophic signalling by the retrograde transport of TrkB/BDNF loaded receptors localized at autophagosomes. An interaction of LC3 with the endocytic receptor AP2 mediates this transport, and it could be demonstrated that disruption in the retrograde transport of autophagosomes led to decreased neuronal complexity (Kononenko et al. 2017). Furthermore, it was shown that BDNF ablation induced

autophagosome formation *in-vitro* (Nikoletopoulou et al. 2017) and impairment in LTP caused by BDNF deficiency could be rescued by the inhibition of autophagy. Additionally, it was shown that LTP activates mTOR and led to autophagy inhibition subsequently (Kelleher et al. 2004; Tang et al. 2002).

Another study demonstrated the role of autophagy in memory formation, which is induced during learning and memory and required for novel memory formation. Impairment of autophagy by selective downregulation of autophagy protein level resulted in impaired memory formation. Autophagy contributes to learning and memory formation by enhancing synapses' structural and functional activity-dependent remodelling. Furthermore, the study could show that the induction of autophagy was sufficient to reverse age-related memory deficits (Glatigny et al. 2019).

Autophagy functions also in pruning events, demonstrated with the help of an autism spectrum disorder (ASD) mouse model (*Tsc2*$^{+/-}$) and post-mortem brain tissue of ASD patients that showed increased dendritic spine density with reduced developmental spine pruning in layer V pyramidal neurons in the temporal lobe. Increased spine density was caused by suppressed autophagy-mediated elimination of spines by mTOR overactivation. In contrast, mTOR inhibitor rapamycin corrected ASD-like behaviours and spine pruning defects in *Tsc2*+/ mice, but not in *Atg7*flox:*CamKIIα*-Cre autophagy-deficient mice or *Tsc2*$^{+/-}$:*Atg7*flox:*CamKIIα*-Cre double mutants (Tang et al. 2014).

Another recent study has shown that autophagy regulates microtubule dynamics by LC3 association with ELKS1, an active zone located protein. The upregulation of cytoplasmic LC3 levels stabilized ELKS1 protein leading to increased binding of ELKS1 to CLASP2, a microtubule plus-end trafficking protein. Especially at en-passant synapses, this interaction is indispensable for maintaining neurotransmitter release and preventing axonal pathology (Negrete-Hurtado, Overhoff et al. 2020).

6.1.11 Autophagy in epileptogenesis and epilepsy-induced neuronal alterations

Epilepsy is a disorder affecting around 1% of all people (Wong 2010), defined by the recurrent and unpredictable interruptions of normal brain functions by abnormal excessive or

synchronous neuronal activity in the brain. These events are termed epileptic seizures, which are transient, demarcated in time, with a clear start and finish. Epileptic seizures can interfere with sensory, motor, and autonomic functions, consciousness, emotional state, memory, cognition and behaviour, depending on seizure onset localization, propagation pattern and a variety of other factors (Fisher et al. 2005). Several studies indicate that alterations in autophagy are present in neurodegenerative diseases and acute neurological insults like epileptic seizures (Giorgi et al. 2015). Studies using forebrain specific knockout mouse models of TSC1 and Tensin, genetic mouse models for epilepsy, could show that mTOR is hyperactive with a simultaneous downregulation of autophagy activity. In these mouse models, hyperactivation of mTOR is believed to be primarily responsible for the epileptogenic process (Cao et al. 2009; Wong 2010). The finding that mTOR activity is induced by aberrant synaptic activity could be demonstrated in a study that used kainate, an ionotropic glutamate receptor agonist, to induce epileptic seizures experimentally. They found mTOR pathway upregulation at 1-24 hours after seizure onset and 3 days till 5 weeks after status epilepticus (30 minutes extending long-lasting epileptic seizure). Furthermore, they could show that the pretreatment with mTOR inhibitor, rapamycin, did not alter the epileptic seizure characteristic (latency, duration, and severity) but weakened neuronal degeneration (Zeng et al. 2009). In contrast, the lack of autophagy in forebrain confined *Atg7*-deficient knockout mice lead to the appearance of epileptic seizures (McMahon et al. 2012). Therefore, autophagy could be an attractive target for drug development to improve epilepsy treatment.

The control of epileptic seizures by anti-epileptic medication is effective in 65% of epilepsy patients. Another 8-10% can undergo surgery for release, but the remaining 25% have medication-resistant epileptic seizures (Mormann et al. 2007). Anti-epileptic drugs are designed to block voltage-dependent sodium channels, prevent selectively high-frequency repetitive neuronal firing, potentiate GABAergic inhibition, inhibit GABA transaminase or GABA reuptake, or block calcium channels (Perucca 2005). Patients affected by medication-resistant epileptic seizures are often treated with a special diet, the ketogenic diet. The ketogenic diet is a special high-fat, low-carbohydrate diet, which is an effective treatment in some patients with multi-resistant catastrophic epilepsies and is likely based on starvation-induced autophagy activation (Giorgi et al. 2015). This treatment method has a long history and goes back to findings in 1920, where fasting was reported to improve cognition and

seizure frequency after 2-3 days of fasting (summarized in (Wheless 2008)). The classical ketogenic diet is rich in lipids (90%) and low in carbohydrates and proteins to induce ketosis and slightly neuronal starvation. The goal of the diet is to decrease the blood glucose level with a simultaneous increase of ketone bodies produced in the liver, forcing the neurons to use ketone bodies instead of glucose for energy supply. This anaerobic metabolism slowed down the energy availability compared to the rapidly available energy produced by the glucose metabolism. However, rapidly available energy is necessary for seizure activity and can be suppressed successfully with the change to the slower anaerobic metabolism (D'Andrea Meira et al. 2019). Another beneficial effect of the ketogenic diet and fasting is the mTOR-dependent induction of autophagy that can contribute to synaptic homeostasis (Liśkiewicz et al. 2021; McCarty et al. 2015; Wang et al. 2018; Alirezaei et al. 2010; Young et al. 2009; McDaniel et al. 2011). Nevertheless, today's treatments are symptomatic and suppress seizures but do not correct the underlying brain abnormalities causing epilepsy, making autophagy an exciting target for future drug development.

6.1.12 Genetic mouse models of autophagy

To achieve a deep understanding of autophagy protein function in neurons/ the brain, several ATG KO mouse lines were investigated over the last decades. It has been noticed that a conventional knockout of ATG proteins causes embryonic or neonatal lethality. However, several conditional mouse models have been investigated to understand the function of autophagy in the brain, primarily developed under the *Nestin*-Cre (Nes) promotor that affects neuronal and glial cells (Dahlstrand et al. 1995). Among them are conditional mouse models for ATG5 (Hara et al. 2006), ATG7 (Komatsu et al. 2006), FIP200 (Liang et al. 2010), ULK1/2 (Joo et al. 2016), and ATG9a (Yamaguchi et al. 2018). Autophagy deficient mice are born normally but show increased mortality within the first week and a reduced life span, progressive neurodegeneration in different brain areas, growth retardation and motoric dysfunction. Another characteristic that most mice models share (except the Ulk1/2 KO mouse model) is the accumulation of ubiquitinated protein aggregates, highly positive for adaptor protein p62, in the cell body and aberrant membranous structures and amorphous materials. The formation of axonal swellings, a form of axonal pathology associated with

neurodegeneration, was detected in WD40 repeat-containing PtdIns(3)P binding protein (WDR45 / WIPI4) deficient mouse model (Zhao et al. 2015). Next to the autophagy-deficient mouse models under the *Nestin*-Cre, neuronal subtype-specific mouse models were generated to investigate the role of autophagy in different neuronal subtypes. A mouse model lacking ATG7 in Purkinje neurons (*Atg7*flox:*Pcp2*-Cre) showed cell-autonomous, progressive dystrophy (manifested by axonal swellings) and degeneration of the axon terminals followed by cell-autonomous Purkinje cell death and mouse behavioural deficits (Komatsu et al. 2007b). But in contrast, neurodegeneration was not observed in several other neuronal subtype-confined autophagy-deficient mouse models (e.g. *Atg5*flox:*CamkIIα*-Cre, *Atg7*flox:*DAT*-Cre, *Atg7*flox:*BAC*^{drd1acre}, *Atg7*flox:*BAC*^{A2Acre}). Other cellular alterations were observed in these mouse models, suggesting a role of autophagy in several cellular pathways independent of its function in degradation. These include the regulation of axonal microtubule dynamics demonstrated in excitatory forebrain neurons (Negrete-Hurtado, Overhoff et al. 2020), the regulation of presynaptic neurotransmission demonstrated in dopaminergic neurons (Hernandez et al. 2012), and the regulation of intrinsic neuronal excitability demonstrated in the striatum, spiny projection neurons (Lieberman et al. 2020). These mouse models show that the role of autophagy is multifaceted and might be different between cell types, which makes it worth it to look at it more in detail in different cell types to elucidate autophagy functions.

6.2 cAMP-dependent protein kinase A (PKA)

PKA was discovered in 1968, as the second protein kinase (Walsh et al. 1968), and since then, much research has been done elucidating its function. So far, four regulatory (R1-α, R1-β, R2-α, R2-β) and three catalytic subunits (C-α, C-β, C-γ) are identified in eukaryotic cells, each encoded by a unique gene (McKnight et al. 1988; Døskeland et al. 1993). In an inactive state, the catalytic subunits assemble to the regulatory subunit forming a holoenzyme complex. This complex comprises two regulatory and two catalytic subunits forming a heterotetrameric structure (R_2C_2). When cAMP binds to the regulatory subunits, they undergo a conformational change, releasing the catalytic subunits, which gets released to phosphorylate downstream targets (Fig. 3) (Taylor et al. 2012). Thereby, the regulatory subunits type 1 (R1) show a higher

binding affinity for cAMP (40-50 nM; (Woodford et al. 1989)) than the regulatory subunit type 2 (R2) (50-200 nM; (Robinson-Steiner et al. 1984)), suggesting that the bulk of the cytoplasmic PKA activity derives from R1.

PKA mediated signalling is controlled tightly in time and location by A-kinase anchoring proteins (AKAPs) that bind to the regulatory subunits of protein kinase A, confining the holoenzyme to discrete locations within the cell (Langeberg and Scott 2005), whereas they show a higher binding affinity for R2 than R1 (Kirschner et al. 2009). The R1-α and R2-α subunits are ubiquitously expressed in every cell. Nevertheless, the RI-β is expressed in the brain and spinal cord and R2-β is expressed predominantly in the brain, endocrine, fat, liver and reproductive tissues (Cadd and Stanley McKnight 1989). The most significant difference between R1 and R2 is the serine residue at the inhibitory side of R2, which makes R2 itself a substrate of the PKA catalytic subunit, whereas R1 contains an alanine or glycine residue that mimics the substrate (Diskar et al. 2007; Martin et al. 2007). The four subunits are functionally non-redundant, which was shown by the usage of different knockout studies.

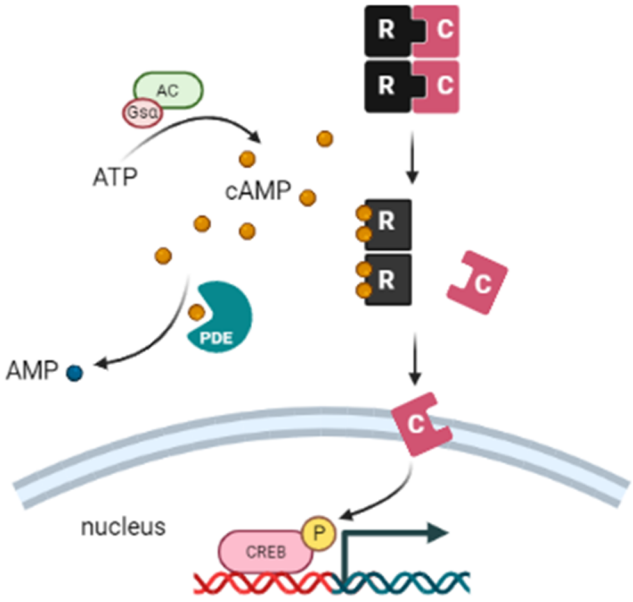

Figure 3: cAMP-dependent protein kinase A (PKA) signalling.

cAMP-dependent protein kinase A holoenzyme complex (R_2C_2) gets activated by cAMP binding. That induces a conformational change of the regulatory subunits (R), causing the release of the catalytic subunits (C) to induce phosphorylation (P) of downstream targets like transcription factor CREB. cAMP is generated by adenylyl cyclase (AC) and gets degraded by phosphodiesterases (PDE) (picture generated using BioRender, Agreement number: LX238ALJ51).

6.2.1 Knockout mouse models of PKA elucidating kinase function

The knockout of the catalytic subunit C-α (prkaca$^{-/-}$) led to an increased perinatal lethality (circa 27% of knockout mice survived till adulthood), a decrease in overall body size, resulting in the 65% leaner phenotype and male infertility caused by deficient sperm development and overall reduced sperm count (Skålhegg et al. 2002). In an independent study, they observed that C-α null mice showed decreased epithelial growth factor receptor protein level, which could lead to an impaired ability for cells to convey growth signals resulting in the presented lean phenotype (Oksvold et al. 2008). In contrast to the strong phenotype of C-α knockout mice, PKA C-β (prkacb$^{-/-}$) mice are phenotypically normal but show learning deficits in contextual learning (Qi et al. 1996) and cued learning (Howe et al. 2002). Additionally, it was observed that the knockout of PKA C-β resulted in a compensatory increase of PKA C-α protein level, which stabilized the activation potential for PKA in the brain. The knockout of both catalytic subunits (prkaca$^{-/-}$; prkacb$^{-/-}$) resulted in early embryonic lethality (Huang et al. 2002). Knockouts in which one allele of the subunits remained (prkaca$^{+/-}$; prkacb$^{-/-}$ / prkaca$^{-/-}$; prkacb$^{+/-}$) presented spinal neural tube defects leading to Spina Bifida suggesting a role for PKA signalling during neural tube development (Huang et al. 2002).

Studies to identify the physiological functions of PKA regulatory subunits were performed with mouse models targeting the single subunits. Knockout of PKA R1-α (prkar1a$^{-/-}$), the most highly and widely expressed regulatory subunit, led to embryonal lethality by embryonic day 10.5 due to a failure of normal mesodermal development (Amieux et al. 2002). The additional knockout of PKA C-α (prkar1a$^{-/-}$; prkaca$^{-/-}$) improved the genotype but did not restore post-embryonic viability (Amieux et al. 2002). The heterozygous knockout of PKA R1-α (prkar1a$^{+/-}$) was viable and are used as a genetic model organism to study Carney Complex syndrome (Kirschner et al. 2009). Knockout mice lacking PKA R1-β (prkar1b$^{-/-}$) are viable, fertile with an inconspicuous phenotype (Brandon et al. 1995). PKA activity was maintained on an average level in brain tissue due to a compensatory increase of PKA R1-α protein level increase (Amieux et al. 1997). Because dysregulated PKA activity is associated with a disruption in long-term synaptic potentiation (Abel and Nguyen 2008), memory processes were studied in these knockout mice. It was shown that the lack of PKA R1-β resulted in deficits in the long-term

depression at the Shaffer collateral-CA1 synapses, at pyramidal cells and the lateral perforant path-dentate synapse on granular cells. Additionally, a reduction in the depotentiation of CA1 synapses was observed, suggesting an essential function of PKA signalling for long term depression (LTD) and depotentiation and low-frequency stimulation-induced LTD (Brandon et al. 1995). The knockout mice of PKA R2-α appeared normal without phenotype (Burton et al. 1997). General PKA activity was reduced but without a lack of functionality. Even the interaction of PKA with the L-type calcium channels, usually controlled by PKA R2-α phosphorylation, was not altered, most likely due to the compensational effort of the other subunits (Burton et al. 1997). The knockout of PKA R2-β (prkar2b$^{-/-}$) appeared normal with a reduction of white adipose tissue, resulting in a lean phenotype, despite normal food intake (Brandon et al. 1998; Cummings et al. 1996). It could be shown that the compensatory increase on the protein level of PKA R1-α due to the lack of PKA R2-β resulted in a switch to PKA type 1 signalling that induced a higher metabolic rate and body temperature with enhanced energy utilization. It could be shown that PKA R2-β KO mice have lower body weight, low insulin levels and improved total-body glucose disposal than WT controls (Schreyer et al. 2001). Additionally, the brain function of the dopaminergic system was investigated because of PKA R2-β prominent expression in striatal tissue. It could be demonstrated that PKA R2-β functions in the coordination of motor control because KO mice showed defects in the performance of the Rotarod task (Brandon et al. 1998). To sum up, the four regulatory subunits of PKA are widely expressed in different tissues and function in different signalling pathways. However, it was noted that PKA R1-α seems to act as a buffer for PKA activity (Brandon et al. 1997). PKA R1-α was upregulated compensatively when catalytic subunits were overexpressed (Uhler and McKnight 1987) and in PKA regulatory subunit KO mice (Otten and McKnight 1989; Brandon et al. 1995; Cummings et al. 1996). Another compensatory effect of PKA R1-β could be observed in PKA R2-β mice (Brandon et al. 1997). Surprisingly, the compensatory effect on the protein level of PKA R1-α was not based on an increased mRNA level or translation rate but a decrease in the rate of selective protein degradation. Pulse-chase experiments could show that the half-time of the PKA R1-α was 4-5 fold increased as it becomes incorporated into the holoenzyme (Amieux et al. 1997).

6.2.2 PKA signalling is crucial for learning and memory formation

The signalling of cAMP/PKA is necessary to establish short- and long-lasting forms of synaptic plasticity, learning and memory, demonstrated in landmark studies using *Aplysia* (Kandel 2001) and *Drosophila* (Dubnau and Tully 1998). The targets of PKA phosphorylation differ in both short- and long-term memory. PKA phosphorylates ion channels during short-term synaptic facilitation, whereas PKA signalling modulates gene expression and protein synthesis for long-term memory formation by the phosphorylation-dependent activation of transcription factors (Kandel 2001). To elucidate the function of PKA during learning and memory formation in mammals, the generation of PKA mice models were very supportive. Transgenic mice overexpressing a dominant-negative version of PKA R1-α under the *CamKIIα*-Cre promotor showed reduced hippocampal PKA activity, resulting in a decreased late-phase long-term potentiation without affecting the basal synaptic transmission or the early phase of long-term potentiation (LTP). Behaviorally, normal short-term memory but defective long-term memory led to deficits in spatial memory and contextual fear conditioning in PKA R1-α overexpressing mice. The observed effects mirror the finding in mice with pharmacologically blocked protein synthesis, pointing to an essential role of PKA in LTP-induced protein synthesis for memory consolidation (Abel et al. 1997). Additionally, the pharmacological inhibition of PKA by a bilateral intrahippocampal infusion of PKA inhibitor H89 into the CA1 hippocampal region worsened the performance of treated mice in the Morris water maze, indicating a role for PKA signalling during spatial learning and memory (Sharifzadeh et al. 2005). Memory storage and acquirement are defective also in several neurodegenerative diseases, which are hypothesized based on defective PKA signalling. In i*n-vitro* experiments, using cultured primary neurons, the application of the amyloid beta-peptide led to the inactivation of PKA due to the persistence of its regulatory subunit PKA R2-α. As a result, the CREB phosphorylation as a response to glutamate was decreased. That effect could be rescued by cAMP level raising substrates as rolipram, a phosphodiesterase inhibitor blocking the degradation of cAMP, or Forskolin, an adenylyl cyclase-activating agent supporting the conversion of ATP to cAMP. The observed rescue could be blocked by PKA inhibitor H89 (Vitolo et al. 2002).

Several critical proteins in hippocampal long-term potentiation and targets of PKA phosphorylation include NMDA (N-methyl-D-aspartate), AMPA (alpha-amino-3-hydroxy-5-

methyl-4-isoxazole propionate), glutamatergic receptors, RIM1α, inhibitor-1, and the transcription factor CREB. LTP is the strengthening of a synaptic contact induced by synaptic signalling. Presynaptic released glutamate binds to AMPA and NMDA receptors in the postsynaptic density membrane. Due to the glutamate binding, AMPA receptor channels open and allow the influx of Na^{2+} ions into the cell inducing neuronal depolarization. The NMDA receptor has a high binding affinity for glutamate but only opens when the cell depolarizes, which causes Mg^{2+}, that block the NMDA receptor channel pore, to delocalize. When the Mg^{2+} block is released, Ca^{2+} ions flow into the cell along the concentration gradient. The influx of calcium from the extracellular space and release from intracellular storages activates several signalling cascades in the cell that have long-lasting effects like protein synthesis via activation of transcription factors leading to synaptic strengthening.

6.2.3 PKA phosphorylation on AMPA receptors

PKA phosphorylation can modulate AMPA receptor-mediated signalling in two ways, by phosphorylation of AMPA receptors and modulation of AMPA receptor trafficking. PKA can phosphorylate the AMPA subunit GLUR1 at the serine residues S831 and S845 (Roche et al. 1996), which modulates AMPA receptor opening frequency and channel opening duration. This modulatory effect could be demonstrated in hippocampal neurons treated with PKA stimulating agent Forskolin or the intracellular application of PKA catalytic subunit that enhances whole-cell EPSC amplitudes (Greengard et al. 1991; Wang et al. 1991; Banke et al. 2000). In contrast, applying a PKI inhibitor peptide blocked the expression of long-lasting synaptic potentiation in hippocampal neurons (Duffy and Nguyen 2003). However, PKA is also a modulator of activity-dependent AMPA receptor trafficking, including AMPA receptor recycling and sorting, a mechanism that contributes to synaptic plasticity. AMPA receptors have four subunits, GLUR1-GLUR4, and those subunits form heterotetrameric channels, composed of two dimers, predominantly expressed in hippocampal neurons in combinations GLUR1/2 or GLUR2/3 (Wenthold et al. 1996). Receptors with only short cytoplasmic termini (GLUR3/2) continuously cycle in and out of the synapse, whereas the subunits with long cytoplasmic tails (GLUR4/2, GLUR1/2) are recruited into the postsynaptic membrane by strong synaptic activity (Passafaro et al. 2001; Shi et al. 2001). An important modulator of AMPA

receptor trafficking is the phosphorylation of long cytoplasmic tail containing receptor subunits by CamKII and PKA. Thereby, PKA is known to phosphorylate the AMPA receptor subunits GLUR4 at serine 842 and GLUR1 at serine 845, which leads to the incorporation of the receptors into the postsynaptic membrane (Esteban et al. 2003). The dynamic phosphorylation and dephosphorylation of the GLUR1 phosphorylation site were reported to be a critical factor in NMDA-dependent AMPA receptor internalization and, therefore, proper LTP and LTD (Man et al. 2007).

To ensure proper PKA signalling, numerous structuring proteins coordinate PKA localization in the postsynaptic density. These proteins are inserted into membranous structures or attached to the cytoskeleton and regulate the localization of their distinct targets, including PKA. The scaffold proteins targeting PKA, the AKAPs, place PKA close to AMPA receptors for spatially-confined, selective phosphorylation (Nguyen and Woo 2003). The localization of PKA is crucial for proper AMPA receptor function. A study using a PKA displacing peptide Ht31 reduced the amplitude of AMPA receptors in cultured hippocampal neurons. This effect is overcome by directly applying a catalytic subunit of PKA (Rosenmund et al. 1994).

6.2.4 PKA modulates NMDA receptors in a calcium-dependent manner

PKA is coupled to NMDA receptors via AKAP, yotiao (Westphal et al. 1999). PKA phosphorylation of NMDA receptors and other surrounding proteins leads to an altered pore size of the NMDA channel to regulate the calcium influx and determine the type of plasticity (LTP or LTD) (Abel and Nguyen 2008). Blockers of PKA mediated phosphorylation reduced calcium permeability of NMDA receptors, leading to reduced calcium signalling in the neurons (Skeberdis et al. 2006). However, calcium influx through NMDA receptors indirectly modulates PKA signalling in a feedback loop. Calcium sensitive adenylyl cyclases (AC; e.g. AC1) gets activated by the calcium influx induced by synaptic activity and convert ATP to second messenger cAMP, which binds to PKA regulatory subunits and induce PKA signalling (Fig. 4) (Mons et al. 1995; Antoni et al. 1998; Hanoune and Defer 2001). The calcium-dependent regulation of PKA signalling seems to play a significant role in LTP, considering the enrichment of Ca^{2+}-sensitive ACs in areas exposed to high intracellular free calcium such as dendritic spines

(Mons et al. 1995) and the observation that genetic mouse models with disruption of the AC1 gene show deficiencies in spatial learning (Wu et al. 1995; Storm et al. 1998).

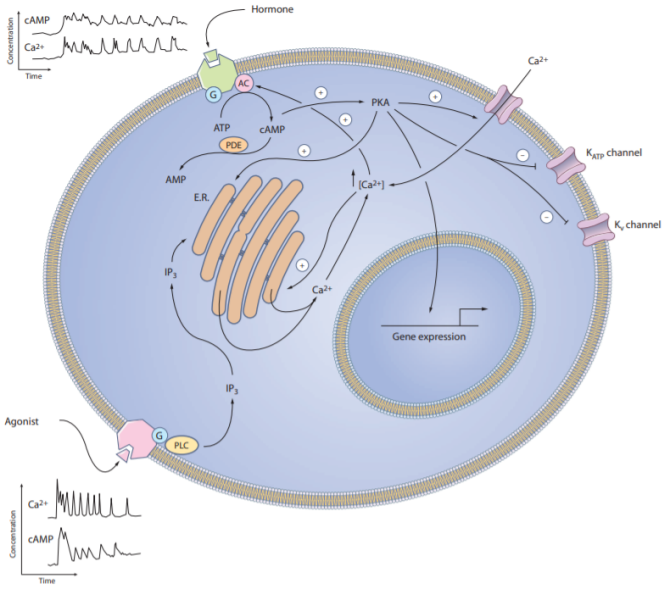

Figure 4: Cross-communication of PKA and calcium.

Synaptic activity is causing neuronal depolarization that free NMDA receptors from their channel, blocking Mg^{2+} ions. The NMDA channel pore opening allows Ca^{2+} ion influx into the neuron, activating several pathways involved in learning and long-term memory formation. One of these pathways is PKA-mediated phosphorylation, initiated through calcium-induced adenylyl cyclase mediated conversion of ATP to cAMP (figure taken from (Borodinsky and Spitzer 2006)).

6.2.5 cAMP response element-binding protein (CREB)

CREB is a transcription factor constitutively expressed and activated via posttranslational modifications such as phosphorylation. A variety of cellular signalling processes can trigger this phosphorylation, including an increase in intracellular calcium (Ca^{2+}) via activation of voltage- or ligand-gated channels (e.g. NMDA receptor) after synaptic activity, an increase of intracellular cAMP concentration mediated by adenylyl cyclase or G-coupled receptors, or activation of receptor tyrosine kinase by growth factors (Lonze and Ginty 2002). Transcription factor CREB specifically recognizes the palindromic octanucleotide sequences TGACGTCA, referred to as cAMP response element (CRE) (Montminy et al. 1990). CREB mediated function

and gene expression are critical for several neuronal functions in the nervous system, including neurogenesis and neuronal survival, development, and differentiation, neuroprotection, axonal outgrowth and regeneration, circadian rhythms, addiction, synaptic plasticity, and memory formation (Barco and Kandel 2005; Carlezon et al. 2005; Dragunow 2004; Mioduszewska et al. 2003; Montminy et al. 2004; Persengiev and Green 2003; Silva et al. 1998). One of the kinases phosphorylating and thereby activating CREB is PKA. Increased cAMP levels lead to PKA activation and subsequently to phosphorylation mediated activation of CREB at serine 133. CREB has several phosphorylation sites, and the different phosphorylation patterns of CREB are correlated with distinct cellular functions and can exert opposite effects. Phosphorylation of CREB at serine 111 or 121 inhibits transcription, whereas phosphorylation of CREB at serine 129 and 133 induces transcription (Steven et al. 2020). This induction of transcription mediated by PKA phosphorylation of CREB, at serine 133, was demonstrated to be an essential factor during late-phase LTP (memory consolidation), which requires gene transcription and new protein synthesis to induce long-term changes at the postsynapse. PKA activity or transcription blockers inhibit late-phase LTP (Nayak et al. 1998). The precise role of CREB in learning and memory formation was studied in great detail in *Aplysia* (Kandel 2012) and *Drosophila* (Yin and Tully 1996). Nevertheless, CREB is also crucial for memory formation in vertebrates, demonstrated by impaired memory consolidation and reconsolidation in a mice model expressing dominant-negative CREB (Kida et al. 2002).

6.2.6 PKA signalling in neurodegenerative diseases

6.2.6.1 Alzheimer's disease

One of the hallmarks in AD pathology is the formation of neurofibrillary tangles, and those numbers correlate with cognitive decline. Neurofibrillary tangles are composed of phosphorylated tau proteins generated by a variety of kinases, including PKA mediated phosphorylation at serine 214 and serine 409 (Jicha et al. 1999), as well as phosphorylation at threonine 231 by several other kinases, for example, CamKII, GSK-3 and cdk5 (Sengupta et al. 1998). The level of intracellular neurofibrillary tangles increases in an age-dependent manner, most likely due to increased calcium signalling in the aged brain that leads to the loss of cAMP-phosphodiesterase PDE4A (Carlyle et al. 2014). During ageing, impaired calcium signalling

results from alterations of Ca^{2+}-regulating proteins in the plasma membrane (ligand- and voltage-gated Ca^{2+} channels, ion-motive ATPases, and glucose and glutamate transporters), ER and mitochondria (Mattson 2007). The increased calcium influx across the plasma membrane was further elucidated in CA1 pyramidal neurons from young and aged rats. An additional buffer balances the increase in calcium influx in aged neurons following a small number of action potentials. However, it is overwhelmed during sustained or theta-like activity, which causes a massive increase in intracellular calcium concentration compared to young neurons (Oh et al. 2013). The misregulated calcium signalling could be one of the underlying reasons for the cognitive decline in AD patients and the underlying reason for impaired PKA signalling. PKA signalling is induced by cAMP, which is tightly controlled by adenylyl cyclase and phosphodiesterase. Increased calcium levels upregulate cAMP production by adenylyl cyclase and suppress PDE activity. Increased PKA leads to an increase of PKA mediated tau phosphorylation, which favours the formation of tau fibrils (Carlyle et al. 2014).

Another critical protein in AD disease pathology is the Aβ, which was reported in several studies to impact PKA-mediated signalling in neurons strongly. It could be shown that the pretreatment of cortical neurons with a sublethal concentration of Aβ(1-42) suppressed the phosphorylation of CREB, induced by exposure to either 30 mM KCl or 10-micron N-methyl-d-aspartate. Suppression of CREB phosphorylation affected CREB downstream targets like the expression of brain-derived neurotrophic factor (BDNF) and could contribute to the cognitive deficit in Alzheimer's disease (Tong et al. 2001). Additionally, Aβ(1-42) treatment of hippocampal neurons led to a rapid and severe impairment of mitochondrial transport, which the stimulation of PKA could rescue using Forskolin (Rui et al. 2006). Another effect of Aβ(1-42) on PKA mediated signalling was observed in cortical neurons were Aβ(1-42) treatment led to a desensitization of β(2) adrenergic receptor, which leads to decreased cAMP level. Decreased cAMP level resulted in a decline in PKA activity and, therefore, decreased phosphorylation of serine 845 on AMPA receptors, leading to decreased AMPA receptor-mediated miniature excitatory postsynaptic currents (Wang et al. 2011). Since PKA activity seems to be adversely affected by Aβ(1-42), pharmacological modulation of PKA could be considered as a putative therapeutic target. Therefore, hippocampal neurons were stimulated with rolipram, a phosphodiesterase inhibitor, and Forskolin. Both led to increased cAMP

concentration, which could compensate for the decline of CREB phosphorylation after Aβ(1-42) treatment. The observed reversal could be blocked by applying PKA inhibitor H89 (Vitolo et al. 2002). Another substance, Nobiletin that enhances PKA/CREB-dependent signalling, was also able to rescue the decreased phosphorylation level of CREB in cultured hippocampal neurons and improved learning ability in behavioural tests in a chronically Aβ(1-40) infused AD rat model (Matsuzaki et al. 2006).

6.2.6.2 Parkinson's disease

Gene mutations in the *LRRK2* gene are the underlying cause of autosomal dominant PD and a risk locus for sporadic PD (Zimprich et al. 2004). Cellular LRRK2 activity could be linked to signalling cascades, including cAMP-PKA signalling (Parisiadou et al. 2014). In LRRK2 knockout mice, abnormal morphology of dendritic spines was observed, which could be correlated with defective PKA signalling. Immunostainings of brain sections revealed mislocalization of PKA R2-β in dendritic spines leading to increased PKA-mediated phosphorylation of actin-disassembling enzyme cofilin and glutamate receptor GLUR1, resulting in abnormal synaptogenesis and synaptic transmission (Parisiadou et al. 2014). These observations indicate that LRRK2 functions as an anchoring protein for PKA regulatory subunits to control localization and signalling (Greggio et al. 2017). Mutations in the *Lrrk2* gene alter PKA signalling and contribute to the disease pathology.

Another protein associated with PD is α-synuclein, a small, highly conserved presynaptic protein involved in the SNARE complex assembly (Burré et al. 2014) and the modulation of neurotransmitter vesicle pool structure (Diao et al. 2013). Overexpression of wild-type or mutant α-synuclein in norepinephrine-producing cells in-vitro interfered with the binding of Forskolin induced phosphorylated CREB localization to CRE by competitive binding (Kim et al. 2014). This finding was supported by another study overexpressing wild-type and mutant A30P and A53T α-synuclein in SK-N-BE(2)C cells. Forskolin-induced increases in TH promoter activity and CRE-dependent transcription were significantly suppressed (Kim et al. 2011b). The CREB target genes also include growth factors such as brain-derived neurotrophic factor (BDNF), which support neuronal survival. The mRNA levels of BDNF were significantly decreased in dopaminergic neurons in the *substantia nigra* prior to neurodegeneration in

clinically and neuropathologically typical PD (Howells et al. 2000), which could be a potential reason for neurodegeneration. Furthermore, PKA signalling was shown to stimulate dopamine uptake (Liu et al. 2001) and to activate tyrosine hydroxylase, the rate-limiting enzyme in dopamine synthesis (Riederer et al. 2002). Impairments in PKA signalling likely mess up the dopaminergic homeostasis. Pharmacological studies using 6-hydroxydopamine, a neurotoxin to model PD neuronal pathology, in B65 neuronal cells led to an aberrant mislocalization of phosphorylated CREB from the nucleus to the cytosol. This led to decreased mRNA level of BDNF, supporting the concept that impaired PKA signalling contributes to PD pathology (Chalovich et al. 2006). Accumulation of phosphorylated CREB was also found in postmortem patients brain tissue in the cytoplasm of *substantia nigra* dopaminergic neurons, supporting the findings *in-vitro* (Chalovich et al. 2006). Pharmacologically treatment of PKA signalling using Rolipram, a PDE4 specific inhibitor, could significantly attenuate dopamine depletion in the striatal neurons of MPTP-treated mice by cAMP-mediated PKA signalling, which had a neuroprotective effect (Yang et al. 2008).

6.2.6.3 The implication of PKA signalling in other neurodegenerative diseases

The induction of PKA signalling is beneficial in amyotrophic lateral sclerosis (ALS), where PKA drives activity-dependent neuroprotection of motoneurons. In a transgenic mouse model of ALS, a mouse line carrying a mutated human *SOD1* gene display a phenotype similar to late-onset ALS in humans. Electrophysiological recordings from presymptomatic mice showed reduced excitatory responses due to stimulation, which could be correlated to a disrupted postsynaptic clustering of several postsynaptic scaffold proteins like Homer1b, Shank, and AMPAR subunits. This phenotype could be rescued by the intracellular application of cAMP, which activated PKA signalling (Bączyk et al. 2020).

The role of PKA signalling can be diverse in different subtypes of neurons could be demonstrated using a transgenic mouse model for Huntington's disease. R6/2 mice express mutated Huntington (mHTT) with increased CAG repeats (circa 125) within the *Huntington* gene exon 1. Severe cognitive impairments were reported in these mice in behavioural tests like Morris water maze even before the onset of motor symptoms. The underlying cause of hyperactivated PKA signalling was observed, which led to a selective hyper-phosphorylation

of some downstream targets, including NMDA receptor subunit 1, Ras-guanine nucleotide releasing factor-1 and striatal-enriched protein tyrosine phosphatase. However, others like CREB and tau were unaffected. Additionally, PDE4 was decreased, and the mice phenotype could be reproduced applying rolipram, which induced learning and memory deficits (Giralt et al. 2011). In contrast, a beneficial effect of PKA activity could be observed in the same mouse model in striatal neurons, in which PKA signalling was reported to be impaired due to proteasome impairments. The mHTT was reported to interfere with proteasomal function, which led to the selective accumulation of PKA regulatory subunits and thereby decreased PKA activity. Induction of PKA signalling via the A_{2A} adenosine receptor could rescue the impairment of the proteasomal system via phosphorylation of proteasomal component Rpt6 (Lin et al. 2013b).

6.2.7 Treatment options targeting PKA signalling

The cAMP/PKA signalling pathway is involved in a wide variety of cellular processes from metabolism to ion channel activation, cell growth and differentiation, gene expression and apoptosis and disturbances in cAMP-mediated signalling have been implicated in several diseases, for example, AD, PD, HD, ALS (see above) and neuropsychiatric disorders like depressive disorder (Shelton et al. 1996) and tardive dyskinesia (Sasaki et al. 1995). Therefore, PKA appears as an exciting candidate for drug-induced therapy. Potential drug components are designed to modulate intracellular cAMP levels or interfere with PKA localization targeting AKAPs. One of the best-investigated substances is Rolipram, a PDE4 inhibitor. Inhibition of PDE4 leads to a rise in intracellular cAMP levels and showed beneficial effects in *in-vitro* and *in-vivo* studies in rodents mimicking neurodegenerative conditions (see above). Based on these observations, clinical trials were initiated for drug discovery and development. It was used in studies with patients meeting the DSM-III criteria for major depression as an antidepressant but could not prevail against the conventional treatment with amitriptyline, and the patients reported nausea as a side effect (Scott et al. 1991). In another study with depressive patients, the treatment with Rolipram showed efficient treatment in half of the patients (Zeller et al. 1984), and another study even reported better tolerance of Rolipram (Fleischhacker et al. 1992). In another study with multiple sclerosis patients, Rolipram was

tested as an anti-inflammatory drug, but could not be reported to decrease inflammatory events and was poorly tolerated by the patients due to side effects like severe insomnia, gastroesophageal reflux and balance changes, which led to premature termination of the study (Bielekova et al. 2009). Until today Rolipram never reached the drug market due to the reported side effects, including headache, gastric hyper secretion and emesis (nausea and even vomiting) (Prickaerts et al. 2017). Other studies using different phosphodiesterase inhibitors, such as Vinpocetine (PDE1 Inhibitor) and Cilostazol (PDE3), were performed in patients with AD with varying success. Vinpocetine showed promising results in healthy patients during early clinical trials (Subhan and Hindmarch 1985) but did not improve disease symptoms in patients (Thal et al. 1989; Szatmari and Whitehouse 2003). In contrast, Cilostazol seemed to increase cognitive function in AD patients (Tai et al. 2017; Arai and Takahashi 2009). Until today, the targeting of several phosphodiesterases for clinical treatment is ongoing. The challenge is to selectively target the isoform mainly expressed in the affected tissue to minimize side effects (for a detailed overview of ongoing studies, see (Prickaerts et al. 2017)). Another approach for drug development is the control of PKA signalling localization targeting AKAPs. AKAPs create spatially constrained signalling microdomains, and since there are numerous AKAPs, all of them under tight spatial and temporal control, the modulation of PKA signalling can be done for specific cellular compartments. To prevent the binding of AKAPs to PKA regulatory subunit isoforms, the disruptors need to bind to the AKAP helix with high affinity and recognize the unique structural features of one AKAP helix preferentially (Nygren and Scott 2015). However, studies focusing on identifying such small AKAP disruptors (Gold et al. 2013; Christian et al. 2011) are still in formative stages and are far from being tested in patients.

6.2.8 PKA and the maintenance of cellular homeostasis

Next to protein synthesis during long-LTP, PKA plays a role in maintaining cellular homeostasis phosphorylating proteins of the autophagy machinery and the ubiquitin-proteasome system (UPS) (Hershko et al. 2000) to regulate and modulate protein biogenesis and turnover. The UPS is a large multicomplex protein that requires ATP to exert its proteolytic activity. It degrades misfolded proteins that are marked for degradation by ubiquitin. The proteasome also referred to as 26S proteasome, is composed of a barrel-like core complex termed the 20S,

involved in the proteolysis of proteins. Two regulatory complexes termed 19S complexes cap each site of the 20S. The 19S complex binds the ubiquitinated substrate, removes the ubiquitin chain, unfolds the protein substrate, and translocates it through a narrow gated channel into the channel of the 20S particle, where the proteins become digested (Finley 2009). PKA can modulate the UPS degradation via phosphorylation of 26S proteasomes on Rpn6/PSMD11 (Lokireddy et al. 2015). The phosphorylation of the 26S proteasome increases proteasomal degradation and thus the breakdown of misfolded proteins, which could be shown in several *in-vitro* systems (myoblasts, cardiomyocytes, neuroblastoma cells and primary rat spinal cord neurons) (Myeku et al. 2012; Lokireddy et al. 2015). Additionally, PKA maintains cellular homeostasis modulating protein degradation via autophagy. As described above, the principal regulator of autophagy is mTORC1 that phosphorylates ULK1 and thereby hinders the induction of autophagy. During starvation, the mTORC1 mediated phosphorylation of ULK1 decays and autophagy gets initiated and degrades harmful cellular components. However, PKA-mediated phosphorylation depends on cell growth, nutrients, and stress (Torres-Quiroz et al. 2015). A proteomic approach performed in *Saccharomyces cerevisiae* showed that key regulator protein ATG1 (in mammals ULK1/ ULK2) was controlled by PKA phosphorylation *in-vitro* (Budovskaya et al. 2005). In another study, it could be demonstrated that in addition to ATG1 also ATG13, a conserved regulator of ATG1 kinase activity, can be directly phosphorylated by PKA (Stephan et al. 2009). Inhibiting PKA activity by downregulating cAMP levels was enough to induce autophagy (Stephan et al. 2009), whereas the induction of PKA signalling had been shown to inhibit autophagy (Budovskaya et al. 2004). Recently, it was shown that PKA is a regulator of autophagy induction and a selective target of autophagy. Using autophagy-deficient knockout (*ATG7*flox:*Syn*-Cre, *ATG14*flox:*Syn*-Cre) mice brain lysates, the protein level of PKA R1-α were selectively upregulated. In contrast, the protein level of PKA R2-α remained unchanged. Furthermore, it could be shown that AKAP11 binds to LC3 via the LIR motif domain, functioning as an autophagy receptor for PKA R1-α, recruiting PKA R1-α to the growing autophagophore in non-neuronal cells. The selective degradation of the PKA R1-α subunits could decrease PKA signalling and subsequently increase autophagy during glucose starvation in HEK cells (Deng et al. 2021).

7. Aim of study

Loss of autophagy in murine neurons does not induce their cell loss (Komatsu et al. 2007b; McMahon et al. 2012; Hernandez et al. 2012; Lieberman et al. 2020; Negrete-Hurtado, Overhoff et al. 2020), although these mouse models are characterized by autism spectrum disorder-like behavioural deficits (Hui et al. 2019) and reveal impairments in synaptic plasticity, learning and memory formation (Hernandez et al. 2012; Negrete-Hurtado, Overhoff et al. 2020). These phenotypes are also accompanied by increased excitability of autophagy-deficient neurons (Lieberman et al. 2020; McMahon et al. 2012; Kuijpers et al. 2021; Hui et al. 2019). These published data raise a hypothesis that autophagy might fulfil additional survival-independent roles in postmitotic brain cells, i.e. neurons. Furthermore, recently published data from our lab (Negrete-Hurtado, Overhoff et al. 2020) and another study (McMahon et al. 2012) identified the appearance of seizures in mice lacking ATG5 and/or ATG7 in excitatory forebrain neurons, whereas the absence of seizures was reported in mice lacking ATG7 in inhibitory forebrain neurons (Hui et al. 2019). Since the difference in brain excitability in mice with conditional autophagy deletion in either excitatory or inhibitory neurons could be a result of the differential role of autophagy in these two neuronal subclasses, the following central question was asked:

"Does autophagy regulate brain excitability independently of its role in cell survival, and is this function of autophagy different in excitatory and inhibitory neurons?"

Two conditional autophagy-deficient mouse lines lacking crucial autophagy protein ATG5 in forebrain inhibitory (*Atg5*flox:*VGAT*-Cre) or excitatory (*Atg5*flox:*CamKIIα*-Cre) neurons were investigated by a combination of SILAC and label-free quantitative proteomics, high-content screening microscopy, and live-cell imaging approaches to achieve three specific goals that would answer the central question:

1. What is the phenotype of neuronal subtype-confined autophagy-deficient mice?
2. Are there differences in autophagic cargo degraded in excitatory and inhibitory neurons?
3. Are defects in neuronal excitability in autophagy-deficient mice a result of an accumulation of cargo-specific proteins?

8. Results

8.1 ATG5 deficiency in excitatory and inhibitory neurons results in differential excitability phenotype.

To elucidate how autophagy contributes to neuronal function, two mouse lines lack crucial autophagy component ATG5 either in forebrain excitatory (*Atg5*flox:*CamKIIα*-Cre mice) or inhibitory (*Atg5*flox:*VGAT*-Cre) neurons were used. The *Atg5*flox:*CamKIIα*-Cre mice, which was already described in another study (Negrete-Hurtado, Overhoff et al. 2020), shows a significant decrease of ATG5 in cortical brain lysates (Fig. 5A) and a strong increase of autophagy receptor p62 that is known to accumulate under autophagy-deficient conditions (Fig. 5B) (Komatsu et al. 2007a). The protein level of LC3 shows a decrease of LC3II isoform, confirming a block in the autophagosomal flux (Fig. 5C). The lack of ATG5 was also detectable in striatal brain lysates of *Atg5*flox:*VGAT*-Cre KO mice (Fig. 5D), which was accompanied by an increase of p62 protein level (Fig. 5E) and decreased level of LC3II isoform (Fig. 5F). Both mouse lines showed a cessation of weight gain in KO mice at about one month of age compared to their WT littermates (Fig. 5G,H). In line with other papers that did not observe neurodegeneration in neuronal subtype confined autophagy-deficient mice (Komatsu et al. 2007b; McMahon et al. 2012; Hernandez et al. 2012), *Atg5*flox:*CamKIIα*-Cre and *Atg5*flox:*VGAT*-Cre KO mice did not show signs of neurodegeneration in Nissl staining's of affected brain areas (Fig. 5I,J).

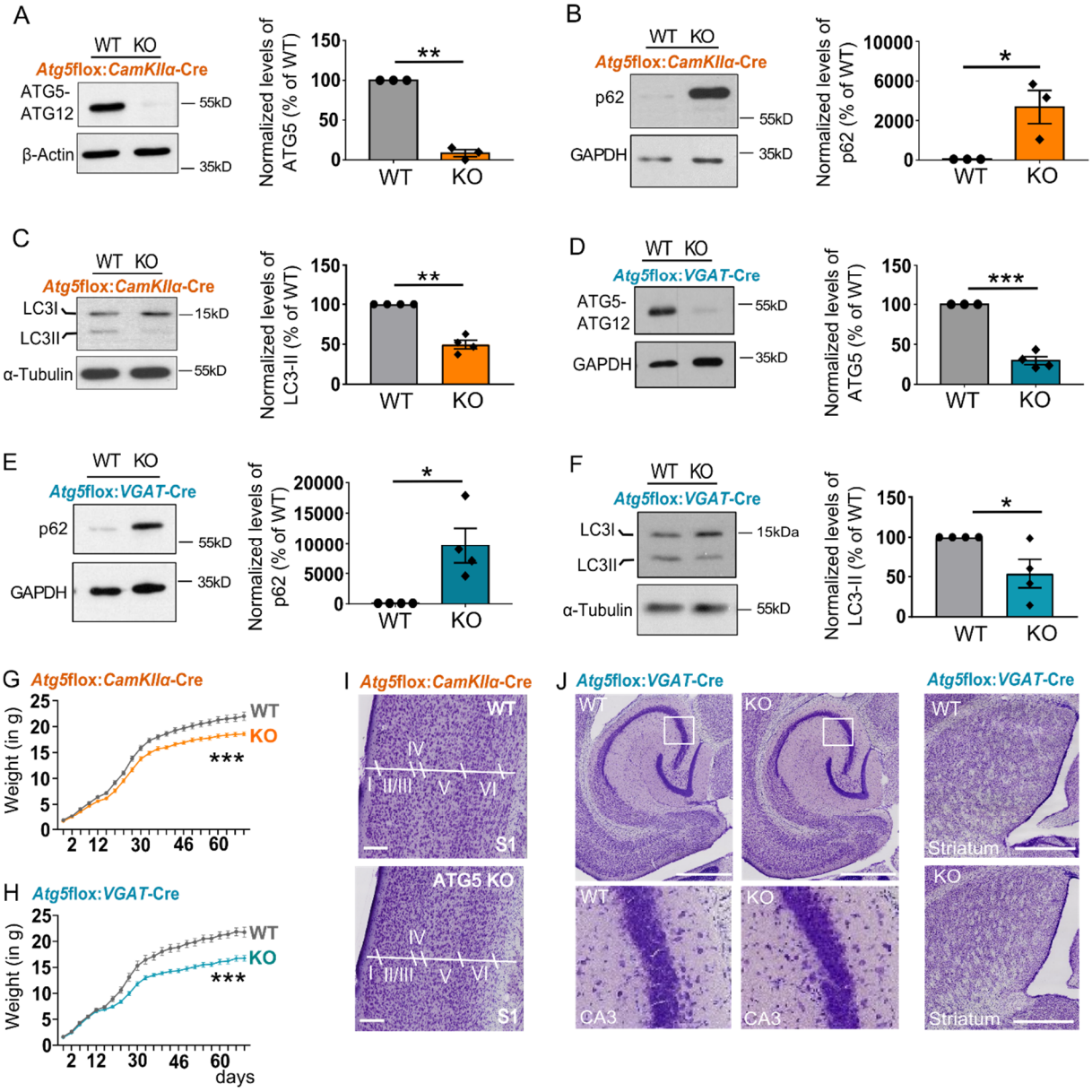

Figure 5: Lack of neurodegeneration in excitatory or inhibitory autophagy-deficient forebrain neurons.

(A) Protein levels of ATG5 are significantly decreased in cortical brain lysates of 13-weeks old *Atg5*flox:*CamKIIα*-Cre KO mice (WT set to 100%, KO: 14.22± 4.80%). p<0.0001, n=4. Performed one-tailed unpaired t-test. **(B)** Autophagy receptor p62 were significantly increased in *Atg5*flox:*CamKIIα*-Cre KO brains (WT set to 100%, KO: 6697± 2105%). p=0.0175; n=3. Performed one-tailed unpaired t-test. **(C)** LC3 lipidation is defective in *Atg5*flox:*CamKIIα*-Cre KO brains (WT set to 100%, KO: 49.73± 5.34%). p=0.0026; n=4. Performed one-tailed unpaired t-test. **(D)** Protein levels of ATG5 are significantly decreased in striatal brain lysates of 13-weeks old *Atg5*flox:*VGAT*-Cre KO mice (WT set to 100%, KO: 29.70± 5.043%). p<0.0001; n=4. Performed one-tailed unpaired t-test. **(E)** Autophagy receptor protein p62 was significantly increased in striatal lysates of autophagy-deficient *Atg5*flox:*VGAT*-Cre KO mice (WT set to 100%, KO: 2956± 839.3%). p=0.0072, n=4. Performed one-tailed unpaired t-test. **(F)** The reduced protein level of lipidated LC3 (LC3II) demonstrates autophagic flux blockage in autophagy-deficient *Atg5*flox:*VGAT*-Cre mice (WT set to 100%, KO: 53.69± 17.69%). p=0.0199; n=4. Performed one-tailed

unpaired t-test. **(G)** *Atg5*flox:*CamKIIα*-Cre and *Atg5*flox:*VGAT*-Cre KO mice present a lean phenotype compared to WT littermates, starting after weaning (at 2 months of age; WT: 21.3± 0.68 g; $KO_{CamKII\alpha\text{-}Cre}$: 18.2± 0.35 g; p=0.000115, n_{WT}=18, $n_{KO\ CamKII\alpha\text{-}Cre}$=17. WT: 20.6± 0.68 g; $KO_{VGAT\text{-}Cre}$: 15.6± 0.43 g; p=<0.0001, n_{WT}=18, $n_{KO\ VGAT\text{-}Cre}$=20.) Performed unpaired t-test for each time point. **(I)** Representative (from n=3 couples) nissl staining of 40 µM thick horizontal brain slices revealed no signs of neurodegeneration in the cortex of 12-weeks old *Atg5*flox:*CamKIIα*-Cre KO mice. Scale bar 300 µm. **(J)** Representative (from n=3 couples) nissl staining of 40 µM horizontal brain slices revealed no overt alteration of the morphology and the number of neurons in 12-weeks old *Atg5*flox:*VGAT*-Cre mice neither in the hippocampus (H-I) nor striatum (J). White rectangular boxes depict the zoom area shown in the panel below. Scale bars: 200µm.

Even though ATG5 was equally dispensable for the survival of excitatory and inhibitory neurons, the conditional loss of autophagy caused some phenotypical differences between *Atg5*flox:*CamKIIα*-Cre and *Atg5*flox:*VGAT*-Cre mice. A primary screen test, a basic test to determine behavioural or motoric changes in mice, called SHIRPA analysis, was performed to observe differences in the presenting phenotype (Rogers et al. 1997). Whereas *Atg5*flox:*CamKIIα*-Cre were unaffected in their ability to explore the environment (Fig. 6A), *Atg5*flox:*VGAT*-Cre animals were less likely to exhibit a spontaneous rearing behaviour in the open field when compared to their control littermates (Fig. 6B), whereas the total locomotor activity (freely voluntary movement, number of passed squares in the arena over a specific time) was unaltered in both conditional mice lines (Fig. 6C,D). The rearing, defined as standing on both hind paws in a vertical upright posture, is considered exploratory behaviour and has been used as a read-out for changes in anxiety behaviour in several studies (Ennaceur 2014). Since decreased rearing in mice is associated with increased anxiety, which can potentiate the startle reflex, both mouse lines were subjected to a loud noise presentation, and the startle response was measured. ATG5-deficient mice from both lines responded with a significantly potentiated startle reflex to stimulus presentation (Fig. 6E,F). Furthermore, *Atg5*flox:*CamKIIα*-Cre revealed epileptic seizures appearance at the age of 10 weeks in homozygous and at 22 weeks of age in heterozygous mice. Interestingly, seizures were also present in a small percentage of animals with decreased levels of ATG5 in GABAergic neurons, but their onset was significantly later (>10 months of age) and a minimal number of affected animals (Fig. 6G). Seizure activity can be either a result of intrinsic neuronal hyperexcitability or be a cause of neuronal network re-organization due to neurodegeneration. The differential effect on the

appearance of seizures in mice with autophagy-deficiency either in excitatory or inhibitory neurons combined with the absence of neurodegeneration in these animals (Fig. 5) suggests that ATG5 functions in two classes of neurons to intrinsically regulate their excitability. The appearance of spontaneous recurrent seizures was also reported in another study using *Atg7*flox:*CamKII*α-Cre at 20-weeks of age (McMahon et al. 2012). The appearance of seizures was coming along with a reduced life span of conditional KO mice lacking autophagy in excitatory neurons (McMahon et al. 2012; Negrete-Hurtado, Overhoff et al. 2020).

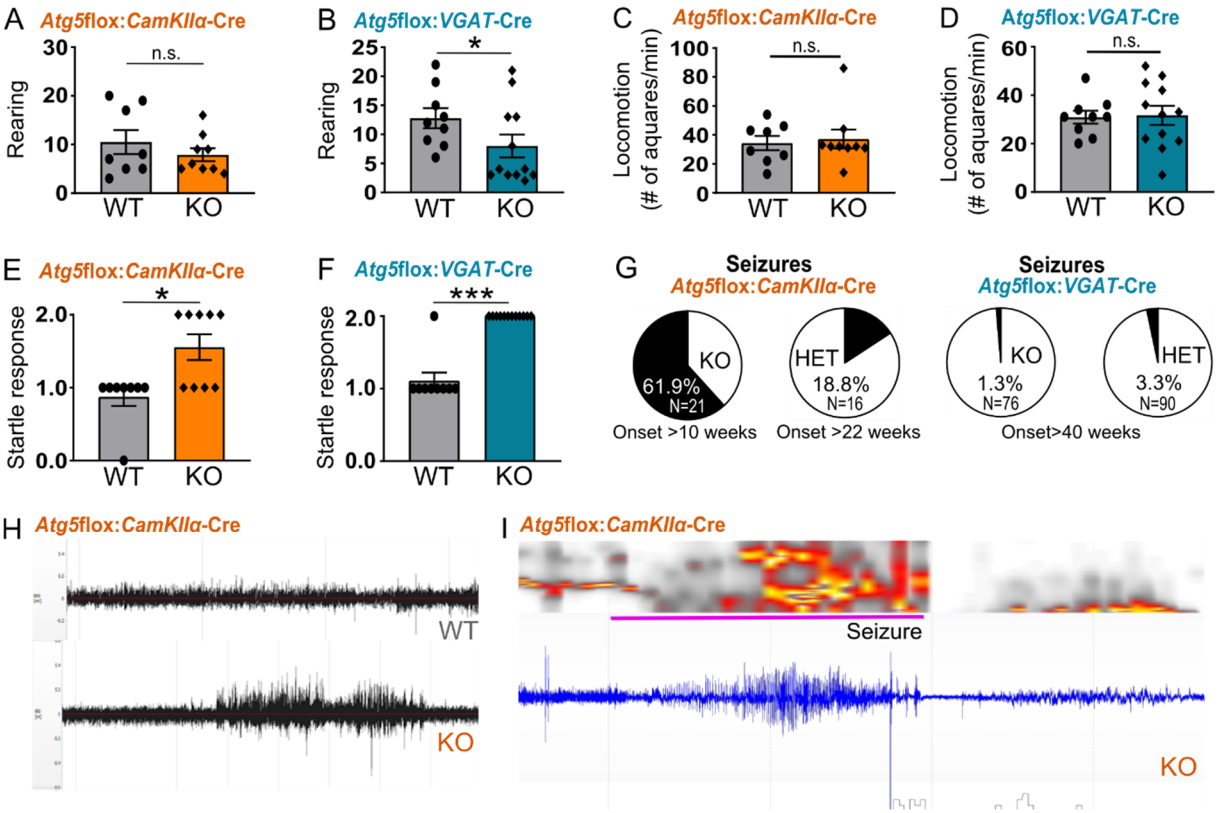

Figure 6: ATG5 deficiency in excitatory and inhibitory neurons results in differential behavioural phenotypes with the appearance of seizures mainly in mice lacking ATG5 in excitatory neurons.

(A) SHIRPA analysis, a basic test, detecting phenotypic differences in mice, did not show alterations in the rearing behaviour of 12-weeks old *Atg5*flox:*CamKII*α-Cre KO mice (WT: 10.50± 2.464, KO: 7.889± 1.338, n_{WT}=8, n_{KO}=9). Performed a two-tailed unpaired t-test. **(B)** In contrast, 12-weeks old *Atg5*flox:*VGAT*-Cre KO mice showed a decreased rearing behaviour/ explorative behaviour (WT: 12.78± 1.730, KO: 6.818± 1.715, p=0.0262, n_{WT}=9, n_{KO}=11). Performed a two-tailed unpaired t-test. **(C,D)** Alterations in locomotion, tracked by the number of passed squares per time of freely moving mice, could not be detected in *Atg5*flox:*CamKII*α-Cre KO mice (WT: 34.38± 4.931, $KO_{CamKIIα\text{-}Cre}$: 37.22± 6.606; n_{WT}=8, n_{KO}=9) as well as *Atg5*flox:*VGAT*-Cre KO mice compared to WT (WT: 30.89± 2.679, $KO_{VGAT\text{-}Cre}$: 31.67± 3.938; n_{WT}=9, n_{KO}=12). Performed a two-tailed unpaired t-test for each

dataset. **(E,F)** An increased startle response (reaction to a loud spontaneous noise) could be detected during SHIRPA analysis in *Atg5*flox:*CamKII*α-Cre KO mice ($p=0.0204$, $n_{WT}=9$, $n_{KO}= 11$) as well as *Atg5*flox:*VGAT*-Cre KO mice ($p<0.0001$, $n_{WT}=9$, $n_{KO}=12$). Performed a two-tailed unpaired Mann-Whitney test for each dataset. **(G)** Percentage of KO and heterozygous mice developing seizures during their lifespan lacking autophagy protein ATG5 in a different subtype of neurons (the animal number, age of seizure onset and percentage of affected animals is indicated in the graph). **(H)** Example electrocorticogram traces from *Atg5*flox:*CamKII*α-Cre mice display increased hippocampal and cortical neuronal activity in ATG5 knockout mice. **(I)** Example electrocorticogram trace from a seizure measured in *Atg5*flox:*CamKII*α-Cre KO mice.

8.2 PKA regulatory subunits 1-α and 1-β are among the highest upregulated proteins in autophagy-deficient excitatory and inhibitory neurons.

What is the mechanism by which ATG5 upregulates neuronal excitability of neurons? A recent study using mice lacking ATG5 in cortical (pallial) progenitors suggested that ATG5 regulates neurotransmission by selective degradation of presynaptic tubular ER components (Kuijpers et al. 2021), whereas another study proposed that autophagy regulates neuronal excitability by governing the degradation of damaged synaptic vesicle proteins (Hoffmann et al. 2019). To reveal whether the changes in axonal ER components and/or bulk synaptic proteome are reflected in brains conditionally lacking ATG5 in either excitatory or inhibitory neurons, quantitative proteomics studies were conducted. Global proteomic profiling of conditional ATG5 KO mice was performed using spike-in heavy isotope labelled brain lysate (SILAC) as a reference into brain lysates of control mice or mice lacking ATG5 in either excitatory (*Atg5flox:CamKII*α-Cre, cortex) or inhibitory neurons (*Atg5*flox:*VGAT*-Cre, striatum) (Fig. 7A). In fact, except for known autophagy receptors such as GABARAPL2 and p62 (SQSTM1), only a few proteins were highly upregulated ($p<0.05$, fold-change (FC)>2) in brains of mice with autophagy deficiency either in excitatory or inhibitory neurons (Fig. 7B,C). Interestingly, in striatal lysates of *Atg5*flox:*VGAT*-Cre KO mice, recently identified reticulophagy receptors TEX264 (An et al. 2019) and SEC62 (Chino et al. 2019) were among the highest upregulated proteins, implicating this type of autophagy in maintaining the physiology of inhibitory neurons. Intriguingly, in both types of autophagy-deficient neurons, regulatory subunits of PKA holoenzyme R1-α (PRKAR1a) and R1-β (PRKAR1b) were among the most significantly upregulated proteins. In agreement with Kuijpers et al. (2021), most synaptic proteins were unchanged in brains lacking ATG5 either in excitatory or inhibitory neurons, except Bassoon

and Piccolo, whose protein levels were slightly decreased in global proteomic analysis (Fig. 7D,E).

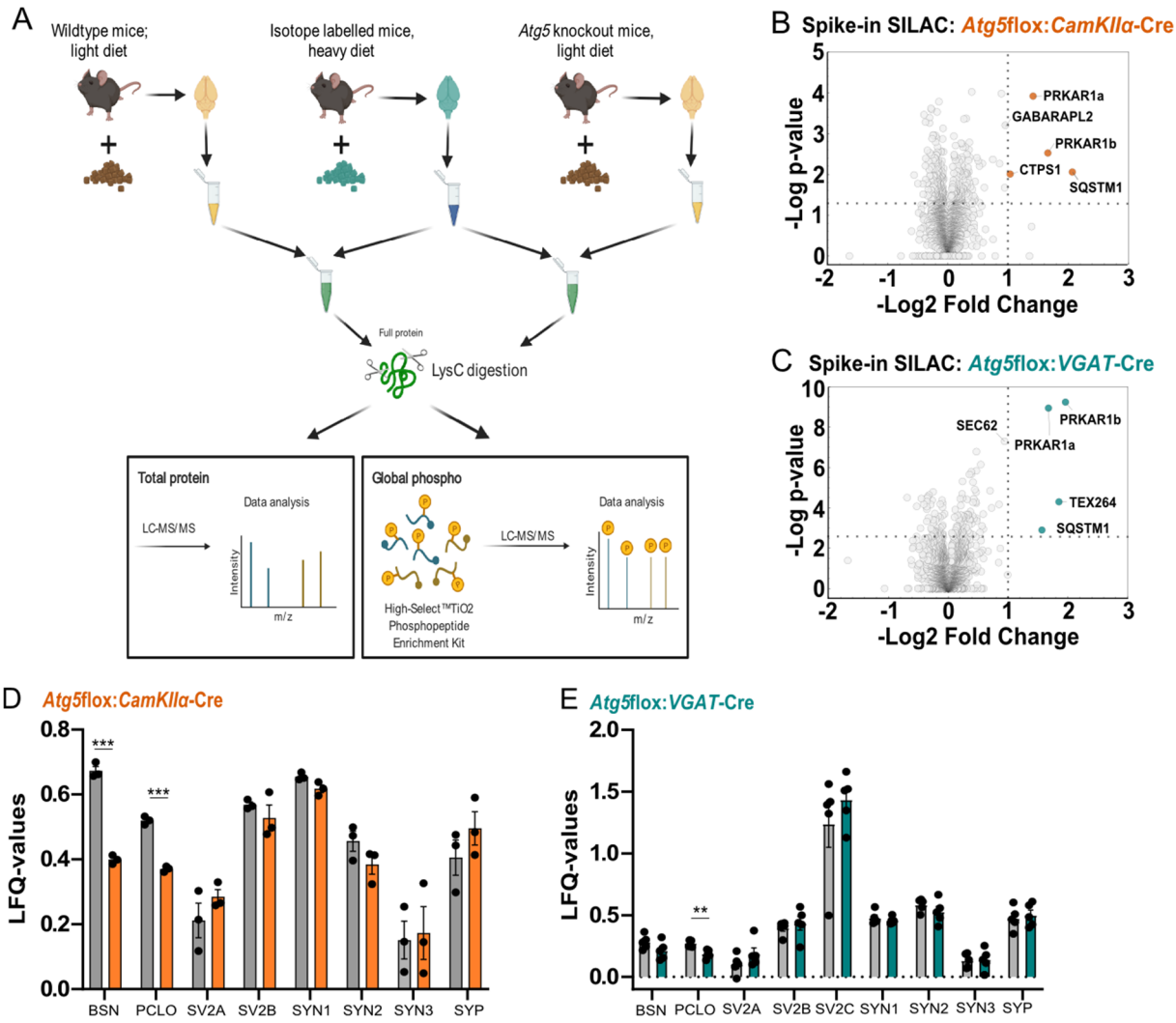

Figure 7: SILAC-based proteomic analysis identifies PKA regulatory subunits 1-α and 1-β as potential autophagic cargo in autophagy-deficient brains in-vivo.

(A) Schematic illustration of performed spike-in analysis. Brain regions of interest from *Atg5*flox:*CamKIIα*-Cre, *Atg5*flox:*VGAT*-Cre and isotope-labelled spike-in mice were dissected and homogenized. Unlabelled and isotope labelled brain lysates were mixed in a 1:1 ratio, and proteins were digested into peptides using LysC. Part of the samples was forwarded to total proteome analysis, whereas most were processed to acquire the global phosphoproteome. The illustration was done using BioRender (Agreement number: RF238L00IB) **(B-C)** Volcano plots of proteome changes in the cortex of *Atg5*flox:*CamKIIα*-Cre (B) and striatum of *Atg5*flox:*VGAT*-Cre (C) identified using isotope labelled mouse-based proteomic analysis ($n_{Atg5flox:CamKII\alpha\text{-}Cre}$=3, $n_{Atg5flox:VGAT\text{-}Cre}$=5 mice per genotype). Highlighted are the identified proteins with a $p<0.05$ and a FC>2 (log2 FC>1). **(D-E)** LFQ values of the global proteome analysis reveal no changes on the protein level of most synaptic proteins, except Bassoon that is significantly decreased in *Atg5*flox:*CamKIIα*-Cre KO mice and Piccolo that is decreased in autophagy-deficient

mice of both lines (*Atg5*flox:*CamKIIα*-Cre KO: WT_{BSN}: 0.6730± 0.01357, KO_{BSN}: 0.3994± 0.0008042, p<0.0001; WT_{PCLO}: 0.5199± 0.007423, KO_{PCLO}: 0.3703± 0.005192, p <0.0001; n=3; *Atg5*flox:*VGAT*-Cre: WT_{PCLO}: 0.2739± 0.01210, KO_{PCLO}: 0.1858± 0.01552, p=0.0021; n=5). Performed a two-tailed unpaired t-test between WT and KO for each protein separately.

To understand whether changes in levels of PKA R1-α and R1-β represent a cell-autonomous role of autophagy in neurons, a fluorescence-activated cell sorting (FACS)–based strategy to perform label-free proteomic analysis on WT and ATG5 KO neurons isolated from brains of 3/4-weeks-old *Atg5*flox:*CamKIIα*-Cre and *Atg5*flox:*VGAT*-Cre reporter mouse lines carrying tdTomato allele was developed (Fig. 8A,B). Proteomic analysis of FACS-sorted neurons identified significantly more dysregulated proteins in both classes of autophagy-deficient neurons compared to the SILAC-based approach. A significant decrease of ATG5 protein levels in FACS-sorted *Atg5*flox:*CamKIIα*-Cre:tdTomato$^+$ KO neurons were observed (Fig. 8C), and its complete loss in neurons isolated from *Atg5*flox:*VGAT*-Cre:tdTomato$^+$ KO mice (Fig. 8D), reflecting the reliability of the used FACS-sorting protocol. In agreement with the data from SILAC-based proteomics, R1-α and R1-β were among significantly upregulated proteins in FACS-sorted autophagy-deficient neurons. This upregulation was less robust in autophagy-deficient excitatory neurons, likely reflecting their confinement to peripheral synaptic processes (see Fig. 13), which are absent in the FACS-based proteomics approach. Although among significantly upregulated proteins (p<0.05, log2 FC>0.5,), a few presynaptic (RIMS2, CPLX1, HAP1 and SYP) and postsynaptic proteins (GRIA1, CNIH2, GRIA4, TANC2, GRID2IP, DAGLB) were detected (Fig. 8F), the majority of neuronal autophagy cargo was associated with the molecular function in nucleic acid (DNA and RNA) and enzyme binding (Fig. 8G). Interestingly, in GO cellular component and GO molecular function analysis, the PKA-associated pathway was among the highest enriched gene ontology terms in autophagy-deficient excitatory and inhibitory neurons (Fig. 8E-I). As described above, cAMP-dependent protein kinase (PKA) is essential in the regulation of neuronal and network activities, where PKA takes a major role in the regulation of AMPA and NMDA glutamate receptor and sodium channels activity at synapses (Abel and Nguyen 2008; Roche et al. 1996; Man et al. 2007). This established role of PKA in the regulation of synaptic function together with our findings indicating strong upregulation in the levels of inhibitory R1-α and R1-β subunits of PKA

complex in autophagy-deficient neurons suggest a scenario where autophagy might control neuronal excitation by the regulation of PKA signalling.

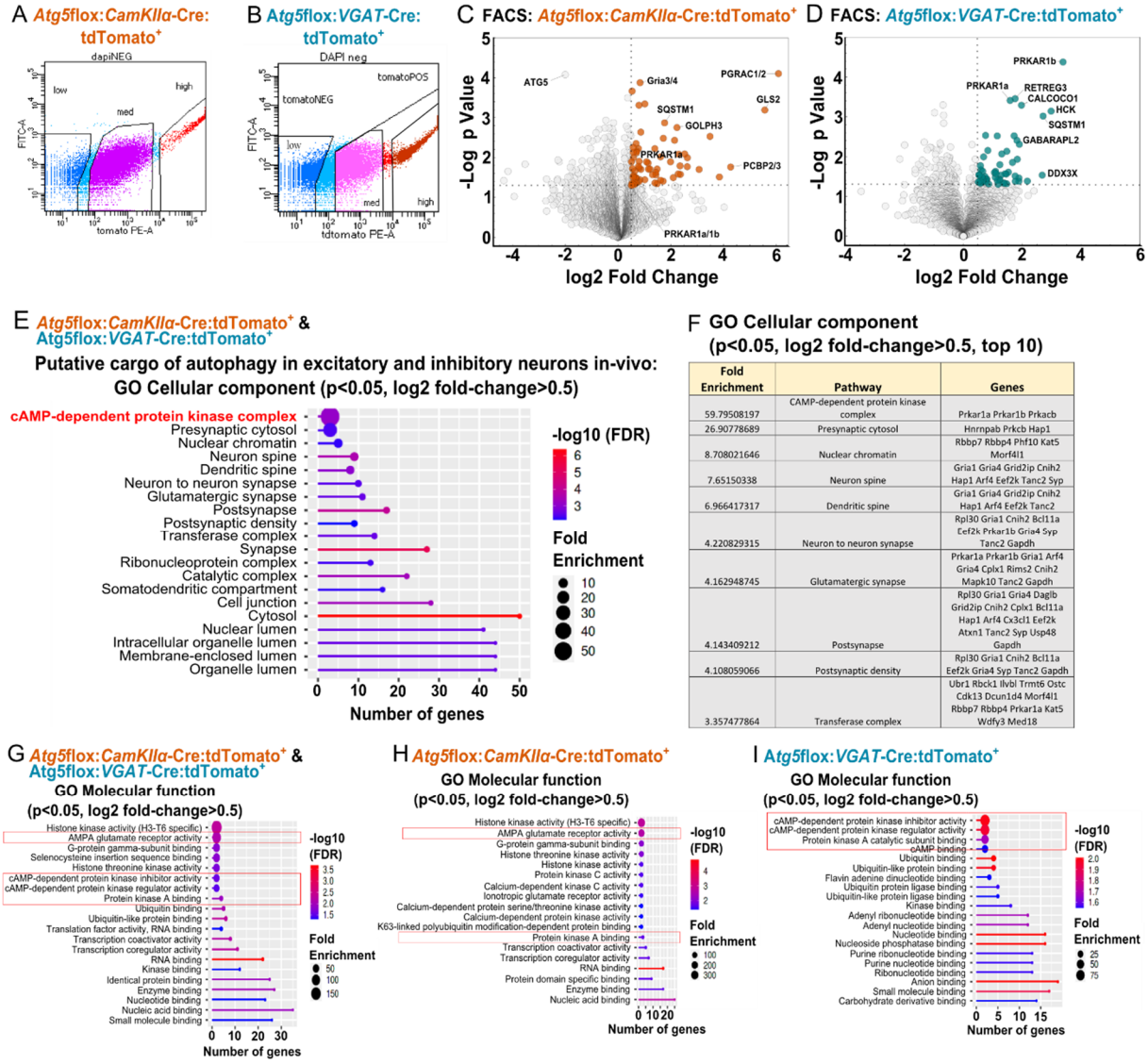

Figure 8: PKA-associated pathway is among the highest enriched gene ontology terms in autophagy-deficient excitatory and inhibitory neurons.

(A-B) Exemplary illustration of *Atg5*flox:*CamKIIα*-Cre:tdTomato$^+$ (A) and *Atg5*flox:*VGAT*-Cre:tdTomato$^+$ (B) fluorescence-based cell sorting (FACS). The cells were categorized into three populations depending on their tdTomato fluorescence intensity expression. The cells labelled with low did not express tdTomato, and the scatter was set with the help of an in parallel processed brain sample without tdTomato expression. The cell population expressing tdTomato was divided into middle and highly tdTomato positive cells based on fluorescence intensity. The populations of highly tdTomato positive cells were used for downstream experiments. **(C-D)** Label-free proteomic analysis of FACS-sorted neurons from *Atg5*flox:*CamKII*α-Cre:tdTomato$^+$ and *Atg5*flox:*VGAT*-Cre:tdTomato$^+$ mice confirmed the selective upregulation of the PKA R1-α and R1-β ($n_{Atg5flox:CamKII\alpha\text{-}Cre:tdTomato+}$=4, $n_{Atg5flox:VGAT\text{-}Cre:tdTomato+}$= 5 mice per genotype). Highlighted in the volcano blot are enriched proteins forwarded to GO Cellular component analysis (p<0.05 and log2 FC>0.5) **(E)** GO Cellular

component analysis of upregulated proteins (cut-off p<0.05, log2 FC>0.5) detected in proteomic approaches of FACS sorted neurons from both lines shows strong enrichment of proteins from the cAMP-dependent protein kinase complex. ShinyGO v0.741 platform was used for analysis and illustration. **(F)** Numeric overview about the data shown in (E). Displayed are the top 10 pathways and the detected, corresponding genes that are misregulated in autophagy-deficient neurons *in-vivo*. **(G)** GO molecular function analysis of significantly upregulated proteins detected in FACS sorted neurons of *Atg5*flox:*CamKIIα*-Cre:tdTomato^{+} and *Atg5*flox:*VGAT*-Cre:tdTomato^{+} mice brain tissue. **(H,I)** GO molecular function analysis performed on single datasets of *Atg5*flox:*CamKIIα*-Cre:tdTomato^{+} (H) and *Atg5*flox:*VGAT*-Cre:tdTomato^{+} (I) mice show that cargo selection of autophagy differs slightly between neuronal subtypes.

8.3 Neuronal autophagy selectively regulates the levels of type 1 PKA inhibitory subunits, which are confined to synapses and mitochondria

The data described above suggest that autophagy regulates the levels of regulatory subunits of PKA holoenzyme R1-α and R1-β in excitatory and inhibitory neurons. To further test this hypothesis, the results from the proteomic studies were confined by western blotting. The levels of R1-α and R1-β were robustly upregulated in the cortex and hippocampus of 12/13-week-old *Atg5*flox:*CamKIIα*-Cre KO mice (Fig. 9A-D), as well as in the striatum, cortex and cerebellum of 12/13-week-old *Atg5*flox:*VGAT*-Cre KO mice (Fig. 9E-H), indicating that autophagy regulates levels of the regulatory subunits of PKA holoenzyme across different brain regions.

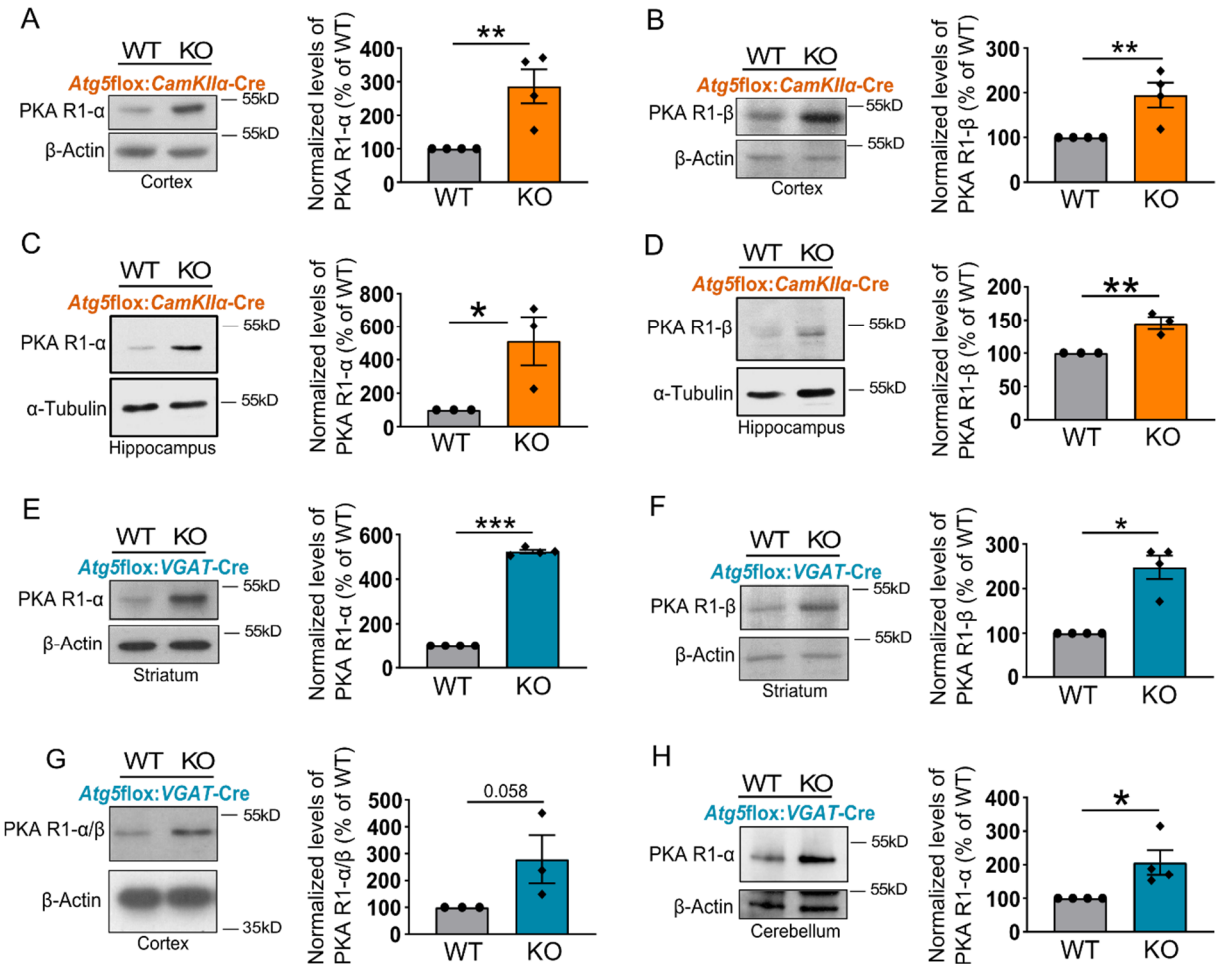

Figure 9: PKA regulatory subunits 1-α and 1-β are robustly upregulated in autophagy-deficient brains.

(A,B) The protein level of PKA R1-α (KO: 286.1± 50.53%; p=0.0051, n=4) and PKA R1-β ((KO: 194.7± 27.82%; p=0.0072, n=4) were significantly increased in cortical brain lysates from 12/13-weeks old *Atg5*flox:*CamKII*α-Cre knockout mice compared to WT. **(C,D)** Significant upregulation of PKA R1-α (KO: 513.1± 146.8%; p=0.0241, n=3) and PKA R1-β (KO: 145.3± 9.578%; p= 0.0046, n=3) protein level were also detected in hippocampal brain lysates from 12/13-weeks old *Atg5*flox:*CamKII*α-Cre knockout mice compared to WT. **(E,F)** The protein level of PKA R1-α (KO: 524.1± 8.346%; p<0.0001, n=4) and PKA R1-β (KO: 247.9± 26.26%, p=0.0007; n=4) were significantly increased in striatal brain lysates from 12/13-weeks old *Atg5*flox:*VGAT* mice knockout mice compared to WT. **(G)** Cortical lysates of *Atg5*flox:*VGAT*-Cre mice showed increased PKA R1-α/β protein level in KO compared to WT (KO: 278.9± 89.7%; p= 0.0584, n=3). **(H)** Significantly upregulated protein levels of PKA R1-α were detected in cerebellar brain lysates of *Atg5*flox:*VGAT*-Cre KO mice (KO: 206.6± 36.70%). p=0.0136, n=4. Representative immunoblot examples are shown for WT and KO lysates; the number of animals is indicated for each experiment. The WT was set to 100% for all Western blots, and a one-tailed unpaired t-test was performed for analysis.

In mammals, four inhibitory, regulatory subunit (R1-α, R1-β, R2-α, and R2-β) have been identified, comprising the type 1 or the type 2 PKA isozymes, respectively (see above). Since all regulatory subunits are ubiquitously expressed in the brain, R2-α and R2-β protein levels in brain lysates of autophagy-deficient mice were assessed to investigate if autophagy functions to regulate type 1 PKA signalling selectively. The levels of R2-α and R2-β were neither altered in cortical brain lysates of *Atg5*flox:*CamKIIα*-Cre KO mice (Fig. 10A,B) nor in striatal brain lysates of *Atg5*flox:*VGAT*-Cre KO mice (Fig. 10E). ATG5 was also dispensable for regulating levels of catalytic PKA-Cα subunits in cortical and hippocampal brain lysates of *Atg5*flox:*CamKIIα*-Cre KO mice (Fig. 10C,D) as well as in striatal and cerebellar brain lysates of *Atg5*flox:*VGAT*-Cre KO mice (Fig. 10F,G).

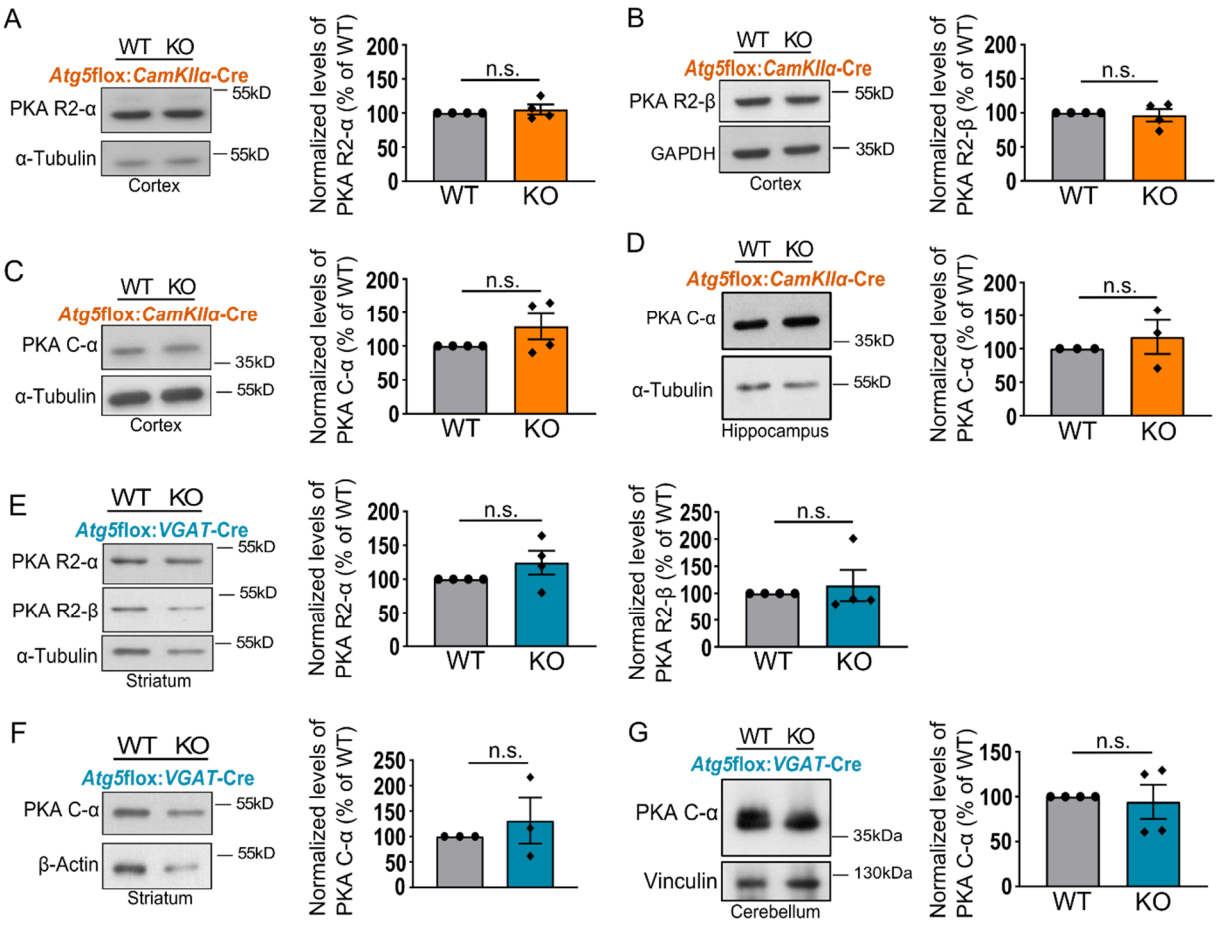

Figure 10: Neuronal autophagy loss induces selective upregulation of protein levels of PKA regulatory subunits type 1 and does not affect PKA R2-α, R2-β or the catalytic subunits C-α.

(A) Protein upregulation was selective for regulatory subunits type 1 since the levels of PKA R2-α are unchanged in cortical brain lysates of autophagy-deficient *Atg5flox*:*CamKIIα*-Cre KO mice (KO: 105.3± 7.399%). n=4. **(B)** Also, PKA R2-β protein levels are unchanged (KO: 96.40± 9.226%). n=4. **(C)** In cortical brain lysates from

*Atg5*flox:*CamKIIα*-Cre mice, no upregulation of the PKA catalytic subunit α could be observed compared to WT controls (KO: 129.1±19.39%). p= 0.0921, n=4. **(D)** As observed in cortical tissue, the protein level of PKA C-α was not upregulated in hippocampal brain lysates of *Atg5*flox:*CamKIIα*-Cre KO mice compared to WT (KO: 117.6± 25.45%). p=0.2637, n=3. **(E)** Upregulation of protein level was also selective to the regulatory subunits type 1 in striatal brain lysates of *Atg5*flox-*VGAT*-Cre KO mice, and no alterations were observed for PKA R2-α (KO: 124.6± 17.45%) or PKA R2-β (KO: 114.6± 28.94%). n=4. **(F)** In striatal brain lysates of *Atg5*flox:*VGAT*-Cre mice, the PKA C-α was not changed compared to WT (KO: 131.2± 45.27%). p=0.2644, n=3. **(G)** No change in the protein level of PKA C-α could be detected in cerebellar brain lysates of *Atg5*flox:*VGAT*-Cre KO mice (KO: 94.36± 19.02%). p=0.3884, n=4. Representative immunoblot examples are shown for WT and KO lysates; the number of experiments is indicated for each experiment. The WT was set to 100% for all Western blots, and a one-tailed unpaired t-test was performed for analysis.

Additionally, the levels of R1-α and R1-β, but not PKA-Cα, were also dysregulated in an in-vitro cortico-hippocampal culture system, where the deletion of ATG5 was driven by a tamoxifen-dependent activation of the CAG-Cre promoter (Atg5flox:CAG-CreTmx) (Negrete-Hurtado, Overhoff et al. 2020). The upregulation of PKA R1-α protein level was upregulated in mass MS analysis (Fig. 11A), a finding validated using western blotting with an antibody recognizing PKA R1-α and R1-β (Fig. 11B). The PKA C-α protein levels were unchanged in the autophagy-deficient *in-vitro* system (Fig. 11C).

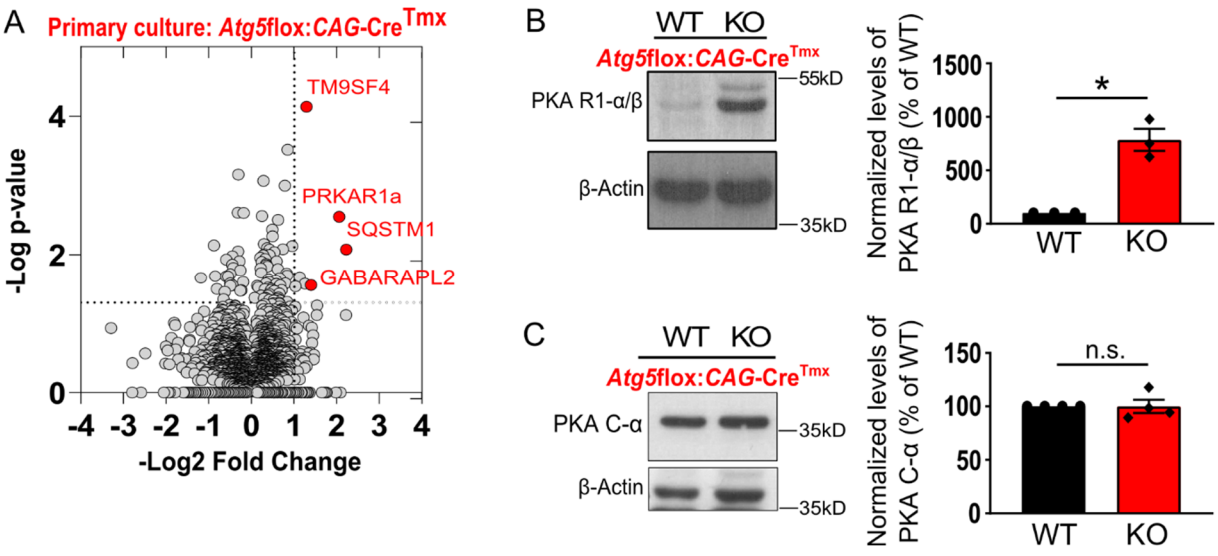

Figure 11: PKA regulatory subunits type 1 are upregulated in autophagy-deficient neurons *in-vitro*.

(A) Proteomic analysis performed on *Atg5*flox:*CAG*-Cre^{Tmx} primary cortical and hippocampal neurons at DIV15-16 showed increased protein level of PKA R1-α in Mass Spectrometry. Next to PKA R1-α also autophagy-receptors

p62 and GABARAPL2 were highly upregulated. Results were illustrated in a volcano blot plotting the logarithmic p-value against the difference between WT and KO (n=3). Performed Student's t-test. Highlighted are the proteins with a p<0.05 and high upregulation in KO compared to WT. **(B)** Upregulation of PKA R1-α and R1-β in KO neurons could be validated by western blotting using an antibody detecting RKA R1-α and R1-β (KO: 784.6± 103.3%). p=0.0013, n=3. **(C)** No upregulation of the PKA C-α could be observed in primary ATG5 KO neurons (KO: 100± 6.220%). p=0.4984, n=4. The WT was set to 100% for all shown immunoblot analyses, and a one-tail unpaired t-test was used for statistical analysis.

This effect was not specific to ATG5 since R1-α and R1-β were also accumulated in cortical and hippocampal primary neurons isolated from Atg16L1flox:CAG-CreTmx KO mice (Negrete-Hurtado, Overhoff et al. 2020) in MS analysis (Fig.12A), which is a component of the ATG12-ATG5-ATG16L1 complex, crucial for LC3 lipidation to autophagosome membranes. Additionally, the levels of PKA R1-α/β were upregulated in cortical brain lysates of *Atg16L1*flox:*VGAT*-Cre KO mice (Fig. 12B). Taken together, the data indicate that neuronal autophagy functions *in-vivo* and *in-vitro* to regulate the levels of type 1 PKA regulatory subunits selectively.

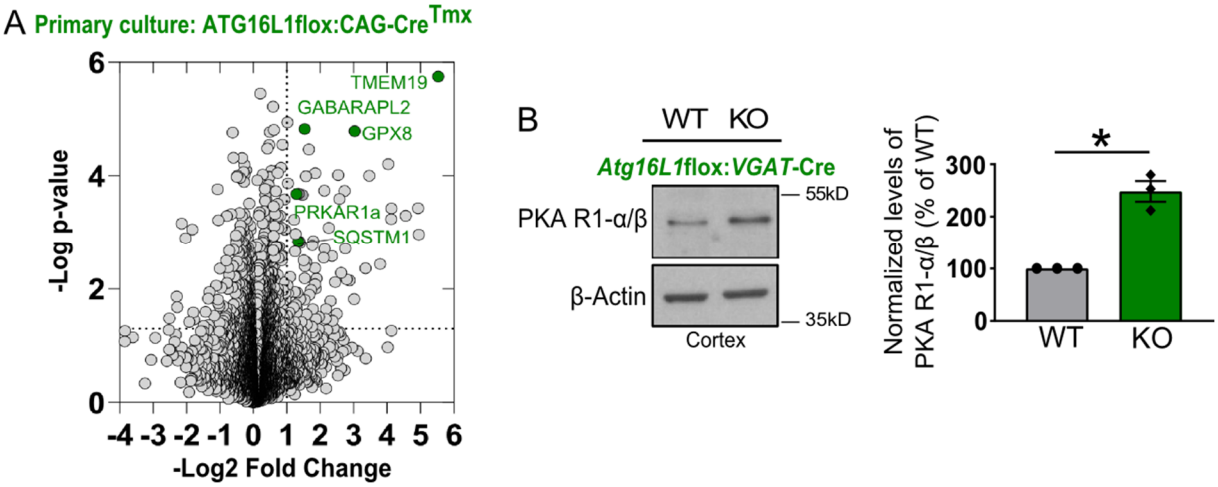

Figure 12: Protein levels of PKA regulatory subunits type 1 are upregulated in ATG16L1 KO neurons *in-vitro* and *in-vivo*

(A) Proteomic analysis performed on *Atg16L1*flox:*CAG*-Cre^{Tmx} primary cortico-hippocampal neurons at DIV15-16 showed a significant increase for PKA R1-α protein level. Underneath the highly upregulated proteins, autophagy-receptors p62 and GABARAPL2 were detectable. Results were illustrated in a volcano blot plotting the logarithmic p-value against the difference between WT and KO (n=3). Performed Student's t-test. **(B)** The selective upregulation of PKA R1-α/β was not limited to autophagy-deficient mice lacking ATG5 but also detectable in

cortical brain lysates of *Atg16L1*flox:*VGAT*-Cre KO mice compared to WT (WT set to 100%, KO: 248.4± 19.64%). p=0.0008, n=3. Performed one-tailed unpaired t-test.

Next, the exact cellular and sub-cellular localization of R1-α and R1-β in neurons were determined. Therefore, immunohistochemical imaging of R1-α and R1-β in brains of *Atg5*flox:*CamKIIα-Cre* and *Atg5*flox:*VGAT-Cre* WT and KO mice was performed, using R1-α and R1-β antibodies. PKA R1-β was prominently expressed in the hippocampus and cortex's cell soma and synaptic neuropil. This expression pattern was intensified by ATG5 deletion (Fig. 13A,B), which could be impressively demonstrated by 3D remodelling (Fig. 13C). Co-staining of PKA R1-β and synaptic marker Bassoon and subsequently 3D remodelling suggested increased recruitment of enriched PKA R1-β to the synaptic compartment (Fig. 13D), an observation that is in agreement with the dendritic localization of R1-β in wild-type mice (Ilouz et al. 2017). PKA R1-α was, similar to PKA R1-β, enriched in processes and co-localized with postsynaptic density marker PSD95 in autophagy-deficient excitatory neurons (Fig. 13E). Although mouse R1-α and R1-β share 82% sequence identity, they are not functionally redundant functionally (see above), which can be partially explained by their differential subcellular localization, where R1-α is merely cytosolic, and R1-β enriched at mitochondria (Ilouz et al. 2012). The sub-cellular localization of R1-α and R1-β in autophagy-deficient neurons was determined using immunogold labelling on Tokuyasu cryosections of the CA1 neuropil area of the hippocampus in WT and *Atg5*flox:*CamKIIα-Cre* KO mice. As previously reported (Ilouz et al. 2012), the immunogold analysis revealed sparse cytoplasmic labelling for R1-α in wild-type neurons and its accumulation on the cytosol of dendrites and at the postsynaptic density of autophagy-deficient neurons (Fig. 13F). However, the sparse content of R1-α antibody labelling in the WT made it impossible to quantify these differences. In contrast, the antibody recognizing R1-α and R1-β subunits were efficient in labelling R1-α and R1-β subcellular distribution in both WT and ATG5-deficient excitatory neurons (Fig. 13G,H). PKA R1-α/β showed enrichment at synapses and mitochondria under autophagy-deficient conditions. Accumulation of R1-α and R1-β at autophagy-deficient synapses, especially their presence at the postsynaptic density in-vivo, agreed with changes observed in the total proteome, where the gene ontology analysis indicated that the proteins accumulated in neurons lacking ATG5 mainly were enriched at the postsynaptic compartment (see Fig. 8).

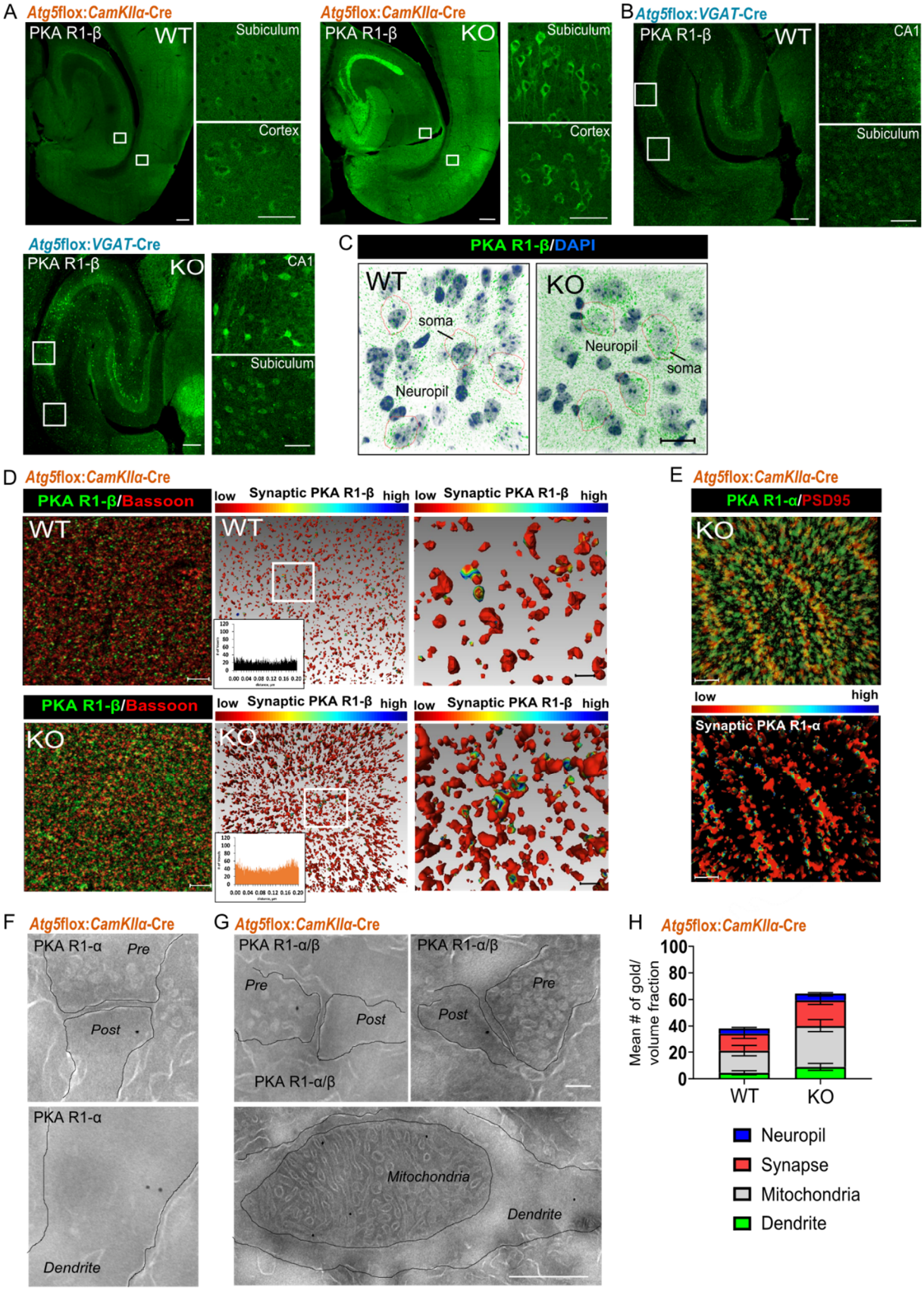
A
Atg5flox:CamKIIα-Cre
PKA R1-β
WT
Subiculum
Cortex
Atg5flox:CamKIIα-Cre
PKA R1-β
KO
Subiculum
Cortex
B
Atg5flox:VGAT-Cre
PKA R1-β
WT
CA1
Subiculum
Atg5flox:VGAT-Cre
PKA R1-β
KO
CA1
Subiculum
C
PKA R1-β/DAPI
WT
soma
Neuropil
KO
Neuropil
soma
D
Atg5flox:CamKIIα-Cre
PKA R1-β/Bassoon
low Synaptic PKA R1-β high
WT
KO
E
Atg5flox:CamKIIα-Cre
PKA R1-α/PSD95
KO
low
high
Synaptic PKA R1-α
F
Atg5flox:CamKIIα-Cre
PKA R1-α
Pre
Post
PKA R1-α
Dendrite
G
Atg5flox:CamKIIα-Cre
PKA R1-α/β
Pre
Post
PKA R1-α/β
PKA R1-α/β
Pre
Post
Mitochondria
Dendrite
H
Atg5flox:CamKIIα-Cre
Mean # of gold/ volume fraction
100
80
60
40
20
0
WT
KO
Neuropil
Synapse
Mitochondria
Dendrite

Figure 13: PKA R1-α and R1-β subunits are enriched in synapses and mitochondria in autophagy-deficient brains.

(A) Representative confocal images (from n=3 couples) of the cortex and hippocampus from *Atg5*flox:*CamKIIα*-Cre immunostained for PKA R1-β, which was intensified by lack of ATG5. White rectangular boxes indicate areas magnified to the right. Scale bar: 200 µM in large panels, 50 µM in small panels. **(B)** Representative confocal images (from n=3 couples) of PKA R1-β on *Atg5*flox:*VGAT*-Cre mice brain sections showed a prominent localization to CA1 hippocampal neurons and neurons of the subiculum, which was intensified by lack of ATG5. Scale bar: 200 µM in large panels, 50 µM in small panels. **(C)** 3D visualization of PKA R1-β in brain sections of *Atg5*flox:*CamKIIα*-Cre mice underpinned a strong enrichment in neuronal cell bodies and the neuropil, depending on ATG5 protein level. Scale bar 20 µm. **(D)** Co-staining of PKA R1-β and synaptic marker bassoon shows recruitment of accumulated PKA R1-β to the synaptic compartment in *Atg5*flox:*CamKIIα*-Cre KO mice plotted in the histogram. Amira 2020.2 software was used for 3D reconstruction. Scale bar 5 µm in dual-channel, 1 µm in 3D-reconstruction zoom. **(E)** Co-staining of PKA R1-α with postsynaptic density protein PSD95 *in-vivo* pointed towards recruitment of PKA regulatory subunits to the postsynaptic density in *Atg5*flox:*CamKIIα*-Cre KO mice. Scale bar 2 µm. **(F)** Immunogold labelling of PKA R1-α was detectable at postsynapses and the dendritic compartment in *Atg5*flox:*CamKIIα*-Cre, whereas the labelling was absent in WT (not quantified). **(G,H)** Immunogold labelling with an antibody detecting PKA R1-α/β showed an increased level of both regulatory subunits type 1 at synapses (WT: 12.762± 3.625, KO: 19.323± 3.172), dendritic compartment (WT: 4.462± 1.539, KO: 8.869± 2.559) and mitochondria (WT: 16.618±3.865, KO: 31.291±4.829, all values show the mean number of gold particles per volume fraction of n=2 mice. At least 8 images per animal were analysed with a grid size of 500k. Scale bar: upper row 50 nm, 500 nm lower picture.

8.4 PKA regulatory subunits 1-α and 1-β are degraded by starvation-induced autophagy, and their accumulation sequesters PKA catalytic subunit.

The observed changes in the levels of PKA R1-α and R1-β could be attributed either to its accumulation as autophagy substrate or to related secondary effects due to enhanced or decreased activation of signalling pathways. In response to the block of autophagy by Bafilomycin A (67nM, 6 hrs) in NSC34 cells, the protein level of PKA R1-α increased significantly (Fig. 14A), suggesting PKA R1-α as a target of autophagy. To further test this hypothesis, autophagy was induced in NSC34 cells subjected to starvation or treatment with an ATP-competitive inhibitor of mTOR, Torin1 (Fig. 14B). The protein level of PKA R1-α was significantly decreased under starvation conditions (Fig. 14C,D). In contrast to starvation, the decrease in PKA R1-α protein level was not evident upon treating NSC34 cells with Torin1 (Fig. 14C). Nevertheless, the phosphorylation levels of S6 Ribosomal Protein (pS6), used as a

readout of mTOR activity, were equally decreased (Fig. 14F), suggesting that starvation decreases R1-α levels independently of mTOR. The decrease in PKA R1-α was rescued by acute suppression of autophagy using a specific V-ATPase inhibitor Bafilomycin A1 (BafA) (Fig. 14E). Furthermore, PKA R1-α intensity was decreased in brain slices staining of mice subjected to 4 hours fasting, suggesting that starvation also induces autophagy-mediated PKA R1-α degradation *in-vivo* (Fig. 14G). Next, autophagosomes isolated from WT brains were lysed and analysed with Western blotting to proof, that the R1-α and R1-β subunits of PKA holoenzyme are autophagy substrates (Fig. 14H). Furthermore, immunogold labelling on WT brain cryosections revealed that PKA R1-α and R1-β are localized to brain autophagosomes, confined to autophagosome lumen and autophagosome membrane (Fig. 14I). All in all, the data indicated that PKA R1-α and R1-β protein levels could be controlled by autophagy.

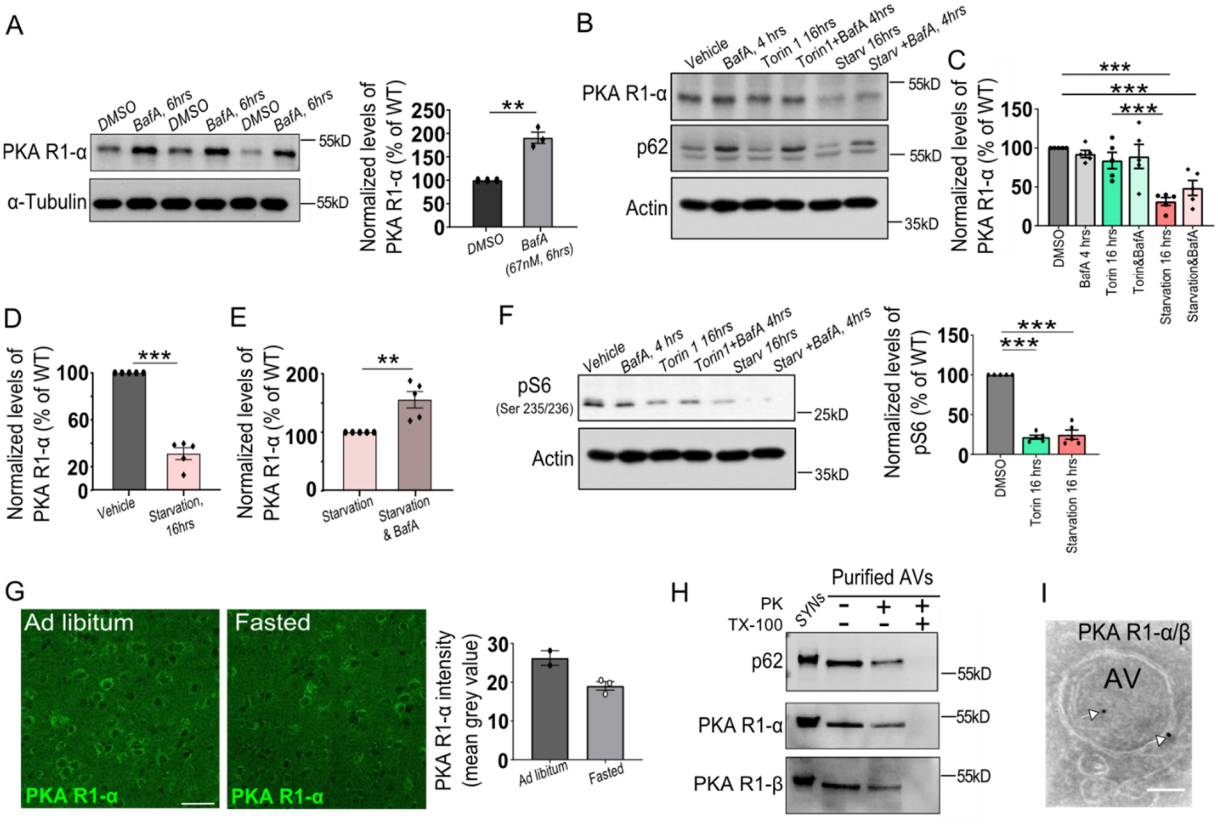

Figure 14: Starvation-induced autophagy degrades PKA R1-α and R1-β subunits.

(A) The treatment of NSC34 cells with autophagy inhibitor Bafilomycin A for 6 hrs (BafA; 67nM) led to a significantly increased protein level of PKA R1-α compared to DMSO control group set to 100% (BafA: 191.0±12.12%) p=0.0008, n=3. Performed one-tail unpaired t-test. **(B)** NSC34 cells were treated with Torin A (250 nM), an mTOR inhibiting drug, or starved for 16 hrs to induce autophagy. Additionally, lysosomal degradation was blocked in the last 4 hrs of the experiment treating the cells with 67 nM BafA prior to harvesting.

(C) Autophagy induced by starvation led to a decrease of PKA R1-α total protein level compared to DMSO control or Torin 1 treated cells (DMSO: set to 100%, BafA 4 hrs: 92.28± 4.612%, Torin 16 hrs: 83.90± 10.48%, Torin & BafA: 89.15± 15.47%, Starvation 16 hrs: 31.19± 5.085%, Starvation 16 hrs & BafA: 48.52± 9.627%). $p_{DMSO/starvation\ 16\ hrs}<0.0001$, $p_{Torin\ 16\ hrs/starvation\ 16\ hrs}=0.0007$, $p_{DMSO/starvation\ 16\ hrs\ \&\ BafA}=0.0009$, n=5. Performed Two-Way ANOVA with Tukeys' multiple comparison test. **(D)** The protein level of PKA R1-α decreased drastically under starvation-induced autophagy compared to the control group (starvation: 31.19± 5.085%). p<0.0001; n=5. Performed one-tail unpaired t-test. **(E)** The block of lysosomal degradation using BafA in the last 4 hrs of starvation stopped PKA R1-α degradation and resulted in significantly higher PKA R1-α protein level than starvation (starvation&BafA: 48.52± 9.627%). p=0.0020, n=5. Performed one-tail unpaired t-test. **(F)** The induction of starvation and the treatment of Torin 1 activated autophagy mirrored by the significant decrease of pS6 protein level in NSC34 cells due to starvation/ drug-induced mTOR activity depression (DMSO set to 100%, Torin 16 hrs: 21.65± 2.541%, Starvation 16 hrs: 24.82± 5.819%). $p_{DMSO/Torin\ 16\ hrs}<0.0001$, $p_{DMSO/starvation\ 16\ hrs}<0.0001$, n=5. Performed Two-Way ANOVA with Tukeys' multiple comparison test. **(G)** Example pictures of brain slices stained for PKA R1-α from fasted wild-type mice. The mice were fasted for 4 hours prior to perfusion. The fasting period decreased PKA R1-α protein level in fasted mice, suggesting autophagy-mediated regulation of PKA R1-α protein level (Ad libitum: 26.25± 1.9, Fasted: 19.07± 1.08). $n_{Ad\ libitum}=2$, $n_{Fasted}=3$, 6 pictures/mouse were analysed. Scale bar 50 µm **(H)** Western blot analysis of purified AVs (50µg AVs/lane) with and without Proteinase K (PK) treatment. Triton-X 100 (1% final) was used as a positive control for the activity of PK. Synaptosome lysates (30µg/lane) were also used as a positive control for the signal of antibodies used against the synaptic proteins PKA R1-α and PKA R1-β and p62. **(I)** Immunogold labelling targeting PKA R1-α/β showed specific labelling in autophagosomes, autophagosome lumen and autophagosome membrane on WT brain sections (example picture). Scale bar: 50 nm.

The data above indicate R1-α and R1-β as selective cargos of neuronal autophagosomes. In that case, their recruitment to autophagosomes should be based on the binding to autophagy receptors, and autophagy dysfunction should lead to their accumulation in p62 (SQSTM1)-positive aggregates, which are known to accumulate in autophagy-deficient systems (Komatsu et al. 2007a). In agreement with this hypothesis, confinement of R1-α and R1-β to p62-containing puncta in cell soma of neurons of *Atg5*flox:*CamKIIα*-Cre KO mice could be observed (Fig. 15A). Loss of ATG5 in GABAergic neurons also caused the soma-confined accumulation of R1-β to inclusion bodies containing p62, as well as another selective autophagy receptor NBR1 (Fig. 15B). In the soma of WT neurons *in-vitro*, the colocalization of R1-α and p62 was regulated by starvation and could be facilitated by autophagy inhibition using autophagy blocker Bafilomycin A (Fig. 15C). The enrichment of R1-β at ATG5 KO deficient synapses (described above) was not sequestered by p62 inclusion bodies in processes as observed in

the cell soma (Fig. 15D), suggesting full functionality of the regulatory subunits in neuronal processes. Its interaction with LC3 might mediate selective PKA R1-α and R1-β to autophagosomes (Fig. 15E).

Finally, significantly more R1-α and R1-β was associated with PKA catalytic subunit in autophagy-deficient brains, suggesting a misbalance in PKA complex formation (Fig. 15F). As described above, PKA regulatory subunits function as catalytic subunits carriers for spatially controlled PKA signalling. However, if the catalytic subunits are bound to the regulatory subunits, they cannot phosphorylate their downstream target, suggesting a dominant-negative role for R1-α and R1-β in regulating PKA signalling in ATG5-deficient neurons. Furthermore, the induction of autophagy by starvation and thereby the degradation of the PKA regulatory subunits type 1 was sufficient to induce PKA signalling displayed by the increase of PKA phosphorylation substrate protein levels (Fig. 15G). A block of PKA signalling by H89 treatment abolished the observed effect. These results demonstrate that starvation-dependent autophagy regulates the protein levels of PKA regulatory subunits type 1 in neurons and thereby PKA signalling. A lack of autophagy results in the stabilization of R1-α and R1-β protein levels, ultimately causing the sequestration of the PKA catalytic subunit.

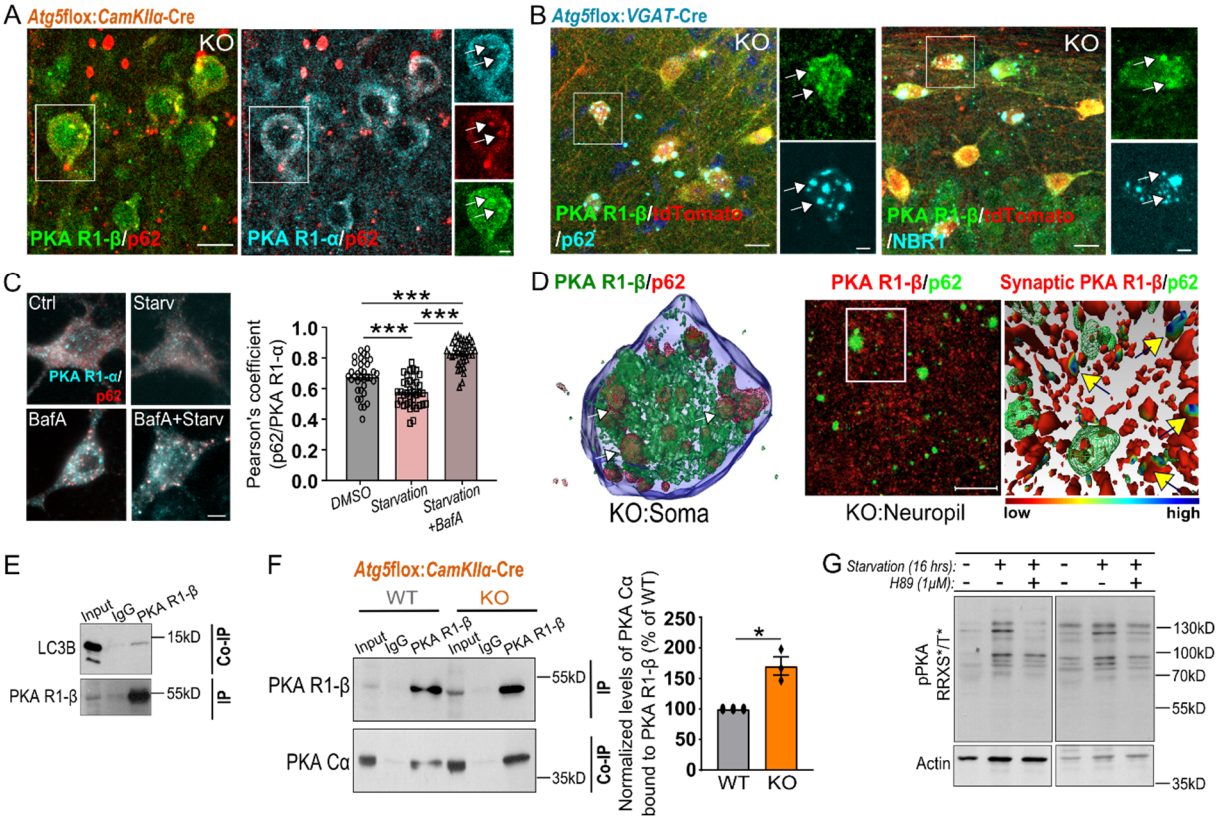

Figure 15: Autophagy degrades PKA regulatory subunits type 1 in neurons and a lack of autophagy results in the sequestration of the PKA catalytic subunit.

(A) Representative confocal images of hippocampal brain sections from *Atg5*flox:*CamKIIα*-Cre WT and KO mice immunostained for PKA R1-α and R1-β and co-immunostained for p62. White rectangular boxes indicate areas magnified to the right. White arrows indicate p62 inclusion bodies positive for PKA R1. Scale bar: large panel 15 µm, small panel: 5 µm. **(B)** Representative confocal images of hippocampal brain sections from *Atg5*flox:*VGAT*-Cre:tdTomato^{+} WT and KO mice immunostained for PKA R1-β and co-immunostained for p62 and NBR1. White rectangular boxes indicate areas magnified to the right. White arrows indicate p62/ NBR1 inclusion bodies positive for PKA R1-β. Scale bar: large panels: 15 µm, small panels: 5 µm. **(C)** Example pictures of primary cortico-hippocampal neurons, forwarded to 16 hours starvation to induce autophagy. The induction of autophagy by neuronal starvation (16 hrs) induced PKA R1-β protein degradation. The degradation of PKA R1-β was diminished by the supplementation of BafA (67nM) in the media (control: 0.6767± 0.01896 n=36 neurons, starvation: 0.5776± 0.01537 n=38 neurons, starvation + BafA: 0.8325± 0.01383 n=36 neurons). $p<0.0001$, analysed number of neurons coming from n=3 independent experiments. Performed Two-Way ANOVA with Tukeys' multiple comparison test. Scale bar: 5 µm. **(D)** 3D-modulation of *Atg5*flox:*CamKIIα*-Cre KO soma and neuropil show that PKA R1-β colocalizes in the soma with p62 inclusion bodies but not in processes. Scale bar: 10 µM. **(E)** Co-Immunoprecipitation analysis of PKA R1-β revealed LC3 as a binding partner in mouse brain lysates. Input, 1.5% of lysate was added to the assay. **(F)** Enriched protein levels of PKA R1-β were functional in the neurons and bound a bigger proportion of PKA catalytic subunit C-α in *Atg5*flox:*CamKIIα*-Cre KO mice, which could be shown using immunoprecipitation analysis of brain lysates (WT set to 100%, KO: 170.3± 14.88%). $p=0.0046$; n=3. Performed one-tail unpaired t-test. **(G)** The phosphorylation level of proteins containing a PKA

phosphorylation motif was increased upon 16 hours of starvation in primary cortico-hippocampal neurons. The observed phosphorylation increase was suppressed by 1 µM H89 supplementation in the media. Blots from two independent experiments are shown.

8.5 ATG5 regulates the cAMP/PKA signalling axis, and its neuronal loss interferes with the CREB phosphorylation response in the brain.

Considering the data described above, it can be hypothesized that upregulated PKA regulatory subunits type 1 in neurons with ATG5 deletion diminishes PKA signalling. PKA activity is tightly controlled by cAMP and can be elevated upon supplementation of cells with cAMP-elevating agent Forskolin, a phenotype reflected in phosphorylation of CREB (pCREB) at Serine 133. CREB phosphorylation was increased upon treatment with 10 µM of Forskolin for 5 min in cultured WT primary cortico-hippocampal neurons, whereas total CREB levels were unaltered (Fig. 16A). In contrast, the pCREB response to Forskolin stimulation was undetectable in *Atg5*flox:*CAG*-Cre^{Tmx} KO neurons, indicating that cAMP-dependent PKA signalling is inhibited upon autophagy deficiency in neurons (Fig. 16A). The observed phenotype was not neuron-specific since a decreased pCREB response to Forskolin stimulation could also be observed in autophagy-deficient (ATG5-deficient) mouse embryonic fibroblasts (MEF cells) (Fig. 16B). To investigate whether neuronal ATG5 regulates PKA/pCREB activation *in-vivo*, quantitative high content screening (HCS) microscopy was performed. The pCREB staining intensity in response to Forskolin stimulation of thousands of cortical neurons isolated from 8-week-old *Atg5*flox:*CamKIIα*-Cre:tdTomato^{+} WT or KO mice revealed that Forskolin-mediated activation of pCREB was abolished in autophagy-deficient cortical neurons *in-vivo* (Fig. 16C). These changes were independent of cAMP levels that were unaltered in hippocampal brain lysates of *Atg5*flox:*CamKIIα*-Cre KO mice compared to WT (Fig. 16D) and isolated neurons of *Atg5*flox:*CamKIIα*-Cre:tdTomato^{+} KO mice (Fig. 16E). After neuronal stimulation, cAMP/PKA signalling can be induced to mediate the LTP (described above). Chemical depolarization of neurons with KCl application activates NMDA receptor-mediated CREB phosphorylation and CRE-mediated gene expression (Macías et al. 2001). Activation of pCREB using a brief pulse of depolarizing KCL solution (40 µM) was also impaired (Fig. 16C), suggesting that ATG5 could regulate neuronal activity-dependent pCREB activation.

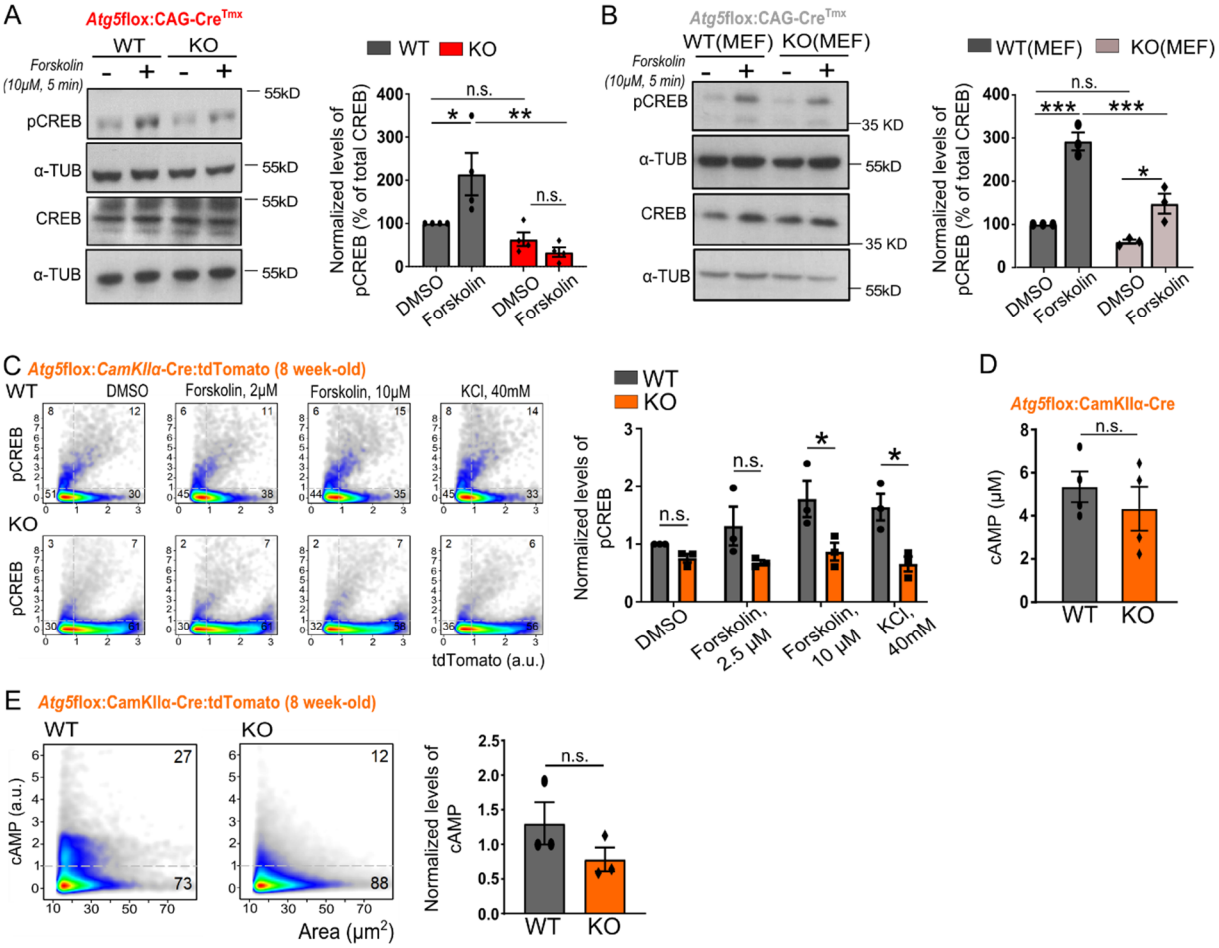

Figure 16: ATG5 regulates the cAMP/PKA signalling axis, and its neuronal loss interferes with CREB phosphorylation response in the brain without alterations in intracellular cAMP concentrations.

(A) *Atg5*flox:*CAG*-Cre^{Tmx} KO primary cortico-hippocampal neurons show a decreased pCREB response to cAMP level stimulating agent Forskolin (10 μM, 5 min) compared to WT neurons. pCREB signal was normalized to the total CREB protein level (WT_{DMSO} set to 100%, $WT_{Forskolin}$: 214.17± 48.87%, KO_{DMSO}: 63.26± 15.85%, $KO_{Forskolin}$: 33.50± 10.84%). $p_{WT\ DMSO/WT\ Forskolin}$=0.0416, $p_{WT\ Forskolin/KO\ Forskolin}$=0.0019; n=4. Analysed using two-way ANOVA with Tukey's multiple comparisons test. **(B)** ATG5-deficient MEF cells also showed impaired PKA signalling due to Forskolin stimulation using pCREB level normalized to total CREB as a readout for PKA activity (WT DMSO set to 100%, WT Forskolin: 292.36± 20.76%, KO DMSO: 59.96± 4.85%, KO Forskolin: 148.10± 23.20%). $p_{WT\ DMSO/WT\ Forskolin}$=0.0001, $p_{WT\ Forskolin/KO\ Forskolin}$=0.0009, $p_{KO\ DMSO/KO\ Forskolin}$=0.0176; n=3. Analysed using two-way ANOVA with Tukey's multiple comparisons test. **(C)** Quantitative high content screening microscopy analysis from isolated neurons of 8 weeks old *Atg5*flox:*CamKII*-Cre:tdTomato WT and KO mice treated either with DMSO, 2 μM or 10 μM Forskolin revealed a decreased pCREB staining intensity in KO neurons in a dose-dependent manner. The pCREB response to neuronal depolarization, using KCl was also reduced in KO neurons compared to WT (WT_{DMSO} set to 1, KO_{DMSO}: 0.76± 0.07%, $WT_{Forskolin\ 2μM}$: 1.31± 0.34%, $KO_{Forskolin\ 2μM}$: 0.68± 0.04%, $WT_{Forskolin\ 10μM}$: 1.78± 0.31%, $KO_{Forskolin\ 10μM}$: 0.87± 0.15%, $WT_{KCl\ 40mM}$: 1.64± 0.23%, $KO_{KCl\ 40mM}$: 0.66± 0.13%). $p_{WT\ Forskolin\ 10μM/KO\ Forskolin\ 10μM}$=0.0280, $p_{WT\ KCl\ 40mM/KO\ KCl\ 40mM}$=0.0336; n=3 independent experiments. Analysed using two-way ANOVA with Tukey's multiple comparisons test. **(D)** Second messenger cAMP concentration was unaltered in hippocampal brain

lysates of autophagy-deficient *Atg5*flox:*CamKII*-Cre KO mice compared to WT (WT: 5.340±0.7111, KO: 4.327±1.014). p=0.4448, n=4. Performed Two-tailed unpaired t-test. **(E)** Quantitative high content screening microscopy analysis using a cAMP detecting antibody also revealed no changes in intracellular levels of second messenger cAMP in isolated neurons from *Atg5*flox:*CamKII*-Cre:tdTomato KO mice compared to WT (WT: 1.303± 0.3055, KO: 0.7839± 0.1722). p=0.2127, n=3. Performed Two-tailed unpaired t-test.

CREB belongs to the CREB/CREM subgroup of transcription factors, which bind to cAMP-responsive elements (CRE) in target genes. To understand whether alterations of PKA signalling are reflected in the expression of CREM/CREB target genes, next-generation sequencing of FACS-sorted WT and KO *Atg5*fl*ox:VGAT*-Cre:tdTomato^{+} neurons (see Fig. 8A,B) were done to determine gene expression pattern in autophagy-deficient neurons. The deletion of ATG5 caused downregulation of 732 transcripts (Fig. 17A,B). Although only a few genes were differentially expressed based on the corrected p-value (Fig. 17B). Analysis of transcription factor binding signatures ($p<0.01$, $FC<2$, 115 genes in total) revealed that 29.6% of downregulated genes contained CREB1 response elements in their promoter region (Fig. 17C). On the other side, 66 out of 238 significantly upregulated genes ($p<0.01$, $FC>2$) were regulated by the WT1 transcription activity (Fig. 17D). Intriguingly, among highly downregulated genes with CREB1 response element, genes encoding for proteins with the function in protein and vesicle trafficking, for example, *Clasp1, Gdi2, Sgms1, Vps13b*, were identified (Fig. 17E), suggesting that autophagy might indirectly regulate intracellular membrane trafficking by controlling the PKA signalling.

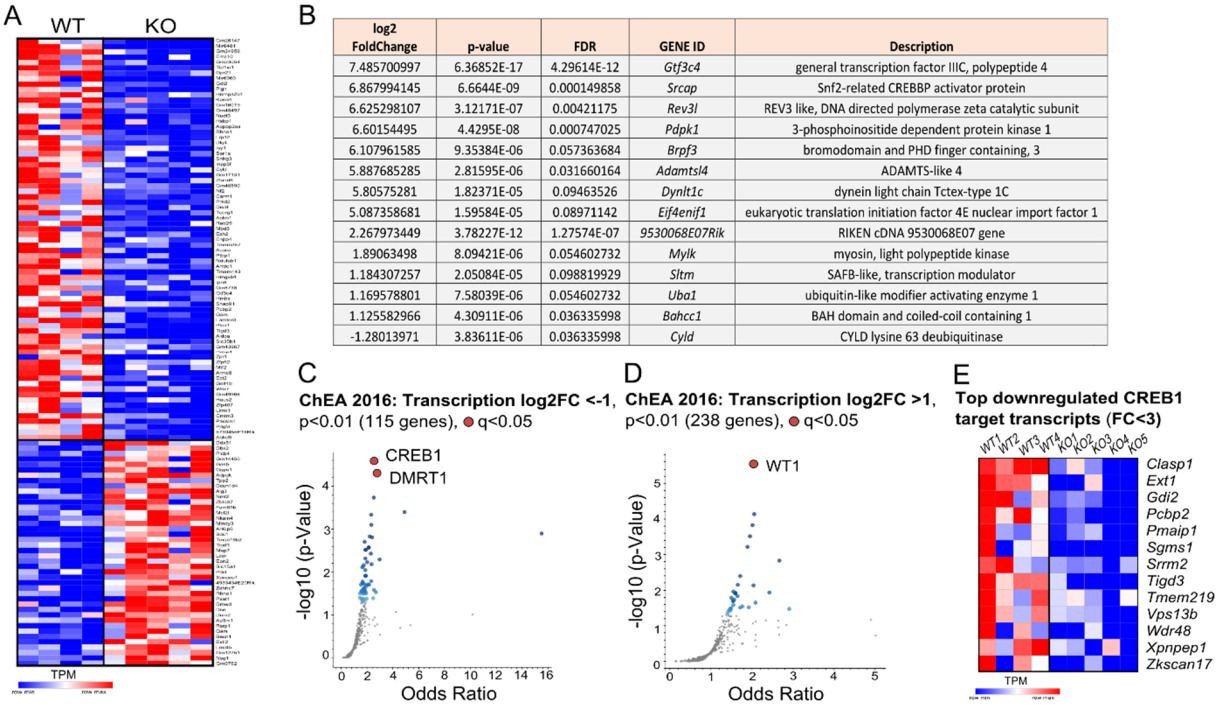

log2 FoldChange	p-value	FDR	GENE ID	Description
7.485700997	6.36852E-17	4.29614E-12	*Gtf3c4*	general transcription factor IIIC, polypeptide 4
6.867994145	6.6644E-09	0.000149858	*Srcap*	Snf2-related CREBBP activator protein
6.625298107	3.12171E-07	0.00421175	*Rev3l*	REV3 like, DNA directed polymerase zeta catalytic subunit
6.60154495	4.4295E-08	0.000747025	*Pdpk1*	3-phosphoinositide dependent protein kinase 1
6.107961585	9.35384E-06	0.057363684	*Brpf3*	bromodomain and PHD finger containing, 3
5.887685285	2.81595E-06	0.031660164	*Adamtsl4*	ADAMTS-like 4
5.80575281	1.82371E-05	0.09463526	*Dynlt1c*	dynein light chain Tctex-type 1C
5.087358681	1.59584E-05	0.08971142	*Eif4enif1*	eukaryotic translation initiation factor 4E nuclear import factor 1
2.267973449	3.78227E-12	1.27574E-07	*9530068E07Rik*	RIKEN cDNA 9530068E07 gene
1.89063498	8.09421E-06	0.054602732	*Mylk*	myosin, light polypeptide kinase
1.184307257	2.05084E-05	0.098819929	*Sltm*	SAFB-like, transcription modulator
1.169578801	7.58039E-06	0.054602732	*Uba1*	ubiquitin-like modifier activating enzyme 1
1.125582966	4.30911E-06	0.036335998	*Bahcc1*	BAH domain and coiled-coil containing 1
-1.28013971	3.83611E-06	0.036335998	*Cyld*	CYLD lysine 63 deubiquitinase

Figure 17: The expression of genes containing CREB1 response elements in their promoter region is downregulated upon ATG5 deletion in neurons.

(A) *Atg5*flox:*VGAT*-Cre FACS sorted neurons were forwarded to new generation sequencing. All significant (p<0.02) up- and downregulated transcripts (fold change <>2) from Kallisto TPM output are displayed in the heatmap (117 displayed transcripts, 75 downregulated, 42 upregulated, n_{WT}=4, n_{KO}=5). **(B)** Table displays most dysregulated genes in autophagy-deficient inhibitory neurons based on the corrected p-value. **(C-D)** ChEA enrichment analysis, performed on down- (C) and upregulated (D) Kallisto transcripts that were further processed by Sleuth differential gene expression analysis, revealed a strong downregulation of genes containing CREB1 and DMRT1 response elements in their promoter region and strong upregulation of genes under WT1 transcription activity. **(E)** Heatmap displays the Kallisto output values of the most downregulated genes after Sleuth differential gene expression analysis, pointing forward to a role of autophagy in PKA mediated membrane trafficking.

If neuronal levels of PKA type I inhibitory subunits are negatively regulated by starvation-induced autophagy (see Fig. 14&15), then the starvation should facilitate CREB translocation to the nucleus due to degradation of the regulatory subunits that can no longer sequester the catalytic subunits and enable PKA signalling. In agreement with this hypothesis, a proportion of wildtype primary cortico-hippocampal neurons with nuclear pCREB was significantly increased upon amino acid and serum deprivation. This phenotype was PKA-dependent since blocking the catalytic activity of PKA by H89 diminished pCREB translocation to the nucleus

(Fig. 18A-C). To understand whether ATG5 is directly responsible for regulating the PKA/pCREB signalling axis, MEF cells overexpressing ATG5 tagged with eGFP or eGFP alone as control were stimulated with Forskolin (10 µM, 5 min). Overexpression of ATG5 augmented CREB phosphorylation responses upon Forskolin treatment (Fig. 18D), indicating that ATG5 directly regulates PKA activity, likely by facilitating PKA R1 inhibitory subunit degradation. Strikingly, pCREB levels were also increased in ATG5-overexpressing MEFs under Forskolin-free conditions (Fig. 18D,E), indicating that ATG5, and thus autophagy, could potentially fine-tune the sensitivity of PKA to cAMP levels in cells.

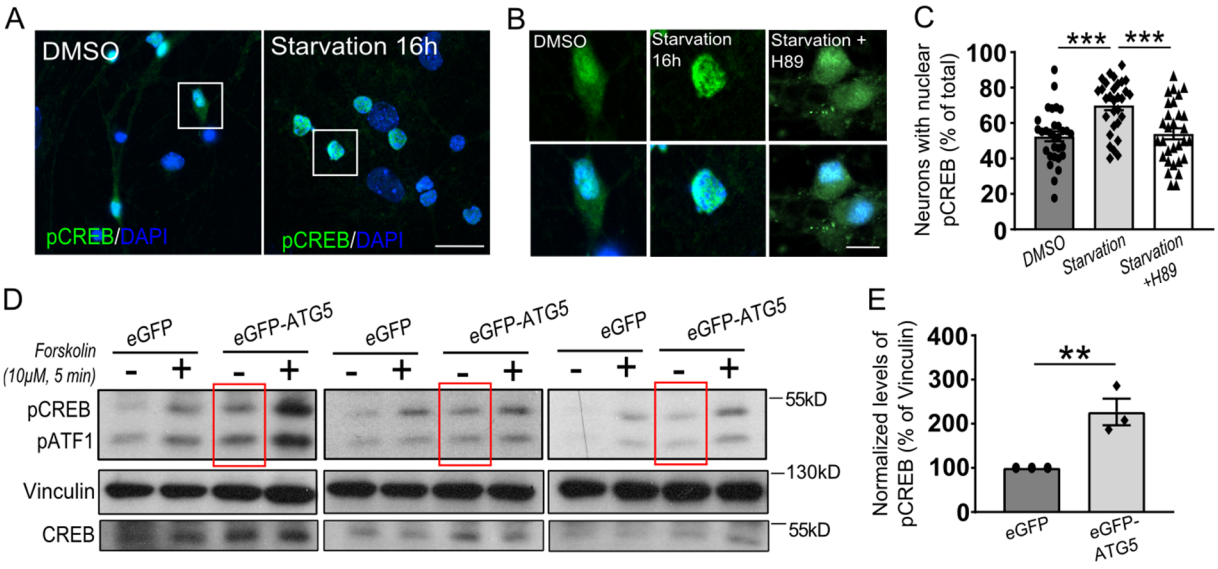

Figure 18: ATG5 fine-tunes cAMP/PKA mediated signalling in neuronal and non-neuronal cells.

(A-C) Primary cortico-hippocampal WT neurons showed a significant increase of pCREB positive neurons after starvation compared to the control group treated with DMSO. Inhibition of PKA signalling applying 1 µM PKA inhibitor H89 diminished the increasing percentage of pCREB positive neurons, indicating that autophagy regulates PKA mediated signalling (DMSO: 52.50± 2.76, starvation: 70.00± 2.70, starvation+H89: 53.92± 3.15). $p_{DMSO/starvation}$=0.0001, $p_{starvation/starvation+H89}$=0.0004; n=30 images from n=3 independent experiments. Analysed using ordinary one-way ANOVA with Tukey's multiple comparisons test. Scale bar: large panels: 15 µm, small panels: 5 µm. **(D-E)** MEF cells overexpressing eGFP-ATG5 or eGFP as control were treated with 10 µM Forskolin or DMSO for 5 min. The overexpression of ATG5 in MEF cells significantly increased the basal level of pCREB (E) and led to a strong response to Forskolin stimulation ($eGFP_{DMSO}$ set to 100%, $eGFP\text{-}ATG5_{DMSO}$: 223.4± 26.87%). p=0.0068; n=3. Performed one-tail unpaired t-test.

8.6 Neuronal ATG5 regulates PKA-mediated phosphorylation of proteins enriched at postsynaptic density of excitatory synapses.

PKA-mediated regulation of CREB-dependent gene expression is known to be crucial for long-term memory (Kandel et al. 2014). In addition, PKA-mediated phosphorylation can regulate neurotransmission by acting directly on presynaptic proteins regulating synaptic vesicle exo-/endocytosis and PSD-localized neurotransmitter receptors (Greengard et al. 1991; Cho et al. 2015). The latter function of PKA in synaptic potentiation is an essential regulator of neuronal excitation. Thus, the findings above raise the question of whether autophagy regulates neuronal excitability by controlling PKA-dependent phosphorylation of the synaptic proteome. When PKA is activated, it phosphorylates substrates preferably on the recognition motif Arg-Arg-X-Ser/Thr-Y, and phosphorylated phospho-Ser/Thr residues can be monitored by using a specific antibody (RRXS/T). In WT neurons, application of Forskolin-induced a robust increase in phosphorylated phospho-Ser/Thr residues, whereas Forskolin-dependent phosphorylation of PKA substrates was abolished in neurons lacking ATG5 *in-vitro* (Fig. 19A) and *in-vivo* (Fig. 19B), suggesting a global reduction in PKA-dependent proteome phosphorylation upon autophagy deficiency.

To directly analyze phosphoproteome changes in the brains of ATG5 KO mice, global phosphoproteome analysis was performed of *Atg5*flox*:CamKIIα-Cre* and *Atg5*flox:*VGAT-Cre* WT and KO brains using an isotope-labelled spike-in mouse approach (already described above). Phosphoproteome analysis revealed significant downregulation of 31 phosphosites in *Atg5*flox*:CamKIIα-Cre* KO mice and 82 phosphosites in *Atg5*flox:*VGAT-Cre* KO mic*e* when normalized to total protein levels ($p<0.05$, $FC<-1.2$). Surprisingly, several postsynaptic and a few presynaptic proteins were among proteins with the strongest downregulated phosphorylation, including PALM, TNIK, DNAJC5, DLGAP4, RIMS1 EPB4.1L1, DLG1, SYNGAP1 and CASKIN1 (Fig. 20A,B). Furthermore, gene ontology (GO) analysis for cellular component enrichment revealed that most proteins with decreased phosphorylation were localized to the PSD of glutamatergic synapses in both mouse lines (Fig. 20C,D). On the general level, these data argue that autophagy deficiency decreases global phosphorylation of PSD proteins at excitatory glutamatergic synapses in both excitatory and inhibitory neurons.

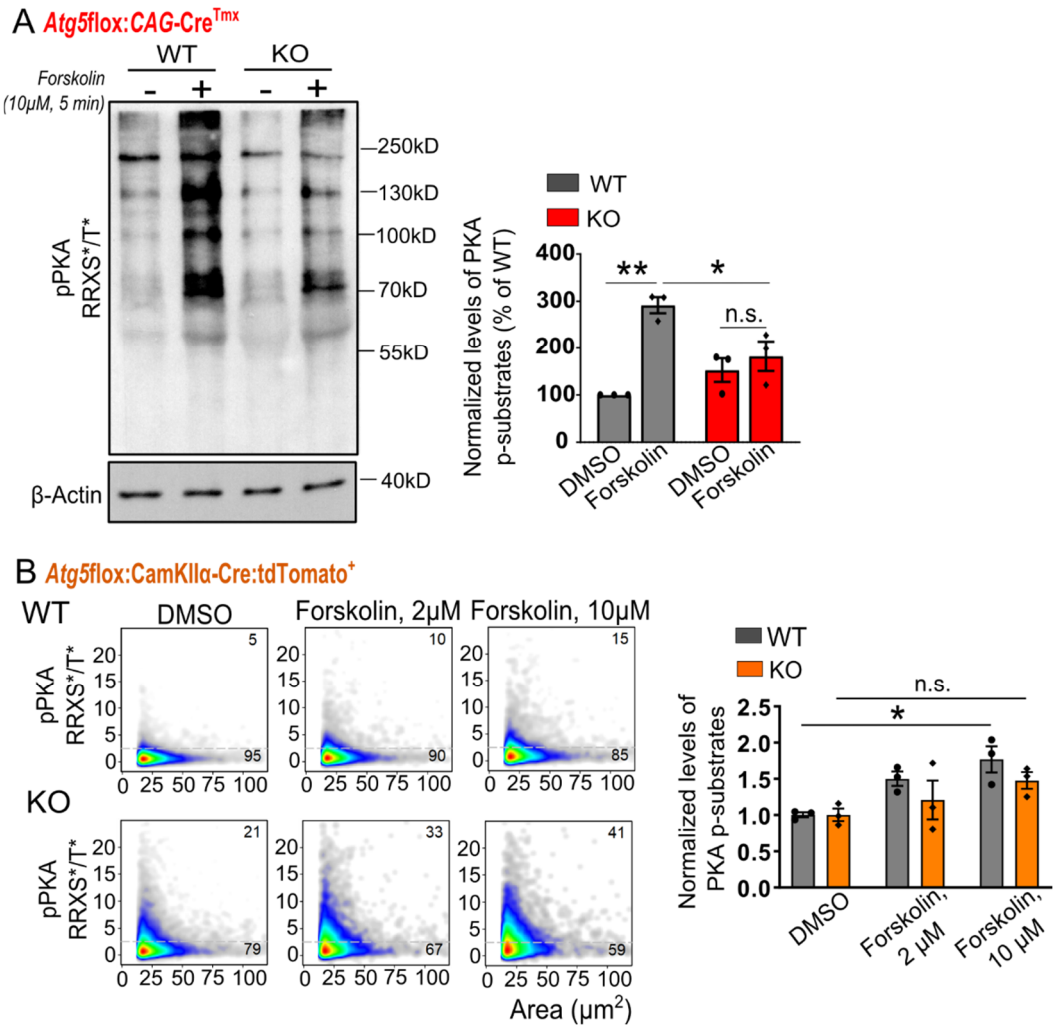

Figure 19: Phosphorylation levels of PKA targets are reduced in autophagy-deficient neurons *in-vitro* and *in-vivo*.

(A) Immunoblot analysis of primary cortico-hippocampal *Atg5*flox:*CAG*-Cre^{Tmx} WT and KO neurons treated with 10 µM Forskolin for 5 min prior to harvesting showed a significantly decreased response to Forskolin stimulation in WT compared to KO investigating the level of phosphorylated PKA substrate targets (WT_{DMSO} set to 100%, $WT_{Forskolin}$: 291.85± 17.02%, KO_{DMSO}: 152.97± 25.26%, $KO_{Forskolin}$: 182.56± 31.89%). $p_{WTDMSO/WTForskolin}$=0.0012, $p_{WTForskolin/KOForskolin}$=0.0328; n=3. Performed two-way ANOVA with Tukey's multiple comparisons test for analysis.

(B) Quantitative high content screening microscopy analysis from isolated neurons of 8 weeks old *Atg5*flox:*CamKII*-Cre:tdTomato^{+} WT and KO mice using an antibody detecting phosphorylated substrates carrying the PKA motif (RRXS) showed a significant increase of phosphorylated targets in WT after Forskolin stimulation (10 µM) but not in KO neurons (WT_{DMSO}: 1.004± 0.034, KO_{DMSO}: 1.004± 0.086, $WT_{Forskolin\ 2µM}$: 1.502± 0.098, $KO_{Forskolin\ 2µM}$: 1.209± 0.269, $WT_{Forskolin\ 10µM}$: 1.770± 0.182, $KO_{Forskolin\ 10µM}$: 1.476± 0.116). $p_{WT\ DMSO/WT\ Forskolin\ 10µM}$=0.0342, n=3. Two-Way ANOVA with Tukeys' multiple comparison test was used for analysis.

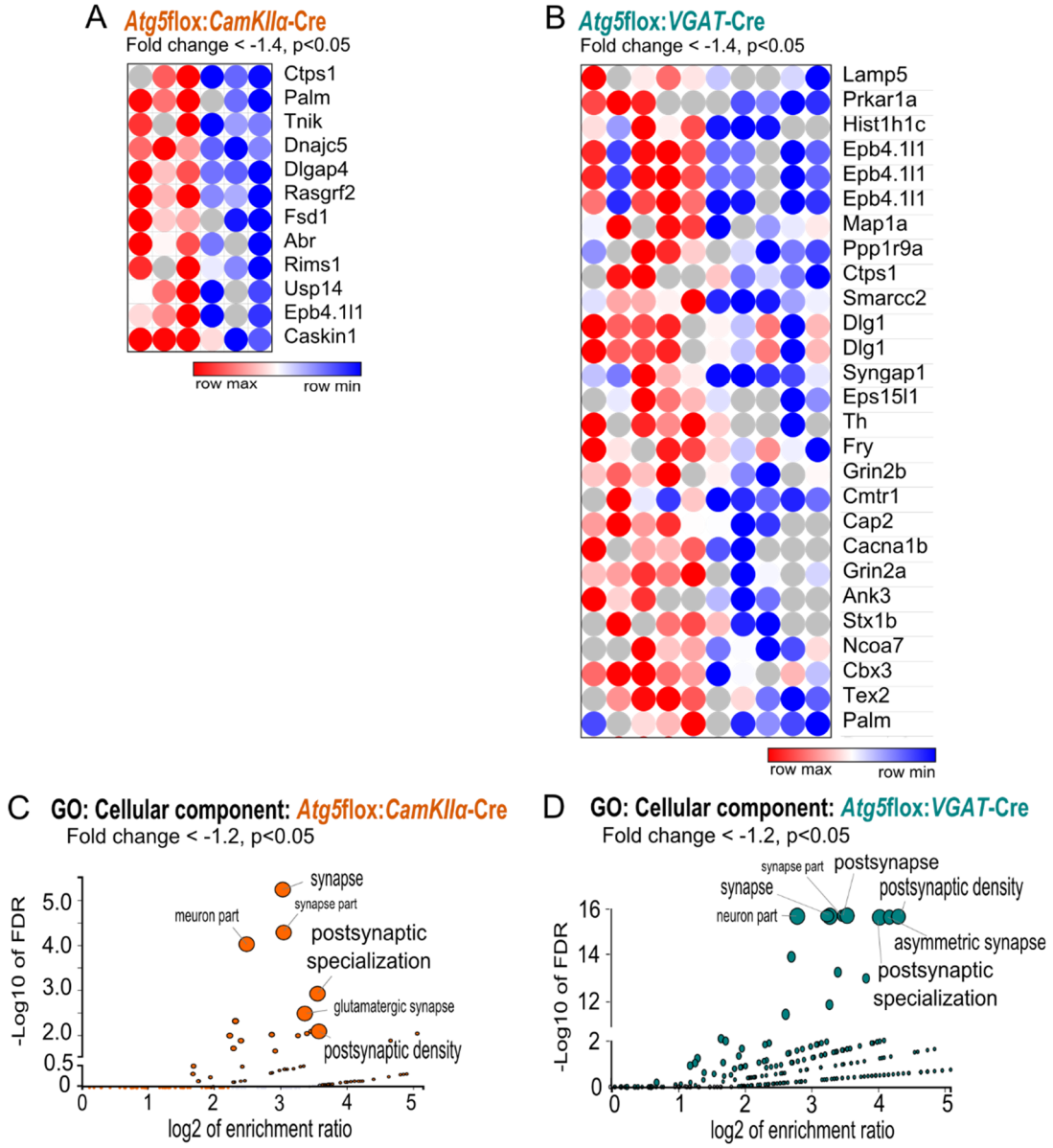

Figure 20: Phosphorylation state of postsynapse-localized proteins is regulated by neuronal autophagy.

(A-B) Cortical lysates of *Atg5*flox:*CamKIIα*-Cre and striatal lysates of *Atg5*flox:*VGAT*-Cre mice were forwarded to isotope labelled spike-in phosphoproteome analysis. There was a significant ($p<0.05$) downregulation of 31 phosphosites in *Atg5*flox:*CamKIIα*-Cre KO mice and 82 phosphosites in *Atg5*flox:*VGAT*-Cre KO mice, detected when normalized to total protein levels. **(D)** GO Cellular component analysis with significantly downregulated phosphoproteins with a FC< -1.2 in KO compared to WT revealed associated with postsynaptic density. GO Cellular component analysis was done using WebGestalt.

Phosphorylation of PKA substrates in neurons is maintained at a relatively high state under basal conditions (Hilfiker et al. 2001). To identify the phosphorylation targets of PKA in wildtype brain tissue co-immunoprecipitation, followed by mass spectrometry was performed

using PKA phosphorylation state-specific antibody (RRXS/T) and IgG as control (Fig. 21A). Proteins that were significantly enriched using the PKA phosphorylation state-specific antibody (RRXS/T) for co-immunoprecipitation were forwarded to GO cellular component analysis, which revealed that most PKA-phosphorylation targets in the brain are associated with the postsynaptic density (Fig. 21B). Several of the targets detected during co-immunoprecipitation analysis were also downregulated in the phosphoproteome data of *Atg5*flox:*CamKIIα*-Cre and *Atg5*flox:*VGAT*-Cre mice (Fig. 21C). Targets detected using the PKA phosphorylation state-specific antibody and downregulated in autophagy-deficient brains could be associated with a postsynaptic localization using GO cellular component analysis (Fig. 21D). Thus, global phosphorylation changes in brains lacking ATG5 could at least partially result from diminished PKA signalling.

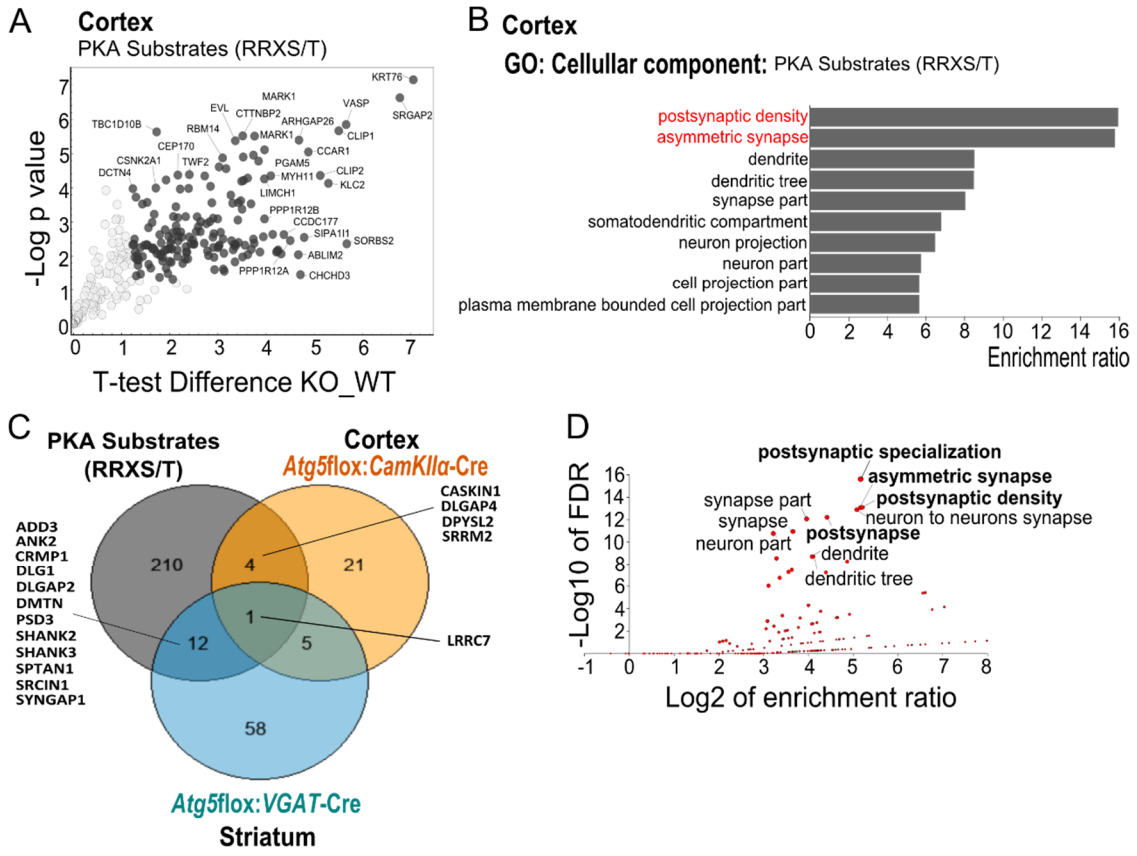

Figure 21: PKA phosphorylation in the brain targets proteins at the postsynaptic density of excitatory synapses.

(A) Co-immunoprecipitation analysis using PKA substrates antibody in WT brain lysates identified several binding partners of PKA *in-vivo*. The volcano blots illustrate the proteome of enriched proteins detected with the PKA phosphorylation state-specific antibody (RRXS/T). Highlighted are significant proteins ($p<0.05$) with an FC>1.2. **(B)** All proteins highlighted in (A) were forwarded to GO cellular component analysis using WebGestalt. PKA

phosphorylation targets in mice brain lysates were allocated to the postsynaptic density. **(C)** Venn diagram analysis revealed that several candidates identified to be less phosphorylated *in-vivo* were PKA phosphorylation targets identified using co-immunoprecipitation analysis. For the PKA pSubstrates dataset, all upregulated hits with a q<0.05 were used for analysis. For autophagy-deficient brain lysates, phosphoproteome hits with a p<0.05 and FC<-1.2 were used. **(D)** GO cellular component analysis performed on proteins identified in (C) revealed that PKA target proteins with decreased phosphorylation levels in autophagy-deficient mice are associated with postsynaptic localization.

To test this hypothesis, PKA phosphorylation targets in WT mice were determined after Forskolin or DMSO stimulation of cortical and hippocampal acute brain slices (Fig. 22A). Forskolin caused an increase in phosphorylation of several known PKA substrates, for example, MAPT, RIMS1, STMN1, IP3R1, RASGRP2, SNAP-25 and TH. GO Cellular component analysis revealed that significantly upregulated (p<0.05, FC>1.2) phosphosites due to Forskolin stimulation in mice brain tissue were associated with postsynaptic function/ localization (Fig. 22B). Comparing the list of identified PKA phosphorylation targets in WT (FC>1.2, p<0.05) with decreased phosphorylation targets identified in global phosphoproteome of autophagy-deficient brains (Fig. 22C), 11 phosphosites with decreased phosphorylation in *Atg5*flox:*CamKIIα*-Cre KO brains and 25 phosphosites from *Atg5*flox:*VGAT*-Cre KO mice were identified that could be potential PKA targets. Subsequent analysis of these 34 substrates revealed that 20 of them contained a potential PKA phosphorylation motif (based on Perseus software used for analysis). Next, *Atg5*flox:*CamKIIα*-Cre KO cortical slices were stimulated with Forskolin or DMSO as control (Fig. 22D). PKA phosphorylation targets identified to be less phosphorylated in bulk analysis *in-vivo* (Fig. 20A,B) were less sensitive to Forskolin treatment in *Atg5*flox:*CamKIIα*-Cre KO cortico-hippocampal brain slices compared to WT (Fig. 22E). In agreement with the data above, cellular component GO enrichment analysis indicated that most of the putative PKA phospho-targets affected by the ATG5 deletion were localized to PSD of glutamatergic synapses in both mouse lines (Fig. 22F). Finally, the vast majority of substrates significantly downregulated in global phosphoproteome (Fig. 20A,B) were not reacting to forskolin treatment in cortical slices prepared from *Atg5*flox:*CamKIIα*-Cre KO mice (Fig. 22G) and this identified Forskolin-“irresponsive” targets in KO neurons contained proteins enriched at the PSD of excitatory synapses (Fig. 22H).

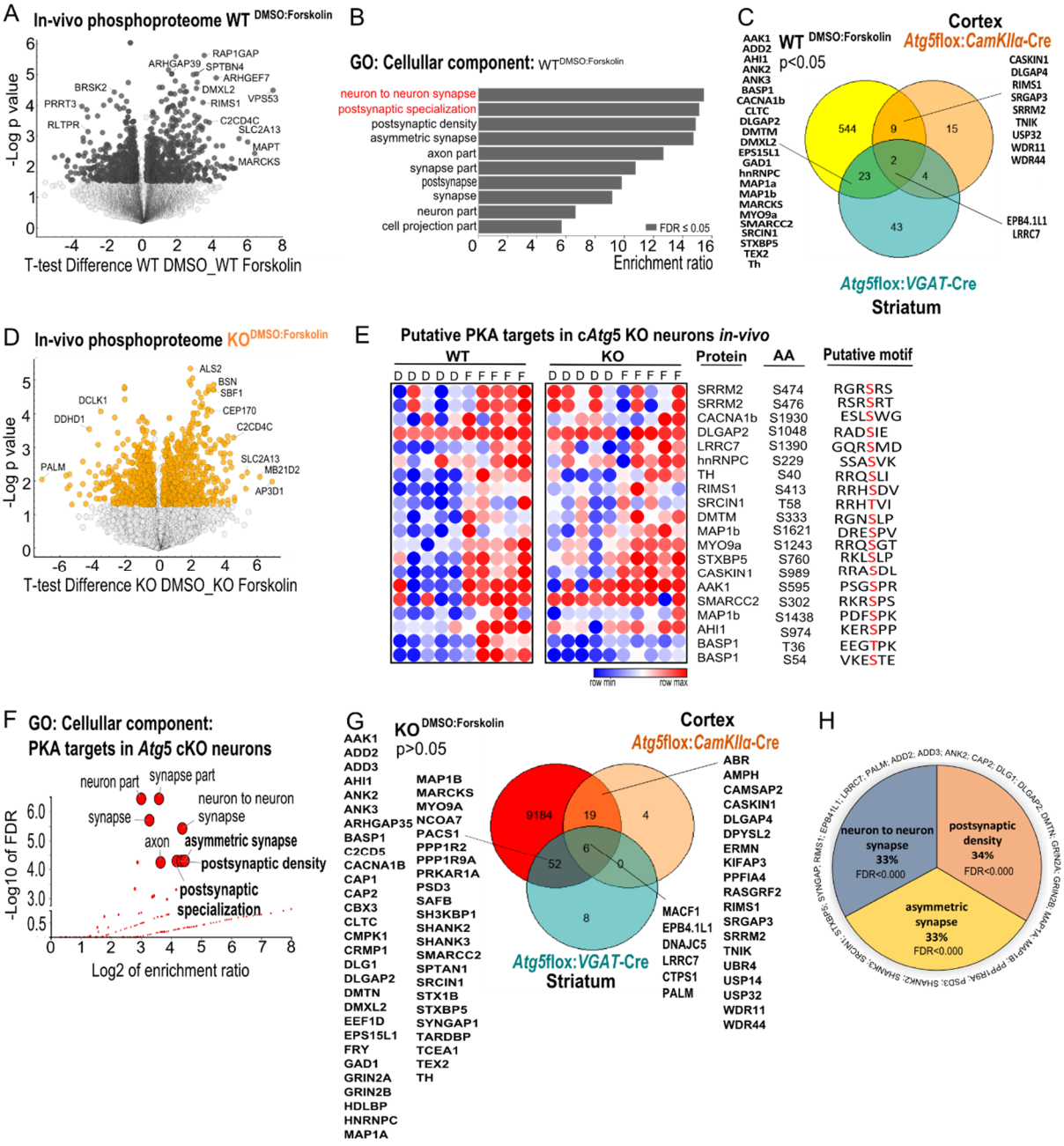

Figure 22: Neuronal ATG5 deficiency diminishes PKA-mediated phosphorylation of proteins enriched at postsynaptic density of excitatory synapses.

(A) Phosphoproteome analysis of acute cortico-hippocampal brain slices (300 µm) from wild-type mice stimulated with 50 µM Forskolin or DMSO as a control for 15 min prior to homogenization. The volcano blot illustrates all detected phosphosites. Highlighted are the proteins with p<0.05 and a FC>1.2/<-1.2. **(B)** GO Cellular component pathway analysis revealed that most phosphosites responding to Forskolin (dataset shown in A) in WT brain slices (p<0.05, FC>1.2) are associated with the synapses, primarily the postsynaptic density. **(C)** Venn diagram analysis on the phosphoproteome data of *Atg5*flox:*CamKII*-Cre (Fig. 20A), *Atg5*flox:*VGAT*-Cre (Fig. 20B) and Forskolin responsive phosphosites (p<0.05, FC>1.2) showed that several proteins with decreased phosphorylation in autophagy-deficient mice brain lysates were upregulated due to Forskolin treatment. **(D)** Global phosphoproteome analysis was performed on 300 µm thick brain slices of *Atg5*flox:*CamKII*-Cre KO mice

either incubated with 50 µM Forskolin (15 min) or DMSO as control prior to homogenization. The Forskolin treatment increased/ decreased phosphorylation of several proteins illustrated in the volcano blot. Highlighted are the proteins with p<0.05 and a FC>1.2. **(E)** Several putative PKA phosphorylation targets, responding to Forskolin stimulation, detected in WT (C) showed no reaction to Forskolin stimulation in *Atg5*flox:*CamKII*-Cre KO acute brain slices as illustrated by the heatmap. Several of the proteins reacting to Forskolin stimulation in WT brain but were Forskolin irresponsive in KO brain contained a putative PKA phosphorylation motif (based on Persues software). **(F)** GO cellular component pathway analysis revealed that putative PKA targets *in-vivo* (G) could be associated with a postsynaptic density function/ localization. **(G)** Venn diagram analysis was performed with Forskolin irresponsive phosphosites detected in *Atg5*flox:*CamKII*-Cre KO brain slices (G) and the phosphoproteome data of brain lysates from autophagy-deficient mice (Fig. 20A,B). The graph demonstrates that the proteins, which are not phosphorylated as a response to Forskolin stimulation (p>0.05), are also downregulated in the brains of autophagy-deficient mice (p<0.05 and an FC< -1.2). **(H)** GO Cellular component analysis showed that phosphosites irresponsive to Forskolin stimulation in KO brains that show a decreased phosphorylation in total global phosphoproteome analysis are functional at the postsynaptic density.

The posttranslational modification of PSD-confined proteins by serine or threonine phosphorylation has been shown to profoundly affect localization, clustering characteristics and synaptic shape (Wu et al. 2017a; Wang et al. 2014; Koh et al. 1999). DLG was shown to localize at synapses when dephosphorylated, whereas phosphorylation induces dissociation (Koh et al. 1999). If ATG5-dependent cAMP/PKA-dependent signalling is a crucial regulator of phosphorylation of PSD-confined protein, then decreased phosphorylation of these proteins in the absence of ATG5 might affect the morphological property of the postsynaptic density in autophagy-deficient neurons. In agreement with this hypothesis, electron microscopic analysis reveals that the area of the postsynaptic density was significantly increased in neurons lacking ATG5 (Fig. 23A,B).

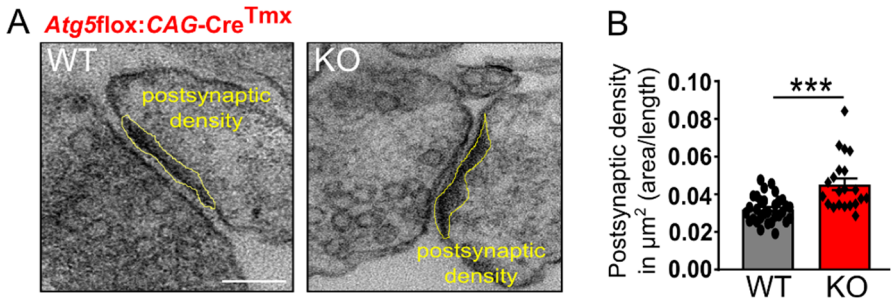

Figure 23: Decreased PKA signalling drives changes in postsynaptic density morphology.

(A,B) The thickness of the postsynaptic density was increased in electron microscope acquired pictures of ultrathin (70nm) sections from primary *Atg5*flox:CAG-Cre^{Tmx} cortico-hippocampal KO neurons pointing to

morphologically changes based on autophagy-mediated alterations in PKA signalling (WT: 0.032± 0.0013, KO: 0.045± 0.003). p <0.0001, n_{WT}=31, n_{KO}=21 from n=3 independent experiments. Scale bar: 120 nm.

Collectively, the data indicate that ATG5 functions in neurons to modulate PKA-dependent phosphorylation of the (post)synaptic proteome independently of their total protein level. Furthermore, the data suggest that ATG5-dependent protein phosphorylation can serve as a crucial regulator of postsynaptic protein localization and trafficking.

8.7 Autophagy-dependent PKA signalling regulates postsynaptic GLUR1 localization and is responsible for regulating neuronal excitability.

What are the mechanistic implications of decreased phosphorylation of postsynaptic density-confined proteins for the physiology of ATG5 KO neurons? The postsynaptic density of synapses includes cytoskeletal, scaffold proteins, receptors and ion channels, and the phosphorylation state of these components is known to be central to synaptic transmission (Esteban et al. 2003; Poisbeau et al. 1999; Uematsu et al. 2015; Wu et al. 2017a). The size of postsynaptic density is a common characteristic of neuronal excitability per se, where the larger size of the PSD is positively correlated with higher numbers of AMPA-type glutamate (AMPA) receptors (Takumi et al. 1999; Tao-Cheng 2019). Furthermore, PKA directly regulates synaptic function via neuronal activity-dependent internalization of AMPAR subunit GLUR1 from the postsynaptic plasma membrane (Lee et al. 2003). This function of PKA requires the interaction of its type II regulatory subunit α with AKAP79/150 (Tavalin et al. 2002; Carr et al. 1992) and involves PKA-dependent phosphorylation of GLUR1 at Ser845 (Esteban et al. 2003; Ehlers 2000). Thus, it is likely that autophagy-dependent PKA signalling regulates synaptic neurotransmission by directly controlling the trafficking of AMPA receptors. To test this hypothesis, the levels of total GLUR1 and phosphorylated GLUR1 at Ser845 were analyzed in *Atg5*flox:*CamKIIα*-Cre and *Atg5*flox:*VGAT*-Cre WT and KO mice by western blotting. The total protein level of GLUR1 was unaltered in brains lacking ATG5 (Fig. 24A,C). This finding agreed with the data from global proteome analysis in which robust changes (p<0.05, FC1.2) for AMPA receptor subunits were undetectable (data not shown). In addition to the unchanged level of GLUR1 also the level of phosphorylated GLUR1 (Fig. 24B) as well as the level of anchor protein AKAP79/150, the protein that recruits and allocate PKA close to AMPA receptors were

unchanged in global proteomic analysis from *Atg5*flox:*CamKIIα*-Cre KO mice (Fig. 24E; demonstrated by LFQ values). Interestingly, GLUR1 phosphorylation at Ser845 was slightly reduced in striatal lysates from *Atg5*flox:*VGAT*-Cre KO mice, although this effect did not reach significance (Fig. 24D). This phenotype was accompanied by a significant reduction in total levels of AKAP79/150 in inhibitory ATG5-deficient neurons (Fig. 24F), suggesting that PKA-dependent phosphorylation of GLUR1 might be differentially regulated in excitatory and inhibitory neurons.

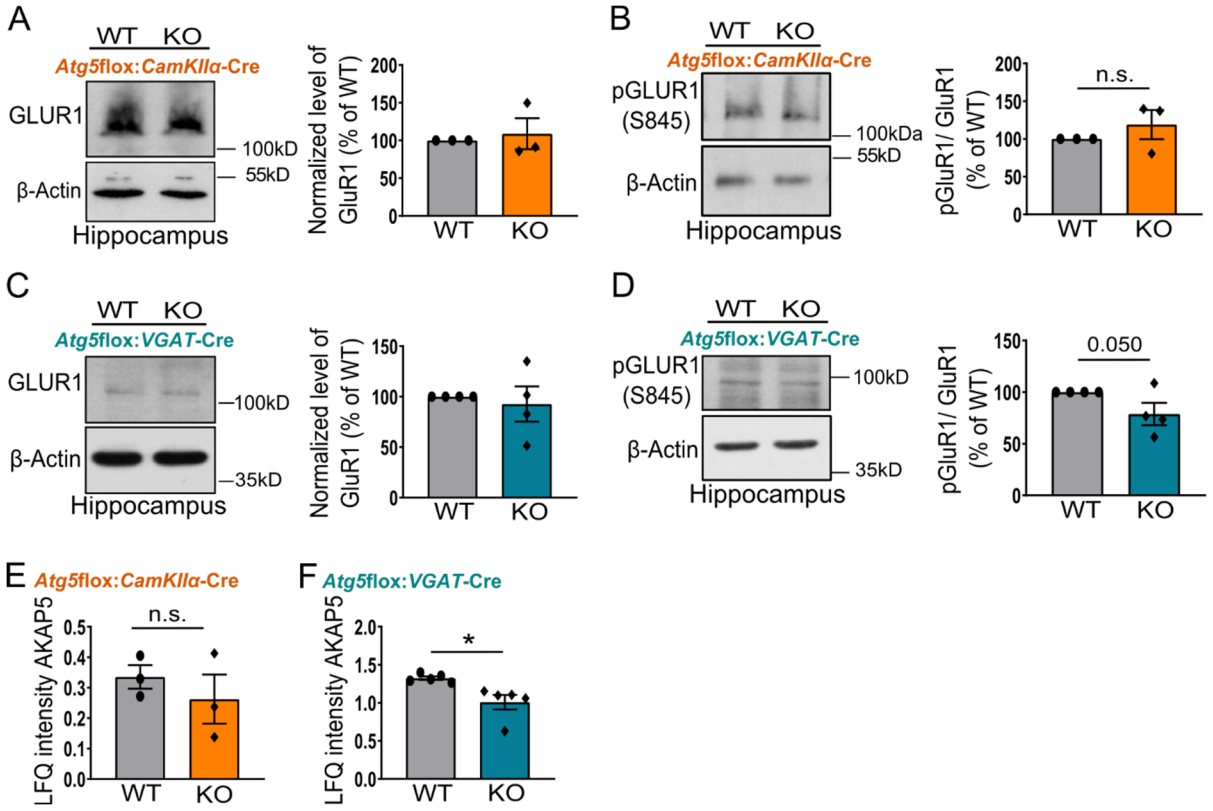

Figure 24: Autophagy-dependent PKA signalling does not directly affect total or phosphorylation levels of GLUR1.

(A) Total protein levels of AMPA receptor subunit GLUR1 were unaltered in *Atg5*flox:*CamKIIα*-Cre hippocampal brain lysates (WT set to 100%, KO: 108.9± 20.47%). p=0.3427, n=3. Performed one-tailed unpaired t-test. **(B)** Protein levels of phosphorylated GLUR1 at serine 845 were unchanged in *Atg5*flox:*CamKIIα*-Cre hippocampal KO brain lysates compared to WT (WT set to 100%, KO: 104.2± 16.97%). p=0.4086, n=3. Performed one-tailed unpaired t-test. **(C)** The total protein level of GLUR1 was also unchanged in *Atg5*flox:*VGAT*-Cre hippocampal brain lysates in KO compared to WT (WT set to 100%, KO: 92.74± 17.48%). p=0.3462, n=4. Performed one-tailed unpaired t-test. **(D)** The phosphorylation of AMPA receptor subunit GLUR1 at serine 845 was decreased in hippocampal brain lysates of *Atg5*flox:*VGAT*-Cre KO mice compared to WT, but the p-value did not reach significance (WT set to 100%, KO: 66.10± 9.464%). p=0.0058, n=4. Performed one-tailed unpaired t-test. **(E)** LFQ values from isotope labelled spike-in analysis (Fig. 20A) were used to detect changes in AKAP5 (AKAP79) protein

level in *Atg5*flox:*CamkIIα*-Cre KO mice and revealed no changes (WT: 0.3356±0.03859, KO: 0.2625± 0.08046). p=0.4588, n=3. Performed a two-tailed unpaired t-test. **(F)** LFQ values from isotope labelled spike-in analysis (Fig. 20B) from *Atg5*flox:*VGAT*-Cre KO mice revealed a significant downregulation of anchor protein AKAP5 (AKAP79) in autophagy-deficient inhibitory neurons (WT: 1.325±0.02370, KO: 1.008± 0.09625). p=0.0128, n=5. Performed a two-tailed unpaired t-test.

To further unravel the mechanism of hyperexcitability of autophagy-deficient neurons, GO molecular function analysis was performed using g:Profiler (Raudvere et al. 2019) and the dataset of "forskolin- irresponsive" PKA phosphorylation targets in KO condition. In agreement with the fact that PKA phosphorylates many cytoskeletal substrates in non-neuronal cells (Shabb 2001; Howe 2004), "cytoskeletal protein binding" (32% of proteins) and "actin-binding" (20% of proteins) proteins were the most abundant GO molecular function terms among downregulated phospho-targets in autophagy-deficient neurons (Fig. 25A). Strikingly, analysis performed using the human phenotype ontology database (g:Profiler) indicated that proteins identified as being decreased in their phosphorylation state in brains of autophagy-deficient mice are associated with EEG abnormality and seizure onset in humans (Fig. 25A). These data, taken together with the fact that about 37% of "cytoskeletal protein binding" proteins identified in Fig. 25A are directly involved in endocytosis (CLTC) and trafficking (ANK3, DLG1, DPYSL2, EPB41L1, PPP1R9A, SHANK3 and STXBP5 (Carroll et al. 1999; Smith et al. 2014; Leonard et al. 1998; Zhang et al. 2020; Shen et al. 2000; Wu et al. 2008; Uchino et al. 2006; Shen et al. 2020) of GLUR1 subunit of AMPARs (Fig. 25B), suggested that GLUR1 trafficking rather than its direct phosphorylation by PKA might be a crucial determinant of neuronal excitability in ATG5 KO neurons. In line with this hypothesis and the data described above, the colocalization of GLUR1 and postsynaptic density marker PSD95 was increased in primary cortico-hippocampal ATG5 KO neurons (Fig. 25C,D). This phenotype directly resulted from the loss of ATG5 function since overexpression of ATG5 tagged with eGFP normalized postsynaptic density (PSD)-confined GLUR1 localization (Fig. 25E). On the other hand, overexpression of PKA subunits R1-α and R1-β mimicked the phenotype of ATG5 KO neurons and induced the accumulation of GLUR1 at the PSD (Fig. 25F), indicating that increased postsynaptic levels of GLUR1 in autophagy-deficient neurons resulted from diminished PKA signalling. Since total levels of GLUR1 were not altered in either proteomic datasets or the western blotting analysis

(see above), GLUR1 accumulation at the postsynapse could be caused by a decreased endocytosis rate from the plasma membrane. To directly probe whether the defects in GLUR1 distribution reflect diminished retrieval of GLUR1 from the plasma membrane, autophagy-deficient neurons were transfected with a commercially available plasmid expressing GLUR1 and a pH-sensitive variant of GFP that undergoes quenching within the acidic SV lumen and is unquenched on exocytic fusion with the plasma membrane (Kononenko et al. 2013). In KO neurons, superfused with buffers titrated either to pH 5.5 (to reveal the surface exposure of pHluorin) or to pH 8.5 (to reveal the total levels of pHluorin) (Fig. 25G,H), the surface-stranded/total GLUR1-pHluorin ratio was elevated in KO neurons compared with their WT littermates (Fig. 25I).

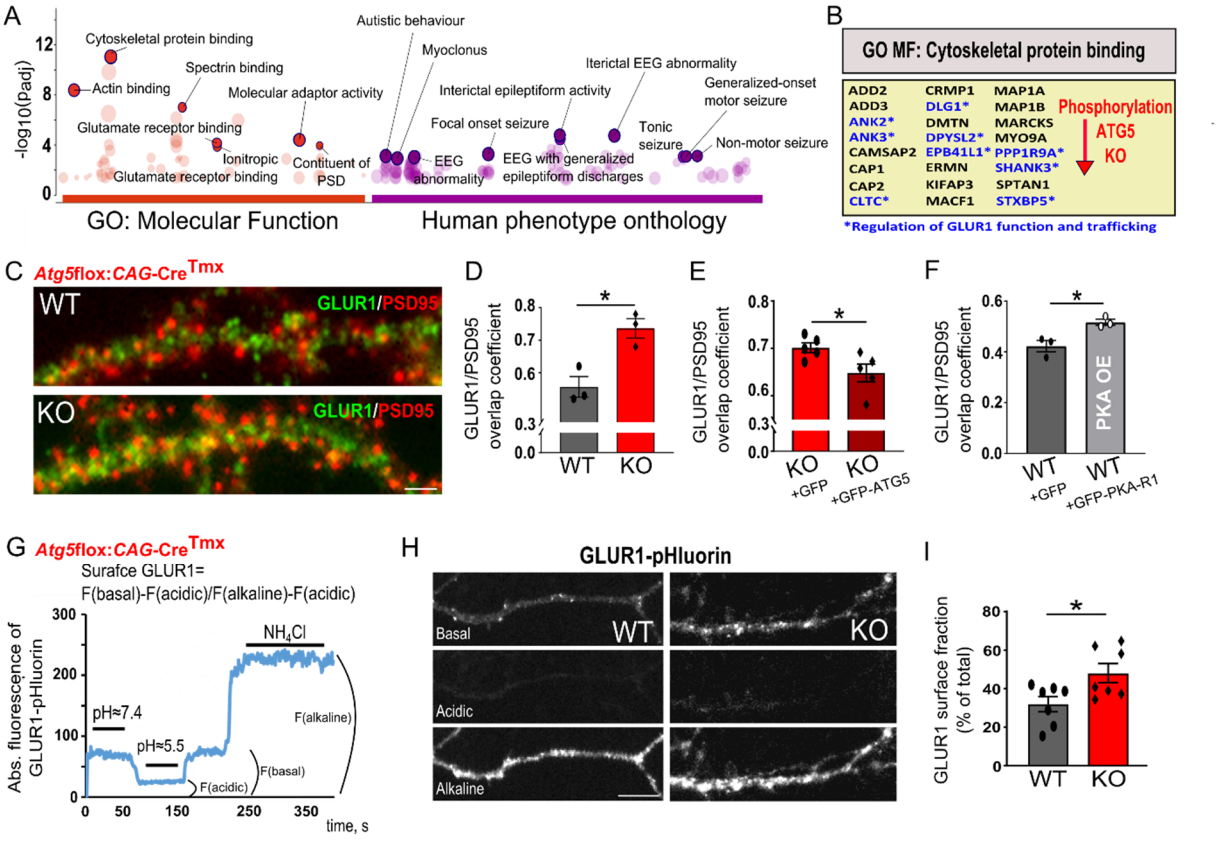

Figure 25: Autophagy-dependent PKA signalling regulates postsynaptic GLUR1 localization.

(A) GO molecular function analysis and human phenotype ontology database analysis were performed on phosphosites with decreased phosphorylation in *Atg5*flox:*CamKIIα*-Cre and *Atg5*flox:*VGAT*-Cre KO mice brain tissue ($p<0.05$, FC< -1.2) that were irresponsive to Forskolin induction in *Atg5*flox:*CamKIIα*-Cre KO brain slices ($p>0.05$). Several cytoskeletal proteins showed decreased phosphorylation in autophagy-deficient brains. Analysis was done using g:Profiler. **(B)** Several phosphosites that were classified as "cytoskeletal protein binding" during molecular function analysis are known to be involved in AMPA receptor function and

trafficking. **(C-D)** Co-localization analysis of GLUR1 and PSD95 in *Atg5*flox:*CAG*-Cre^{Tmx} WT and KO neurons showed an increased localization of GLUR1 at the postsynaptic density of autophagy-deficient neurons (WT: 0.56±0.03, KO: 0.74±0.02). p=0.0144, n_{WT}=23, n_{KO}=26 pictures analysed from n=3 independent experiments. Scale bar: 2 µm. Performed unpaired two-tailed t-test. **(E)** *Atg5*flox:*CAG*-Cre^{Tmx} KO neurons were transfected with GFP or ATG5 tagged with GFP to rescue ATG5 protein level. The rescue of ATG5 restored GLUR1 and PSD95 colocalization (WT: 0.70± 0.017, KO: 0.65± 0.02). p=0.0379, n_{KO+GFP}=33, $n_{KO+GFP-ATG5}$=37 pictures analysed from n=5 independent experiments. Performed unpaired two-tailed t-test. **(F)** The overexpression of PKA R1-α and PKA R1-β in wildtype cortico-hippocampal neurons resulted in a significantly increased GLUR1 and PSD95 overlap coefficient mimicking the KO situation (WT: 0.42± 0.025, KO: 0.51± 0.03). p=0.0213, n_{WT+GFP}=46, $n_{WTGFP+PKA\ R1\ OE}$=46 pictures analysed from n=3 independent experiments. Performed unpaired two-tailed t-test. **(G-I)** To assess receptor localization/ endocytosis rate in the postsynaptic density of *Atg5*flox:*CAG*-Cre^{Tmx} WT and KO neurons, neurons were transfected with GLUR1 tagged with pHlourin and forwarded to live-cell imaged in changing buffer conditions. The total surface located GLUR1 was determined from the difference in fluorescence intensity between acidic and alkaline buffer conditions (normalized by baseline). Significantly more GLUR1 was inserted into the postsynaptic density membrane in KO than WT (WT: 31.94± 3.99, KO: 48.01± 4.93). p=0.0262; n_{WT}=35, n_{KO}=48 from n=7 independent experiments. Scale bar in (H): 5 µm. Performed unpaired t-test.

The increased amount of GLUR1-containing AMPAR receptors at the postsynaptic density could be the underlying cause of the increased neuronal excitability observed in *Atg5*flox:*CamKIIα*-Cre KO mice (Fig. 6G). Therefore, an *in-vitro* GCAMP6f imaging assay was employed to measure neuronal excitability. During action potential firing, voltage-dependent Ca^{2+} channels are activated, leading to an activity-dependent rise in intracellular Ca^{2+} levels, which can be detected using genetically encoded Ca^{2+}-sensing probe GCAMP7f. To monitor calcium signals by live-cell imaging, primary cortico-hippocampal neurons isolated from *Atg5*wt:tdTomato or *Atg5*flox:tdTomato mice were infected with an adeno-associated (AAV) virus encoding a *CamKIIα*-GCaMP7f construct and, additionally, with *CamKIIα*-Cre AAV to induce the ATG5 KO. As a *CamKIIα* promoter controls the GCaMP7f reporter, only neuronal calcium signals from excitatory neurons were captured. The calcium responses evoked by tetanic stimulation (four tetani, 100 APs at 100Hz, 3 s stimulus interval) was analysed per cell. KO excitatory neurons had significantly increased facilitation of evoked calcium signals compared to controls (Fig. 26A,C). This facilitation was entirely abolished by pre-incubation of KO neurons with the broad-spectrum AMPA/kainate receptor antagonist CNQX, confirming

that neuronal excitability in autophagy-deficient neurons is driven by glutamate-bound AMPA receptors (Fig. 26B,C). This function of autophagy in the regulation of neuronal excitability was cell-autonomous for excitatory neurons (Fig. 26D,E). It required PKA activity since the application of PKA inhibitor H89 facilitated evoked calcium responses in control neurons (Fig. 26F,G). Furthermore, the cAMP elevating agent forskolin was enough to diminish the frequency action potential firing in excitatory ATG5 KO primary neurons (Fig. 26H, J), whereas Forskolin did not affect the frequency of action potentials in WT neurons (Fig. 26H,I).

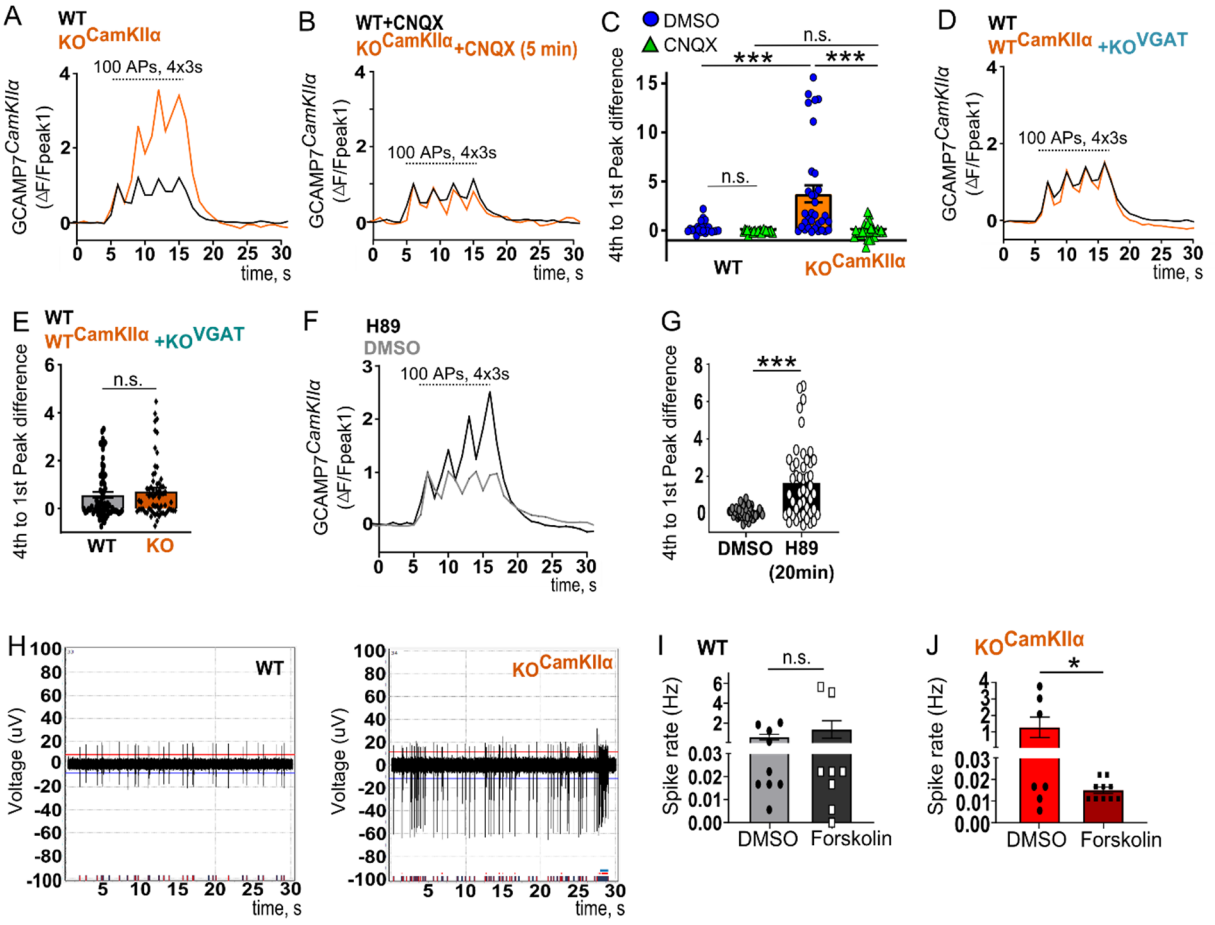

Figure 26: Autophagy-dependent PKA signalling regulates neuronal excitability.

(A-C) Primary cortico-hippocampal *Atg5*flox:tdTomato and *Atg5*wt:tdTomato neurons were virus transfected with *CamKII*α-Cre and *CamKII*α-GCaMP7f. The neurons were stimulated applying consecutive electrical field stimulation (100 action potentials at 100 Hz, 4 stimulations with 3 s interval). Autophagy deficient cells showed significantly increased stimulus-induced facilitation (ΔF/Fpeak1) compared to WT neurons. After the first stimulation the cells were treated with 10 µM CNQX for 5 min which inhibited facilitation in autophagy-deficient neurons (WT_{DMSO}: 0.28± 0.12, WT_{CNQX}: -0.07± 0.03, KO_{DMSO}: 3.74± 0.86, KO_{CNQX}: -0.014± 0.13). $p_{WT\ DMSO/\ KO\ DMSO}$<0,0001, $p_{KO\ DMSO/KO\ CNQX}$<0,0001; $n_{WT\ DMSO}$= 25, $n_{WT\ CNQX}$= 27, $n_{KO\ DMSO}$= 33, $n_{KO\ CNQX}$= 30 from n=4 independent experiments. Analysed using two-way ANOVA with Tukey's multiple comparisons test. **(D,E)** Primary cortico-

hippocampal *Atg5*flox:tdTomato and *Atg5*wt:tdTomato neurons were virus transfected with *GAD67*-Cre and *CamKII*α-GCaMP7f. The neurons were stimulated applying consecutive electrical field stimulation (100 action potentials at 100 Hz, 4 stimulations with 3 s interval). No facilitation of excitatory neurons, calculating the difference between the fourth and the first peak of stimulation, could be detected (WT: 0.5611± 0.1253, KO: 0.7215± 0.1470). p=0.4058; n_{WT}=69, n_{KO}=64 from n=4 independent experiments. Performed a two-tailed unpaired t-test. **(F,G)** WT primary cortico-hippocampal neurons were virus transfected with *CamKII*α-GCaMP7f and treated either with 10 µM H89 or DMSO, respectively, for 20 min prior to electrical stimulation. The neurons were stimulated applying consecutive electrical field stimulation (100 action potentials at 100 Hz, 4 stimulations with 3 s interval) (DMSO: 0.07± 0.04, H89: 1,668± 0.28). p<0.0001; n_{DMSO}=48, n_{H89}=47 neurons from n=3 independent experiments. Performed unpaired t-test. **(H-J)** Network activity (spike rate) of primary cortico-hippocampal *Atg5*flox neurons transfected with *CamKIIα*-GFP-Cre (KO) or *CamKIIα*-GFP (WT) were investigated using the MEA system. Example traces show an increased spike rate of autophagy-deficient neurons compared to WT. The increased spike rate could be rescued in autophagy-deficient cells applying cAMP elevating agent Forskolin (10µM for 72 hrs) to induce PKA signalling (WT_{DMSO}: 0.56± 0.29, $WT_{Forskolin}$: 1.35± 0.88, KO_{DMSO}: 1.27± 0.62, $KO_{Forskolin}$: 0.02± 0.001). $p_{WT\ DMSO/WT\ Forskolin}$=0.40, $p_{KO\ DMSO/KO\ Forskolin}$=0.0270; $n_{WT\ DMSO}$=9, $n_{WT\ Forskolin}$=8, $n_{KO\ DMSO}$: 7, $n_{KO\ Forskolin}$=10. Performed unpaired t-test.

Collectively, the described data reveal a previously unknown role for autophagy in controlling neuronal excitability via regulation of the phosphorylation status of postsynaptic density-confined proteins. Mechanistically, this function of autophagy involves starvation-induced activation of type 1 PKA signalling at synapses, which via cytoskeletal proteins phosphorylation controls the synaptic accumulation of AMPARs.

9. Discussion

The data presented here unravel a new function of the autophagy ubiquitin-like conjugation machinery in neuronal signalling, which maintains excitability in inhibitory and excitatory forebrain neurons. This study shows that ATG5, which regulates the intracellular availability of PKA R1 subunits by starvation-induced selective autophagy, is not only dispensable for the survival of forebrain excitatory neurons (Negrete-Hurtado, Overhoff et al. 2020) but also for forebrain inhibitory neurons. Autophagy modulates AMPA receptor trafficking and surface localization at the postsynaptic density of glutamatergic synapses by PKA-mediated phosphorylation of postsynaptic density cytoskeletal proteins.

9.1 Autophagy-deficiency increases neuronal excitability

The conditional loss of autophagy protein ATG5 in the two mouse models (*Atg5*flox:*CamKIIα*-Cre and *Atg5*flox:*VGAT*-Cre) led to a significant weight reduction, starting after weaning, but had no impact on neuronal survival of cortical (*Atg5*flox:*CamKIIα*-Cre) or hippocampal and striatal (*Atg5*flox:*VGAT*-Cre) neurons, in contrast to several other studies, where autophagy-deficiency was induced using neuronal progenitor-specific promotor, *Nestin* (Hara et al. 2006; Komatsu et al. 2006; Liang et al. 2010; Zhao et al. 2015; Yamaguchi et al. 2018). The mice showed an increased startle response during SHIRPA analysis, often associated with the onset of seizures, which appeared with a difference in the percentage of affected mice per line and considerable differences in the age of onset. The appearance of spontaneous recurrent seizures was also reported in another study using *Atg7*flox:*CamKIIα*-Cre KO mice at 20 weeks of age (McMahon et al. 2012), suggesting that alterations in excitation are based on the lack of autophagy rather than ATG5. Recurring, unprovoked seizures characterize epilepsy, representing the abnormally synchronous activity of neurons in a focal area of the brain or throughout the entire brain, initiated by glutamate triggered EPSPs. Multiple, synchronously EPSPs are responsible for epileptic field potentials mainly driven by surface located AMPA receptors at the postsynaptic density of neurons (Rogawski 2013). The fact that autophagy is involved in neuronal signalling at the presynaptic, as well as the postsynaptic site, was already demonstrated in an emerging number of studies (reviewed in (Liang 2019; Nikoletopoulou and Tavernarakis 2018)), in which autophagy has been described to degrade synaptic vesicles

under control of presynaptic protein Bassoon (Okerlund et al. 2018) or Endophilin A and Synaptojanin that interact with autophagy-related proteins to promote synaptic autophagy (Soukup et al. 2016; Murdoch et al. 2016; Vanhauwaert et al. 2017). Other proteins of the autophagy core machinery are known to mediate synaptic vesicle pool size like ATG16L1, which can bind to GTPase Rab26, localized at the synaptic vesicle membrane, facilitating the recruitment of the autophagy-machinery onto synaptic vesicles to induce their clearance (Binotti et al. 2015), thereby controlling the number of synaptic vesicles available for release (Nikoletopoulou and Tavernarakis 2018). In another study, ATG7, a core component of the autophagy-machinery, was deleted in dopaminergic neurons (*Atg7*flox:*DAT*-Cre), leading to increased axonal profiles and elevated dopamine release upon stimulation (DeJesus-Hernandez et al. 2011). At the postsynapse, autophagy is involved in the degradation of several postsynaptic proteins, like PSD95, PICK1 and SHANK3, (Nikoletopoulou et al. 2017) and receptors like $GABA_A$ and AMPA (Rowland et al. 2006; Shehata et al. 2012). Recently, a published study showed that autophagy could also modulate postsynaptic density organization by degradation of phosphorylated PSD95 at position T19 after NMDA stimulation resulting in a lateral movement of AMPA receptors and LTD (Kallergi et al. 2020). With the selective degradation of postsynaptic density proteins, autophagy is believed to play an essential role in LTD and synaptic pruning events (Lieberman et al. 2019). Autophagy selectively degrades superfluous postsynaptic material to adapt dynamically to changed signalling conditions, contributing to the remodelling of synapses. That could be shown by *in-vitro* stimulation of neurons with a low-dose pulse of NMDA, inducing LTD and a robustly increase in autophagic flux measured by the amount of GFP-LC3 formed puncta in dendrites and spines (Shehata et al. 2012). With these functions, autophagy is believed to play a role also in learning and memory formation since several studies could demonstrate that the induction of autophagy rescued cognitive impairments at the cellular and organismal level (Yan et al. 2018; Zhai et al. 2018; Fu et al. 2017; Li et al. 2016). In line with that, memory impairment, scored by the number of c-FOS positive neurons in the hippocampal dentate gyrus after novel object recognition in an open field arena, was observable in *Atg5*flox:*CamKIIα*-Cre mice (Negrete-Hurtado, Overhoff et al. 2020). This study indicates that autophagy contributes to the regulation of synaptic function by additionally controlling the phosphorylation state of postsynaptic proteins, a function mediated by the PKA.

The current study took advantage of global spike-in proteome analysis on brain lysates and label-free proteome analysis of FACS-sorted KO neurons from two autophagy-deficient mice lines. Besides a downregulation on the total protein level of Bassoon in *Atg5*flox:*CamKIIα*-Cre and Piccolo in both lines, the protein level of prominent synaptic vesicle endo- and exocytosis associated proteins were unchanged. Furthermore, autophagy at presynapses was reported to maintain the pool of functional mitochondria by selective degradation, called mitophagy mediated by LRRK2 and Endophilin A (Soukup et al. 2016; Arranz et al. 2015). Global spike-in proteome data from *Atg5*flox:*CamKIIα*-Cre but not *Atg5*flox:*VGAT*-Cre revealed a minor enrichment of mitochondrial located proteins (data not shown), and analysis of electron microscopy acquired pictures from *Atg5*flox:*CAG*-Cre^{Tmx} KO neurons showed an increased average number of mitochondria at the active zone. However, mitochondrial function was unchanged in cultured ATG5 KO neurons compared to WT, measured via oxygen consumption rate using Seahorse XFe96 analyser (Negrete-Hurtado, Overhoff et al. 2020). Another recently published study observed accumulation of tubular ER in axons of ATG5-deficient primary granular neurons, suggesting an increased calcium release from the accumulated tubular ER as the underlying reason for increased stimulation-dependent SV release (Kuijpers et al. 2021). Global spike-in proteome analysis revealed an enrichment of endoplasmic reticulum-associated proteins in KO brain lysates of both lines, a finding that was abolished entirely in *Atg5*flox:*CamKIIα*-Cre FACS-sorted KO neurons. Furthermore, in cortico-hippocampal primary ATG5-deficient neurons *in-vitro*, no changes in neurotransmitter release were observable, making usage of a pH-sensitive fluorescent protein pHluorin fused to Synaptobrevin2 (SYB2) to track synaptic vesicle release upon electrical stimulation (Negrete-Hurtado, Overhoff et al. 2020). Next to autophagy receptor proteins known to accumulate under autophagy-deprived conditions (e.g. GABARAPL2, SQSTM1/p62), PKA R1-α and R1-β subunits, but neither PKA R2 nor catalytic subunits were significantly enriched, a finding that could be robustly proven by western blotting. The upregulation of PKA regulatory subunits type 1 was detectable in both classes of autophagy-deficient excitatory and inhibitory forebrain neurons and is, therefore, not a neuronal subtype-specific cargo. PKA R1 subunits were found to locate at synapses and mitochondria primarily, a pattern intensified by the deletion of ATG5. PKA signalling in neurons is known to be a key player in the LTP induced protein synthesis (Kandel 2001), modulation of neurotransmitter receptor channel conductance (Roche et al. 1996; Greengard

et al. 1991; Wang et al. 1991; Banke et al. 2000) and activity-dependent AMPA receptor trafficking (Esteban et al. 2003; Ehlers 2000). These functions of PKA are based on precise spatio-temporal regulation of the PKA holoenzyme and the level of intracellular cAMP. The PKA regulatory subunits type 2 are recruited to membranous compartments by anchoring proteins (AKAPs), whereas the PKA regulatory subunits type 1 are mainly cytosolic (Walker-Gray et al. 2017). As the catalytic subunits of PKA are bound to the regulatory subunits, their phosphorylation targets differ based on the regulatory subunits localization. Necessary for the PKA signalling dynamic is that the protein level of the regulatory subunits vastly outnumbers the catalytic subunits to support rapid catalytic subunit reassociation (Walker-Gray et al. 2017; Aye et al. 2010). PKA signalling is induced due to an increase of intracellular cAMP level, which can be induced, among others, by synaptic signalling dependent rise of intracellular calcium concentration (Halls and Cooper 2011). Autophagy seems to modulate this well-established signalling pathway by controlling the abundance of the regulatory subunit type 1.

9.2 Autophagy modulates PKA signalling by the degradation of PKA R1 subunits

This study could show that PKA R1 subunits are autophagy targets since a block in lysosomal degradation increased and the induction of autophagy, applying starvation, decreased the protein level of PKA R1-α and PKA R1-β and induced the colocalization with autophagy-receptors p62 and NBR1. Furthermore, PKA R1-a and R1-β were detectable in lysates of autophagosomes isolated from mouse brains and localized to autophagosome vesicles at immunogold labelled brain slices. Accumulation of PKA R1-α was recently described to be associated with impaired autophagy in *Atg7*flox:*Syn*-Cre and *Atg14*flox:*Syn*-Cre KO mice (Deng et al. 2021) and linked to autophagy function in glucose metabolism in cancer cells. Subsequently, performed experiments in the study of Deng et al. (2021) identified AKAP11 as a selective autophagy receptor for PKA R1-α degradation. However, the current study showed that autophagy degradation was not selective for PKA R1-α but also targeted PKA R1-β and is not limited to glucose starvation, but in contrary, can be induced by amino acid and serum starvation in neurons. Furthermore, from all the performed global proteome analyses, AKAP11 was only enriched in the global proteome of *Atg16L1*flox:*CAG*-Cre KO primary neurons, making it questionable that AKAP11 functions as an autophagy-receptor for PKA R1-

α in neurons. Another study aiming to define the impact of autophagy on the half-time of proteins could show that the block of autophagy in ATG5- and ATG7-deficient fibroblasts increased PKA R1-α half-time (Zhang et al. 2016), underpinning its autophagic degradation. Close regulation of PKA and autophagy was already observed in *Saccharomyces cerevisiae*, in which elevated levels of PKA activity inhibited autophagy and wise versa the inactivation of PKA signalling robustly induced autophagy (Stephan et al. 2009), pointing forward to feedback regulation. In contrast to this finding, a study performed in mammalian (MEF) cells showed that PKA R1-α colocalized with LC3 labelled autophagosomes, suggesting autophagosomal degradation, but they report a negative regulation of mTOR activity by PKA (Mavrakis et al. 2006). In this study, the relationship between mTOR regulated autophagy and PKA R1-α and R1-β protein levels was not noticeable. The application of Torin 1, an mTOR inhibitor, was not sufficient to decrease the PKA R1 subunit protein level significantly in contrast to 16 hours of starvation. Nevertheless, the protein level of pS6, a downstream target of mTOR, was significantly reduced in both conditions, leaving the door open for further investigation if PKA degradation is mTOR-dependent or independent. Two pathways that could likely mediate mTOR-independent regulation of PKA by autophagy in response to starvation are the AMPK/TSC pathway and the JNK1/Beclin-1/PI3KC3 pathway (Sarkar 2013). AMPK is phosphorylated and activated by LKB1 under low energy conditions during nutrient deprivation (Inoki et al. 2003; Inoki et al. 2006). The activation of AMPK increases autophagy, usually through mTORC1 inactivation, but was also shown to induce autophagy directly through phosphorylation of ULK1 and Beclin-1, in a mechanism distinct to that mediated by amino acid starvation (Egan et al. 2011; Kim et al. 2011a). Starvation also induces the activation of JNK1, initiating the JNK1/Beclin-1/PI3KC3 pathway. Activated JNK1 phosphorylates BCL-2 leading to its dissociation from Beclin-1, thereby promoting the formation of autophagy-stimulatory Beclin-1–hVps34 complex (Pattingre et al. 2005; Wei et al. 2008). This pathway was shown to be independent of mTOR since rapamycin showed no effect on JNK1 and Bcl-2 phosphorylation (Sarkar et al. 2011). Taken together, several studies, including this study, report that the PKA regulatory subunits type 1 are autophagy targets. However, the current study is the first to identify that PKA regulatory subunit type 1 autophagy-dependent degradation in neurons is induced by amino acid and serum starvation.

This function is independent of mTOR, but how autophagy is induced remains to be elucidated.

PKA signalling is induced by cAMP binding to the regulatory subunits, which undergo a conformational change, releasing the catalytic subunits to phosphorylate their downstream targets (Taylor et al. 2012). This study could show that the enriched protein level of PKA regulatory subunits type 1 in ATG5-deficient neurons sequestered a bigger proportion of the catalytic subunits compared to control conditions. The observed misbalance led to impaired PKA signalling in autophagy-deficient cells after signalling induction using cAMP-elevating agent Forskolin and downstream target pCREB protein level as a readout. This finding was supported by RNA-sequencing data, which revealed a downregulation of genes containing a CREB responsive binding element. It could be excluded that altered levels of intracellular cAMP were the underlying reason for decreased PKA phosphorylation since the levels were unchanged in autophagy-deficient mouse brain lysates and isolated neurons. Furthermore, this study could demonstrate that autophagy modulates PKA signalling in neurons since starvation not only decreased the protein level of the PKA R1 subunits but was also sufficient to elevate the phosphorylation level of PKA targets and pCREB protein level in neurons. The regulation of PKA signalling by autophagy was also shown in another study, in which glucose starvation led to increased phosphorylation of CREB, a well-known PKA substrate, likely caused by elevated PKA activity in both HEK293T and HCT116 cells due to selective degradation of PKA R1-α mediated by AKAP11 (Deng et al. 2021). In the study of Deng et al. (2021), starvation was initiated by a lack of glucose in non-neuronal cells, whereas the present study induced starvation by amino acids and serum starvation in neurons. These differences leave space for further investigations to unravel differences and similarities for the role of autophagy regulated PKA signalling in non-neuronal and neuronal cells. Furthermore, the present study could show that the overexpression of ATG5 in WT cells was sufficient to elevate PKA activity using pCREB protein level as readout. These findings unravel a new function of autophagy: the selective degradation of PKA R1-α and R1-β subunits under nutrient deprivation and, more importantly, shows for the first time that autophagy modulates PKA signalling in neurons.

9.3 Diminished PKA signalling in autophagy-deficient neurons affects AMPA receptor localization, leading to increased excitability of excitatory neurons

Global spike-in phosphoproteome analysis was performed to identify which target proteins are mainly affected by decreased PKA phosphorylation in brain lysates of autophagy-deficient mice. GO cellular component analysis identified that decreased phosphorylation affected mainly proteins in the postsynaptic density of excitatory synapses in both mouse lines. Subsequently, PKA phosphorylation targets in brain tissue were identified, treating acute cortico-hippocampal brain slices with cAMP elevating agent Forskolin. GO cellular component analysis showed that mainly postsynaptic proteins are phosphorylation targets of PKA, and several of them were observed to be less phosphorylated in brain lysates of autophagy-deficient mice. When treating brain slices from *Atg5*flox:*CamKIIα*-Cre KO mice with Forskolin, several previously identified target proteins were irresponsive to Forskolin stimulation, even though they contained a PKA phosphorylation motif, supporting the finding of diminished PKA signalling. Several of these irresponsive phosphorylation sites showed decreased phosphorylation in the spike-in global phosphoproteome dataset. Interestingly, GO molecular function analysis revealed that Forskolin irresponsive phosphosites in autophagy-deficient mice could be associated with the cytoskeleton of the excitatory synapses' postsynaptic density involved in glutamate receptor trafficking. The phosphorylation state of cytoskeletal proteins at the postsynaptic density was recently associated with homeostatic plasticity, also called synaptic scaling, and associated with PKA signalling (Desch et al. 2021). Homeostatic plasticity allows neurons to bidirectionally scale excitatory postsynaptic strengths to prevent neuronal hyper- or hypoactivity that could otherwise result in neuronal network dysfunction (Wu et al. 2021; Chowdhury and Hell 2018; Fox and Stryker 2017). Homeostatic adaptation of synaptic strength is achieved through the functional availability of AMPA receptors at the postsynaptic site (Chowdhury and Hell 2018; Turrigiano et al. 1998) and is believed to counteract the positive feedback process, the Hebbian plasticity (Pozo and Goda 2010; Rabinowitch and Segev 2008). The scaling of glutamatergic synapses mainly depends on network activity-mediated, calcium-dependent AMPA receptor trafficking, leading to alterations in AMPA receptor surface presentation (O'Brien et al. 1998; Turrigiano 2008). Studies addressing the process of homeostatic plasticity use TTX to inhibit neuronal signalling, inducing synaptic upscaling, leading to increased insertion of AMPA receptors into the PSD

membrane, and Bicculin, a GABA receptor inhibitor, inducing synaptic downscaling leading to internalization of AMPA receptors (Moulin et al. 2020). A study investigating synaptic scaling in cortical neurons *in-vitro* focused on the changes in the global phosphoproteome (Desch et al. 2021). They found that synaptic down-scaling, but not up-scaling, requires the rapid phosphorylation of cytoskeletal proteins at the postsynaptic density. Surprisingly, several of the identified candidates essential for synaptic homeostasis, more precisely the down-scaling of glutamatergic synapses after Bicculine treatment (Desch et al. 2021), for example, LRRC7, DLG4, MAP1A, DLGAP4, RIMS1, DLGAP2, SHANK3, STXBP5, SYNGAP1, EPB1L1, were downregulated in autophagy-deficient brains and several of the proteins can be associated with the trafficking of AMPA receptors (SHANK3, STXBP5, EPB1L1, DLG1). Furthermore, PKA activity was found to be induced after Bicculine treatment (Diering et al. 2014), and PKA R1 was identified as the kinase mainly involved in the down-scaling of synapses (Desch et al. 2021), bringing PKA into the spotlight of postsynaptic cytoskeletal remodelling in excitatory synapses. Homeostatic synaptic plasticity is known to be induced by prolonged changes in neuronal activity to maintain network stability and to prevent runaway excitation (Turrigiano 2008; Siddoway et al. 2014) mediated by the number of AMPA receptors at the surface (O'Brien et al. 1998; Siddoway et al. 2014) and was associated with the genesis of aberrant states, such as addiction, epilepsy or autism (Turrigiano 2008; Lignani et al. 2020; Tien and Kerschensteiner 2018). Defects in PKA-signalling activity, as observed in autophagy-deficient cells, and the association of PKA R1 signalling functioning in down-scaling of synapses (Desch et al. 2021), could interfere with AMPA receptor internalization at glutamatergic synapses resulting in increased excitability in ATG5 depleted neurons. Strikingly, human gene ontology analysis of the less phosphorylated proteins identified during global spike-in phosphoproteome could be associated with different forms of epilepsy, suggesting that alterations in cytoskeletal protein phosphorylation leading to AMPA receptor misdirection are the underlying cause for the observed seizures appearing in autophagy-deficient mice.

To further investigate if diminished PKA signalling leads to misdirection of AMPA receptors at the postsynaptic density, colocalization analyses of AMPA receptor subunit GLUR1 and postsynaptic density protein PSD95 were performed. This study could show that enrichment of GLUR1 at the postsynaptic density depends on ATG5 protein level/ autophagy function since the overexpression of ATG5 in autophagy-deficient neurons rescued the enrichment of

GLUR1 at the postsynaptic density. GLUR1 recruitment to postsynaptic densities was PKA-dependent since the overexpression of PKA regulatory subunits type 1 mimicked the observation made in autophagy-deficient neurons. Furthermore, it could be shown that enriched AMPA receptors were inserted into the postsynaptic density membrane, leading to an increased surface presentation of AMPA receptors in autophagy-deficient neurons. Increased AMPA receptor presentation at the postsynapse is associated with increased excitation (Rogawski 2013), a finding supported by increased postsynaptic density thickness in autophagy-deficient neurons.

Four different AMPA receptor subunits are known so far, GLUR1-GLUR4 that presents different characteristics. One AMPA receptor consists of 4 subunits, which can differ in their subunit composition. Thereby the dominant AMPA receptor composition (80%) at CA1 neurons of the hippocampus are heterotetramers of GluA1 and GluA2 (Lu et al. 2009), which seems to be the case for several brain regions as it was shown by co-immunoprecipitation analysis of the rat nucleus accumbens, dorsal striatum, prefrontal cortex, and hippocampus (Reimers et al. 2011). AMPA receptor trafficking is activity-dependent, and the cycling into and out of the postsynaptic membrane is highly dynamic, whereas NMDA receptors are relatively stable at synapses and undergo only minimal cycling (Anggono and Huganir 2012). A former study linked GLUR1 phosphorylation and PKA activity to bidirectional homeostatic plasticity, showing that homeostatic scaling-up required the phosphorylation of GLUR1 at S845 by AKAP5 recruited PKA, whereas the process of scaling-down leads to decreased phosphorylation level of GLUR1 S845 (Diering et al. 2014). In general, the dephosphorylation of GLUR1 S845 is believed to destabilize AMPA receptor surface presentation at the synapse (Ehlers 2000; Lee et al. 2000; Man et al. 2007). However, in autophagy-deficient brain lysates, the total protein level of GLUR1 was unchanged, the phosphorylation of GLUR1 S845 appeared to be unchanged in *Atg5*flox:*CamKIIα*-Cre KO and slightly decreased in *Atg5*flox:*VGAT*-Cre KO brain lysates, whereas the AKAP5 protein levels were unchanged in autophagy-deficient brain lysates. The fact that there are no changes on the total receptor level, the phosphorylation and the anchoring receptor, recruiting PKA to GLUR1, exclude the possibility that the observed, increased neuronal excitability is based on alterations in GLUR1 S845 phosphorylation, the known PKA phosphorylation site that increases peak response open

probability (Banke et al. 2000), AMPA currents and GLUR1 membrane expression (Dias et al. 2012).

Subsequently, performed calcium imaging to measure neuronal activity in *CamKIIα* positive excitatory neurons revealed that autophagy-deficient neurons reacted with a facilitating amplitude to recurrent electrical field stimulation depending on AMPA receptor levels, since a blockage of AMPA receptors could rescue increased excitation in autophagy-deficient neurons. Epileptic seizures are characterized by recurring, unprovoked seizures, representing the abnormally synchronous activity of neurons in a focal area of the brain or throughout the entire brain, initiated by glutamate triggered EPSPs. Multiple, synchronously EPSPs are responsible for epileptic field potentials mainly driven by surface located AMPA receptors at the postsynaptic density of neurons (Rogawski 2013). With the help of non-selective blockers of non-NMDA glutamate receptors, it could be demonstrated that the block of AMPA receptors markedly reduced or even abolished epileptiform activity in hippocampal neurons *in-vitro* (Lee and Hablitz 1989; McBain et al. 1988; Neuman et al. 1988), whereas the selective blockage of NMDA receptors did not alter epileptiform activity but led to a reduction in the discharge duration (Traub et al. 1993). Since epileptic seizures are often driven by AMPA receptor-mediated hyperexcitation, combined with an increased surface localization of GLUR1 at the PSD membrane and the observed rescue after AMPA receptor blockage, mislocalized AMPA receptors are the primary cause for the appearance of epileptic seizures in autophagy-deficient mice with glutamatergic forebrain-confined ATG5 deletion.

Furthermore, PKA is essential to maintain excitability at glutamatergic synapses since applying H89, a PKA inhibitor that causes competitive inhibition of the PKA catalytic subunits' ATP site, led to increased amplitude facilitation in WT neurons. Additionally, an increased network spike rate was detected in neuronal networks with autophagy-deficient excitatory neurons, mimicking the situation of the *Atg5*flox:*CamKIIα*-Cre KO mice. Strikingly, elevated network activity could be rescued by applying Forskolin, demonstrating that network alterations were PKA-dependent. This data could show for the first time that autophagy modulates PKA signalling to maintain neuronal excitability by AMPA receptor localization.

9.4 Closing remarks

This study aimed to understand how autophagy affects neuronal excitability in two subsets of neurons: excitatory and inhibitory forebrain neurons. This study could show that the lack of autophagy resulted in an early onset of an epileptic seizure phenotype affecting excitatory neurons, whereas epileptic seizures were mainly absent when affecting inhibitory neurons. Surprisingly, differences in neuronal excitability were not caused by significant alterations in autophagic cargo degradation. In both neuronal subclasses, autophagy-deficiency led to selective enrichment of PKA regulatory subunits type 1, without impacting other PKA subunits. The selective enrichment of PKA R1-α and R1-β created a misbalance in PKA signalling, causing a decrease of postsynaptic cytoskeleton phosphorylation resulting in increased AMPA receptor surface presentation in autophagy-deficient neurons, which leads to increased network activity in *Atg5*flox:*CamKIIα*-Cre KO neurons.

All in all, the mechanism described here relies on the autophagy-dependent AMPA receptor surface presentation by regulating the protein level of PKA R1-α and R1-β subunits and thereby PKA activity to maintain proper neuronal excitability. Further studies should address autophagy in known homeostatic plasticity settings using Bicculine to induce down-scaling at synapses and trace autophagy induction and autophagic vesicle cargo content. Furthermore, the measurement of mEPSP as a functional readout after Bicculine treatment in autophagy-deficient neurons would be beneficial. Another interesting point to tackle would be to see if autophagy controlled PKA mediated phosphorylation of postsynaptic density cytoskeleton proteins affects the trafficking of different receptors in other classes of neurons.

Another interesting point to elucidate would be to compare the role and induction mechanisms of autophagy in LTD and its possible role in homeostatic plasticity. During LTD, autophagy mediates the degradation of several postsynaptic proteins, whereas autophagy induction during homeostatic plasticity seems to be more selective, leading to PKA-mediated structural changes at the postsynaptic density.

Autophagy and cAMP/PKA signalling is known to decline during ageing and play a role in the disease progression of several neurodegenerative diseases like AD, PD, ALS and HD (Chang et al. 2017; Hansen et al. 2018; Carlyle et al. 2014). Ageing affects all tissues and organs, but the

brain seems to be particularly vulnerable, reflected by the gradual decrease in synaptic function and the deterioration of synaptic plasticity (Di Benedetto et al. 2021). The decline of autophagy is often associated with the accumulation of intracellular toxic protein aggregates (Ravikumar et al. 2002; Menzies et al. 2015), hallmarking several neurodegenerative diseases. However, autophagy is also involved in age-associated memory decline (Gupta et al. 2013; Menzies et al. 2017), similar to impaired PKA signalling, which is associated with a decline in memory consolidation (Wild and Dell'Acqua 2018; Kim et al. 2013) due to alterations in CREB phosphorylation (Ramos et al. 2003; Bach et al. 1999; Porte et al. 2008). These alterations are caused by impaired calcium homeostasis (Carlyle et al. 2014), decreased AMPA receptor phosphorylation (Wang et al. 2011; Parisiadou et al. 2014) or disrupted postsynaptic clustering of several postsynaptic scaffold proteins (Bączyk et al. 2020). The presented study shows that autophagy at synapses is a crucial regulator of PKA-mediated phosphorylation of cytoskeletal proteins confined to the postsynaptic density, enabling proper AMPA receptor localization. The induction of PKA signalling in mutSOD1 mice, a model system for amyotrophic lateral sclerosis (ALS), achieved synaptic restoration, normalizing motor neuron excitability due to rescue of disrupted postsynaptic clustering of HOMER1b, SHANK and AMPA receptor subunits (Bączyk et al. 2020). In other studies, the induction of cAMP/PKA signalling was sufficient to improve learning and memory in a chronically Aβ(1-40) infused AD rat model (Matsuzaki et al. 2006) or to attenuate dopamine depletion in an MPTP-treated PD mice model (Yang et al. 2008). Unfortunately, drug-induced targeting of PKA is accompanied by several severe side effects. The induction of autophagy in studies using AD and PD model organisms increased the clearance of aggregated protein accumulations (Dehay et al. 2010; Jiang et al. 2014; Ozcelik et al. 2013) and delayed or even reversed nearly every age-related disease or decline in functionality in mice (Lin et al. 2013a), but were also accompanied by several severe side effects. Nevertheless, autophagy and cAMP/PKA signalling remain exciting candidates for treating neurodegenerative diseases and unravelling the regulation of PKA signalling by autophagy could be beneficial to target PKA signalling in the future.

10.Materials and Methods

10.1 Materials

10.1.1 General laboratory equipment

Table 1: List of devices and machines working in the lab.

Instrument	**Manufacturer**	**Catalogue number**
BioRupter, Picorupter	Diagenode	B01060010
Cabinet, Horizontal laminar flow	Thermo Fisher Scientific	Heraguard ECO
Cabinet, Vertical laminar flow cabinet (cell lines)	Scanlaf	Mars Safety Class 2
Cabinet, vertical laminar flow (primary cells)	Thermo Fisher Scientific	Safe 2020
Centrifuges	Eppendorf Hettich VWR	5702R 320R MicroSTAR 17R
Double Edge Coated Blades (Washed version)	Electron Mircoscopy Science	#72000-WA
EASY-nLC™ 1200 System	Thermo Scientific	LC140
Electrophoresis Power Source	VWR	300V
Electrophoresis chamber (PCR)	VWR	700-0569
Electrophoresis chamber (WB)	Bio-Rad	Mini-Protean Tetra Cell
EVOSEP ONE	Evosep	EV-1000
Dissection tools	FST	

Forceps Scissors Scalpel		11253-27 16020-14 11270-20 14090-09 13002-10 14002-13 10073-14
Freezer (-20°C)	LIEBHERR	9988187-12
Fridge (4°C)	LIEBHERR	9983491-10
Gel imager system (PCRs)	Bio-Rad	Gel Doc™ XR+
Incubator CO_2 (cell lines)	Binder	C170
Incubator CO_2 (primary neurons)	Eppendorf	Galaxy 1705
Incubator Shaker	Eppendorf	M1335-0002
Mass Spectrometer Orbitrap Eclipse™ Tribrid™ Q Exactive Exploris™ 480 Q Exactive™ Plus Orbitrap™	 Thermo Scientific Thermo Scientific Thermo Scientific	 FSN04-1000 BRE725539
McIlwain Tissue Chopper	Cavey laboratory engineering Co. LTD	MTC/5E
Microscope, inverted (cell culture)	Leica	Leica DMi1
Microscope, inverted fluorescence Camera	Zeiss Hamamatsu	Axiovert 200M C11440

Temperature module	Zeiss	TempMoudleS
LED Light source	CoolLED	pE-4000
Software	Micro-Manager	MicroManager1.4
Objectives:		
40x/1.4 oil DIC	Zeiss	420762-9900
63x/1.4 oil	Zeiss	420780-9900
10x/0.3	Zeiss	420304-9901
Microscope, inverted confocal	Leica	TCS SP8
Camera	Leica	HyVolution 2
Detector	Leica	4 HyD's, 1 PMT
Software	Leica	LAS X
Objectives:		
40x/0.85	Leica	Apo CORR CS
63x/1.20	Leica	PL APO W motCORR CS2
Microscope, light (histoscanner)	Leica	SCN400
Software	Leica	Digital Image Hub
Microscope, stereo (dissection)	Leica	Leica M80
Microscope, transmission electron	Jeolusa	JEM-2100 Plus
Camera	Gatan	OneView 4K 16 bit
Software	Gatan	DigitalMicrograph
Microtom	Thermo Fisher Scientific	Microm HM 430
Microwave	Inverter	Sharp

Neubauer chamber	Marienfeld	0640110
Osmometer	Gonotec	Osmomat 3000
Perfusion pump	WPI	Peri-Star Pro
pH-meter	Mettler Toledo	Seven Easy
Photometer	Eppendorf	Bio Photomer plus
Real-time PCR Thermocyler	Applied Biosciences	7500 RealTimePCR System
Sonicator	BRANSON	Sonifier 250
Scales	OHAUS VWR	EX225D T1502746
SpeedVac Eppendorf Concentrator plus	Eppendorf	5305000509
Thermocycler	VWR	peqSTAR
Thermoschaker	CellMedia	Thermomixer basic
Water bath	VWR	VWB6
96-well plates 96-well V-bottom plates	Greiner NerbePlus	#655896 #10-111-000
Vortex	Scientific Industries	Vortex-Genie 2

10.1.2 Chemicals

Table 2: Chemicals used for solutions and buffers.

Chemical	Manufacturer	Identifier
2-ß-Mercaptoethanol	Roth	4227.1
2-Propanol	Roth	CP41.3
Acetic acid 100%	Roth	3738.4
Acetone	Roth	5025.1
Aceton (Proteomics)	Merck	1.00020.2500
Acetonitrile hypergrade for LC-MS LiChrosolv	Merck	1.00029.2500
Ammonium chloride	Roth	K298.2
Ammonium peroxidisulfate (APS)	Merck	1.012.001.000
Ampicillin sodium salt	Roth	K029.2
Bafilomycin A	MilliporeSigma™	5.08409.0001
Boric acid	VWR	J67202
Bovine Serum Albumin	Sigma	A7906
Bromophenol blue	Sigma	B5525
2-Chloracetamid (CAA)	Merck	CAS 79-07-2
Calcium chloride dihydrate	Roth	5239.2
Calcium chloride hexahydrate	Roth	T886.1
Cresyl violet acetate	Sigma	C5042

1,4-Dithioerythritol (DTT)	Applichem	CAS 3483-12-3
D-(+)-Glucose	Sigma	G5767
D-Mannitol	Sigma	M4125
Dimethyl sulfoxide (DMSO)	Roth	A994.2
di-Potassium hydrogenphoshate	Roth	6875.1
di-Sodium hydrogen phosphate dihydrate	Roth	4984.1
di-Sodium hydrogen phosphate anhydrous	Merck	106559
EDTA	AppliChem	A1104.1000
EGTA	Roth	3054.2
Entellan®	Merck	107960
Ethanol	Omnilabs	A1613.2500PE
Formic Acid	Honeywell/FLUKA	607-001-00-0
Forskolin	Tocris	1099
Gelatin from porcine skin	Sigma	G2500
Glycerol	Roth	7530.1
Glycine	Roth	3908.3
H89	Tocris	2910
HEPES	Sigma	H4034
Hydrochloric acide 32%	Roth	X896.2
IGEPAL	Sigma	I8896

Kanamycinsulfat	Roth	T832
LB-Agar (Lennox)	Roth	X965.2
LB-Medium (Lennox)	Roth	X964.2
Luminol	Roth	4203.1
Lysyl Endopeptidase (LysC)	WAKO	129-02541
Magnesium chloride hexahydrate	Roth	2189.1
Magnesium sulphate heptahydrate	Roth	P027.2
Methanol	Roth	4627.5
Methanol LC-MS grade (Proteomics)	VWR	83638.32
Milk powder	Roth	T145.2
Normal Goat Serum (NGS)	Thermo Fisher Sci	16210064
Paraformaldehyde (PFA)	Merck	104.005.100
p-coumaric acid	Sigma	C9008
Phenol red	Sigma	P3532
PIPES	Sigma	P8203
Ponceau S	Roth	5938.1
Potassium acetate	Roth	T874.1
Potassium chloride	Roth	6781.1
Potassium dihydrogen phosphate	Roth	3904.1
Potassium disulfite	Sigma	60508

Potassium hypochlorid	Carl Roth	9062.3
Saponin	Serva	34655
Sodium chloride	Roth	3957.1
Sodium hydrogen carbonate	Roth	6885.1
Sodium hydroxide	Roth	6771.1
Sodium dodecyl sulfate (SDS) ultra-pure	Roth	2326.2
Sodium tetraborate	VWR	1303964
Sucrose	Sigma	S0389
Tetramethylenediamine (TEMED)	AppliChem	A1148.0028
Torin 1	APE BIO	A8312
Tris (hydrogenmethyl) aminomethane (Tris-base)	VWR	28.808.294
Trizma hydrochloride (Tris-HCl)	Sigma	T3253
Trypan blue	Roth	CN76.1
Tween 20	VWR	663684B
Urea	Sigma	U1250
Xylene	VWR	28975.291

10.1.3 Reagents

Table 3: Reagents used in this study.

Reagent	Manufacturer	Identifier
Acryl/Bis™ solution (30%) 37.5:1	VWR	E347
Bradford Reagent	Sigma	B6916
Buffer A (0,1% Formic acid in water)	VWR	84867.290
Buffer B (80% acetonitril, 0,1% formic acid)	Fisher scientific	LS 122-500
Complete Mini Protease Inhibitor	Roche	11836153001
DNA ladder (100 bp/ 1 kb)	Thermo Fisher Sci	SM0323/SM0311
DNA Gel Loading Dye (6X)	Thermo Fisher Sci	R0611
DreamTaq DNA polymerase	Thermo Fisher Sci	EP0703
Dynabeads™ Protein G	Invitrogen	10003D
ECL™ WB detection reagents	GE Healthcare	RPN2106
LongAmp Taq DNA polymerase	BioLabs	M03235
Normal Goat Serum	Gibco	16210064
Nuclease-free water	Ambion	AM9938
PageRuler Plus Prestained Prot. Ladder	Thermo Fisher Sci	26619
Pierce™ Protease and phosphatase inhibitor mini tablets	Thermo Fisher Sci	A32959
Proteinase K	Sigma	AM2546
SuperSignal™ West Femto	Thermo Fisher Sci	34094

10.1.4 Cell culture media ingredients and reagents

Table 4: Cell culture media ingredients and reagents used for media preparation.

Reagent	Manufacturer	Identifier
B-27 Supplement (50X)	Thermo Fisher Sci	17504-044
Conconamycin A	Sigma	C9705
Cytosine ß-D-arabinofuranpsode hydrochloride	Sigma	C6645
DMEM (1X)+GlutaMAX™	Thermo Fisher Sci	31966-021
Deoxyribonuclease I from bovine pancreas	Sigma	D5025
EBSS	Thermo Fisher Sci	14155-048
Fetal Bovine Serum	Merck	S0115
Fetal Bovine Serum (sterile filtered) (FBS)	Sigma	F7524
GlutaMAX™	Thermo Fisher Sci	35050-061
HBSS (1X) [-] $CaCl_2$, [-] $MgCl_2$	Thermo Fisher Sci	14175-053
HEPES (1M)	Thermo Fisher Sci	15630-080
Hibernate®-A	Gibco	A12475-01
Hibernate A (-$CaCl_2$))	BrainBits	HACA500
Insulin, human recombinant zinc	Thermo Fisher Sci	12585-014
MEM	Thermo Fisher Sci	51200-046
MG132	Sigma	M7449

MEM NEAA	Gibco	11140050
Neurobasal®-A Medium	Gibco	12349-015
OptiPrep® Density Gradient Medium	Sigma	100M1278
Papain (lypholized)	Worthington	LS003119
Penicillin/Streptomycin (P/S)	Thermo Fisher Sci	15140-122
Poly-D-lysine (1mg/mL)	Merck	A-003-E
Sodium Pyrubate	Thermo Fisher Sci	11360-039
Transferrin, Holo, Bovine Plasma	Merck	616420
Trypsin from bovine pancreas	Sigma	T1005
(Z)-4-Hydroxytamoxifen (Tamoxifen)	Sigma	H7904

10.1.5 Media composition for primary neuronal cell culture, NSC34 and MEF cells

All cell culture media was filtered through 0.2 µm pore size membranes after preparation and stored at 4°C.

Table 5: Overview of media composition used for primary neuronal cell culture and cell line maintenance.

Name	**Composition**
Basic Media	1L MEM; 5g Glucose; 200mg $NaHCO_3$, 100mg Transferrin
Borate Buffer 0.1M	1.24g boric acid; 1.9g sodium tetraborate in 400ml autoclaved ddH2O
Digestion Solution	137mM NaCl; 5mM KCl; 7mM Na_2HPO_4; 25mM HEPES dissolved in autoclaved ddH_2O. pH 7.2
Dissociation Solution	Hank's + 12mM MgSO4x7H_2O

Growth Media	100mL Basic Media; 5mL sterile filtered FBS; 0.25mL GlutaMAX; 2mL B-27; 1mL P/S
Hank's solution	500 mL HBSS; 5mL Sodium pyrubate; 5mL HEPES; 5mL P/S
Hank's + 20% FBS	Hank's + 20% (v/v) sterile filtered FBS
Plating Media	100 mL Basic Media; 10 mL sterile filtered FBS; 1mL GlutaMAX; 625µL Insulin; 1.1 mL P/S
Cell line media	DMEM + 10% (v/v) FBS + 1% (v/v) P/S + 1% NEAA

10.1.6 Reagents for animal perfusion

Table 6: Mice were transcardially perfused after deep anaesthesia.

Reagent	Manufacturer	Identifier	Concentration
Isofluran	Piramal	B73E16A	
Ketamin hydrochloride	Sigma	K2753	100mg/ml
Rompun 2% (Xylazine)	Bayer	KP0BZPE	20mg/ml

10.1.7 Kits and other equipment

Table 7: Commercial kits that were used in this study.

Reagent	Manufacturer	Identifier
cAMP measurement Kit	abcam	ab138880
Endotoxin-free plasmid DNA purification	Macherey-Nagel	740420.10
High Capacity cDNA Reverse Transcription	Thermo Fisher Sci	4368814
Lipofectamine 3000	Thermo Fisher Sci	L3000-008

High-Select™ TiO2 Phosphopeptide Enrichment Kit	Thermo Scientific	A32993
ProFection Mammalian Transfection System-Calcium Phosphate	Promega	E1200
RNeasy® Plus Micro Kit (50)	Qiagen	74034

10.1.8 Antibodies & DNA labelling dyes

Table 8: Antibodies & DNA labelling dyes and thier used concentration in Immunoblotting (WB), Immunocytochemistry (ICC), Immunohistochemistry (IHC) and Immunoprecipitation (IP) analysis.

Antibodies	**Used concentration**				**Manufacturer**	**Catalog number**
Target protein	WB	ICC	IHC	IP		
ATG5	1:1000	-	-	-	Abcam	ab108327
β-Actin	1:1000	-	-	-	Sigma	A-5441
Bassoon	-	-	1:500	-	Synaptic Systems	141002 & 141004
CREB	1:1000	-	-	-	Cell Signaling	9197
cAMP	-	1:500	-	-	Abcam	ab24856
GAPDH	1:1000	-	-	-	Sigma-Aldrich	G8795
GFP	-	1:2000	1:1000	-	Abcam	ab13970
GluA1	1:1000	1:500	1:500	-	Synaptic Systems	182011
Glutamate receptor 1 (AMPA subtype) phospho S845	1:1000	-	-	-	Abcam	ab76321

LC3B	1:2000	-	-	-	Novus Biologicals	NB600-1384SS
MAP2	-	1:500	-	-	Sigma-Aldrich	M9942
NBR1	-	-	1:300	-	Santa Cruz Biotechnology	sc-130380
Normal Rabbit IgG	-	-	-	2 µg	Cell Signaling	2729
Normal Mouse IgG	-	-	-	2 µg	Millipore	12-371
Normal Sheep IgG	-	-	-	2 µg	Jackson Immuno Research	713-005-147
p62	1:1000	1:1000	1:1000	-	Progen	GP62-C
pCREB (Ser133)	1:1000	1:500	-	-	Cell Signaling	9198
pCREB (S133)	-	1:500	-	-	Thermo Fisher (Pierce)	MA5-11192
pGluR1 (S845)	1:1000	-	-	-	Abcam	ab76321
pPKA-R2-α	-	1:500	-	-	Abcam	ab32390
pPKA-Substrate	1:1000	-	-	2 µg	Cell Signaling	9624
PKA C-α	1:1000	-	-	-	Cell Signaling	5842
PKA R1-α	1:1000	1:300	1:300	2 µg	Cell Signaling	5675
PKA R1-α/β	1:1000	-	-	-	Cell Signaling	3927
PKA R1-β	1:1000	1:300	1:300	2 µg	R&D Systems	AF4177
PKA R2-α	1:1000	-	-	-	BD Transduction Laboratories	612242
PKA R2-β	1:1000	-	-	-	Abcam	Ab32390

PSD95	-	1:300	1:300	-	Synaptic Systems	124 008
S6 Ribosomal Protein (phosho Ser235/236)	1:1000	-	-	-	Cell Signaling	2211
α-Tubulin	1:1000	-	-	-	Synaptic Systems	302 211
Vinculin [EPR8185]	1:1000	-	-	-	Abcam	ab129002
DNA labelling dyes						
DAPI	-	1:10000	-	-	Roth	6335.1
DRAQ5	-	1:1000	-	-	Thermo Scientific	62254

Table 9: Secondary antibodies with HRP (WB) or flourescence (ICC / IHC) tag and their used concentration.

Antibody target	**Used concentration**			**Manufacturer**	**Catalog number**
	WB	ICC	IHC		
Goat anti-Mouse IgG (H+L) peroxidase-conjugated	1:5000	-	-	Jackson Immuno Research	115-035-003
Goat anti-Rabbit IgG (H+L) peroxidase-conjugated	1:5000	-	-	Jackson Immuno Research	111-035-003
Goat anti-Guinea Pig IgG (H+L) peroxidase-conjugated	1:5000	-	-	Jackson Immuno Research	106-035-003
Goat anti-Sheep IgG (H+L) peroxidase-conjugated	1:5000	-	-	Invitrogen	A16041

Alexa Fluor 488 Goat anti-Mouse IgG	-	1:500	-	Life Technologies GmbH	A11029
Alexa Fluor 488 Goat anti-Rabbit IgG	-	1:500	1:500	Life Technologies GmbH	A11034
Alexa Fluor 488 Goat anti-Chicken IgG	-	1:500	1:500	Life Technologies GmbH	A11039
Alexa Fluor 488 Goat anti-Guinea Pig IgG	-	1:500	1:500	Life Technologies GmbH	A11073
Alexa Fluor 488 Donkey anti-Sheep IgG		1:500	1:500	Life Technologies GmbH	A11015
Alexa Fluor 568 Goat anti-Mouse IgG	-	1:500	1:500	Life Technologies GmbH	A-11031
Alexa Fluor 568 Goat anti-Rabbit IgG	-	1:500	1:500	Life Technologies GmbH	A11036
Alexa Fluor 568 Goat anti-Guinea Pig IgG	-	1:500	1:500	Life Technologies GmbH	A11075
Alexa Fluor 568 donkey anti-mouse IgG	-	1:500	1:500	Life Technologies GmbH	A10037
Alexa Fluor 555 Donkey anti-Sheep IgG	-	1:500	1:500	Life Technologies GmbH	A21436
Alexa Fluor 647 Goat anti-Mouse IgG	-	1:500	1:500	Life Technologies GmbH	A21236

Alexa Fluor 647 Goat anti-Mouse IgG	-	1:500	-	Life Technologies GmbH	A327728
Alexa Fluor 647 Goat anti-Rabbit IgG	-	1:500	1:500	Life Technologies GmbH	A21245
Alexa Fluor 647 Goat anti-Guinea Pig IgG	-	1:500	1:500	Life Technologies GmbH	A21450
Alexa Fluor 647 Donkey anti-Rabbit IgG	-	1:500	1:500	Life Technologies GmbH	A31573

10.1.9 Plasmids & Viral vectors

Table 10: Plasmid DNA used for transfection of cells in-vitro.

Plasmid (source gene)	**Manufacturer**	**Identifier**
GFP	Clontech	pT3027.5
pEGFP-C1-hAPG5 (ATG5-GFP)	addgene	#22952
Prkar1a shRNA	OriGene	TL501735
Prkar1a shRNA	OriGene	TL501736
pcDNA3-mouse PKA-RIalpha-mEGFP	addgene	#45525
pcDNA3-mouse PKA-RIbeta-mEGFP	addgene	#45526
pCMV-SEP-GluA1	addgene	#64942

Table 11: Viral vectors used *in-vitro*.

Name	Full description	Manufacturer	Identifier
GAD67-Cre	ssAAV-5/2-hGAD67-chl-iCre-SV40p(A)	Viral Vector Facility VVF	V197-5
CamKIIα-Cre	ssAAV-9/2-mCaMKIIα-iCre-WPRE-hGHp(A)	Viral Vector Facility VVF	V206-9
CamKIIα:GCAMP7	ssAVV-9/2-mCaMKIIα- jGCaMP7f-WPREbGHp(A)	Viral Vector Facility VVF	V493-9

10.1.10 Genotyping primers

Table 12:Primer sequences for genotyping.

Gene	Sequence (5'- 3')
Atg5	
Atg5 forward 1	GAA TAT GAA GCC ACA CCC CTG AAA TG
Atg5 forward 2	ACA ACG TCG AGC ACG CTG GCG AAG G
Atg5 reverse	GTA CTG CAT AAT GGT TTA ACT CTT GC
Atg16L1	
Atg16L1_1	CAG AAT AAT TTC CGG CAG AGA CCG G
Atg16L1_2	AGC CAA AGA AGG AAG GTA AGC AAC GAA
Cre	
Cre_1	GAA CCT GAT GGA CAT GTT CAG G
Cre_2	AGT GCG TTC GAA CGC TAG AGC CTG T

Cre_3	TTA CGT CCA TCG TGG ACA
Cre_4	TGG GCT GGG TGT TAG CC
tdTomato	
tdTomato_1	AAG GGA GCT GCA GTG GAG TA
tdTomato_2	CCG AAA ATC TGT GGG AAG TC
tdTomato_3	GGC ATT AAA GCA GCG TAT CC
tdTomato_4	CTG TTC CTG TAC GGC ATG G

10.1.11 Cell lines

Table 13: Cell lines and origin.

Cell line	**Manufacturer**	**Identifier**
Mouse embryonic fibroblast (MEFs)	Kind gift from Prof Dr. Thomas Langer	N/A
Mouse motor neuron-like hybrid cell line (NSC-34)	Kind gift from Prof Dr Brunhilde Wirth	N/A

10.1.12 Mouse models

Table 14: Mouse line identification.

Mouse model	**Manufacturer**	**Identifier**
C57BL/6J	CECAD *in vivo* facility	N/A
*Atg5*flox:CAG-Cre^{Tmx}	Kononenko et al. (2017)	N/A
*Atg5*flox:*CamKIIα*-Cre	Kononenko lab	N/A

*Atg5*flox*:Slc32a1-Cre*	Kononenko lab	N/A
*Atg16L1*flox*:CamKIIα-Cre*	Kononenko lab	N/A
*Atg5*flox:*CamKIIα*-Cre:tdTomato	The Jackson Laboratory	Ai9(RCL-tdT) line
*Atg5*flox:Slc32a1-Cre:tdTomato	Kononenko lab	N/A
Atg5flox:tdTomato	Kononenko lab	N/A

10.1.13 Buffers & Solutions

If not mentioned, solutions were stored at room temperature (RT)

Table 15: Description of buffer composition.

Name	**Composition**
1.5M Tris pH 8.8	181.65g Tris Base; 0.4% (w/v) SDS; 1L ddH_2O ; pH 8.8
0.5M Tris pH 6.8	6g Tris Base; 0.4% (w/v) SDS; 100 mL ddH_2O; pH 6.8
10% Acrylamide gel	8.04 ml H_2O; 5ml 1.5M Tris pH 8.8, 6.67ml 30% acrylamide/bis, 200µl 10% SDS, 100µl APS 10%, 10µL TEMED
15% Acrylamide gel	5.04 ml H_2O; 5ml 1.5M Tris pH 8.8, 9.67ml 30% acrylamide/bis, 200µl 10% SDS, 100µl APS 10%, 10µL TEMED
4% Acrylamide gel (Stacking)	6mL ddH_2O; 2.52 mL 0.5 M Tris pH 6.8, 1.32 mL acrylamide/bis, 100µL 10%SDS, 50µL 10% APS, 10µL TEMED
2% agarose gel	2% (w/v) agarose in TBE 1X
B buffer	35.6g Na_2HPO_4*2H_2O, 31.7g Na_2HPO_4 in 500mL, pH=7.4 in 500mL H_2O
Blocking solution WB (BSA)	5% (w/v) BSA in TBS-T

Blocking solution WB (milk powder)	5% (w/v) milk powder in TBS-T
DMSO post-fixation	31.25 mL 0.4M PB, 46.75 mL H2O, 25.2g glycerin, 2mL DMSO
ICC blocking/permeabilizing solution	5% (v/v) NGS; 0.3% (w/v) Saponin, in PBS
Imaging Buffer	1mL B buffer; 100µL NaCl 5M; 4.9 µL $MgCl_2$, 13µL $CaCl_2$ 1M; total volume 10 mL
Neutralization Buffer	1.3g Tris-HCl in 200Ml ddH_20. pH=5
Lammeli Buffer (4x)	250mM Tris-HCL;1% (w/v) SDS; 40% (v/v) Glycerol; 4% (v/v) ß-mercaptoethanol; 0.02% Bromophenol
PFA 4% (perfusion)	4% (w/v) PFA in PB 0.125 M, 60°C. pH 7.4
PFA 4% (ICC fixation)	4% (w/v) PFA, 4% (w/v) Sucrose, dissolved in PBS. pH 7.4
PBS	0.137M NaCl; 0.0027M KCl; 0.01M Na_2HPO_4; 1.8mM KH2PO4
Phosphate Buffer 0.4M (PB)	27.6g NaH_2PO_4, 35.6g $Na_2HPO_4*2H_2O$, 31.7g Na_2HPO_4 in 500mL, pH=7.4
Proteinase K solution	50mM Tris-HCl; 1mM $CaCl_2$; 50% Glycerol, in ddH_2O to generate dilution Buffer. + 20g Proteinase K for 1mL of dilution buffer.
Ponceau staining solution	1% (w/v) Ponceau S; 2% (v/v) acetic acid in ddH_2O
Ringer	0.85% (w/v) NaCl, 0.025% (w/v) KCl, 0.02% (w/v) $NaHCO_3$ in ddH_2O
RIPA buffer	50mM Tris-Base; 150 mM NaCl ; 1% (v/v) IGEPAL; 0.5% (w/v) Sodim deoxycholate; 0.1% (w/v) SDS dissolved in ddH2O (1 tablet of protease inhibitor and phosphatase inhibitor/10mL RIPA buffer)
Running Buffer 10X	25mM Tris-Base; 192mM Glycine; 0.1% (w/v) SDS in ddH_2O
Transfer Buffer 10X	25mM Tris-Base; 192mM Glycine; 0.025% (w/v) SDS in ddH_2O
Transfer Buffer 1X	10% (v/v) Transfer Buffer 10X; 20% (v/v) methanol; 70% (v/v) ddH_2O

Tail lysis buffer	1M Tris-Base; 0.5M EDTA; 20% (w/w) SDS, 5M NaCl, in ddH_2O, pH 8.5
TBE 10X	108g Tris-Base; 55g Boric acid; 7.4g EDTA in 1L ddH_2O
TBS-T	20mM Tris; 137 Mm NaCl; 0.1% (v/v) Tween 20
Lysis buffer for IP (Co-IP buffer)	50 mM Tris-HCl; 1% IGEPAL; 100mM NaCl; 2mM $MgCl_2$ in ddH_2O (1 tablet of protease and phosphatase inhibitors/10Ml of lysis buffer)

10.2 Methods

10.2.1 Animals

All mice were housed in ventilated polycarbonate cages at standard 12/12 hour day/night cycles. Food and water were provided *ad libitum*. All animal experiments are approved by the LANUV Cologne and ethics committee and are conducted to the committee's guidelines. Conditional tamoxifen-inducible *Atg5* KO (*Atg5*flox/flox: B6.Cg-Tg(CAG-Cre/Esr1*)5Amc/J) is described in the results section, and (Kononenko et al. 2017). Conditional KO mice were created by crossing *Atg5*flox/flox mice with *CamKIIα*-Cre line (Dragatsis and Zeitlin 2000), kindly provided by Prof. Aleksandra Trifunovic (CECAD, Cologne, Germany) or crossing *Atg5*flox/flox mice with *Vgat-ires*-cre (*VGAT*-Cre, #016962, The Jackson Laboratory) line kindly provided by Prof. Matthew Poy (Johns Hopkins University School of Medicine, St. Petersburg, USA). Reporter lines were created by crossing both lines to Ai9(RCL-tdT) (tdTomato) line (The Jackson Laboratory) that was received from Prof. Matteo Bergami (CECAD, Cologne, Germany). *Atg16L1*$^{flox/flox}$ mice (Adolph et al. 2013) were received from Prof. Philip Rosenstiel (University Hospital Kiel, Germany). Conditional tamoxifen-inducible ATG16L1 KO mice were created by crossing *Atg16L1*$^{lox/lox}$ mice with a Tamoxifen-inducible CAG-Cre line (B6.Cg-Tg(CAG-Cre/Esr1*)5Amc/J; The Jackson Laboratory).

10.2.2 Genotyping

10.2.2.1 Tissue preparation

For the mice's genetic determination, small tissue probes from the ears were taken 3 weeks after birth (ear punches) or 1mm tail tip of newborn pups (tails cut) at postnatal day 1-5. The samples were stored at -20°C before extraction.

10.2.2.2 DNA extraction

DNA extraction from tissue was performed depending on the target genes. For the phenotype lines, *Atg5*flox:*CamKIIα*-Cre, *Atg5*flox:*VGAT*-Cre, and *Atg16L1*flox:*VGAT*-Cre and corresponding reporter lines carrying tdTomato the tissue probes were incubated in 300µL Proteinase K overnight at 55°C on a shaker. The next day, the samples were centrifuged for 5 min at 13 000 rpm. The supernatant was transferred into a fresh tube, and 400µL isopropanol was added to the solution. The mixture was incubated for 15 minutes at room temperature (RT) before centrifuging at 13 000 rpm for 10 minutes (min). The supernatant was discarded, and 300 µL of 70% EtOH was added to the sample. The sample was again centrifuged for 10 min at 13 000 rpm to wash the DNA and subsequently placed on a heater at 55°C for a minimum of 30-45 min to dry out the pellet. Afterwards, the pellet was dissolved in 100 µL autoclaved water.

For *in-vitro* experiments, tail cuts of the *Atg5*flox:*CAG*-Cre^{Tmx} mice were processed with a short DNA extraction protocol. Therefore, 50 µL Alkaline Lysis Reagent was added to the tissue before incubation at 95°C in a heating block for 30 min. Afterwards, the samples were centrifuged and allowed to cool down before 50 µL of Neutralization buffer was added.

10.2.2.3 PCR

The genetic determination for single genes was done via polymerase chain reaction following the displayed protocols and machine settings. For the PCR, the samples were placed first into the tubes, and other components were added as a master mix afterwards.

Table 16: PCR pipetting protocols for master mixes.

ATG5, CAG-Cre CamKII-Cre, Slc32a1-Cre, tdTomato	
Sample	1 µL
DreamTaq Buffer	2 µL
25mM $MgCl_2$	2 µL
2mM dNTPs	1.5 µL
Primer (10mols/µL)	1 µL / primer
DreamTaq Polymerase	0.2 µL
Autoclaved water	Filled up to 20 µL

ATG16L1	
Sample	1 µL
LongAmp® Buffer	2 µL
2mM dNTPs	1.5 µL
Primer (10mols/µL)	1 µL / primer
LongAmp® Taq Polymerase	0.2 µL
Autoclaved water	Filled up to 20 µL

Table 17: PCR programs.

		ATG5		ATG16L1		Cre		tdTomato	
Cycle number		36		35		35		10 / 28	
		T (°C)	Time (min)	T (°C)	Time (min)	T (°C)	Time (min)	T (°C)	Time (sec)
Initial denaturation		94	4	94	2	95	5	94	2
cycles	denaturation	94	0.5	94	0.5	95	0.5	94	2/15
	annealing	63	0.5	65	0.5	62	0.5	65/60	15/15
	elongation	72	1s	68	5	72	0.5	68/72	10
Final extension		72	1s	68	8	72	5	72	120
Hold		4	∞	4	∞	4	∞	4	∞

10.2.2.4 Electrophoresis

After PCR samples were run in 2% Agarose gel (ATG5, Cre, tdTomato) / 1 % Agarose gel (ATG16L1) with SYBR safe, at a concentration indicated by the manufacture guidelines, at 120V for 40 min (2% Agarose gels) or 120V, and 120 min (1% Agarose gels). Results were visualized by the gel imager system (BioRad).

10.2.3 Primary neuronal cultures

10.2.3.1 PDL-coating

Coverslips for imaging and dishes for biochemistry experiments were coated with 0.1 M PDL diluted in borate buffer. PDL was allowed to stay on the corresponding surface for 2-4 hours before wells/dishes were washed twice with autoclaved water and placed for drying at 37°C.

10.2.3.2 Preparation of primary cultures

Postnatal pups (P1-5) were decapitated, and brains were collected in Hank's & 20% FBS. Hippocampus and cortex were dissected and chopped into small pieces (McIlwain tissue chopper, Cavey Laboratory Engineering Co. LTD.). The pieces were washed twice with Hank's & 20% FBS and Hank's before being digested with 10 mg trypsin and 10 µL DNase dissolved in 2 mL digestion solution for 15 min at 37°C. Trypsination was stopped by washing twice with Hank's & 20% FBS and Hank's, and samples were transferred into 2 mL dissociation solution containing 10 µL DNase afterwards. Samples were mechanically dissociated by pipetting 2-3 times with a fire-polished glass pipette, then centrifuging cells at 0.3 rcf, 8 min at 4°C. The supernatant was discarded, and cells were resuspended in plating medium, counted with a Neubauer counting chamber, and plated in a concentration of 2200cells/µL. Cells were fed after settling (1 hour after plating) with plating medium. After 24 hrs, half of the media was removed and replaced by an equal amount of growth media supplemented with 2 µM cytosine ß-D-arabinofuranoside hydrochloride (AraC). 48 hrs after plating, growth media containing 4 µM AraC were added in a ratio of 1:1.

Homologous recombination of Atg5 (*Atg5*flox:CAG-Cre^{Tmx} line) alleles was induced by tamoxifen. Cultured neurons were fed with 0.2 µM (Z)-4-hydroxytamoxifen 1 hr after plating and 0.4 µM of tamoxifen after 24 hrs. Ethanol was added to control neurons (WT) equal to the tamoxifen.

Neurons were kept under constant culture conditions set to 37°C/5% CO2 for 14-16 days.

10.2.4 Starvation/ Fasting experiments

10.2.4.1 In-vitro experiments

Neurons and NSC34 cells were starved by replacing regular culturing media with homemade starvation media. Note that the media provided to neurons was osmolarity adjusted to avoid osmotic stress of the cells. Cells were starved overnight (16 hrs) and harvested/ PFA fixated the following day.

For the NCS34 cells starvation experiment, Bafilomycin was added in a concentration of 67nM in the last 4 hours before harvesting and in neurons for the whole starvation period. PKA signalling during starvation was inhibited by adding 1 µM H-89 dihydrochloride to the starvation media.

Table 18: Starvation media composition.

Components	**mM**
Calcium Chloride (CaCl2) (anhyd.)	1.8
Magnesium Sulfate (MgSO4) (anhyd.)	0.8
Potassium Chloride (KCl)	5.3
Sodium Bicarbonate (NaHCO3)	26.2
Sodium Chloride (NaCl)	117.2
Sodium Phosphate monobasic (NaH2PO4-H2O)	1.0
D-Glucose (Dextrose)	5.6

10.2.4.2 In-vivo experiments

Adult wild-type mice were subjected to fasting 4 hours prior to perfusion, whereas the control group retained access to food ad libitum. The mice's fasting period was introduced at the beginning of their dark cycle. After perfusion, the brains were sliced and forwarded to immunohistochemistry staining.

10.2.5 Immunoblotting

10.2.5.1 Brain tissue and cell culture

Mice were sacrificed at the age of 10-13 weeks via cervical dislocation. Brains were isolated, dissected, shock frozen in liquid nitrogen, and stored at -80°C till further use. Brain tissue was

homogenized in RIPA buffer containing Protease Inhibitor (Roche) and Phosphatase Inhibitor (ThermoScientific) using a Wheaton Potter-Elvehjem Tissue Grinder.

Primary neurons, MEF cells, and NSC34 cells were harvested in RIPA buffer containing Protease Inhibitor (Roche) and Phosphatase Inhibitor (ThermoScientific) using a cell scraper.

All samples were sonicated before being incubated on ice for 45 min. Afterwards, the lysates were centrifuged at 13 000 rpm for 20 min at 4°C. Supernatants were transferred into fresh tubes, and protein concentration was assessed using Bradford assay (Sigma). Depending on the experiment, 10-20 µg of protein per sample was loaded onto SDS-page gels for protein separation. For better denaturation of the proteins, samples were boiled for 5 min at 95°C before gel loading. After the run, proteins were transferred to nitrocellulose or methanol-activated PVDF membranes (LC3). Membranes were blocked with 5% skim milk or 5% bovine serum albumin (BSA) in TBS containing 1% Tween (TBS-T) for 1 hour before incubation with the primary antibody in TBS overnight shaking at 4°C. The next day, the membranes were washed three times with TBS-T for 10 minutes before incubation with secondary HRP-tagged secondary antibody for 1 hour at RT. After incubation, the membranes were washed three times, as mentioned above, and protein levels were visualized using an ECL-based autoradiography film system (Super RX-N, Fujifilm;) for documentation. Films were analyzed using the Gel Analyzer plugin from Image J.

10.2.5.2 Isolated autophagosomes from rat brain tissue

10.2.5.2.1 Purification of autophagosomes (AVs) from cortical and hippocampal murine tissue

The isolation of purified AVs was performed from ten cortices and hippocampi of adult (postnatal day 60, P60) C57BL/6J male mice as described previously (Nikoletopoulou et al. 2017). Briefly, the tissue was homogenized in 10% sucrose, 10 mM Hepes and 1 mM EDTA (pH 7.3) by 20 strokes using a Dounce glass homogenizer. The material was then diluted in half volume of homogenization buffer (HB) (250 mM sucrose, 10 mM Hepes and 1 mM EDTA, pH 7.3) containing 1.5 mM glycyl-L-phenylalanine 2-napthylamide (GPN). After incubation at 37°C for 7 min, the material was centrifuged at 2000 xg for 2 min at 4°C, and the nuclear pellet was discarded. The isolated post-nuclear supernatant was then loaded on discontinuous Nycodenz

gradients that were centrifuged at 141.0000g for 1 hr at 4°C, to remove the cytosolic, mitochondrial and peroxisomal fraction. The isolated autophagosomal and endoplasmic reticulum material was diluted with an equal volume of HB buffer and overlaid on Nycodenz-Percoll gradients for centrifugation at 72000 xg for 30 min at 4°C. After centrifugation, to remove the Percoll silica particles, the AVs' resulting interface was then diluted with 0.7 volumes of 60% Buffered Optiprep overlaid by 30% Buffered Optiprep and HB buffer. The Optiprep gradients were then centrifuged at 71000g for 30min at 4°C. The collected AVs were diluted in three volumes of HB buffer and centrifuged for 30min at 16000g at 4°C. The concentration of the purified isolated AVs was then measured by BCA, following the manufacturer's instructions.

10.2.5.2.1 Proteinase K protection assay

Purified AVs were treated with Proteinase K (PK) (20ng/µl) on ice for 20 min, in the presence or absence of 1% Triton X-100, and then 4 mM of PMSF was added for 10min on ice for PK inactivation. The samples were then centrifuged at 16.900 xg for 10 min at 4°C, and the autophagosomal pellets were resuspended in Laemmli buffer, boiled for 5 min at 95°C and analyzed by Western blot.

10.2.6 SHIRPA analysis of *Atg5*flox:*CamKIIα*-Cre and *Atg5*flox:*VGAT*-Cre mice

The primary screening of the SHIRPA analysis, a basic test to determine behavioural or motoric changes in mice, was performed in mice from both lines (Rogers et al. 1997). The mice were weighted before being placed in a glass beaker (15 cm diameter, 19 cm height) for 2 minutes. During this time, the number of rears (Rearing), the level of arousal, and deviating external appearance characteristics were noted. Afterwards, the mice were transferred into an arena (55 cm x 33cm, 18cm height) in which the floor was subdivided into uniform squares. The number of squares passed during 1 minute was noted and displayed as locomotion (# of squares/min). After 1 minute, the response to a loud, spontaneous noise was measured and ranked from 0-2 (0 – no response; 1 – Preyer reflex; 2 –Reaction in addition to Preyer reflex) and displayed as startle response.

10.2.7 Electrocorticogram recording of *Atg5*flox:*CamKIIα*-Cre mice

Data were collected as previously described (Marguet et al. 2015). Telemetric electrocorticogram analyses were performed using implantable radio transmitters (models TA11EA-F20 or TA11ETA-F20, DataSciences International). Adult (at least 3 months old) male mice received 0.05 mg/kg buprenorphine (subcutaneously) for analgesia and were anaesthetized with 1.5–2% isoflurane in 100% oxygen. Midline skin incisions were made on the top of the skull and neck. The transmitter body was implanted subcutaneously. The tips of the leads were placed 2 mm posterior to bregma and 1.8 mm right to the midline for the recording electrode, and 1 mm posterior to lambda and 1–2 mm left to the midline for the reference electrode. The electrodes were fixed with dental cement. Radio transmitters allowed simultaneous monitoring of electrocorticogram and motor activity in undisturbed, freely moving mice housed in their home cages. Telemetry data and corresponding video data were recorded 24-48 hrs after surgery and were stored digitally using Ponemah software v5.1 (Data Sciences International). Electrocorticogram recordings lasted over 50 h, sampled at 500 Hz, with continuous video recording.

10.2.8 Network activity of primary neurons- MEA System

Neurons from postnatal *Atg5*flox mice were isolated as described before and plated in 24-well plates with gold electrodes on epoxy (24W700/100F-288, Catalogue number: 890852, multichannel*systems). Feeding was done as described previously. At DIV5, the knockout was induced by virus transfection with *CamKIIα*-Cre or *CamKIIα*-eGFP for the control group. MEA recordings were acquired at DIV15 using Multiwell-Analyzer software (multichannel*systems). Recordings were taken for 3 min with a sampling rate of 20000 Hz and automatic threshold estimation. Per well, the best channel electrode was selected for analysis. A well was considered active when at least 3 active electrodes were detected in the well (out of 12). Results were analysed and visualized using GraphPad Prism.

10.2.9 Immunohistochemical analysis of brain sections

10.2.9.1 Perfusion

Mice at the age of 12-15 weeks were euthanized by an overdose of 1.2% ketamine and 0.16% xylazine in PBS (i.p., 10 µl per 10 g body weight) before transcardial perfusion with 25 mL Ringer solution at pre-warmed to 37°C, followed by 25 ml ice-cold freshly depolymerized 4% (w/v) PFA in PBS. Brains were carefully dissected and post-fixated in 4% PFA overnight before being transferred into a mixture of 20% (v/v) glycerol and 2% (v/v) dimethylsulfoxide in 0.4 M PB (DMSO) for 24 hrs for cryoprotection. Horizontal sections (40 µm) were collected in six series in DMSO using the microtome and stored at -80°C till further use. For stainings, corresponding sections from WT and KO littermates were processed simultaneously.

10.2.9.2 Immunofluorescence staining

Sections were rinsed for 5 min in PBS to remove DMSO before permeabilization in 0.3% Triton X-100 diluted in PBS (PBS-T; 2x 5 min). Afterwards, the sections were blocked with 10% normal goat serum (NGS) or normal donkey serum (NDS) in 0.5% PBS-T for 1 hour at RT. Primary antibodies were diluted in3% NGS/NDS and 0.3% PBS-T overnight at 4°C. The next day, the brain sections were washed three times 10 min in 0.3% PBS-T before being incubated with fluorescence labelled secondary antibodies in 3% NGS/ NDS and 0.3% PBS-T for 1 hour at RT protected from light. Finally, the sections were rewashed as described above and mounted on gelatin-coated glass slides.

Pictures of brain sections were taken at the Leica SP8 confocal microscope (Leica Microsystems) equipped with a 63x/1.32 oil DIC objective and a pulsed excitation white light laser (WLL; ~80-ps pulse width, 80-MHz repetition rate; NKT Photonics).

10.2.9.3 3D-analysis and reconstruction

For high-resolution 3D analysis, samples were scanned using Plan-Apochromat 63×/1.32 Oil DIC objective at a resolution of 1,024 × 1,024 pixels with 8-bit sampling in sequential scanning frame-by-frame mode. Single optical sections were acquired using identical acquisition settings, with the pinhole of 1 Airy Unit. Stacks of 8–29 optical sections yielded voxel dimensions between 100 and 300 nm for the X, Y and Z planes. 3D reconstructions were generated with Amira Software 2020.2 (Thermo Fisher Scientific). First, the surface area of the

Bassoon-positive synaptic contacts was reconstructed using the Amira segmentation editor. Bassoon/PKA R1-β-positive contacts were defined by colour-coding the surface of PKA R1-β cells found within 250 nm from Bassoon-positive varicosities. Subsequently, the surface of '250-nm-distant' PKA R1-β -positive voxels was mapped onto Bassoon-positive contact using the "surface distance" tool and plotted as a histogram.

10.2.9.4 Cresyl-violet staining

Brain sections were mounted on gelatin-coated "super frost plus" glass slides and dried overnight. The next day, the sections were hydrophilized in water for 1 min before incubation in Cresyl violet solution for 6-10 min, depending on designated staining intensity. The staining solution was removed by 3 washing steps using water, each lasting 2 min. Afterwards, the brain sections were dehydrated in an ascending ethanol row (70% EtOH, 80% EtOH, 90% EtOH, 96% EtOH, 100% EtOH), staying in each solution for 2 min. The brain sections were placed in Xylene for 2 min before mounting in Entellan® (Merck). Images were acquired using a slide scanner (SCN400, Leica).

10.2.10 Immunocytochemistry of neuronal cultures

10.2.10.1 Staining procedure

Neuronal cultures were fixed in 4% PFA/sucrose in phosphate-buffered saline (PBS) for 15 min at room temperature (RT) at DIV 14-16. Neurons were washed 3x with PBS before permeabilization and blocking with 5% NGS and 0.3% Saponin in PBS (blocking solution) for 1 hour. After blocking, the neurons were incubated with the primary antibody in a blocking solution for 1 hour in a humidified chamber. Coverslips were rinsed 3x with PBS before incubation with the corresponding fluorescence tagged secondary antibodies in blocking solution for 30 min. After washing, the coverslips were mounted in Immu-mount (Thermo Fisher Sci). Fixed neurons were imaged using either Zeiss Axiovert 200M microscope equipped with 40x/1.4 oil DIC objective and the Micro-Manager software (Micro-Manager1.4, USA) or with Leica SP8 confocal microscope (Leica Microsystems) equipped with a 63x/1.32 oil DIC objective and a pulsed excitation white light laser (WLL; ~80-ps pulse width, 80-MHz repetition rate; NKT Photonics).

10.2.10.2 Colocalization analysis

Colocalization of AMPA receptor subunit GluR1 and postsynaptic density marker protein PDS95 were assessed in *Atg5*flox:*CAG*-Cre^{Tmx} neurons using an ROI set in an area devoid of somata for colocalization analysis. Each channel was individually smoothened and binarized with a user-defined threshold before calculating overlap area, Manders' and Pearson coefficients in a semi-automated fashion using a custom ImageJ macro (script can be provided upon request). The graphs display the calculated overlap areas of the GLUR1 signal with PSD95:

$$GLUR1\ I\ PSD95\ overlap\ coefficient = \frac{overlap}{Area\ of\ GLUR1}$$

10.2.10.3 Determination of pCREB positive neurons after starvation

The percentage of pCREB positive neurons in different culture media was determined by counting DAPI positive neuronal cell bodies (differentiated by size). Afterwards, pCREB positive neuronal cell bodies were counted and the percentage calculated.

10.2.11 Plasmid transfection

10.2.11.1 Primary neuronal cultures

Neurons were transfected at DIV7 via calcium phosphate transfection using the ProFection Mammalian Transfection System- Calcium Phosphate Kit (Promega) following manufacturers' guidelines. Therefore, 6 µg plasmid DNA (concentration 1 µg/µL) was mixed with 12.5 µL 2M $CaCl_2$ and 81.5 µL H_2O. The mixture was allowed to sit on the bench briefly before it was mixed (1:1) with 100 µL 2x HEPES buffered saline before it got vortexed and incubated in the dark for 20 min to allow precipitate formation. Meanwhile, neurons were transferred into osmolarity adjusted NeurobasalA (Gibco). After incubation, plasmid solution was added in a ratio of 1:5 to media on top of the cells. Neurons were incubated with plasmid solution for 30 min before washing 3x with osmolarity adjusted HBSS (Gibco). Afterwards, the neurons were transferred back to the original plate/culture media. Imaging was performed on DIV 14-16, 7-9 days after transfection.

10.2.11.2 Mouse embryonal fibroblasts

MEF cells were transfected 24-48 hrs after seeding, when the culture reached a confluency of approximately 50-70%, using Lipofectamine™ 3000 Transfection Reagent (Invitrogen) following manufacturers' guidelines. In brief, 5 µg Plasmid DNA (concentration 1 µg/µL) was mixed with 125 µL Opti-MEM medium and 5 µL P3000TM enhancer and added in a ratio 1:1 to a prepared solution containing Lipofectamine™ 3000 reagent in 125 µL Opti-MEM medium. The mixture was allowed to sit on the bench for 5 min before 250 µL were added to the cells cultured in 6-well plates. After 48 hours, the cells were harvested in RIPA buffer for immunoblotting analysis.

10.2.12 cAMP Direct Immunoassay

cAMP concentration in brain tissue of autophagy-deficient mice was measured using the cAMP Direct Immunoassays Kit (Fluorometric) from Abcam (ab138880) following the manufacturers' instructions. Brains of *Atg5*flox:*CamKIIα*-Cre WT and KO mice were dissected at 12-weeks of age, snap-frozen and stored at -80°C. Hippocampi were weighted and homogenized in lysis buffer depending on tissue weight using a Wheaton Potter-Elvehjem Tissue Grinder (VWR). Insoluble material was removed by centrifugation before the supernatant was pipetted into the anti-cAMP coated 96-well plate. A standard with pre-defined cAMP concentrations was loaded in parallel. Total cAMP content was calculated using a set amount of HRP*-cAMP conjugate and HRP-dependent fluorescent substrate detected by a microplate reader at Ex/Em=540/590 nm.

10.2.13 EM analysis

10.2.13.1 Immunogold labelling on brain sections

Mice were perfused with warm Ringer solution, followed by 4% PFA before the brains were sliced at a vibratome (400 µm). Slices were briefly stained with 0.2% methylene blue in PBS buffer. Small blocks with visible CA1 pyramidal cell layer and adjacent Stratum Radiatum were cut out by the razor and placed into the 2.3 M sucrose in 0.1 M PB solution for 24 hrs at 4°C. Following sucrose infiltration, blocks were placed at pins and plunge frozen in the liquid Ethan.

Ultrathin (80 nm) cryosections (Slot and Geuze 2007) were collected and thawed at sucrose drop (as described), placed at EM grids, blocked and washed in PBS supplemented with 1% BSA and 0.1% glycine, stained with R1 alpha or R1 alpha/beta antibodies 1:50. Following secondary antibody labelling 1:50 (12 nm gold goat anti-rabbit antibodies (Dianova), ultrathin sections were embedded and contrasted with 3% Tungstosilicic acid hydrate (w/v) in 2.8% polyvinyl alcohol (w/v), dried and imaged in Zeiss 900 transmission electron microscope. Images of CA1 Stratum radiatum were taken without prior knowledge of genotype or antibody labelling conditions. The reference area of subneuropil structures was determined by superimposing a grid over the neuropil images (volume fraction estimation). The number of gold particles found at those structures was normalized to the volume fraction of corresponding structures in the neuropil.

10.2.13.2 Assessment of postsynaptic density thickness

The preparation of neurons for postsynaptic density thickness detection was described before (Negrete-Hurtado, Overhoff et al. 2020). In brief, neurons cultured on 18 mm Ø coverslips were fixed with pre-warmed fixative solution (2% glutaraldehyde, 2.5% sucrose, 3 mM $CaCl_2$, 100 mM HEPES, pH 7.4) at RT for 30 min, followed by the post-fixation at 4°C for 30 min. Afterwards, the cells were washed with 0.1 M sodium cacodylate buffer, incubated with 1% OsO_4, 1.25% sucrose, 10 mg/ml $K_4[Fe(CN)_6]\cdot 3H_2O$ in 0.1 M cacodylate buffer for 1 hr on ice and washed three times with 0.1 M cacodylate buffer. Subsequently, the cells were dehydrated at 4°C using ascending ethanol series (50, 70, 90, 100%, 7 min each), incubated with ascending EPON series (EPON with ethanol (1+1) for 1 hr; EPON with ethanol (3+1) for 2 hrs; EPON alone ON; 2 x 2 h with fresh EPON at RT) and finally embedded for 48-72 hrs at 62°C. Coverslips were removed with liquid nitrogen and heat consecutively. Ultrathin sections of 70 nm were made using an ultramicrotome (Leica, UC7) and stained with uranyl acetate for 15 min at 37°C and lead nitrate solution for 4 min. Electron micrographs were taken with a JEM-2100 Plus Electron Microscope (JEOL), Camera OneView 4K 16 bit (Gatan), and software DigitalMicrograph (Gatan). Postsynaptic density was measured using Image J.

10.2.14 Co-Immunoprecipitation experiments

For immunoprecipitation experiments, 20 µL Dynabeads Protein G (Thermofischer) were coated with 2 µg antibody targeting the protein of interest and corresponding IgG as a negative control. Therefore, the bead's storing solution was replaced by 100 µL PBS, and 2 µg of antibody was added. The beads were incubated with the antibody for 2-3 hrs at 4°C on a shaker before washing once with 200 µL to remove excess antibodies.

Neurons were harvested / tissue was homogenized using a Wheaton Potter-Elvehjem Tissue Grinder in Co-Immunoprecipitation (Co-IP) buffer supplemented with Proteinase Inhibitor (Roche) und Phosphatase Inhibitor (ThermoScientific). Lysates were sonicated, incubated on ice for 45 min, and subsequently centrifuged at 13 000 for 20 min at 4°C. Protein concentration was assessed using Bradford assay (Sigma). An equal amount of protein was added to the beads coated with antibodies against the protein of interest and control IgG for overnight incubation at 4°C. The next day, lysates were removed, and beads were washed 3 times with Co-IP buffer before they were dissolved in 20 µL Co-IP buffer and 20 µL 4s SDS buffer and boiled at 95°C for 5 min. Precipitation of proteins was detected via SDS-page gel.

10.2.15 Fluorescence-activated cell sorting (FACS) of isolated neurons

10.2.15.1 Neuronal isolation

Neurons for FACS sorting were isolated from 2-3 weeks old *Atg5*flox:*CamkIIα*-Cre:tdTomato and *Atg5*flox:*VGAT*-Cre:tdTomato reporter mice to receive a pure fraction of autophagy-deficient *in-vivo* neurons. Therefore, the mice were transcardially perfused with artificial cerebrospinal fluid (ACSF) to remove blood cells. Isolated brains were dissected in HibernateA (HA) and cortex, hippocampus and striatum isolated and transferred into a fresh dish containing HABG (Hibernate-A, 2% B27, 1% GlutaMax). The tissue was cut into pieces and digested in activated Papain (Worthington) for 40 min at 37°C. Afterwards, tissue pieces were transferred back into fresh HABG. They were allowed to sit on the bench for 5 min at RT before homogenization with a fire-polished Pasteur pipette (triturate approximately ten times in 1 min). The cell suspension was applied on an OptiPrep®Density Gradient Medium (Sigma) centrifuged at 800 xg for 15 min at 22°C to force cell type separation. Neuron enriched

fractions were maintained for further processing. Gradient material was diluted with 10 mL HABG and cells were pelleted down at 3000 xg for 3 min at 22°C to clean cell suspension from debris contaminations. This step was repeated once before the cells were resuspended in NBA supplemented with 2% B27. Cells were stained with DRAQ5 (1:1000) and DAPI (1:1000) before FACS sorting to label and exclude dead cells.

10.2.15.2 Cell sorting by flow cytometry

To obtain purified lysates from autophagy-deficient neurons, cells in suspension were stained with DAPI and DRAQ5. Cell sorting was performed using BD FACSAria Fusion IIu and BD FACSAria IIIu with FACSDiva 8.0.1 software. Cells/Neurons were sorted at 4°C using a 100 µm nozzle, and sheath pressure was set at 20 psi. 0.9% NaCl was used as sheath fluid. The tdTomato highly positive/ DAPI negative/ DRAQ5 positive cell population was selected. Cells were collected in chilled 1.5 mL Eppendorf tubes containing DPBS. After sorting, the cells were centrifuged at 3000 xg for 3 min and lysed in buffers depending on subsequent analysis.

10.2.16 Total proteome analyses

10.2.16.1 Atg5flox:CAG-Cre^{Tmx}

For total proteome analysis *Atg5*flox:CAG-Cre^{Tmx} cultured neurons were harvested at DIV15-16 in RIPA buffer and processed as described for Immunoblotting (see above). A total of 50µg were forwarded for proteomic analysis using an in-gel digestion protocol for sample preparation. In brief, samples were loaded onto an SDS-PAGE gel and run for 1-2 cm. The whole running line was chopped into small pieces and transferred in a 1.5 ml Eppendorf tube. Samples were reduced (10 mM DTT) and alkylated (55 mM CAA). Protein was digested overnight using Trypsin (10 ng/µL 90% Trypsin) and LysC (50 mM). Peptides were extracted and purified using Stagetips. Eluted peptides were dried in vacuo, resuspended in 1% formic acid/4% acetonitrile and stored at -20°C prior to MS measurement.

All samples were analyzed on a Q Exactive Plus Orbitrap (Thermo Scientific) mass spectrometer coupled to an EASY nLC (Thermo Scientific). Peptides were loaded with solvent A (0.1% formic acid in water) onto an in-house packed analytical column (50 cm — 75 µm I.D.,

filled with 2.7 µm Poroshell EC120 C18, Agilent). Peptides were chromatographically separated at a constant flow rate of 250 nL/min using the following gradient: 4-5% solvent B (0.1% formic acid in 80 % acetonitrile) within 1.0 min, 5-28% solvent B within 200.0 min, 28-50% solvent B within 28.0 min, 50-95% solvent B within 1.0 min, followed by washing and column equilibration. The mass spectrometer was operated in data-dependent acquisition mode. The MS1 survey scan was acquired from 300-1750 m/z at a resolution of 70,000. The top 10 most abundant peptides were isolated within a 2.0 Th window and subjected to HCD fragmentation at a normalized collision energy of 27%. The AGC target was set to 5e5 charges, allowing a maximum injection time of 55 ms. Product ions were detected in the Orbitrap at a resolution of 17,500. Precursors were dynamically excluded for 40.0 sec. Each sample was injected twice.

Using default parameters, all mass spectrometric raw data were processed with Maxquant (version 1.5.3.8). Double injections from each sample were combined in MaxQuant by naming them identically. MS2 spectra were searched against the Uniprot mouse reference proteome containing isoforms (UP000000589, downloaded at 26.08.2020), including a list of common contaminants. The target-decoy approach estimated false discovery rates on protein and PSM levels to 1% (Protein FDR) and 1% (PSM FDR), respectively. The minimal peptide length was set to 7 amino acids, and carbamidomethylation at cysteine residues was considered a fixed modification. Oxidation (M), Phospho (STY), and Acetyl (Protein N-term) were included as variable modifications. The match-between runs option was enabled. LFQ quantification was enabled using default settings.

10.2.16.2 Atg16L1flox:CAG-Cre^{Tmx}

For total proteome analysis *Atg16L1*flox:*CAG*-Cre^{Tmx} sample preparation was done as described for *Atg5*flox:*CAG*-Cre^{Tmx} cultured neurons (see above).

Peptide digests were analyzed on a Q Exactive plus Orbitrap (Thermo Scientific) mass spectrometer coupled to an EASY nLC (Thermo Scientific). Samples were loaded onto an in-house packed analytical column (50 cm — 75 µm I.D., filled with 2.7 µm Poroshell EC120 C18, Agilent). Peptides were separated at a 250 nL/min flow rate using 2 hrs runs with data-

independent acquisitions (DIA) or 4 hrs runs with the data-dependent acquisition (DDA). The gradients were: (2 hrs) 3-5% solvent B (0.1% formic acid in 80 % acetonitrile) within 1.0 min, 5-30% solvent B within 91.0 min, 30-50% solvent B within 17.0 min, 50-95% solvent B within 1.0 min, followed by washing with 95 % solvent B for 10 min or (4h) 4-5% solvent B (0.1% formic acid in 80 % acetonitrile) within 1.0 min, 5-28% solvent B within 200.0 min, 28-50% solvent B within 28.0 min, 50-95% solvent B within 1.0 min, followed by washing with 95 % solvent B for 10 min.

DDA runs for spectrum library generation were acquired from each sample. MS1 survey scans were acquired at a resolution of 70,000. The top 10 most abundant peptides were isolated within a 2.0 Th window and subjected to HCD fragmentation with a normalized collision energy of 27. The AGC target was set to 5e5 charges, allowing a maximum injection time of 55 ms. Product ions were detected in the orbitrap at a resolution of 17,500. Precursors were dynamically excluded for 20.0 s.

Sample runs were acquired in DIA mode using 10 variable windows covering the mass range from m/z 450 to m/z 1200. MS1 scans were acquired at 140,000 resolution, and maximum IT restricted to 120 ms and an AGC target set to 5e6 charges. The settings for MS2 scans were 17,500 resolution, maximum IT restricted to 60 ms and AGC target set to 5e6 charges. The default charge state for the MS2 was set to 4. Stepped normalized collision energy was set to 27. All spectra were acquired in profile mode.

An assay-specific hybrid spectrum library was generated in Spectronaut 13 (Bruderer et al. 2015) using DDA library runs, DIA sample runs, and a mouse sequence file (up000000589) downloaded from Uniprot. Spectronaut default settings were used for the analysis of the DIA runs. Protein identifications were filtered for q-values below 0.01, and normalized intensities were exported for subsequent statistical analysis in Perseus 1.6.1.1 (Tyanova et al. 2016). Intensities were transformed to log2 values, and the dataset was filtered for at least 3 out of 3 values in at least one condition. The remaining missing values were imputed with random values from the left end of the intensity distribution (with 0.3 sd, downshift 2 sd). Two runs were removed from the analysis since the projection in the principal component analysis were outside median plus/minus 4 times interquartile range for component 1 or 2. Two sample Student´s T-tests were calculated using permutation-based FDR estimation.

10.2.16.2 Atg5flox:CamKIIα-Cre/tdTomato & Atg5flox:VGAT-Cre/tdTomato mice

10.2.16.2.1 Sample preparation

Isolations of neurons for total proteome of autophagy-deficient cells (*Atg5*flox:CamKIIα-Cre:tdTomato, *Atg5*flox:VGAT-Cre:tdTomato) was done using FACS isolation as described above. Sorted cells were pelleted and resuspended in SP3 lysis buffer (5% SDS in PBS). Chromatin was degraded using a Biorupter (Diagenode, 10 min, cycle 30/30). The samples were reduced (5 mM DTT) and alkylated (40 mM CAA), and protein content was measured with the Pierce BCS protein assay. 20 µg were used for protein digestion according to the single-pot solid-phase-enhanced sample preparation (Hughes et al. 2019)

10.2.16.2.2 LCMS Data Independent Acquisition- Atg5flox:CamKIIα-Cre/tdTomato

The LCMS analysis approach was adjusted to handle low input volume. Samples were analyzed on a Q Exactive Exploris 480 (Thermo Scientific) mass spectrometer that was coupled to an Evosep ONE (Evosep) in the recommended “whisper” setup. Samples were loaded onto EvoTips following the manual instructions (Evosep). Peptides were chromatographically separated by the predefined “whisper 20 SPD” set on a 58 min gradient on a PepSep 15 cm column with a 75 µm inner diameter filled with 1.9 µm Dr Maisch resin. MS1 scans were acquired from 380 m/z to 900 m/z at 45k resolution. Maximum injection time was set to 60 ms and the AGC target to 100%. MS2 scans ranged from 400 m/z to 880 m/z and were acquired at 45 k resolution with a maximum injection time of 84 msec and an AGC target of 1000%. DIA scans covering the precursor range from 400 - 880 m/z were acquired in 15 x 30 m/z staggered windows resulting in 30 nominal 15 m/z windows after demultiplexing. All scans were stored as a centroid.

Thermo raw files were demultiplexed and transformed to mzML files using the msconvert module in Proteowizard. MzML files were converted to dia file format in DIA-NN 1.7.15 . A Mouse canonical Swissprot fasta file was converted to a Prosit upload file with the convert tool in encyclopedia 0.9.0 (Searle et al. 2018) using default settings: Trypsin, up to 1 missed cleavage, range 396 m/z – 1004 m/z, charge states 2+ and 3+, default charge state 3 and NCE 33. The csv file was uploaded to the Prosit webserver and converted to a spectrum library in

generic text format (Gessulat et al. 2019). The resulting library (16998 protein isoforms, 21694 protein groups and 1404872 precursors was used in DIA-NN 1.7.15 (Demichev et al. 2020) to search acquired data in double-pass mode. The applied settings were: Output will be filtered at 0.01 FDR, N-terminal methionine excision enabled, Maximum number of missed cleavages set to 1, Min peptide length set to 7, Max peptide length set to 30, Min precursor m/z set to 400, Max precursor m/z set to 1000, Cysteine carbamidomethylation enabled as a fixed modification.

10.2.16.2.3 LCMS Data Independent Acquisition- Atg5flox:VGAT-Cre/tdTomato

Samples were analysed on a Q Exactive Exploris 480 (Thermo Scientific) mass spectrometer equipped with a FAIMSpro differential ion mobility device coupled to an EASY-nLC 1200 (Thermo Scientific). Samples were loaded onto an in-house packed analytical column (30 cm — 75 µm I.D., filled with 2.7 µm Poroshell EC120 C18, Agilent). Peptides were chromatographically separated at a constant flow rate of 300 nL/min and the following gradient: initial 4% B (0.1% formic acid in 80 % acetonitrile), up to 30% B in 74 min, up to 55% B within 8.0 min and up to 95% solvent B within 2.0 min, followed by a 6 min column wash with 95% solvent B. The FAIMS pro was operated at -47V compensation voltage and electrode temperatures of 99.5 °C for the inner and 85 °C for the outer electrode. Identical HPLC settings were used for library generation and sample runs.

Aliquots from each sample were pooled, and the pool was used for spectrum library generation by narrow window DIA of six 100 m/z gas phase fractions (GPF) covering the range from 400 m/z to 1000 m/z (Searle et al. 2020). The Orbitrap was operated in DIA mode. MS1 scans of the respective 100 m/z gas-phase fraction were acquired at 60k resolution. Maximum injection time was set to 60 ms and the AGC target to 100%. MS2 scans of the corresponding 100 m/z regions were acquired in 24 x 4 m/z staggered windows resulting in 48 nominal 2 m/z windows after demultiplexing. MS2 settings were 30 k resolution, 60 ms maximum injection time and an AGC target of 100%. All scans were stored as a centroid.

MS1 scans were acquired from 390 m/z to 1010 m/z at 60k resolution. Maximum injection time was set to 60 ms and the AGC target to 100%. MS2 scans ranged from 300 m/z to 1500 m/z and were acquired at 15 k resolution with a maximum injection time of 22 msec and an

AGC target of 100%. DIA scans covering the precursor range from 400 - 1000 m/z were acquired in 50 x 12 m/z staggered windows resulting in 100 nominal 6 m/z windows after demultiplexing. All scans were stored as a centroid.

Thermo raw files were demultiplexed and transformed to mzML files using the msconvert module in Proteowizard. MzML files were converted to dia file format in DIA-NN 1.7.11

A Mouse canonical Swissprot fasta file was converted to a Prosit upload file with the convert tool in encyclopedia 0.9.0 (Searle et al. 2018) using default settings: Trypsin, up to 1 missed cleavage, range 396 m/z – 1004 m/z, charge states 2+ and 3+, default charge state 3 and NCE 33. The csv file was uploaded to the Prosit webserver and converted to a spectrum library in generic text format (Gessulat et al. 2019). The resulting library (16998 protein isoforms, 21698 protein groups and 1404872 precursors) was searched in DIA-NN 1.7.11 (Demichev et al. 2020) with the 6 GPF runs to generate a project-specific library (6275 protein isoforms, 6523 protein groups and 26215 precursors). The applied settings were: Output will be filtered at 0.01 FDR, N-terminal methionine excision enabled, the maximum number of missed cleavages set to 1, min peptide length set to 7, max peptide length set to 30, min precursor m/z set to 400, Max precursor m/z set to 1000, cysteine carbamidomethylation enabled as a fixed modification,

10 sample files were searched with DIA-NN 1.7.11 and the project library. In addition to the settings used for library generation, Rt dependent normalization was used.

10.2.17 PKA pSubstrate Immunoprecipitation

WT brains were homogenized in Co-IP buffer and processed as described above. A total amount of 2 mg protein was provided to the beads. The samples were loaded onto an SDS-PAGE gel, and sample preparation followed the in-gel digestion protocol (described above). Eluted peptides were dried in vacuo, resuspended in 1% formic acid/4% acetonitrile and stored at -20°C prior to MS measurement.

All samples were analyzed on a Q Exactive Plus Orbitrap mass spectrometer coupled with an EASY nLC (Thermo Scientific). Peptides were loaded with solvent A (0.1% formic acid in water) onto an in-house packed analytical column (50 cm, 75 µm I.D., filled with 2.7 µm Poroshell

EC120 C18, Agilent). Peptides were chromatographically separated at a constant flow rate of 250 nL/min using the following gradient: 3-5% solvent B (0.1% formic acid in 80 % acetonitrile) within 1.0 min, 5-30% solvent B within 40.0 min, 30-50% solvent B within 8.0 min, 50-95% solvent B within 1.0 min, followed by washing and column equilibration. The mass spectrometer was operated in data-dependent acquisition mode. The MS1 survey scan was acquired from 300-1750 m/z at a resolution of 70,000. The top 10 most abundant peptides were isolated within a 1.8 Th window and subjected to HCD fragmentation at a normalized collision energy of 27%. The AGC target was set to 5e5 charges, allowing a maximum injection time of 110 ms. Product ions were detected in the Orbitrap at a resolution of 35,000. Precursors were dynamically excluded for 10.0 s. Using default parameters, all mass spectrometric raw data were processed with Maxquant (version 1.5.3.8). Briefly, MS2 spectra were searched against the Uniprot mouse reference proteome containing isoforms (UP000000589, downloaded at 26.08.2020), including a list of common contaminants. False discovery rates on protein and PSM levels were estimated by the target-decoy approach to 1% (Protein FDR) and 1% (PSM FDR), respectively. The minimal peptide length was set to 7 amino acids, and carbamidomethylation at cysteine residues was considered a fixed modification. Oxidation (M), Phospho (STY), and Acetyl (Protein N-term) were included as variable modifications. The match-between runs option was enabled. LFQ quantification was enabled using default settings.

Pathway analysis of proteomic approaches was performed using WebGestalt (WEB-based GEne SeT AnaLysis Toolkit, developed and maintained by the Zhang Lab, Baylor College of Medicine, Houston, Texas) (Liao et al. 2019). Venn diagram analysis was done using Venny[2.1] (Oliveros, J.C. (2007-2015) Venny. An interactive tool for comparing lists with Venn's diagrams. https://bioinfogp.cnb.csic.es/tools/venny/index.html).

10.2.18 Phosphoproteomic analyses

10.2.18.1 Atg5flox:CamKIIα-Cre & Atg5flox:VGAT-Cre mice brain tissue

Experiments using stable isotope labelled animals as an internal control for proteomic/phosphoproteomic analysis of cortex (*Atg5*flox:*CamKIIα*-Cre mice) and striatum (*Atg5*flox:*VGAT*-Cre mice) were performed with 12-14 weeks old mice brain tissue. Brains

from isotope labelled mice and ATG5 KO mice of both lines were homogenized using a Wheaton Potter-Elvehjem Tissue Grinder (VWR) in 6 M Urea/ 2 M Thiourea. Lysates were sonicated and centrifuged at maximum speed. The supernatant was forwarded to protein concentration assessment using Pierce™ 660nm Protein Assay Reagent (Thermo Scientific™). Lysates of ATG5 KO mice were mixed with brain lysates of isotope labelled mice in a ratio of 1:1 (1 mg:1 mg). Samples were incubated with 10 mM DTT for 30 min at RT, followed by 45 min incubation with 55 mM IAA in the dark. Afterwards, samples were pre-digested with LysC in an enzyme:substrate ratio of 1:50 for 2 hrs. The samples were diluted three times with 50 mM ABC buffer to reach a concentration of 2 M Urea before LysC was added again in an enzyme:substrate ratio of 1:100 for overnight digestion at RT. The next day, desalting and phosphopeptide enrichment were performed.

10.2.18.2 In-vivo phosphoproteome WT & Atg5flox:CamKIIα-Cre brain$^{DMSO:Forskolin}$

Experiments with acute brain slices treated with the cAMP-inducing agent Forskolin were performed with 12-14 weeks old mice. The brain was isolated and chopped into 400µm thick sections. The sections were washed with HBSS, transferred into media, and placed in the incubator for 1 hour. Afterwards, they were treated with 50µM Forskolin for 15 min before being washed with ice-cold PBS for albumin removal. The sections were snap-frozen and stored at -80°C till further use. On the day of the experiment, slices were homogenized in 1.5 mL 8 M Urea buffer using a Wheaton Potter-Elvehjem Tissue Grinder (VWR). The lysates were sonicated and centrifuged at 13000 rpm for 10 min. Protein concentration was assessed using Pierce™ 660nm Protein Assay Reagent (Thermo Scientific™) and 1 mg protein of each sample taken for the experiment. The samples were pre-digested in 5 mM TCEP, 27.5 mM CAA and LysC, in an enzyme:substrate ratio of 1:50 for 3 hours at RT after vortexing. Afterwards, the samples were diluted to a concentration of 2 M Urea using 50 mM ABC buffer. Trypsin was added to an enzyme:substrate ratio of 1:100 and incubated overnight at RT. The next day, desalting and phosphopeptide enrichment were performed.

10.2.18.3 Desalting and phosphopeptide enrichment

The next day, after Trypsin digestion, the samples were acidified with TFA (1:100 [v/v]) before 10 min centrifugation. Desalting of the samples was performed with 50 mg C_{18} SepPak®Vac cartridges (Waters™). Therefore, the columns were activated with 2 mL 100% CAN and washed three times with 1 mL 0.1% TFA before loading samples. Samples were washed three times with 1 mL 0.1% TFA prior to elution with 0.6 mL elution buffer (60% ACN, 0.1% TFA). 30µg of the sample were taken, desalted and stored on stage tips for total proteome analysis before the remaining sample was dried in a vacuum concentrator. TiO_2 Phosphopeptide extraction was performed using the High-Select™ TiO2 Phosphopeptide Enrichment Kit (Thermo Scientific™) following the manufacturers' instructions. In brief, a lyophilized peptide sample was resuspended in 150 µL Binding/Equilibration Buffer, columns prepared using 20 µL Wash Buffer followed by 20 µL Binding/ Equilibration Buffer. The samples were run twice through the column before the column was washed with 20 µL Binding/ Equilibration Buffer followed by 20 µL Wash Buffer. Afterwards, the columns were washed with 20 µL of LC-MS grade water before the phosphopeptides were eluted from the column in 50 µL Phosphopeptide Elution Buffer. Samples were dried immediately using a vacuum concentrator and subsequently resuspended in 15 µL resuspension buffer (5% FA and 2% ACN). Phosphopeptide samples were stored at -20°C until measurement.

10.2.18.4 Sample measurements- MassSpec

Proteome samples were eluted from stage tips with elution buffer (60% ACN, 1% ammonia), dried in a vacuum concentrator and resuspended in 12µl resuspension buffer. Proteome and phosphoproteome samples were measured on a Thermo Orbitrap Eclipse mass spectrometer with an AIMS interface coupled to a Thermo EASY-nLC system. Each sample was measured in a 90min reverse phase separation using two FAIMS CVs -45V and -65V.

10.2.18.5 Data processing

All raw files were demultiplexed for FAIMS CVs using the Coons lab “FAIMS to Mzxml generator” (https://github.com/coongroup/FAIMS-MzXML-Generator). Mzxml files were analyzed with MaxQuant 1.6.14.0 using a Uniprot mouse protein database (release July 3, 2020). Default settings were used plus: Multiplicity set to 2, label: lys6, enzyme: LysC/P, p(STY)

enabled as variable modification, a match between runs were enabled, unmodified counterpart peptides were not discarded.

The resulting MaxQuant (Tyanova et al. 2015) output was further analyzed in Perseus 1.6.14.0 (Cox and Mann 2012) and InstantClue 0.10.10 (Nolte et al. 2018).

10.2.19 Live-Imaging of cultured neurons

10.2.19.1 GluA1-pHlourin

Neurons were imaged 7-8 days after transfection at DIV14-15 using Zeiss Axiovert 200M microscope (Observer. Z1, Zeiss, USA) equipped with 40x/1.4 oil DIC objective; a pE-4000 LED light source (CoolLED), and a Hamamatsu Orca-Flash4.O V2 CMOS digital camera. Every second, time-lapse image were acquired using Micro-Manager software (Micro-Manager1.4, USA). The imaging chamber was connected to aVC-6 (six-channel valve controller, Warner Instrument Corporation) and plugged into a pump (Mini-Peristaltic Pump II, Harvard Apparatus) to ensure a constant media flow over the neurons. Note that all used media were osmolarity adjusted using D-Mannitol before the experiment. Neurons were imaged in imaging buffer (pH = 7.4) for 1 minute to establish baseline GluA1-pHlourin level. Afterwards, media conditions were switched to an acidic buffer (pH = 5.5) to quench the GluA1-pHlourin signal from membrane inserted receptors until a plateau was reached. For dequenching, the media was switched to a standard imaging buffer again. The total amount of GluA1-pHlourin in the neurons was assessed by a media exchange to an alkaline buffer (NH_4Cl-buffer). To calculate the surface fraction of GluA1-pHlourin receptors, 10 ROIs per neuron along the processes were chosen, and the mean fluorescence intensity signal was plotted over time using Image J (Plot Z-axis Profile). The background was subtracted for each single time point, and the mean of 30 images in the plateau phase of the single conditions was determined. The surface fraction was calculated as demonstrated in the formula for every single neuron:

$$Surface\ GLUR1\ (\%) = \frac{F(basal) - F(acidic)}{F(alkaline) - F(acidic)} * 100$$

10.2.19.1 GCamP7f experiments

Calcium imaging experiments using GCAMP7f$^{CamKII\alpha}$ were performed at *Atg5*flox:tdTomato WT and KO primary cortical and hippocampal neuronal cell culture. The KO was induced via virus transfection with *CamKIIα*-Cre (VVF) and *GAD67*-Cre (VVF) at DIV5. GCAMP7f$^{CamKII\alpha}$ virus-mediated transfection was done on DIV7. Live-cell imaging and stimulation were performed at DIV15-16 using Zeiss Axiovert 200M microscope (Observer. Z1, Zeiss, USA) equipped with 10x/0.3 EC Plan-Neofluar objective; a pE-4000 LED light source (CoolLED), and a Hamamatsu Orca-Flash4.O V2 CMOS digital camera. Neurons were imaged in an osmolarity adjusted imaging buffer, and time-lapse images were taken within a 1-sec interval. For electrical field stimulation, neurons were stimulated four times with 100 action potentials (100 AP) in a 3-sec interval at 100 Hertz (Hz) using an RC-47FSLP stimulation chamber (Warner Instruments). Each coverslip was only stimulated once and was allowed to rest for 5 min in case of subsequent treatment. Afterwards, the buffer was supplemented with 10 µM CNQX for 5 min before imaging as described above.

The cells were incubated with 10µM H89 in DMSO or DMSO as vehicle control for 20 minutes before imaging to mimic decreased PKA signalling observed in autophagy-deficient neurons. Imaging was performed as described above.

For analysis, neuronal cell bodies were chosen as ROI, and the GCAMP7 fluorescence response to the stimulus was plotted over time using Image J (Plot Z-axis Profile). Values were exported to excel for background subtraction per image. Baseline fluorescence levels were calculated by taking the mean of 32 images before stimulation. Baseline value was subtracted, and data normalized to the first peak to visualize facilitation. The 1st and 4th peak difference was calculated and is presented in the bar graphs.

10.2.20 RNA Sequencing

10.2.20.1 RNA isolation

RNA of FACS sorted neurons were isolated using the RNeasy® Plus Micro Kit (Qiagen). Therefore, cell pellets were lysed in 350 µl Buffer RLT Plus and vortexed for 30 sec. The lysates were transferred into gDNA Eliminator spin columns placed in 2 ml collection tubes and

centrifuged for 30 sec at >8000 xg to bind DNA in the sample. After centrifugation, the spin columns were discarded, and 350 µl 70% EtOH was added to the samples. Samples were transferred to RNeasy MinElute spin columns placed in 2 mL collection tubes and centrifuged for 15 sec at >8000 xg. Subsequently, 700 µL of Buffer RW1, 500 µL of Buffer RPE, and 80% EtOH were added to the columns, centrifuged between each solution. After the last centrifugation, the columns were transferred into a fresh collection tube and centrifuged at full speed for 5 min. The columns were again transferred into fresh collection tubes, and RNA was eluted from the columns applying 14 µL RNase-free water and short centrifugation at full speed to elute the RNA. Isolated RNA was forwarded to RNA sequencing analysis

10.2.20.2 Library preparation

Library preparation was performed with the NEBNext® Ultra Directional RNA Library Prep Kit for Illumina. The first step involves the removal of ribosomal RNA using biotinylated target-specific oligos combined with rRNA removal beads from 1ug total RNA input. The NEBNext® rRNA Depletion Kit (Human/Mouse/Rat) depletes samples of cytoplasmic rRNA. Following purification, the RNA is fragmented into small pieces using divalent cations under elevated temperatures. The cleaved RNA fragments are copied into first-strand cDNA using reverse transcriptase and random primers, followed by second-strand cDNA synthesis using DNA Polymerase I and RNase H. These cDNA fragments then have the addition of a single'A' base and subsequent ligation of the adapter. The products are purified and enriched with PCR (20ul template, 15cycles) to create the final cDNA library. After library validation and quantification (Agilent Tape Station), equimolar amounts of the library were pooled. Pools of 4-6 libraries were quantified using the Peqlab KAPA Library Quantification Kit and the Applied Biosystems 7900HT Sequence Detection System and sequenced on a NovaSeq 6000 S4 flowcell 2x100bp.

10.2.20.3 Read Trimming

Illumina adapters were clipped off the raw paired-end reads using cutadapt v2.10 with standard parameters and a minimum read length of 35 base pairs after trimming (shorter reads were discarded).

For read 1, the adapter sequences trimmed were AGATCGGAAGAGCACACGTCTGAACTCCAGTCA, AGATCGGAAGAGCACACGTCTGAAC, TGGAATTCTCGGGTGCCAAGG, AGATCGGAAGAGCACACGTCT, CTGTCTCTTATACACATCT, and AGATGTGTATAAGAGACAG.

For read 2, the sequences were AGATCGGAAGAGCGTCGTGTAGGGAAAGAGTGT, AGATCGGAAGAGCGTCGTGTAGGGA, TGGAATTCTCGGGTGCCAAGG, AGATCGGAAGAGCACACGTCT, CTGTCTCTTATACACATCT and AGATGTGTATAAGAGACAG.

10.2.20.4 Transcript Quantification

Transcript abundance was quantified using kallisto v0.46.1. The transcriptome index was built by kallisto index from file Mus_musculus.GRCm38.rna.fa of Ensembl release 100. Subsequently, the adapter-trimmed RNA-seq reads were matched against the index using kallisto quant with standard parameters and 100 bootstrap samples (-b 100).

Transcript abundances (=TPMs, =estimated Transcripts Per Million) were extracted from the primary output of kallisto using package tximport v1.16.1 of the Bioconductor v3.11 software project in an environment of the R v4.0.0 programming language. Ensembl transcript ids were mapped to Ensembl gene ids and gene symbols in the same environment, using package biomaRt v2.44.4 to access the Ensembl v100 database. A table containing the gene ids, gene symbols, and kallisto TPMs was output as kallisto_tx_abundance.xlsx (141450 transcripts). In table kallisto_tx_abundance_1TPM.xlsx, transcripts represented by less than 1 TPM were filtered out (72659 remaining transcripts).

The TPM values of transcript ids associated with the same Ensembl gene id were summed up for downstream gene-based analysis. That resulted in 53028 unique Ensembl gene ids in the full matrix and 23669 unique Ensembl gene ids in the 1TPM-filtered matrix. The Ensembl ids were associated with 52263 unique gene symbols in the full matrix and 23380 unique gene symbols in the filtered matrix. To resolve cases where >1 Ensembl gene id mapped to the same symbol, we discarded Ensembl gene ids which were not represented in the Ensembl v100 genome annotation file Mus_musculus.GRCm38.100.gtf. (Note that unrepresented Ensembl gene ids were not removed if they did not cause a mapping conflict. That may be an issue as all unrepresented ids came from PATCH contigs rather than canonical chromosomes. On the

other hand, these contigs had been part of the kallisto index used and thus have influenced the mapping process, so they should be represented in the output.) After removing 873 Ensembl gene ids due to conflicts, the final number of genes represented in the full matrix was 52155 and 23319 in the 1TPM-filtered matrix. The full and the 1TPM-filtered gene collapsed matrices are reported in files kallisto_gene_abundance.xlsx and kallisto_gene_abundance_1TPM.xlsx, respectively.

In addition to the TPM values, kallisto also outputs estimated read counts per transcript. We converted these to read counts per gene by summing over associated transcripts as above and retaining the same genes as in the gene-collapsed TPM matrices. Summed estimated counts are reported in files kallisto_gene_counts.xlsx and kallisto_gene_counts_1TPM.xlsx.

10.2.20.5 Differential Gene Expression Analysis

We used the R package sleuth v0.30.0 for differential gene expression because sleuth is explicitly designed to work with kallisto output. Because the experimental samples had been sequenced in two batches, we employed an additive linear model with categorical factors Batch and Genotype. Two of the original samples (BKC515 and BKC437) were left out of the analysis because their genotypic states were ambiguous. (Note that these samples are also left out of the reported kallisto TPM and count matrices).

File newDGE_sleuth_BG_reproduced.xlsx reports the result of the sleuth analysis for model coefficient Genotype, that is, for the effect of genotype state (WT or KO) on transcript expression, corrected for batch membership of the samples.

Sleuth was configured to run Wald tests on the linear model's coefficients and not aggregate the p-values from the individual transcripts contributing to a gene's expression. Therefore a given Ensembl gene id is usually represented in more than one row of the table. The original sleuth output column names "b" (effect strength of the model coefficient), "pval" (p-value = probability of the effect being equal to zero), and "qval" (FDR adjusted p-value using the Benjamini-Hochberg procedure) has been replaced by "logFoldChange", "p-value", and "FDR". (Note that the effect strength "b" is only roughly comparable to the natural logarithm of fold change and that it is not even clear whether in sleuth v0.30.0 the definition has not already been changed to log2 – see https://github.com/pachterlab/sleuth/issues/59). The reported

table contains in addition columns for the Ensembl gene id (“geneid”) and transcript id (“txid”), plus the gene symbol and a description.

10.2.20.6 Data analysis

The p-value of the Kallisto gene counts was calculated, and all significant hits were forwarded to analysis. The means were calculated between the genotypes and the genes sorted by the difference between WT and KO. The dataset was divided into up- and downregulated hits, and both datasets were analyzed using Enrichr (Ma’ayan Lab, Icahn School of Medicine at Mount Sinai, New York) gene set analysis. Results from ChEA 2016 analysis are presented as Clustergrams.

10.2.21 High throughput microscopy assays

Cells were isolated from adult (12-13 weeks) old mice as described for FACS sorting. Afterwards, the cells were resuspended in supplemented NBA medium, were seeded 100 µl/well in clear 96-well plates (Greiner) and were incubated for 3 hours (37 C, 5% CO2) before stimulation. Using an electronic 8-channel pipette (Eppendorf) at low dispense speed, the cells were stimulated for 15 min. The stimulant compound was prepared 10-fold concentrated in 12.5 µl of PBS in 96-well V-bottom plates (NerbePlus). Half of the media (50 µl) was removed from the wells in the cell culture plate, mixed with a stimulant in the V-bottom plate, and added back to the well. Negative controls were stimulated with the vehicle only. The cells were fixed by adding 100 µl 8% PFA (4% final) for 10 min followed by 2X wash with 100 µl PBS. Then the cells were blocked and permeabilized with 50 µl normal goat serum blocking (NGSB) for 1 h at room temperature. Afterwards, the cells were Incubated with 30 µl primary antibodies diluted in 1% BSA overnight at 4°C. Rinsed 3X with 100 µl PBS for 10 min each and were incubated with 50 µl secondary antibodies diluted 1:1000 in PBS for 1 h at room temperature in the dark and rinsed 3X with 100 µl PBS for 10 min each. Finally, the wells were filled with 200 µl PBS and sealed with aluminium sealing.

For imaging, a CellInsight CX7 LZR (ThermoFisher Scientific) microscope with a laser light source was used to acquire images of 1024 * 1024 pixels with a 20X objective. Image analysis was performed using the Cellomics software package. Briefly, images of tdTomato stainings

were background corrected (low pass filtration), converted to binary image masks (fixed threshold), and segmented (geometric method). Inhibitory neurons were then identified by appropriate object selection parameters such as size, circularity, and average tdTomato intensity. These image masks were then overlaid on images obtained at other fluorescence wavelengths to quantify signal intensities. To later determine spillover between fluorescence channels, three respective controls for each triple staining: (1) tdTomato alone, (2) tdTomato + antibody 1, and (3) tdTomato + antibody 2 were included. Single-cell data containing the raw fluorescence data of single cells from the Cellomics software was exported as spreadsheets and analyzed by open-source statistical language R. The raw fluorescence data of the controls were used to calculate the slope of best fit straight lines by linear regression, which were then applied to compensate. Compensated data were scaled to a mean value of 1 for the vehicle-stimulated cells to adjust for variability between experimental treatments. To visualize the data, two-dimensional probability density plots were generated using R. For gating subpopulations, the thresholds were set at the local minima of probability density plots.

10.2.22 Statistical analysis & analysis software

Global proteome and phosphoproteome data were analysed as described for each dataset (see above). MaxQuant and Perseus were used for analysis (Tyanova et al. 2015; Tyanova et al. 2016; Cox and Mann 2012). Volcano blots to visualize global proteome and phosphoproteome data were generated using Instant Clue (Nolte et al. 2018). Heatmaps were created using Morpheus (https://software.broadinstitute.org/morpheus), Gene Ontology (GO) analysis and visualization were done using WebGestalt (WEB-based GEne SeT AnaLysis Toolkit) (Liao et al. 2019) or ShinyGO v0.741: Gene Ontology Enrichment Analysis + more (http://bioinformatics.sdstate.edu/go/), Venn diagrams were created using Gene List Venn Diagram, an interactive tool for comparing lists with Venn's diagrams (http://genevenn.sourceforge.net/). GO functional analysis and human phenotype ontology analysis was done using g:Profiler (Raudvere et al. 2019) (https://biit.cs.ut.ee/gprofiler/gost). 3D-analysis and reconstruction of immunostainings were done using Amira Software 2020.2 (Thermo Fisher Scientific).

Statistical analyses were done on cell values, the number of experiments or single animals indicated by data points. The corresponding figure legend depicts the number of independent

experiments and the dataset's origin. MS Excel (Microsoft, USA) and GraphPad Prism version 9 (GraphPad Software, Inc., USA) were used for statistical analysis and illustration of all shown bar graphs. Statistical analysis of normalized data, including two groups, was assessed using a one-tailed student's t-test. Statistical significance between two groups, for all standard distributed raw data, was evaluated with a two-tailed unpaired student's t-test. Statistical difference between more than two groups was evaluated using Two-Way ANOVA (Tukey posthoc test was used to determine the statistical significance between the groups). Depicted in the figure legend are the p-value and standard error of the mean (SEM). Significant differences were accepted at $p<0.05$ indicated by asterixis in the figures (* $p<0.05$; ** $p<0.01$; *** $p<0.001$).

10.2.23 Data availability

All data supporting the findings described in this study are available upon request.

11.Publication bibliography

A novel gene containing a trinucleotide repeat that is expanded and unstable on Huntington's disease chromosomes. The Huntington's Disease Collaborative Research Group (1993). In *Cell* 72 (6), pp. 971–983.

Abel, Ted; Nguyen, Peter V. (2008): Chapter 6 Regulation of hippocampus-dependent memory by cyclic AMP-dependent protein kinase. In : Essence of Memory, vol. 169: Elsevier (Progress in Brain Research), pp. 97–115.

Abel, Ted; Nguyen, Peter V.; Barad, Mark; Deuel, Thomas A.S; Kandel, Eric R.; Bourtchouladze, Roussoudan (1997): Genetic Demonstration of a Role for PKA in the Late Phase of LTP and in Hippocampus-Based Long-Term Memory. In *Cell* 88 (5), pp. 615–626. DOI: 10.1016/s0092-8674(00)81904-2.

Adolph, Timon E.; Tomczak, Michal F.; Niederreiter, Lukas; Ko, Hyun-Jeong; Böck, Janne; Martinez-Naves, Eduardo et al. (2013): Paneth cells as a site of origin for intestinal inflammation. In *Nature* 503 (7475), pp. 272–276. DOI: 10.1038/nature12599.

Alirezaei, Mehrdad; Kemball, Christopher C.; Flynn, Claudia T.; Wood, Malcolm R.; Whitton, J. Lindsay; Kiosses, William B. (2010): Short-term fasting induces profound neuronal autophagy. In *Autophagy* 6 (6), pp. 702–710. DOI: 10.4161/auto.6.6.12376.

Almeida, Sandra; Gascon, Eduardo; Tran, Hélène; Chou, Hsin Jung; Gendron, Tania F.; Degroot, Steven et al. (2013): Modeling key pathological features of frontotemporal dementia with C9ORF72 repeat expansion in iPSC-derived human neurons. In *Acta neuropathologica* 126 (3), pp. 385–399. DOI: 10.1007/s00401-013-1149-y.

Aman, Yahyah; Schmauck-Medina, Tomas; Hansen, Malene; Morimoto, Richard I.; Simon, Anna Katharina; Bjedov, Ivana et al. (2021): Autophagy in healthy aging and disease. In *Nat Aging* 1 (8), pp. 634–650. DOI: 10.1038/s43587-021-00098-4.

Amieux, P. S.; Cummings, D. E.; Motamed, K.; Brandon, E. P.; Wailes, L. A.; Le, K. et al. (1997): Compensatory regulation of RIalpha protein levels in protein kinase A mutant mice. In *Journal of Biological Chemistry* 272 (7), pp. 3993–3998. DOI: 10.1074/jbc.272.7.3993.

Amieux, Paul S.; Howe, Douglas G.; Knickerbocker, Heidi; Lee, David C.; Su, Thomas; Laszlo, George S. et al. (2002): Increased basal cAMP-dependent protein kinase activity inhibits the formation of mesoderm-derived structures in the developing mouse embryo. In *Journal of Biological Chemistry* 277 (30), pp. 27294–27304. DOI: 10.1074/jbc.M200302200.

An, Heeseon; Ordureau, Alban; Paulo, Joao A.; Shoemaker, Christopher J.; Denic, Vladimir; Harper, J. Wade (2019): TEX264 Is an Endoplasmic Reticulum-Resident ATG8-Interacting Protein Critical for ER Remodeling during Nutrient Stress. In *Molecular cell* 74 (5), 891-908.e10. DOI: 10.1016/j.molcel.2019.03.034.

Anggono, Victor; Huganir, Richard L. (2012): Regulation of AMPA receptor trafficking and synaptic plasticity. In *Current opinion in neurobiology* 22 (3), pp. 461–469. DOI: 10.1016/j.conb.2011.12.006.

Antoni, F. A.; Palkovits, M.; Simpson, J.; Smith, S. M.; Leitch, A. L.; Rosie, R. et al. (1998): Ca 2+ /Calcineurin-Inhibited Adenylyl Cyclase, Highly Abundant in Forebrain Regions, Is Important for Learning and Memory. In *J. Neurosci.* 18 (23), pp. 9650–9661. DOI: 10.1523/JNEUROSCI.18-23-09650.1998.

Arai, Heii; Takahashi, Tadashi (2009): A combination therapy of donepezil and cilostazol for patients with moderate Alzheimer disease: pilot follow-up study. In *The American journal of geriatric psychiatry : official journal of the American Association for Geriatric Psychiatry* 17 (4), pp. 353–354. DOI: 10.1097/JGP.0b013e31819431ea.

Ariosa, Aileen R.; Klionsky, Daniel J. (2016): Autophagy core machinery: overcoming spatial barriers in neurons. In *Journal of molecular medicine (Berlin, Germany)* 94 (11), pp. 1217–1227. DOI: 10.1007/s00109-016-1461-9.

Arranz, Amaia M.; Delbroek, Lore; van Kolen, Kristof; Guimarães, Marco R.; Mandemakers, Wim; Daneels, Guy et al. (2015): LRRK2 functions in synaptic vesicle endocytosis through a kinase-dependent mechanism. In *Journal of cell science* 128 (3), pp. 541–552. DOI: 10.1242/jcs.158196.

Aye, Thin Thin; Scholten, Arjen; Taouatas, Nadia; Varro, Andras; van Veen, Toon A. B.; Vos, Marc A.; Heck, Albert J. R. (2010): Proteome-wide protein concentrations in the human heart. In *Molecular bioSystems* 6 (10), pp. 1917–1927. DOI: 10.1039/C004495D.

Azarnia Tehran, Domenico; Kuijpers, Marijn; Haucke, Volker (2018): Presynaptic endocytic factors in autophagy and neurodegeneration. In *Current opinion in neurobiology* 48, pp. 153–159. DOI: 10.1016/j.conb.2017.12.018.

Baaske, Magdalena K.; Kramer, Edgar R.; Meka, Durga Praveen; Engler, Gerhard; Engel, Andreas K.; Moll, Christian K. E. (2020): Parkin deficiency perturbs striatal circuit dynamics. In *Neurobiology of disease* 137, p. 104737. DOI: 10.1016/j.nbd.2020.104737.

Bach, M. E.; Barad, M.; Son, H.; Zhuo, M.; Lu, Y. F.; Shih, R. et al. (1999): Age-related defects in spatial memory are correlated with defects in the late phase of hippocampal long-term potentiation in vitro and are attenuated by drugs that enhance the cAMP signaling pathway. In *Proceedings of the National Academy of Sciences of the United States of America* 96 (9), pp. 5280–5285. DOI: 10.1073/pnas.96.9.5280.

Bączyk, Marcin; Alami, Najwa Ouali; Delestrée, Nicolas; Martinot, Clémence; Tang, Linyun; Commisso, Barbara et al. (2020): Synaptic restoration by cAMP/PKA drives activity-dependent neuroprotection to motoneurons in ALS. In *The Journal of experimental medicine* 217 (8). DOI: 10.1084/jem.20191734.

Baines, Anthony J.; Lu, Hui-Chun; Bennett, Pauline M. (2014): The Protein 4.1 family: hub proteins in animals for organizing membrane proteins. In *Biochimica et biophysica acta* 1838 (2), pp. 605–619. DOI: 10.1016/j.bbamem.2013.05.030.

Ball, Nicole; Teo, Wei-Peng; Chandra, Shaneel; Chapman, James (2019): Parkinson's Disease and the Environment. In *Frontiers in neurology* 10, p. 218. DOI: 10.3389/fneur.2019.00218.

Banke, T. G.; Bowie, D.; Lee, H.-K.; Huganir, R. L.; Schousboe, A.; Traynelis, S. F. (2000): Control of GluR1 AMPA Receptor Function by cAMP-Dependent Protein Kinase. In *J. Neurosci.* 20 (1), pp. 89–102. DOI: 10.1523/JNEUROSCI.20-01-00089.2000.

Barco, Angel; Kandel, Eric R. (2005): The Role of CREB and CBP in Brain Function. In Gerald Thiel (Ed.): Transcription Factors in the Nervous System. Weinheim, FRG: Wiley-VCH Verlag GmbH & Co. KGaA, pp. 206–241.

Barmada, Sami J.; Serio, Andrea; Arjun, Arpana; Bilican, Bilada; Daub, Aaron; Ando, D. Michael et al. (2014): Autophagy induction enhances TDP43 turnover and survival in neuronal ALS models. In *Nature chemical biology* 10 (8), pp. 677–685. DOI: 10.1038/nchembio.1563.

Bento, Carla F.; Renna, Maurizio; Ghislat, Ghita; Puri, Claudia; Ashkenazi, Avraham; Vicinanza, Mariella et al. (2016): Mammalian Autophagy: How Does It Work? In *Annual review of biochemistry* 85, pp. 685–713. DOI: 10.1146/annurev-biochem-060815-014556.

Berger, Zdenek; Ravikumar, Brinda; Menzies, Fiona M.; Oroz, Lourdes Garcia; Underwood, Benjamin R.; Pangalos, Menelas N. et al. (2006): Rapamycin alleviates toxicity of different aggregate-prone proteins. In *Human molecular genetics* 15 (3), pp. 433–442. DOI: 10.1093/hmg/ddi458.

Bielekova, Bibiana; Richert, Nancy; Howard, Thomas; Packer, Amy N.; Blevins, Gregg; Ohayon, Joan et al. (2009): Treatment with the phosphodiesterase type-4 inhibitor rolipram fails to inhibit blood--brain barrier disruption in multiple sclerosis. In *Multiple sclerosis (Houndmills, Basingstoke, England)* 15 (10), pp. 1206–1214. DOI: 10.1177/1352458509345903.

Binotti, Beyenech; Pavlos, Nathan J.; Riedel, Dietmar; Wenzel, Dirk; Vorbrüggen, Gerd; Schalk, Amanda M. et al. (2015): The GTPase Rab26 links synaptic vesicles to the autophagy pathway. In *eLife* 4, e05597. DOI: 10.7554/eLife.05597.

Bjørkøy, Geir; Lamark, Trond; Brech, Andreas; Outzen, Heidi; Perander, Maria; Overvatn, Aud et al. (2005): p62/SQSTM1 forms protein aggregates degraded by autophagy and has a protective effect on huntingtin-induced cell death. In *The Journal of cell biology* 171 (4), pp. 603–614. DOI: 10.1083/jcb.200507002.

Boda, Attila; Lőrincz, Péter; Takáts, Szabolcs; Csizmadia, Tamás; Tóth, Sarolta; Kovács, Attila L.; Juhász, Gábor (2019): Drosophila Arl8 is a general positive regulator of lysosomal fusion events. In *Biochimica et biophysica acta. Molecular cell research* 1866 (4), pp. 533–544. DOI: 10.1016/j.bbamcr.2018.12.011.

Borodinsky, Laura N.; Spitzer, Nicholas C. (2006): Second messenger pas de deux: the coordinated dance between calcium and cAMP. In *Science's STKE : signal transduction knowledge environment* 2006 (336), pe22. DOI: 10.1126/stke.3362006pe22.

Brandon, E. P.; Zhuo, M.; Huang, Y. Y.; Qi, M.; Gerhold, K. A.; Burton, K. A. et al. (1995): Hippocampal long-term depression and depotentiation are defective in mice carrying a targeted disruption of the gene encoding the RI

beta subunit of cAMP-dependent protein kinase. In *Proceedings of the National Academy of Sciences of the United States of America* 92 (19), pp. 8851–8855. DOI: 10.1073/pnas.92.19.8851.

Brandon, Eugene P.; Idzerda, Rejean L.; McKnight, G. Stanley (1997): PKA isoforms, neural pathways, and behaviour: making the connection. In *Current opinion in neurobiology* 7 (3), pp. 397–403. DOI: 10.1016/S0959-4388(97)80069-4.

Brandon, Eugene P.; Logue, Sheree F.; Adams, Monique R.; Qi, Ming; Sullivan, Sean P.; Matsumoto, Alvin M. et al. (1998): Defective Motor Behavior and Neural Gene Expression in RIIβ-Protein Kinase A Mutant Mice. In *J. Neurosci.* 18 (10), pp. 3639–3649. DOI: 10.1523/JNEUROSCI.18-10-03639.1998.

Bruderer, Roland; Bernhardt, Oliver M.; Gandhi, Tejas; Miladinović, Saša M.; Cheng, Lin-Yang; Messner, Simon et al. (2015): Extending the limits of quantitative proteome profiling with data-independent acquisition and application to acetaminophen-treated three-dimensional liver microtissues. In *Molecular & cellular proteomics : MCP* 14 (5), pp. 1400–1410. DOI: 10.1074/mcp.M114.044305.

Budovskaya, Yelena V.; Stephan, Joseph S.; Deminoff, Stephen J.; Herman, Paul K. (2005): An evolutionary proteomics approach identifies substrates of the cAMP-dependent protein kinase. In *Proceedings of the National Academy of Sciences of the United States of America* 102 (39), pp. 13933–13938. DOI: 10.1073/pnas.0501046102.

Budovskaya, Yelena V.; Stephan, Joseph S.; Reggiori, Fulvio; Klionsky, Daniel J.; Herman, Paul K. (2004): The Ras/cAMP-dependent protein kinase signaling pathway regulates an early step of the autophagy process in Saccharomyces cerevisiae. In *Journal of Biological Chemistry* 279 (20), pp. 20663–20671. DOI: 10.1074/jbc.M400272200.

Burré, Jacqueline; Sharma, Manu; Südhof, Thomas C. (2014): α-Synuclein assembles into higher-order multimers upon membrane binding to promote SNARE complex formation. In *Proceedings of the National Academy of Sciences of the United States of America* 111 (40), E4274-83. DOI: 10.1073/pnas.1416598111.

Burton, K. A.; Johnson, B. D.; Hausken, Z. E.; Westenbroek, R. E.; Idzerda, R. L.; Scheuer, T. et al. (1997): Type II regulatory subunits are not required for the anchoring-dependent modulation of Ca2+ channel activity by cAMP-dependent protein kinase. In *Proceedings of the National Academy of Sciences of the United States of America* 94 (20), pp. 11067–11072. DOI: 10.1073/pnas.94.20.11067.

Cadd, Gary; Stanley McKnight, G. (1989): Distinct patterns of cAMP-dependent protein kinase gene expression in mouse brain. In *Neuron* 3 (1), pp. 71–79. DOI: 10.1016/0896-6273(89)90116-5.

Cao, Ruifeng; Li, Aiqing; Cho, Hee-Yeon (2009): mTOR signaling in epileptogenesis: too much of a good thing? In *J. Neurosci.* 29 (40), pp. 12372–12373. DOI: 10.1523/JNEUROSCI.3486-09.2009.

Carlezon, William A.; Duman, Ronald S.; Nestler, Eric J. (2005): The many faces of CREB. In *Trends in neurosciences* 28 (8), pp. 436–445. DOI: 10.1016/j.tins.2005.06.005.

Carlyle, Becky C.; Nairn, Angus C.; Wang, Min; Yang, Yang; Jin, Lu E.; Simen, Arthur A. et al. (2014): cAMP-PKA phosphorylation of tau confers risk for degeneration in aging association cortex. In *Proceedings of the National Academy of Sciences of the United States of America* 111 (13), pp. 5036–5041. DOI: 10.1073/pnas.1322360111.

Carr, D. W.; Stofko-Hahn, R. E.; Fraser, I. D.; Cone, R. D.; Scott, J. D. (1992): Localization of the cAMP-dependent protein kinase to the postsynaptic densities by A-kinase anchoring proteins. Characterization of AKAP 79. In *Journal of Biological Chemistry* 267 (24), pp. 16816–16823.

Carroll, R. C.; Beattie, E. C.; Xia, H.; Lüscher, C.; Altschuler, Y.; Nicoll, R. A. et al. (1999): Dynamin-dependent endocytosis of ionotropic glutamate receptors. In *Proceedings of the National Academy of Sciences of the United States of America* 96 (24), pp. 14112–14117. DOI: 10.1073/pnas.96.24.14112.

Chalovich, Elisabeth M.; Zhu, Jian-hui; Caltagarone, John; Bowser, Robert; Chu, Charleen T. (2006): Functional repression of cAMP response element in 6-hydroxydopamine-treated neuronal cells. In *Journal of Biological Chemistry* 281 (26), pp. 17870–17881. DOI: 10.1074/jbc.M602632200.

Chang, Jessica T.; Kumsta, Caroline; Hellman, Andrew B.; Adams, Linnea M.; Hansen, Malene (2017): Spatiotemporal regulation of autophagy during Caenorhabditis elegans aging. In *eLife* 6. DOI: 10.7554/eLife.18459.

Chino, Haruka; Hatta, Tomohisa; Natsume, Tohru; Mizushima, Noboru (2019): Intrinsically Disordered Protein TEX264 Mediates ER-phagy. In *Molecular cell* 74 (5), 909-921.e6. DOI: 10.1016/j.molcel.2019.03.033.

Cho, Richard W.; Buhl, Lauren K.; Volfson, Dina; Tran, Adrienne; Li, Feng; Akbergenova, Yulia; Littleton, J. Troy (2015): Phosphorylation of Complexin by PKA Regulates Activity-Dependent Spontaneous Neurotransmitter Release and Structural Synaptic Plasticity. In *Neuron* 88 (4), pp. 749–761. DOI: 10.1016/j.neuron.2015.10.011.

Chowdhury, Dhrubajyoti; Hell, Johannes W. (2018): Homeostatic synaptic scaling: molecular regulators of synaptic AMPA-type glutamate receptors. In *F1000Research* 7, p. 234. DOI: 10.12688/f1000research.13561.1.

Clausen, Terje Høyvarde; Lamark, Trond; Isakson, Pauline; Finley, Kim; Larsen, Kenneth Bowitz; Brech, Andreas et al. (2010): p62/SQSTM1 and ALFY interact to facilitate the formation of p62 bodies/ALIS and their degradation by autophagy. In *Autophagy* 6 (3), pp. 330–344. DOI: 10.4161/auto.6.3.11226.

Coffey, E. E.; Beckel, J. M.; Laties, A. M.; Mitchell, C. H. (2014): Lysosomal alkalization and dysfunction in human fibroblasts with the Alzheimer's disease-linked presenilin 1 A246E mutation can be reversed with cAMP. In *Neuroscience* 263, pp. 111–124. DOI: 10.1016/j.neuroscience.2014.01.001.

Cox, Juergen; Mann, Matthias (2012): 1D and 2D annotation enrichment: a statistical method integrating quantitative proteomics with complementary high-throughput data. In *BMC bioinformatics* 13 Suppl 16, S12. DOI: 10.1186/1471-2105-13-S16-S12.

Cummings, D. E.; Brandon, E. P.; Planas, J. V.; Motamed, K.; Idzerda, R. L.; McKnight, G. S. (1996): Genetically lean mice result from targeted disruption of the RII beta subunit of protein kinase A. In *Nature* 382 (6592), pp. 622–626. DOI: 10.1038/382622a0.

Dahlstrand, Jonas; Lardelli, Michael; Lendahl, Urban (1995): Nestin mRNA expression correlates with the central nervous system progenitor cell state in many, but not all, regions of developing central nervous system. In *Developmental Brain Research* 84 (1), pp. 109–129. DOI: 10.1016/0165-3806(94)00162-s.

D'Andrea Meira, Isabella; Romão, Tayla Taynan; Pires do Prado, Henrique Jannuzzelli; Krüger, Lia Theophilo; Pires, Maria Elisa Paiva; Da Conceição, Priscila Oliveira (2019): Ketogenic Diet and Epilepsy: What We Know So Far. In *Frontiers in neuroscience* 13, p. 5. DOI: 10.3389/fnins.2019.00005.

Dehay, Benjamin; Bové, Jordi; Rodríguez-Muela, Natalia; Perier, Celine; Recasens, Ariadna; Boya, Patricia; Vila, Miquel (2010): Pathogenic lysosomal depletion in Parkinson's disease. In *The Journal of neuroscience : the official journal of the Society for Neuroscience* 30 (37), pp. 12535–12544. DOI: 10.1523/JNEUROSCI.1920-10.2010.

Dehay, Benjamin; Ramirez, Alfredo; Martinez-Vicente, Marta; Perier, Celine; Canron, Marie-Hélène; Doudnikoff, Evelyne et al. (2012): Loss of P-type ATPase ATP13A2/PARK9 function induces general lysosomal deficiency and leads to Parkinson disease neurodegeneration. In *Proceedings of the National Academy of Sciences of the United States of America* 109 (24), pp. 9611–9616. DOI: 10.1073/pnas.1112368109.

Deinhardt, Katrin; Kim, Taeho; Spellman, Daniel S.; Mains, Richard E.; Eipper, Betty A.; Neubert, Thomas A. et al. (2011): Neuronal growth cone retraction relies on proneurotrophin receptor signaling through Rac. In *Science signaling* 4 (202), ra82. DOI: 10.1126/scisignal.2002060.

DeJesus-Hernandez, Mariely; Mackenzie, Ian R.; Boeve, Bradley F.; Boxer, Adam L.; Baker, Matt; Rutherford, Nicola J. et al. (2011): Expanded GGGGCC hexanucleotide repeat in noncoding region of C9ORF72 causes chromosome 9p-linked FTD and ALS. In *Neuron* 72 (2), pp. 245–256. DOI: 10.1016/j.neuron.2011.09.011.

Delorme-Axford, Elizabeth; Popelka, Hana; Klionsky, Daniel J. (2019): TEX264 is a major receptor for mammalian reticulophagy. In *Autophagy* 15 (10), pp. 1677–1681. DOI: 10.1080/15548627.2019.1646540.

Demichev, Vadim; Messner, Christoph B.; Vernardis, Spyros I.; Lilley, Kathryn S.; Ralser, Markus (2020): DIA-NN: neural networks and interference correction enable deep proteome coverage in high throughput. In *Nature methods* 17 (1), pp. 41–44. DOI: 10.1038/s41592-019-0638-x.

Deng, Zhiqiang; Li, Xianting; Blanca Ramirez, Marian; Purtell, Kerry; Choi, Insup; Lu, Jia-Hong et al. (2021): Selective autophagy of AKAP11 activates cAMP/PKA to fuel mitochondrial metabolism and tumor cell growth. In *Proceedings of the National Academy of Sciences of the United States of America* 118 (14). DOI: 10.1073/pnas.2020215118.

Desch, Kristina; Langer, Julian D.; Schuman, Erin M. (2021): Dynamic bi-directional phosphorylation events associated with the reciprocal regulation of synapses during homeostatic up- and down-scaling. In *Cell reports* 36 (8), p. 109583. DOI: 10.1016/j.celrep.2021.109583.

Di Benedetto, Giulietta; Iannucci, Liliana F.; Surdo, Nicoletta C.; Zanin, Sofia; Conca, Filippo; Grisan, Francesca et al. (2021): Compartmentalized Signaling in Aging and Neurodegeneration. In *Cells* 10 (2). DOI: 10.3390/cells10020464.

Diao, Jiajie; Burré, Jacqueline; Vivona, Sandro; Cipriano, Daniel J.; Sharma, Manu; Kyoung, Minjoung et al. (2013): Native α-synuclein induces clustering of synaptic-vesicle mimics via binding to phospholipids and synaptobrevin-2/VAMP2. In *eLife* 2, e00592. DOI: 10.7554/eLife.00592.

Dias, Raquel B.; Ribeiro, Joaquim A.; Sebastião, Ana M. (2012): Enhancement of AMPA currents and GluR1 membrane expression through PKA-coupled adenosine A(2A) receptors. In *Hippocampus* 22 (2), pp. 276–291. DOI: 10.1002/hipo.20894.

Diering, Graham H.; Gustina, Ahleah S.; Huganir, Richard L. (2014): PKA-GluA1 coupling via AKAP5 controls AMPA receptor phosphorylation and cell-surface targeting during bidirectional homeostatic plasticity. In *Neuron* 84 (4), pp. 790–805. DOI: 10.1016/j.neuron.2014.09.024.

Diskar, Mandy; Zenn, Hans-Michael; Kaupisch, Alexandra; Prinz, Anke; Herberg, Friedrich W. (2007): Molecular basis for isoform-specific autoregulation of protein kinase A. In *Cellular signalling* 19 (10), pp. 2024–2034. DOI: 10.1016/j.cellsig.2007.05.012.

Dooley, Hannah C.; Razi, Minoo; Polson, Hannah E. J.; Girardin, Stephen E.; Wilson, Michael I.; Tooze, Sharon A. (2014): WIPI2 links LC3 conjugation with PI3P, autophagosome formation, and pathogen clearance by recruiting Atg12-5-16L1. In *Molecular cell* 55 (2), pp. 238–252. DOI: 10.1016/j.molcel.2014.05.021.

Døskeland, Stein O.; Maronde, Erik; Gjertsen, Bjørn T. (1993): The genetic subtypes of cAMP-dependent protein kinase — Functionally different or redundant? In *Biochimica et Biophysica Acta (BBA) - Molecular Cell Research* 1178 (3), pp. 249–258. DOI: 10.1016/0167-4889(93)90201-y.

Doxaki, Christina; Palikaras, Konstantinos (2020): Neuronal Mitophagy: Friend or Foe? In *Frontiers in cell and developmental biology* 8, p. 611938. DOI: 10.3389/fcell.2020.611938.

Dragatsis, Ioannis; Zeitlin, Scott (2000): CaMKII?-cre transgene expression and recombination patterns in the mouse brain. In *genesis* 26 (2), pp. 133–135. DOI: 10.1002/(sici)1526-968x(200002)26:2<133::aid-gene10>3.0.co;2-v.

Dragunow, Mike (2004): CREB and neurodegeneration. In *Frontiers in bioscience : a journal and virtual library* 9, pp. 100–103. DOI: 10.2741/1197.

Dubnau, J.; Tully, T. (1998): Gene discovery in Drosophila: new insights for learning and memory. In *Annual review of neuroscience* 21, pp. 407–444. DOI: 10.1146/annurev.neuro.21.1.407.

Duffy, Steven N.; Nguyen, Peter V. (2003): Postsynaptic application of a peptide inhibitor of cAMP-dependent protein kinase blocks expression of long-lasting synaptic potentiation in hippocampal neurons. In *J. Neurosci.* 23 (4), pp. 1142–1150.

Egan, Daniel F.; Shackelford, David B.; Mihaylova, Maria M.; Gelino, Sara; Kohnz, Rebecca A.; Mair, William et al. (2011): Phosphorylation of ULK1 (hATG1) by AMP-activated protein kinase connects energy sensing to mitophagy. In *Science (New York, N.Y.)* 331 (6016), pp. 456–461. DOI: 10.1126/science.1196371.

Ehlers, Michael D. (2000): Reinsertion or Degradation of AMPA Receptors Determined by Activity-Dependent Endocytic Sorting. In *Neuron* 28 (2), pp. 511–525. DOI: 10.1016/s0896-6273(00)00129-x.

Ennaceur, A. (2014): Tests of unconditioned anxiety - pitfalls and disappointments. In *Physiology & behavior* 135, pp. 55–71. DOI: 10.1016/j.physbeh.2014.05.032.

Esteban, José A.; Shi, Song-Hai; Wilson, Christopher; Nuriya, Mutsuo; Huganir, Richard L.; Malinow, Roberto (2003): PKA phosphorylation of AMPA receptor subunits controls synaptic trafficking underlying plasticity. In *Nature neuroscience* 6 (2), pp. 136–143. DOI: 10.1038/nn997.

Fader, Claudio Marcelo; Sánchez, Diego Germán; Mestre, María Belén; Colombo, María Isabel (2009): TI-VAMP/VAMP7 and VAMP3/cellubrevin: two v-SNARE proteins involved in specific steps of the

autophagy/multivesicular body pathways. In *Biochimica et biophysica acta* 1793 (12), pp. 1901–1916. DOI: 10.1016/j.bbamcr.2009.09.011.

Fass, Ephraim; Shvets, Elena; Degani, Ilan; Hirschberg, Koret; Elazar, Zvulun (2006): Microtubules support production of starvation-induced autophagosomes but not their targeting and fusion with lysosomes. In *The Journal of biological chemistry* 281 (47), pp. 36303–36316. DOI: 10.1074/jbc.M607031200.

Finley, Daniel (2009): Recognition and processing of ubiquitin-protein conjugates by the proteasome. In *Annual review of biochemistry* 78, pp. 477–513. DOI: 10.1146/annurev.biochem.78.081507.101607.

Fisher, Robert S.; van Emde Boas, Walter; Blume, Warren; Elger, Christian; Genton, Pierre; Lee, Phillip; Engel, Jerome (2005): Epileptic seizures and epilepsy: definitions proposed by the International League Against Epilepsy (ILAE) and the International Bureau for Epilepsy (IBE). In *Epilepsia* 46 (4), pp. 470–472. DOI: 10.1111/j.0013-9580.2005.66104.x.

Fleischhacker, W. W.; Hinterhuber, H.; Bauer, H.; Pflug, B.; Berner, P.; Simhandl, C. et al. (1992): A multicenter double-blind study of three different doses of the new cAMP-phosphodiesterase inhibitor rolipram in patients with major depressive disorder. In *Neuropsychobiology* 26 (1-2), pp. 59–64. DOI: 10.1159/000118897.

Fox, Kevin; Stryker, Michael (2017): Integrating Hebbian and homeostatic plasticity: introduction. In *Philosophical transactions of the Royal Society of London. Series B, Biological sciences* 372 (1715). DOI: 10.1098/rstb.2016.0413.

Frake, Rebecca A.; Ricketts, Thomas; Menzies, Fiona M.; Rubinsztein, David C. (2015): Autophagy and neurodegeneration. In *The Journal of clinical investigation* 125 (1), pp. 65–74. DOI: 10.1172/JCI73944.

Fu, Jingxuan; Wang, Hui; Gao, Jing; Yu, Mei; Wang, Rubin; Yang, Zhuo; Zhang, Tao (2017): Rapamycin Effectively Impedes Melamine-Induced Impairments of Cognition and Synaptic Plasticity in Wistar Rats. In *Molecular neurobiology* 54 (2), pp. 819–832. DOI: 10.1007/s12035-016-9687-7.

Fujioka, Shinsuke; Ogaki, Kotaro; Tacik, Pawel M.; Uitti, Ryan J.; Ross, Owen A.; Wszolek, Zbigniew K. (2014): Update on novel familial forms of Parkinson's disease and multiple system atrophy. In *Parkinsonism & related disorders* 20 Suppl 1, S29-34. DOI: 10.1016/S1353-8020(13)70010-5.

Fumagalli, Fiorenza; Noack, Julia; Bergmann, Timothy J.; Cebollero, Eduardo; Pisoni, Giorgia Brambilla; Fasana, Elisa et al. (2016): Translocon component Sec62 acts in endoplasmic reticulum turnover during stress recovery. In *Nature cell biology* 18 (11), pp. 1173–1184. DOI: 10.1038/ncb3423.

Furuta, Nobumichi; Fujita, Naonobu; Noda, Takeshi; Yoshimori, Tamotsu; Amano, Atsuo (2010): Combinational soluble N-ethylmaleimide-sensitive factor attachment protein receptor proteins VAMP8 and Vti1b mediate fusion of antimicrobial and canonical autophagosomes with lysosomes. In *Molecular biology of the cell* 21 (6), pp. 1001–1010. DOI: 10.1091/mbc.E09-08-0693.

Galluzzi, Lorenzo; Baehrecke, Eric H.; Ballabio, Andrea; Boya, Patricia; Bravo-San Pedro, José Manuel; Cecconi, Francesco et al. (2017a): Molecular definitions of autophagy and related processes. In *EMBO J* 36 (13), pp. 1811–1836. DOI: 10.15252/embj.201796697.

Galluzzi, Lorenzo; Bravo-San Pedro, José Manuel; Levine, Beth; Green, Douglas R.; Kroemer, Guido (2017b): Pharmacological modulation of autophagy: therapeutic potential and persisting obstacles. In *Nature reviews. Drug discovery* 16 (7), pp. 487–511. DOI: 10.1038/nrd.2017.22.

Ganley, Ian G.; Du Lam, H.; Wang, Junru; Ding, Xiaojun; Chen, She; Jiang, Xuejun (2009): ULK1.ATG13.FIP200 complex mediates mTOR signaling and is essential for autophagy. In *The Journal of biological chemistry* 284 (18), pp. 12297–12305. DOI: 10.1074/jbc.M900573200.

Geisler, Sven; Holmström, Kira M.; Skujat, Diana; Fiesel, Fabienne C.; Rothfuss, Oliver C.; Kahle, Philipp J.; Springer, Wolfdieter (2010): PINK1/Parkin-mediated mitophagy is dependent on VDAC1 and p62/SQSTM1. In *Nature cell biology* 12 (2), pp. 119–131. DOI: 10.1038/ncb2012.

Gessulat, Siegfried; Schmidt, Tobias; Zolg, Daniel Paul; Samaras, Patroklos; Schnatbaum, Karsten; Zerweck, Johannes et al. (2019): Prosit: proteome-wide prediction of peptide tandem mass spectra by deep learning. In *Nature methods* 16 (6), pp. 509–518. DOI: 10.1038/s41592-019-0426-7.

Giorgi, Filippo Sean; Biagioni, Francesca; Lenzi, Paola; Frati, Alessandro; Fornai, Francesco (2015): The role of autophagy in epileptogenesis and in epilepsy-induced neuronal alterations. In *Journal of neural transmission (Vienna, Austria : 1996)* 122 (6), pp. 849–862. DOI: 10.1007/s00702-014-1312-1.

Giralt, Albert; Saavedra, Ana; Carretón, Olga; Xifró, Xavier; Alberch, Jordi; Pérez-Navarro, Esther (2011): Increased PKA signaling disrupts recognition memory and spatial memory: role in Huntington's disease. In *Human molecular genetics* 20 (21), pp. 4232–4247. DOI: 10.1093/hmg/ddr351.

Glatigny, Mélissa; Moriceau, Stéphanie; Rivagorda, Manon; Ramos-Brossier, Mariana; Nascimbeni, Anna C.; Lante, Fabien et al. (2019): Autophagy Is Required for Memory Formation and Reverses Age-Related Memory Decline. In *Current biology : CB* 29 (3), 435-448.e8. DOI: 10.1016/j.cub.2018.12.021.

Goldberg, Matthew S.; Fleming, Sheila M.; Palacino, James J.; Cepeda, Carlos; Lam, Hoa A.; Bhatnagar, Anushree et al. (2003): Parkin-deficient mice exhibit nigrostriatal deficits but not loss of dopaminergic neurons. In *The Journal of biological chemistry* 278 (44), pp. 43628–43635. DOI: 10.1074/jbc.M308947200.

Greengard, P.; Jen, J.; Nairn, A. C.; Stevens, C. F. (1991): Enhancement of the glutamate response by cAMP-dependent protein kinase in hippocampal neurons. In *Science (New York, N.Y.)* 253 (5024), pp. 1135–1138. DOI: 10.1126/science.1716001.

Greggio, Elisa; Bubacco, Luigi; Russo, Isabella (2017): Cross-talk between LRRK2 and PKA: implication for Parkinson's disease? In *Biochemical Society transactions* 45 (1), pp. 261–267. DOI: 10.1042/BST20160396.

Grumati, Paolo; Dikic, Ivan; Stolz, Alexandra (2018): ER-phagy at a glance. In *Journal of cell science* 131 (17). DOI: 10.1242/jcs.217364.

Grumati, Paolo; Morozzi, Giulio; Hölper, Soraya; Mari, Muriel; Harwardt, Marie-Lena Ie; Yan, Riqiang et al. (2017): Full length RTN3 regulates turnover of tubular endoplasmic reticulum via selective autophagy. In *eLife* 6. DOI: 10.7554/eLife.25555.

Guardia, Carlos M.; Farías, Ginny G.; Jia, Rui; Pu, Jing; Bonifacino, Juan S. (2016): BORC Functions Upstream of Kinesins 1 and 3 to Coordinate Regional Movement of Lysosomes along Different Microtubule Tracks. In *Cell reports* 17 (8), pp. 1950–1961. DOI: 10.1016/j.celrep.2016.10.062.

Gupta, Varun K.; Scheunemann, Lisa; Eisenberg, Tobias; Mertel, Sara; Bhukel, Anuradha; Koemans, Tom S. et al. (2013): Restoring polyamines protects from age-induced memory impairment in an autophagy-dependent manner. In *Nature neuroscience* 16 (10), pp. 1453–1460. DOI: 10.1038/nn.3512.

Halls, Michelle L.; Cooper, Dermot M. F. (2011): Regulation by Ca2+-signaling pathways of adenylyl cyclases. In *Cold Spring Harbor perspectives in biology* 3 (1), a004143. DOI: 10.1101/cshperspect.a004143.

Hamasaki, Maho; Furuta, Nobumichi; Matsuda, Atsushi; Nezu, Akiko; Yamamoto, Akitsugu; Fujita, Naonobu et al. (2013): Autophagosomes form at ER-mitochondria contact sites. In *Nature* 495 (7441), pp. 389–393. DOI: 10.1038/nature11910.

Hanada, Takao; Noda, Nobuo N.; Satomi, Yoshinori; Ichimura, Yoshinobu; Fujioka, Yuko; Takao, Toshifumi et al. (2007): The Atg12-Atg5 conjugate has a novel E3-like activity for protein lipidation in autophagy. In *The Journal of biological chemistry* 282 (52), pp. 37298–37302. DOI: 10.1074/jbc.C700195200.

Hanoune, J.; Defer, N. (2001): Regulation and role of adenylyl cyclase isoforms. In *Annual review of pharmacology and toxicology* 41, pp. 145–174. DOI: 10.1146/annurev.pharmtox.41.1.145.

Hansen, Malene; Rubinsztein, David C.; Walker, David W. (2018): Autophagy as a promoter of longevity: insights from model organisms. In *Nature reviews. Molecular cell biology* 19 (9), pp. 579–593. DOI: 10.1038/s41580-018-0033-y.

Hara, Taichi; Nakamura, Kenji; Matsui, Makoto; Yamamoto, Akitsugu; Nakahara, Yohko; Suzuki-Migishima, Rika et al. (2006): Suppression of basal autophagy in neural cells causes neurodegenerative disease in mice. In *Nature* 441 (7095), pp. 885–889. DOI: 10.1038/nature04724.

Harper, J. Wade; Ordureau, Alban; Heo, Jin-Mi (2018): Building and decoding ubiquitin chains for mitophagy. In *Nature reviews. Molecular cell biology* 19 (2), pp. 93–108. DOI: 10.1038/nrm.2017.129.

Harrison, David E.; Strong, Randy; Sharp, Zelton Dave; Nelson, James F.; Astle, Clinton M.; Flurkey, Kevin et al. (2009): Rapamycin fed late in life extends lifespan in genetically heterogeneous mice. In *Nature* 460 (7253), pp. 392–395. DOI: 10.1038/nature08221.

Heng, Mary Y.; Duong, Duy K.; Albin, Roger L.; Tallaksen-Greene, Sara J.; Hunter, Jesse M.; Lesort, Mathieu J. et al. (2010): Early autophagic response in a novel knock-in model of Huntington disease. In *Human molecular genetics* 19 (19), pp. 3702–3720. DOI: 10.1093/hmg/ddq285.

Hernandez, Daniela; Torres, Ciara A.; Setlik, Wanda; Cebrián, Carolina; Mosharov, Eugene V.; Tang, Guomei et al. (2012): Regulation of presynaptic neurotransmission by macroautophagy. In *Neuron* 74 (2), pp. 277–284. DOI: 10.1016/j.neuron.2012.02.020.

Hershko, A.; Ciechanover, A.; Varshavsky, A. (2000): Basic Medical Research Award. The ubiquitin system. In *Nature medicine* 6 (10), pp. 1073–1081. DOI: 10.1038/80384.

Hilfiker, S.; Czernik, A. J.; Greengard, P.; Augustine, G. J. (2001): Tonically active protein kinase A regulates neurotransmitter release at the squid giant synapse. In *The Journal of Physiology* 531 (Pt 1), pp. 141–146. DOI: 10.1111/j.1469-7793.2001.0141j.x.

Hill, Sarah E.; Colón-Ramos, Daniel A. (2020): The Journey of the Synaptic Autophagosome: A Cell Biological Perspective. In *Neuron* 105 (6), pp. 961–973. DOI: 10.1016/j.neuron.2020.01.018.

Hoffmann, Sheila; Orlando, Marta; Andrzejak, Ewa; Bruns, Christine; Trimbuch, Thorsten; Rosenmund, Christian et al. (2019): Light-Activated ROS Production Induces Synaptic Autophagy. In *J. Neurosci.* 39 (12), pp. 2163–2183. DOI: 10.1523/JNEUROSCI.1317-18.2019.

Hosokawa, Nao; Hara, Taichi; Kaizuka, Takeshi; Kishi, Chieko; Takamura, Akito; Miura, Yutaka et al. (2009): Nutrient-dependent mTORC1 association with the ULK1-Atg13-FIP200 complex required for autophagy. In *Molecular biology of the cell* 20 (7), pp. 1981–1991. DOI: 10.1091/mbc.e08-12-1248.

Howe, Alan K. (2004): Regulation of actin-based cell migration by cAMP/PKA. In *Biochimica et biophysica acta* 1692 (2-3), pp. 159–174. DOI: 10.1016/j.bbamcr.2004.03.005.

Howe, Douglas G.; Wiley, Jesse C.; McKnight, G. Stanley (2002): Molecular and behavioral effects of a null mutation in all PKA C beta isoforms. In *Molecular and cellular neurosciences* 20 (3), pp. 515–524. DOI: 10.1006/mcne.2002.1119.

Howells, D. W.; Porritt, M. J.; Wong, J. Y.; Batchelor, P. E.; Kalnins, R.; Hughes, A. J.; Donnan, G. A. (2000): Reduced BDNF mRNA expression in the Parkinson's disease substantia nigra. In *Experimental neurology* 166 (1), pp. 127–135. DOI: 10.1006/exnr.2000.7483.

Hu, Zhiping; Yang, Binbin; Mo, Xiaoye; Xiao, Han (2015): Mechanism and Regulation of Autophagy and Its Role in Neuronal Diseases. In *Molecular neurobiology* 52 (3), pp. 1190–1209. DOI: 10.1007/s12035-014-8921-4.

Huang, Yongzhao; Roelink, Henk; McKnight, G. Stanley (2002): Protein kinase A deficiency causes axially localized neural tube defects in mice. In *Journal of Biological Chemistry* 277 (22), pp. 19889–19896. DOI: 10.1074/jbc.M111412200.

Hughes, Christopher S.; Moggridge, Sophie; Müller, Torsten; Sorensen, Poul H.; Morin, Gregg B.; Krijgsveld, Jeroen (2019): Single-pot, solid-phase-enhanced sample preparation for proteomics experiments. In *Nat Protoc* 14 (1), pp. 68–85. DOI: 10.1038/s41596-018-0082-x.

Hui, Kelvin K.; Takashima, Noriko; Watanabe, Akiko; Chater, Thomas E.; Matsukawa, Hiroshi; Nekooki-Machida, Yoko et al. (2019): GABARAPs dysfunction by autophagy deficiency in adolescent brain impairs GABAA receptor trafficking and social behavior. In *Science advances* 5 (4), eaau8237. DOI: 10.1126/sciadv.aau8237.

Ichimura, Y.; Kirisako, T.; Takao, T.; Satomi, Y.; Shimonishi, Y.; Ishihara, N. et al. (2000): A ubiquitin-like system mediates protein lipidation. In *Nature* 408 (6811), pp. 488–492. DOI: 10.1038/35044114.

Ichimura, Yoshinobu; Kumanomidou, Taichi; Sou, Yu-Shin; Mizushima, Tsunehiro; Ezaki, Junji; Ueno, Takashi et al. (2008): Structural basis for sorting mechanism of p62 in selective autophagy. In *Journal of Biological Chemistry* 283 (33), pp. 22847–22857. DOI: 10.1074/jbc.M802182200.

Ilouz, Ronit; Bubis, José; Wu, Jian; Yim, Yun Young; Deal, Michael S.; Kornev, Alexandr P. et al. (2012): Localization and quaternary structure of the PKA RIβ holoenzyme. In *Proceedings of the National Academy of Sciences of the United States of America* 109 (31), pp. 12443–12448. DOI: 10.1073/pnas.1209538109.

Ilouz, Ronit; Lev-Ram, Varda; Bushong, Eric A.; Stiles, Travis L.; Friedmann-Morvinski, Dinorah; Douglas, Christopher et al. (2017): Isoform-specific subcellular localization and function of protein kinase A identified by mosaic imaging of mouse brain. In *eLife* 6. DOI: 10.7554/eLife.17681.

Inoki, Ken; Ouyang, Hongjiao; Zhu, Tianqing; Lindvall, Charlotta; Wang, Yian; Zhang, Xiaojie et al. (2006): TSC2 integrates Wnt and energy signals via a coordinated phosphorylation by AMPK and GSK3 to regulate cell growth. In *Cell* 126 (5), pp. 955–968. DOI: 10.1016/j.cell.2006.06.055.

Inoki, Ken; Zhu, Tianqing; Guan, Kun-Liang (2003): TSC2 Mediates Cellular Energy Response to Control Cell Growth and Survival. In *Cell* 115 (5), pp. 577–590. DOI: 10.1016/S0092-8674(03)00929-2.

Itakura, Eisuke; Kishi-Itakura, Chieko; Mizushima, Noboru (2012): The hairpin-type tail-anchored SNARE syntaxin 17 targets to autophagosomes for fusion with endosomes/lysosomes. In *Cell* 151 (6), pp. 1256–1269. DOI: 10.1016/j.cell.2012.11.001.

Itier, Jean-Michel; Ibanez, Pablo; Mena, Maria Angeles; Abbas, Nacer; Cohen-Salmon, Charles; Bohme, Georg Andrees et al. (2003): Parkin gene inactivation alters behaviour and dopamine neurotransmission in the mouse. In *Human molecular genetics* 12 (18), pp. 2277–2291. DOI: 10.1093/hmg/ddg239.

Jaeger, Philipp A.; Pickford, Fiona; Sun, Chung-Huan; Lucin, Kurt M.; Masliah, Eliezer; Wyss-Coray, Tony (2010): Regulation of amyloid precursor protein processing by the Beclin 1 complex. In *PloS one* 5 (6), e11102. DOI: 10.1371/journal.pone.0011102.

Jiang, Teng; Yu, Jin-Tai; Zhu, Xi-Chen; Zhang, Qiao-Quan; Cao, Lei; Wang, Hui-Fu et al. (2014): Temsirolimus attenuates tauopathy in vitro and in vivo by targeting tau hyperphosphorylation and autophagic clearance. In *Neuropharmacology* 85, pp. 121–130. DOI: 10.1016/j.neuropharm.2014.05.032.

Jicha, Gregory A.; Weaver, Charles; Lane, Eric; Vianna, Cintia; Kress, Yvonne; Rockwood, Julia; Davies, Peter (1999): cAMP-Dependent Protein Kinase Phosphorylations on Tau in Alzheimer's Disease. In *J. Neurosci.* 19 (17), pp. 7486–7494. DOI: 10.1523/JNEUROSCI.19-17-07486.1999.

Johansen, Terje; Lamark, Trond (2011): Selective autophagy mediated by autophagic adapter proteins. In *Autophagy* 7 (3), pp. 279–296. DOI: 10.4161/auto.7.3.14487.

Joo, Joung Hyuck; Wang, Bo; Frankel, Elisa; Ge, Liang; Xu, Lu; Iyengar, Rekha et al. (2016): The Noncanonical Role of ULK/ATG1 in ER-to-Golgi Trafficking Is Essential for Cellular Homeostasis. In *Molecular cell* 62 (4), pp. 491–506. DOI: 10.1016/j.molcel.2016.04.020.

Jung, Chang Hwa; Jun, Chang Bong; Ro, Seung-Hyun; Kim, Young-Mi; Otto, Neil Michael; Cao, Jing et al. (2009): ULK-Atg13-FIP200 complexes mediate mTOR signaling to the autophagy machinery. In *Molecular biology of the cell* 20 (7), pp. 1992–2003. DOI: 10.1091/mbc.E08-12-1249.

Kabeya, Y.; Mizushima, N.; Ueno, T.; Yamamoto, A.; Kirisako, T.; Noda, T. et al. (2000): LC3, a mammalian homologue of yeast Apg8p, is localized in autophagosome membranes after processing. In *The EMBO journal* 19 (21), pp. 5720–5728. DOI: 10.1093/emboj/19.21.5720.

Kallergi, Emmanouela; Daskalaki, Akrivi-Dimitra; Ioannou, Evangelia; Kolaxi, Angeliki; Plataki, Maria; Haberkant, Per et al. (2020): Long-term synaptic depression triggers local biogenesis of autophagic vesicles in dendrites and requires autophagic degradation.

Kandel, E. R. (2001): The molecular biology of memory storage: a dialogue between genes and synapses. In *Science (New York, N.Y.)* 294 (5544), pp. 1030–1038. DOI: 10.1126/science.1067020.

Kandel, Eric R. (2012): The molecular biology of memory: cAMP, PKA, CRE, CREB-1, CREB-2, and CPEB. In *Molecular brain* 5, p. 14. DOI: 10.1186/1756-6606-5-14.

Kandel, Eric R.; Dudai, Yadin; Mayford, Mark R. (2014): The molecular and systems biology of memory. In *Cell* 157 (1), pp. 163–186. DOI: 10.1016/j.cell.2014.03.001.

Kang, Hyejin; Welcher, Andy A.; Shelton, David; Schuman, Erin M. (1997): Neurotrophins and Time: Different Roles for TrkB Signaling in Hippocampal Long-Term Potentiation. In *Neuron* 19 (3), pp. 653–664. DOI: 10.1016/S0896-6273(00)80378-5.

Kang, Liang; Liu, Shiwei; Li, Jingchao; Tian, Yueyang; Xue, Yuan; Liu, Xiaozhi (2019): Parkin and Nrf2 prevent oxidative stress-induced apoptosis in intervertebral endplate chondrocytes via inducing mitophagy and anti-oxidant defenses. In *Life sciences* 243, p. 117244. DOI: 10.1016/j.lfs.2019.117244.

Karanasios, Eleftherios; Stapleton, Eloise; Manifava, Maria; Kaizuka, Takeshi; Mizushima, Noboru; Walker, Simon A.; Ktistakis, Nicholas T. (2013): Dynamic association of the ULK1 complex with omegasomes during autophagy induction. In *Journal of cell science* 126 (Pt 22), pp. 5224–5238. DOI: 10.1242/jcs.132415.

Katsumata, Kiyoshi; Nishiyama, Jun; Inoue, Takafumi; Mizushima, Noboru; Takeda, Junzo; Yuzaki, Michisuke (2010): Dynein- and activity-dependent retrograde transport of autophagosomes in neuronal axons. In *Autophagy* 6 (3), pp. 378–385. DOI: 10.4161/auto.6.3.11262.

Kelleher, Raymond J.; Govindarajan, Arvind; Jung, Hae-Yoon; Kang, Hyejin; Tonegawa, Susumu (2004): Translational Control by MAPK Signaling in Long-Term Synaptic Plasticity and Memory. In *Cell* 116 (3), pp. 467–479. DOI: 10.1016/s0092-8674(04)00115-1.

Khaminets, Aliaksandr; Heinrich, Theresa; Mari, Muriel; Grumati, Paolo; Huebner, Antje K.; Akutsu, Masato et al. (2015): Regulation of endoplasmic reticulum turnover by selective autophagy. In *Nature* 522 (7556), pp. 354–358. DOI: 10.1038/nature14498.

Khobrekar, Noopur V.; Quintremil, Sebastian; Dantas, Tiago J.; Vallee, Richard B. (2020): The Dynein Adaptor RILP Controls Neuronal Autophagosome Biogenesis, Transport, and Clearance. In *Developmental cell* 53 (2), 141-153.e4. DOI: 10.1016/j.devcel.2020.03.011.

Kida, Satoshi; Josselyn, Sheena A.; Peña de Ortiz, Sandra; Kogan, Jeffrey H.; Chevere, Itzamarie; Masushige, Shoichi; Silva, Alcino J. (2002): CREB required for the stability of new and reactivated fear memories. In *Nature neuroscience* 5 (4), pp. 348–355. DOI: 10.1038/nn819.

Kim, Jieun; Kwon, Jeong-Tae; Kim, Hyung-Su; Han, Jin-Hee (2013): CREB and neuronal selection for memory trace. In *Frontiers in neural circuits* 7, p. 44. DOI: 10.3389/fncir.2013.00044.

Kim, Joungmok; Kundu, Mondira; Viollet, Benoit; Guan, Kun-Liang (2011a): AMPK and mTOR regulate autophagy through direct phosphorylation of Ulk1. In *Nature cell biology* 13 (2), pp. 132–141. DOI: 10.1038/ncb2152.

Kim, Myungjin; Sandford, Erin; Gatica, Damian; Qiu, Yu; Liu, Xu; Zheng, Yumei et al. (2016): Mutation in ATG5 reduces autophagy and leads to ataxia with developmental delay. In *eLife* 5. DOI: 10.7554/eLife.12245.

Kim, Sa Suk; Moon, Kyung Rok; Choi, Hyun Jin (2011b): Interference of alpha-synuclein with cAMP/PKA-dependent CREB signaling for tyrosine hydroxylase gene expression in SK-N-BE(2)C cells. In *Archives of pharmacal research* 34 (5), pp. 837–845. DOI: 10.1007/s12272-011-0518-0.

Kim, Sasuk; Park, Ji-Min; Moon, Jisook; Choi, Hyun Jin (2014): Alpha-synuclein interferes with cAMP/PKA-dependent upregulation of dopamine β-hydroxylase and is associated with abnormal adaptive responses to immobilization stress. In *Experimental neurology* 252, pp. 63–74. DOI: 10.1016/j.expneurol.2013.11.009.

Kingwell, Katie (2013): Genetics: Mutations in autophagy gene cause a rare and severe neurodegenerative disease. In *Nature reviews. Neurology* 9 (4), p. 182. DOI: 10.1038/nrneurol.2013.42.

Kirkin, Vladimir; Lamark, Trond; Sou, Yu-Shin; Bjørkøy, Geir; Nunn, Jennifer L.; Bruun, Jack-Ansgar et al. (2009): A role for NBR1 in autophagosomal degradation of ubiquitinated substrates. In *Molecular cell* 33 (4), pp. 505–516. DOI: 10.1016/j.molcel.2009.01.020.

Kirschner, Lawrence S.; Yin, Zhirong; Jones, Georgette N.; Mahoney, Emilia (2009): Mouse models of altered protein kinase A signaling. In *Endocrine-related cancer* 16 (3), pp. 773–793. DOI: 10.1677/ERC-09-0068.

Kitada, T.; Asakawa, S.; Hattori, N.; Matsumine, H.; Yamamura, Y.; Minoshima, S. et al. (1998): Mutations in the parkin gene cause autosomal recessive juvenile parkinsonism. In *Nature* 392 (6676), pp. 605–608. DOI: 10.1038/33416.

Kock, C. P. J. de; Sakmann, B. (2008): High frequency action potential bursts (or= 100 Hz) in L2/3 and L5B thick tufted neurons in anaesthetized and awake rat primary somatosensory cortex. In *The Journal of Physiology* 586 (14), pp. 3353–3364. DOI: 10.1113/jphysiol.2008.155580.

Koh, Y. H.; Popova, E.; Thomas, U.; Griffith, L. C.; Budnik, V. (1999): Regulation of DLG localization at synapses by CaMKII-dependent phosphorylation. In *Cell* 98 (3), pp. 353–363. DOI: 10.1016/s0092-8674(00)81964-9.

Komatsu, Masaaki; Waguri, Satoshi; Chiba, Tomoki; Murata, Shigeo; Iwata, Jun-ichi; Tanida, Isei et al. (2006): Loss of autophagy in the central nervous system causes neurodegeneration in mice. In *Nature* 441 (7095), pp. 880–884. DOI: 10.1038/nature04723.

Komatsu, Masaaki; Waguri, Satoshi; Koike, Masato; Sou, Yu-Shin; Ueno, Takashi; Hara, Taichi et al. (2007a): Homeostatic levels of p62 control cytoplasmic inclusion body formation in autophagy-deficient mice. In *Cell* 131 (6), pp. 1149–1163. DOI: 10.1016/j.cell.2007.10.035.

Komatsu, Masaaki; Wang, Qing Jun; Holstein, Gay R.; Friedrich, Victor L.; Iwata, Jun-ichi; Kominami, Eiki et al. (2007b): Essential role for autophagy protein Atg7 in the maintenance of axonal homeostasis and the prevention of axonal degeneration. In *Proceedings of the National Academy of Sciences of the United States of America* 104 (36), pp. 14489–14494. DOI: 10.1073/pnas.0701311104.

Kononenko, Natalia L.; Claßen, Gala A.; Kuijpers, Marijn; Puchkov, Dmytro; Maritzen, Tanja; Tempes, Aleksandra et al. (2017): Retrograde transport of TrkB-containing autophagosomes via the adaptor AP-2 mediates neuronal complexity and prevents neurodegeneration. In *Nature communications* 8, p. 14819. DOI: 10.1038/ncomms14819.

Kononenko, Natalia L.; Diril, M. Kasim; Puchkov, Dmytro; Kintscher, Michael; Koo, Seong Joo; Pfuhl, Gerit et al. (2013): Compromised fidelity of endocytic synaptic vesicle protein sorting in the absence of stonin 2. In *Proceedings of the National Academy of Sciences of the United States of America* 110 (6), E526-35. DOI: 10.1073/pnas.1218432110.

Korte, Martin; Kang, Hyejin; Bonhoeffer, Tobias; Schuman, Erin (1998): A role for BDNF in the late-phase of hippocampal long-term potentiation. In *Neuropharmacology* 37 (4-5), pp. 553–559. DOI: 10.1016/S0028-3908(98)00035-5.

Krüger, R.; Kuhn, W.; Müller, T.; Woitalla, D.; Graeber, M.; Kösel, S. et al. (1998): Ala30Pro mutation in the gene encoding alpha-synuclein in Parkinson's disease. In *Nature genetics* 18 (2), pp. 106–108. DOI: 10.1038/ng0298-106.

Kuijpers, Marijn; Kochlamazashvili, Gaga; Stumpf, Alexander; Puchkov, Dmytro; Swaminathan, Aarti; Lucht, Max Thomas et al. (2021): Neuronal Autophagy Regulates Presynaptic Neurotransmission by Controlling the Axonal Endoplasmic Reticulum. In *Neuron* 109 (2), 299-313.e9. DOI: 10.1016/j.neuron.2020.10.005.

Kulkarni, Aditi; Chen, Jessica; Maday, Sandra (2018): Neuronal autophagy and intercellular regulation of homeostasis in the brain. In *Current opinion in neurobiology* 51, pp. 29–36. DOI: 10.1016/j.conb.2018.02.008.

Kuma, Akiko; Hatano, Masahiko; Matsui, Makoto; Yamamoto, Akitsugu; Nakaya, Haruaki; Yoshimori, Tamotsu et al. (2004): The role of autophagy during the early neonatal starvation period. In *Nature* 432 (7020), pp. 1032–1036. DOI: 10.1038/nature03029.

Lamark, Trond; Johansen, Terje (2012): Aggrephagy: selective disposal of protein aggregates by macroautophagy. In *International journal of cell biology* 2012, p. 736905. DOI: 10.1155/2012/736905.

Langeberg, Lorene K.; Scott, John D. (2005): A-kinase-anchoring proteins. In *Journal of cell science* 118 (Pt 15), pp. 3217–3220. DOI: 10.1242/jcs.02416.

Langemeyer, Lars; Fröhlich, Florian; Ungermann, Christian (2018): Rab GTPase Function in Endosome and Lysosome Biogenesis. In *Trends in cell biology* 28 (11), pp. 957–970. DOI: 10.1016/j.tcb.2018.06.007.

Langemeyer, Lars; Ungermann, Christian (2015): BORC and BLOC-1: Shared subunits in trafficking complexes. In *Developmental cell* 33 (2), pp. 121–122. DOI: 10.1016/j.devcel.2015.04.008.

Lee, H. K.; Barbarosie, M.; Kameyama, K.; Bear, M. F.; Huganir, R. L. (2000): Regulation of distinct AMPA receptor phosphorylation sites during bidirectional synaptic plasticity. In *Nature* 405 (6789), pp. 955–959. DOI: 10.1038/35016089.

Lee, Hey-Kyoung; Takamiya, Kogo; Han, Jung-Soo; Man, Hengye; Kim, Chong-Hyun; Rumbaugh, Gavin et al. (2003): Phosphorylation of the AMPA Receptor GluR1 Subunit Is Required for Synaptic Plasticity and Retention of Spatial Memory. In *Cell* 112 (5), pp. 631–643. DOI: 10.1016/s0092-8674(03)00122-3.

Lee, Ju-Hyun; Yu, W. Haung; Kumar, Asok; Lee, Sooyeon; Mohan, Panaiyur S.; Peterhoff, Corrinne M. et al. (2010): Lysosomal proteolysis and autophagy require presenilin 1 and are disrupted by Alzheimer-related PS1 mutations. In *Cell* 141 (7), pp. 1146–1158. DOI: 10.1016/j.cell.2010.05.008.

Lee, R.; Kermani, P.; Teng, K. K.; Hempstead, B. L. (2001): Regulation of cell survival by secreted proneurotrophins. In *Science (New York, N.Y.)* 294 (5548), pp. 1945–1948. DOI: 10.1126/science.1065057.

Lee, Sooyeon; Sato, Yutaka; Nixon, Ralph A. (2011): Lysosomal proteolysis inhibition selectively disrupts axonal transport of degradative organelles and causes an Alzheimer's-like axonal dystrophy. In *J. Neurosci.* 31 (21), pp. 7817–7830. DOI: 10.1523/JNEUROSCI.6412-10.2011.

Lee, Wai-Ling; Hablitz, John J. (1989): Involvement of non-NMDA receptors in picrotoxin-induced epileptiform activity in the hippocampus. In *Neuroscience letters* 107 (1-3), pp. 129–134. DOI: 10.1016/0304-3940(89)90804-5.

Leonard, A. S.; Davare, M. A.; Horne, M. C.; Garner, C. C.; Hell, J. W. (1998): SAP97 is associated with the alpha-amino-3-hydroxy-5-methylisoxazole-4-propionic acid receptor GluR1 subunit. In *The Journal of biological chemistry* 273 (31), pp. 19518–19524. DOI: 10.1074/jbc.273.31.19518.

Lesage, Suzanne; Anheim, Mathieu; Letournel, Franck; Bousset, Luc; Honoré, Aurélie; Rozas, Nelly et al. (2013): G51D α-synuclein mutation causes a novel parkinsonian-pyramidal syndrome. In *Annals of neurology* 73 (4), pp. 459–471. DOI: 10.1002/ana.23894.

Levine, Beth; Mizushima, Noboru; Virgin, Herbert W. (2011): Autophagy in immunity and inflammation. In *Nature* 469 (7330), pp. 323–335. DOI: 10.1038/nature09782.

Li, Xiaohua; He, Shikun; Ma, Binyun (2020): Autophagy and autophagy-related proteins in cancer. In *Molecular cancer* 19 (1), p. 12. DOI: 10.1186/s12943-020-1138-4.

Li, Zhigui; Hao, Shuang; Yin, Hongqiang; Gao, Jing; Yang, Zhuo (2016): Autophagy ameliorates cognitive impairment through activation of PVT1 and apoptosis in diabetes mice. In *Behavioural brain research* 305, pp. 265–277. DOI: 10.1016/j.bbr.2016.03.023.

Liang, Chun-Chi; Wang, Chenran; Peng, Xu; Gan, Boyi; Guan, Jun-Lin (2010): Neural-specific deletion of FIP200 leads to cerebellar degeneration caused by increased neuronal death and axon degeneration. In *The Journal of biological chemistry* 285 (5), pp. 3499–3509. DOI: 10.1074/jbc.M109.072389.

Liang, YongTian (2019): Emerging Concepts and Functions of Autophagy as a Regulator of Synaptic Components and Plasticity. In *Cells* 8 (1). DOI: 10.3390/cells8010034.

Liang, YongTian; Sigrist, Stephan (2018): Autophagy and proteostasis in the control of synapse aging and disease. In *Current opinion in neurobiology* 48, pp. 113–121. DOI: 10.1016/j.conb.2017.12.006.

Liao, Yuxing; Wang, Jing; Jaehnig, Eric J.; Shi, Zhiao; Zhang, Bing (2019): WebGestalt 2019: gene set analysis toolkit with revamped UIs and APIs. In *Nucleic acids research* 47 (W1), W199-W205. DOI: 10.1093/nar/gkz401.

Lieberman, Ori J.; Frier, Micah D.; McGuirt, Avery F.; Griffey, Christopher J.; Rafikian, Elizabeth; Yang, Mu et al. (2020): Cell-type-specific regulation of neuronal intrinsic excitability by macroautophagy. In *eLife* 9. DOI: 10.7554/eLife.50843.

Lieberman, Ori J.; McGuirt, Avery F.; Tang, Guomei; Sulzer, David (2019): Roles for neuronal and glial autophagy in synaptic pruning during development. In *Neurobiology of disease* 122, pp. 49–63. DOI: 10.1016/j.nbd.2018.04.017.

Lignani, Gabriele; Baldelli, Pietro; Marra, Vincenzo (2020): Homeostatic Plasticity in Epilepsy. In *Frontiers in cellular neuroscience* 14, p. 197. DOI: 10.3389/fncel.2020.00197.

Lin, Ai-Ling; Zheng, Wei; Halloran, Jonathan J.; Burbank, Raquel R.; Hussong, Stacy A.; Hart, Matthew J. et al. (2013a): Chronic rapamycin restores brain vascular integrity and function through NO synthase activation and improves memory in symptomatic mice modeling Alzheimer's disease. In *Journal of cerebral blood flow and*

metabolism : official journal of the International Society of Cerebral Blood Flow and Metabolism 33 (9), pp. 1412–1421. DOI: 10.1038/jcbfm.2013.82.

Lin, Jiun-Tsai; Chang, Wei-Cheng; Chen, Hui-Mei; Lai, Hsing-Lin; Chen, Chih-Yeh; Tao, Mi-Hua; Chern, Yijuang (2013b): Regulation of feedback between protein kinase A and the proteasome system worsens Huntington's disease. In *Molecular and cellular biology* 33 (5), pp. 1073–1084. DOI: 10.1128/MCB.01434-12.

Liśkiewicz, Daniela; Liśkiewicz, Arkadiusz; Nowacka-Chmielewska, Marta M.; Grabowski, Mateusz; Pondel, Natalia; Grabowska, Konstancja et al. (2021): Differential Response of Hippocampal and Cerebrocortical Autophagy and Ketone Body Metabolism to the Ketogenic Diet. In *Frontiers in cellular neuroscience* 15, p. 733607. DOI: 10.3389/fncel.2021.733607.

Liu, Grace Y.; Sabatini, David M. (2020): mTOR at the nexus of nutrition, growth, ageing and disease. In *Nature reviews. Molecular cell biology*. DOI: 10.1038/s41580-019-0199-y.

Liu, Z.; Zhang, J.; Fei, J.; Guo, L. (2001): A novel mechanism of dopamine neurotoxicity involving the peripheral extracellular and the plasma membrane dopamine transporter. In *Neuroreport* 12 (15), pp. 3293–3297. DOI: 10.1097/00001756-200110290-00029.

Lokireddy, Sudarsanareddy; Kukushkin, Nikolay Vadimovich; Goldberg, Alfred Lewis (2015): cAMP-induced phosphorylation of 26S proteasomes on Rpn6/PSMD11 enhances their activity and the degradation of misfolded proteins. In *Proceedings of the National Academy of Sciences of the United States of America* 112 (52), E7176-85. DOI: 10.1073/pnas.1522332112.

Lonze, Bonnie E.; Ginty, David D. (2002): Function and regulation of CREB family transcription factors in the nervous system. In *Neuron* 35 (4), pp. 605–623. DOI: 10.1016/s0896-6273(02)00828-0.

Lőrincz, Péter; Juhász, Gábor (2020): Autophagosome-Lysosome Fusion. In *Journal of molecular biology* 432 (8), pp. 2462–2482. DOI: 10.1016/j.jmb.2019.10.028.

Lu, Wei; Shi, Yun; Jackson, Alexander C.; Bjorgan, Kirsten; During, Matthew J.; Sprengel, Rolf et al. (2009): Subunit composition of synaptic AMPA receptors revealed by a single-cell genetic approach. In *Neuron* 62 (2), pp. 254–268. DOI: 10.1016/j.neuron.2009.02.027.

Luchsinger, Jose A.; Tang, Ming-Xing; Shea, Steven; Mayeux, Richard (2002): Caloric intake and the risk of Alzheimer disease. In *Archives of neurology* 59 (8), pp. 1258–1263. DOI: 10.1001/archneur.59.8.1258.

Macías, W.; Carlson, R.; Rajadhyaksha, A.; Barczak, A.; Konradi, C. (2001): Potassium chloride depolarization mediates CREB phosphorylation in striatal neurons in an NMDA receptor-dependent manner. In *Brain research* 890 (2), pp. 222–232. DOI: 10.1016/s0006-8993(00)03163-2.

Maday, Sandra; Wallace, Karen E.; Holzbaur, Erika L. F. (2012): Autophagosomes initiate distally and mature during transport toward the cell soma in primary neurons. In *Journal of Cell Biology* 196 (4), pp. 407–417. DOI: 10.1083/jcb.201106120.

Majeski, Amy E.; Dice, J. Fred (2004): Mechanisms of chaperone-mediated autophagy. In *The international journal of biochemistry & cell biology* 36 (12), pp. 2435–2444. DOI: 10.1016/j.biocel.2004.02.013.

Man, Heng-Ye; Sekine-Aizawa, Yoko; Huganir, Richard L. (2007): Regulation of {alpha}-amino-3-hydroxy-5-methyl-4-isoxazolepropionic acid receptor trafficking through PKA phosphorylation of the Glu receptor 1 subunit. In *Proceedings of the National Academy of Sciences of the United States of America* 104 (9), pp. 3579–3584. DOI: 10.1073/pnas.0611698104.

Marguet, Stephan Lawrence; Le-Schulte, Vu Thao Quyen; Merseburg, Andrea; Neu, Axel; Eichler, Ronny; Jakovcevski, Igor et al. (2015): Treatment during a vulnerable developmental period rescues a genetic epilepsy. In *Nature medicine* 21 (12), pp. 1436–1444. DOI: 10.1038/nm.3987.

Martin, Brent R.; Deerinck, Thomas J.; Ellisman, Mark H.; Taylor, Susan S.; Tsien, Roger Y. (2007): Isoform-specific PKA dynamics revealed by dye-triggered aggregation and DAKAP1alpha-mediated localization in living cells. In *Chemistry & biology* 14 (9), pp. 1031–1042. DOI: 10.1016/j.chembiol.2007.07.017.

Martinez-Vicente, Marta; Talloczy, Zsolt; Wong, Esther; Tang, Guomei; Koga, Hiroshi; Kaushik, Susmita et al. (2010): Cargo recognition failure is responsible for inefficient autophagy in Huntington's disease. In *Nature neuroscience* 13 (5), pp. 567–576. DOI: 10.1038/nn.2528.

Maruyama, Hirofumi; Kawakami, Hideshi (2013): Optineurin and amyotrophic lateral sclerosis. In *Geriatrics & gerontology international* 13 (3), pp. 528–532. DOI: 10.1111/ggi.12022.

Matsuda, Noriyuki; Sato, Shigeto; Shiba, Kahori; Okatsu, Kei; Saisho, Keiko; Gautier, Clement A. et al. (2010): PINK1 stabilized by mitochondrial depolarization recruits Parkin to damaged mitochondria and activates latent Parkin for mitophagy. In *The Journal of cell biology* 189 (2), pp. 211–221. DOI: 10.1083/jcb.200910140.

Matsuzaki, Kentaro; Yamakuni, Tohru; Hashimoto, Michio; Haque, Abdul Md; Shido, Osamu; Mimaki, Yoshihiro et al. (2006): Nobiletin restoring beta-amyloid-impaired CREB phosphorylation rescues memory deterioration in Alzheimer's disease model rats. In *Neuroscience letters* 400 (3), pp. 230–234. DOI: 10.1016/j.neulet.2006.02.077.

Mattson, Mark P. (2007): Calcium and neurodegeneration. In *Aging cell* 6 (3), pp. 337–350. DOI: 10.1111/j.1474-9726.2007.00275.x.

Mavrakis, Manos; Lippincott-Schwartz, Jennifer; Stratakis, Constantine A.; Bossis, Ioannis (2006): Depletion of type IA regulatory subunit (RIalpha) of protein kinase A (PKA) in mammalian cells and tissues activates mTOR and causes autophagic deficiency. In *Human molecular genetics* 15 (19), pp. 2962–2971. DOI: 10.1093/hmg/ddl239.

McBain, C. J.; Boden, P.; Hill, R. G. (1988): The kainate/quisqualate receptor antagonist, CNQX, blocks the fast component of spontaneous epileptiform activity in organotypic cultures of rat hippocampus. In *Neuroscience letters* 93 (2-3), pp. 341–345. DOI: 10.1016/0304-3940(88)90106-1.

McCarty, Mark F.; DiNicolantonio, James J.; O'Keefe, James H. (2015): Ketosis may promote brain macroautophagy by activating Sirt1 and hypoxia-inducible factor-1. In *Medical hypotheses* 85 (5), pp. 631–639. DOI: 10.1016/j.mehy.2015.08.002.

McDaniel, Sharon S.; Rensing, Nicholas R.; Thio, Liu Lin; Yamada, Kelvin A.; Wong, Michael (2011): The ketogenic diet inhibits the mammalian target of rapamycin (mTOR) pathway. In *Epilepsia* 52 (3), e7-11. DOI: 10.1111/j.1528-1167.2011.02981.x.

McKnight, G. S.; Clegg, C. H.; Uhler, M. D.; Chrivia, J. C.; Cadd, G. G.; Correll, L. A.; Otten, A. D. (1988): Analysis of the cAMP-dependent protein kinase system using molecular genetic approaches. In *Recent progress in hormone research* 44, pp. 307–335. DOI: 10.1016/B978-0-12-571144-9.50014-4.

McMahon, John; Huang, Xiaoxing; Yang, Jun; Komatsu, Masaaki; Yue, Zhenyu; Qian, Jiang et al. (2012): Impaired autophagy in neurons after disinhibition of mammalian target of rapamycin and its contribution to epileptogenesis. In *J. Neurosci.* 32 (45), pp. 15704–15714. DOI: 10.1523/JNEUROSCI.2392-12.2012.

Mealer, Robert G.; Murray, Alexandra J.; Shahani, Neelam; Subramaniam, Srinivasa; Snyder, Solomon H. (2014): Rhes, a striatal-selective protein implicated in Huntington disease, binds beclin-1 and activates autophagy. In *The Journal of biological chemistry* 289 (6), pp. 3547–3554. DOI: 10.1074/jbc.M113.536912.

Menzies, Fiona M.; Fleming, Angeleen; Caricasole, Andrea; Bento, Carla F.; Andrews, Stephen P.; Ashkenazi, Avraham et al. (2017): Autophagy and Neurodegeneration: Pathogenic Mechanisms and Therapeutic Opportunities. In *Neuron* 93 (5), pp. 1015–1034. DOI: 10.1016/j.neuron.2017.01.022.

Menzies, Fiona M.; Fleming, Angeleen; Rubinsztein, David C. (2015): Compromised autophagy and neurodegenerative diseases. In *Nature reviews. Neuroscience* 16 (6), pp. 345–357. DOI: 10.1038/nrn3961.

Mercer, Thomas J.; Gubas, Andrea; Tooze, Sharon A. (2018): A molecular perspective of mammalian autophagosome biogenesis. In *The Journal of biological chemistry* 293 (15), pp. 5386–5395. DOI: 10.1074/jbc.R117.810366.

Messaoudi, Elhoucine; Ying, Shui-Wang; Kanhema, Tambudzai; Croll, Susan D.; Bramham, Clive R. (2002): Brain-Derived Neurotrophic Factor Triggers Transcription-Dependent, Late Phase Long-Term Potentiation In Vivo. In *J. Neurosci.* 22 (17), pp. 7453–7461. DOI: 10.1523/JNEUROSCI.22-17-07453.2002.

Miller, Richard A.; Harrison, David E.; Astle, C. M.; Baur, Joseph A.; Boyd, Angela Rodriguez; Cabo, Rafael de et al. (2011): Rapamycin, but not resveratrol or simvastatin, extends life span of genetically heterogeneous mice. In *The journals of gerontology. Series A, Biological sciences and medical sciences* 66 (2), pp. 191–201. DOI: 10.1093/gerona/glq178.

Minichiello, Liliana; Korte, Martin; Wolfer, David; Kühn, Ralf; Unsicker, Klaus; Cestari, Vincenzo et al. (1999): Essential Role for TrkB Receptors in Hippocampus-Mediated Learning. In *Neuron* 24 (2), pp. 401–414. DOI: 10.1016/S0896-6273(00)80853-3.

Mioduszewska, Barbara; Jaworski, Jacek; Kaczmarek, Leszek (2003): Inducible cAMP early repressor (ICER) in the nervous system--a transcriptional regulator of neuronal plasticity and programmed cell death. In *Journal of neurochemistry* 87 (6), pp. 1313–1320. DOI: 10.1046/j.1471-4159.2003.02116.x.

Mizushima, N.; Noda, T.; Yoshimori, T.; Tanaka, Y.; Ishii, T.; George, M. D. et al. (1998): A protein conjugation system essential for autophagy. In *Nature* 395 (6700), pp. 395–398. DOI: 10.1038/26506.

Mizushima, N.; Yamamoto, A.; Hatano, M.; Kobayashi, Y.; Kabeya, Y.; Suzuki, K. et al. (2001): Dissection of autophagosome formation using Apg5-deficient mouse embryonic stem cells. In *The Journal of cell biology* 152 (4), pp. 657–668. DOI: 10.1083/jcb.152.4.657.

Mizushima, Noboru; Kuma, Akiko; Kobayashi, Yoshinori; Yamamoto, Akitsugu; Matsubae, Masami; Takao, Toshifumi et al. (2003): Mouse Apg16L, a novel WD-repeat protein, targets to the autophagic isolation membrane with the Apg12-Apg5 conjugate. In *Journal of cell science* 116 (Pt 9), pp. 1679–1688. DOI: 10.1242/jcs.00381.

Mizushima, Noboru; Levine, Beth (2010): Autophagy in mammalian development and differentiation. In *Nature cell biology* 12 (9), pp. 823–830. DOI: 10.1038/ncb0910-823.

Mizushima, Noboru; Levine, Beth; Cuervo, Ana Maria; Klionsky, Daniel J. (2008): Autophagy fights disease through cellular self-digestion. In *Nature* 451 (7182), pp. 1069–1075. DOI: 10.1038/nature06639.

Monastyrska, Iryna; Rieter, Ester; Klionsky, Daniel J.; Reggiori, Fulvio (2009): Multiple roles of the cytoskeleton in autophagy. In *Biological reviews of the Cambridge Philosophical Society* 84 (3), pp. 431–448. DOI: 10.1111/j.1469-185X.2009.00082.x.

Mons, N.; Harry, A.; Dubourg, P.; Premont, R. T.; Iyengar, R.; Cooper, D. M. (1995): Immunohistochemical localization of adenylyl cyclase in rat brain indicates a highly selective concentration at synapses. In *Proceedings of the National Academy of Sciences of the United States of America* 92 (18), pp. 8473–8477. DOI: 10.1073/pnas.92.18.8473.

Montminy, M.; Koo, S-H; Zhang, X. (2004): The CREB family: key regulators of hepatic metabolism. In *Annales d'endocrinologie* 65 (1), pp. 73–75. DOI: 10.1016/s0003-4266(04)95634-x.

Montminy, M. R.; Gonzalez, G. A.; Yamamoto, K. K. (1990): Characteristics of the cAMP response unit. In *Metabolism: clinical and experimental* 39 (9 Suppl 2), pp. 6–12. DOI: 10.1016/0026-0495(90)90198-l.

Mormann, Florian; Andrzejak, Ralph G.; Elger, Christian E.; Lehnertz, Klaus (2007): Seizure prediction: the long and winding road. In *Brain : a journal of neurology* 130 (Pt 2), pp. 314–333. DOI: 10.1093/brain/awl241.

Moulin, Thiago C.; Rayêe, Danielle; Williams, Michael J.; Schiöth, Helgi B. (2020): The Synaptic Scaling Literature: A Systematic Review of Methodologies and Quality of Reporting. In *Frontiers in cellular neuroscience* 14, p. 164. DOI: 10.3389/fncel.2020.00164.

Murdoch, John D.; Rostosky, Christine M.; Gowrisankaran, Sindhuja; Arora, Amandeep S.; Soukup, Sandra-Fausia; Vidal, Ramon et al. (2016): Endophilin-A Deficiency Induces the Foxo3a-Fbxo32 Network in the Brain and Causes Dysregulation of Autophagy and the Ubiquitin-Proteasome System. In *Cell reports* 17 (4), pp. 1071–1086. DOI: 10.1016/j.celrep.2016.09.058.

Myeku, Natura; Wang, Hu; Figueiredo-Pereira, Maria E. (2012): cAMP stimulates the ubiquitin/proteasome pathway in rat spinal cord neurons. In *Neuroscience letters* 527 (2), pp. 126–131. DOI: 10.1016/j.neulet.2012.08.051.

Nakatogawa, Hitoshi; Suzuki, Kuninori; Kamada, Yoshiaki; Ohsumi, Yoshinori (2009): Dynamics and diversity in autophagy mechanisms: lessons from yeast. In *Nature reviews. Molecular cell biology* 10 (7), pp. 458–467. DOI: 10.1038/nrm2708.

Nayak, A.; Zastrow, D. J.; Lickteig, R.; Zahniser, N. R.; Browning, M. D. (1998): Maintenance of late-phase LTP is accompanied by PKA-dependent increase in AMPA receptor synthesis. In *Nature* 394 (6694), pp. 680–683. DOI: 10.1038/29305.

Negrete-Hurtado, A.; Overhoff, M.; Bera, S.; Bruyckere, E. de; Schätzmüller, K.; Kye, M. J. et al. (2020): Autophagy lipidation machinery regulates axonal microtubule dynamics but is dispensable for survival of mammalian neurons. In *Nature communications* 11 (1), p. 1535. DOI: 10.1038/s41467-020-15287-9.

Neuman, R. S.; Ben-Ari, Y.; Cherubini, E. (1988): Antagonism of spontaneous and evoked bursts by 6-cyano-7-nitroquinoxaline-2, 3-dione (CNQX) in the CA3 region of the in vitro hippocampus. In *Brain research* 474 (1), pp. 201–203. DOI: 10.1016/0006-8993(88)90686-5.

Newman, Alice C.; Scholefield, Caroline L.; Kemp, Alain J.; Newman, Michelle; McIver, Edward G.; Kamal, Ahmad; Wilkinson, Simon (2012): TBK1 kinase addiction in lung cancer cells is mediated via autophagy of Tax1bp1/Ndp52 and non-canonical NF-κB signalling. In *PloS one* 7 (11), e50672. DOI: 10.1371/journal.pone.0050672.

Nguyen, P. V.; Woo, N. H. (2003): Regulation of hippocampal synaptic plasticity by cyclic AMP-dependent protein kinases. In *Progress in neurobiology* 71 (6), pp. 401–437. DOI: 10.1016/j.pneurobio.2003.12.003.

Nikoletopoulou, Vassiliki; Sidiropoulou, Kyriaki; Kallergi, Emmanouela; Dalezios, Yannis; Tavernarakis, Nektarios (2017): Modulation of Autophagy by BDNF Underlies Synaptic Plasticity. In *Cell metabolism* 26 (1), 230-242.e5. DOI: 10.1016/j.cmet.2017.06.005.

Nikoletopoulou, Vassiliki; Tavernarakis, Nektarios (2018): Regulation and Roles of Autophagy at Synapses. In *Trends in cell biology* 28 (8), pp. 646–661. DOI: 10.1016/j.tcb.2018.03.006.

Nixon, Ralph A.; Wegiel, Jerzy; Kumar, Asok; Yu, Wai Haung; Peterhoff, Corrinne; Cataldo, Anne; Cuervo, Ana Maria (2005): Extensive involvement of autophagy in Alzheimer disease: an immuno-electron microscopy study. In *Journal of neuropathology and experimental neurology* 64 (2), pp. 113–122. DOI: 10.1093/jnen/64.2.113.

Noda, Sachiko; Sato, Shigeto; Fukuda, Takahiro; Tada, Norihiro; Uchiyama, Yasuo; Tanaka, Keiji; Hattori, Nobutaka (2019): Loss of Parkin contributes to mitochondrial turnover and dopaminergic neuronal loss in aged mice. In *Neurobiology of disease* 136, p. 104717. DOI: 10.1016/j.nbd.2019.104717.

Noda, Takeshi; Suzuki, Kuninori; Ohsumi, Yoshinori (2002): Yeast autophagosomes: de novo formation of a membrane structure. In *Trends in cell biology* 12 (5), pp. 231–235. DOI: 10.1016/s0962-8924(02)02278-x.

Nolte, Hendrik; MacVicar, Thomas D.; Tellkamp, Frederik; Krüger, Marcus (2018): Instant Clue: A Software Suite for Interactive Data Visualization and Analysis. In *Sci Rep* 8 (1), p. 12648. DOI: 10.1038/s41598-018-31154-6.

Nygren, Patrick J.; Scott, John D. (2015): Therapeutic strategies for anchored kinases and phosphatases: exploiting short linear motifs and intrinsic disorder. In *Frontiers in pharmacology* 6, p. 158. DOI: 10.3389/fphar.2015.00158.

Nykjaer, Anders; Lee, Ramee; Teng, Kenneth K.; Jansen, Pernille; Madsen, Peder; Nielsen, Morten S. et al. (2004): Sortilin is essential for proNGF-induced neuronal cell death. In *Nature* 427 (6977), pp. 843–848. DOI: 10.1038/nature02319.

O'Brien, Richard J.; Kamboj, Sunjeev; Ehlers, Michael D.; Rosen, Kenneth R.; Fischbach, Gerald D.; Huganir, Richard L. (1998): Activity-Dependent Modulation of Synaptic AMPA Receptor Accumulation. In *Neuron* 21 (5), pp. 1067–1078. DOI: 10.1016/S0896-6273(00)80624-8.

Oh, M. Matthew; Oliveira, Fernando A.; Waters, Jack; Disterhoft, John F. (2013): Altered calcium metabolism in aging CA1 hippocampal pyramidal neurons. In *J. Neurosci.* 33 (18), pp. 7905–7911. DOI: 10.1523/JNEUROSCI.5457-12.2013.

Okerlund, Nathan D.; Schneider, Katharina; Leal-Ortiz, Sergio; Montenegro-Venegas, Carolina; Kim, Sally A.; Garner, Loren C. et al. (2018): Bassoon Controls Presynaptic Autophagy through Atg5. In *Neuron* 97 (3), p. 727. DOI: 10.1016/j.neuron.2018.01.010.

Oksvold, Morten P.; Funderud, Ane; Kvissel, Anne-Katrine; Skarpen, Ellen; Henanger, Heidi; Huitfeldt, Henrik S. et al. (2008): Epidermal growth factor receptor levels are reduced in mice with targeted disruption of the protein kinase A catalytic subunit. In *BMC cell biology* 9, p. 16. DOI: 10.1186/1471-2121-9-16.

Oliva Trejo, Juan Alejandro; Tanida, Isei; Suzuki, Chigure; Kakuta, Soichiro; Tada, Norihiro; Uchiyama, Yasuo (2020): Characterization of starvation-induced autophagy in cerebellar Purkinje cells of pHluorin-mKate2-human LC3B transgenic mice. In *Sci Rep* 10 (1), p. 9643. DOI: 10.1038/s41598-020-66370-6.

Otten, A. D.; McKnight, G. S. (1989): Overexpression of the Type II Regulatory Subunit of the cAMP-Dependent Protein Kinase Eliminates the Type I Holoenzyme in Mouse Cells. In *Journal of Biological Chemistry* 264 (34), pp. 20255–20260. DOI: 10.1016/S0021-9258(19)47055-5.

Ozcelik, Sefika; Fraser, Graham; Castets, Perrine; Schaeffer, Véronique; Skachokova, Zhiva; Breu, Karin et al. (2013): Rapamycin attenuates the progression of tau pathology in P301S tau transgenic mice. In *PloS one* 8 (5), e62459. DOI: 10.1371/journal.pone.0062459.

Palikaras, Konstantinos; Lionaki, Eirini; Tavernarakis, Nektarios (2018): Mechanisms of mitophagy in cellular homeostasis, physiology and pathology. In *Nature cell biology* 20 (9), pp. 1013–1022. DOI: 10.1038/s41556-018-0176-2.

Pankiv, Serhiy; Alemu, Endalkachew A.; Brech, Andreas; Bruun, Jack-Ansgar; Lamark, Trond; Overvatn, Aud et al. (2010): FYCO1 is a Rab7 effector that binds to LC3 and PI3P to mediate microtubule plus end-directed vesicle transport. In *The Journal of cell biology* 188 (2), pp. 253–269. DOI: 10.1083/jcb.200907015.

Pankiv, Serhiy; Clausen, Terje Høyvarde; Lamark, Trond; Brech, Andreas; Bruun, Jack-Ansgar; Outzen, Heidi et al. (2007): p62/SQSTM1 binds directly to Atg8/LC3 to facilitate degradation of ubiquitinated protein aggregates by autophagy. In *The Journal of biological chemistry* 282 (33), pp. 24131–24145. DOI: 10.1074/jbc.M702824200.

Parisiadou, Loukia; Yu, Jia; Sgobio, Carmelo; Xie, Chengsong; Liu, Guoxiang; Sun, Lixin et al. (2014): LRRK2 regulates synaptogenesis and dopamine receptor activation through modulation of PKA activity. In *Nature neuroscience* 17 (3), pp. 367–376. DOI: 10.1038/nn.3636.

Passafaro, M.; Piëch, V.; Sheng, M. (2001): Subunit-specific temporal and spatial patterns of AMPA receptor exocytosis in hippocampal neurons. In *Nature neuroscience* 4 (9), pp. 917–926. DOI: 10.1038/nn0901-917.

Patterson, Susan L.; Abel, Ted; Deuel, Thomas A.S; Martin, Kelsey C.; Rose, Jack C.; Kandel, Eric R. (1996): Recombinant BDNF Rescues Deficits in Basal Synaptic Transmission and Hippocampal LTP in BDNF Knockout Mice. In *Neuron* 16 (6), pp. 1137–1145. DOI: 10.1016/S0896-6273(00)80140-3.

Pattingre, Sophie; Tassa, Amina; Qu, Xueping; Garuti, Rita; Liang, Xiao Huan; Mizushima, Noboru et al. (2005): Bcl-2 antiapoptotic proteins inhibit Beclin 1-dependent autophagy. In *Cell* 122 (6), pp. 927–939. DOI: 10.1016/j.cell.2005.07.002.

Perrotta, Cristiana; Cattaneo, Maria Grazia; Molteni, Raffaella; Palma, Clara de (2020): Autophagy in the Regulation of Tissue Differentiation and Homeostasis. In *Frontiers in cell and developmental biology* 8, p. 602901. DOI: 10.3389/fcell.2020.602901.

Persengiev, S. P.; Green, M. R. (2003): The role of ATF/CREB family members in cell growth, survival and apoptosis. In *Apoptosis : an international journal on programmed cell death* 8 (3), pp. 225–228. DOI: 10.1023/a:1023633704132.

Perucca, Emilio (2005): An introduction to antiepileptic drugs. In *Epilepsia* 46 Suppl 4, pp. 31–37. DOI: 10.1111/j.1528-1167.2005.463007.x.

Pickford, Fiona; Masliah, Eliezer; Britschgi, Markus; Lucin, Kurt; Narasimhan, Ramya; Jaeger, Philipp A. et al. (2008): The autophagy-related protein beclin 1 shows reduced expression in early Alzheimer disease and regulates amyloid beta accumulation in mice. In *The Journal of clinical investigation* 118 (6), pp. 2190–2199. DOI: 10.1172/JCI33585.

Pickles, Sarah; Vigié, Pierre; Youle, Richard J. (2018): Mitophagy and Quality Control Mechanisms in Mitochondrial Maintenance. In *Current biology : CB* 28 (4), R170-R185. DOI: 10.1016/j.cub.2018.01.004.

Poisbeau, P.; Cheney, M. C.; Browning, M. D.; Mody, I. (1999): Modulation of synaptic GABAA receptor function by PKA and PKC in adult hippocampal neurons. In *The Journal of neuroscience : the official journal of the Society for Neuroscience* 19 (2), pp. 674–683.

Polymeropoulos, M. H.; Lavedan, C.; Leroy, E.; Ide, S. E.; Dehejia, A.; Dutra, A. et al. (1997): Mutation in the alpha-synuclein gene identified in families with Parkinson's disease. In *Science (New York, N.Y.)* 276 (5321), pp. 2045–2047. DOI: 10.1126/science.276.5321.2045.

Porte, Yves; Buhot, Marie-Christine; Mons, Nicole (2008): Alteration of CREB phosphorylation and spatial memory deficits in aged 129T2/Sv mice. In *Neurobiology of aging* 29 (10), pp. 1533–1546. DOI: 10.1016/j.neurobiolaging.2007.03.023.

Pozo, Karine; Goda, Yukiko (2010): Unraveling mechanisms of homeostatic synaptic plasticity. In *Neuron* 66 (3), pp. 337–351. DOI: 10.1016/j.neuron.2010.04.028.

Prickaerts, Jos; Heckman, Pim R. A.; Blokland, Arjan (2017): Investigational phosphodiesterase inhibitors in phase I and phase II clinical trials for Alzheimer's disease. In *Expert opinion on investigational drugs* 26 (9), pp. 1033–1048. DOI: 10.1080/13543784.2017.1364360.

Proukakis, Christos; Houlden, Henry; Schapira, Anthony H. (2013): Somatic alpha-synuclein mutations in Parkinson's disease: hypothesis and preliminary data. In *Movement disorders : official journal of the Movement Disorder Society* 28 (6), pp. 705–712. DOI: 10.1002/mds.25502.

Qi, M.; Zhuo, M.; Skålhegg, B. S.; Brandon, E. P.; Kandel, E. R.; McKnight, G. S.; Idzerda, R. L. (1996): Impaired hippocampal plasticity in mice lacking the Cbeta1 catalytic subunit of cAMP-dependent protein kinase. In *Proceedings of the National Academy of Sciences of the United States of America* 93 (4), pp. 1571–1576. DOI: 10.1073/pnas.93.4.1571.

Rabinowitch, Ithai; Segev, Idan (2008): Two opposing plasticity mechanisms pulling a single synapse. In *Trends in neurosciences* 31 (8), pp. 377–383. DOI: 10.1016/j.tins.2008.05.005.

Rahman, Md Ataur; Rahman, Md Saidur; Uddin, Md Jamal; Mamum-Or-Rashid, A. N. M.; Pang, Myung-Geol; Rhim, Hyewhon (2020): Emerging risk of environmental factors: insight mechanisms of Alzheimer's diseases. In *Environmental science and pollution research international* 27 (36), pp. 44659–44672. DOI: 10.1007/s11356-020-08243-z.

Ramos, Brian P.; Birnbaum, Shari G.; Lindenmayer, Isabelle; Newton, Samuel S.; Duman, Ronald S.; Arnsten, Amy F.T. (2003): Dysregulation of Protein Kinase A Signaling in the Aged Prefrontal Cortex. In *Neuron* 40 (4), pp. 835–845. DOI: 10.1016/S0896-6273(03)00694-9.

Raudvere, Uku; Kolberg, Liis; Kuzmin, Ivan; Arak, Tambet; Adler, Priit; Peterson, Hedi; Vilo, Jaak (2019): g:Profiler: a web server for functional enrichment analysis and conversions of gene lists (2019 update). In *Nucleic acids research* 47 (W1), W191-W198. DOI: 10.1093/nar/gkz369.

Ravikumar, Brinda; Acevedo-Arozena, Abraham; Imarisio, Sara; Berger, Zdenek; Vacher, Coralie; O'Kane, Cahir J. et al. (2005): Dynein mutations impair autophagic clearance of aggregate-prone proteins. In *Nature genetics* 37 (7), pp. 771–776. DOI: 10.1038/ng1591.

Ravikumar, Brinda; Duden, Rainer; Rubinsztein, David C. (2002): Aggregate-prone proteins with polyglutamine and polyalanine expansions are degraded by autophagy. In *Human molecular genetics* 11 (9), pp. 1107–1117. DOI: 10.1093/hmg/11.9.1107.

Ravikumar, Brinda; Imarisio, Sara; Sarkar, Sovan; O'Kane, Cahir J.; Rubinsztein, David C. (2008): Rab5 modulates aggregation and toxicity of mutant huntingtin through macroautophagy in cell and fly models of Huntington disease. In *Journal of cell science* 121 (Pt 10), pp. 1649–1660. DOI: 10.1242/jcs.025726.

Ravikumar, Brinda; Vacher, Coralie; Berger, Zdenek; Davies, Janet E.; Luo, Shouqing; Oroz, Lourdes G. et al. (2004): Inhibition of mTOR induces autophagy and reduces toxicity of polyglutamine expansions in fly and mouse models of Huntington disease. In *Nature genetics* 36 (6), pp. 585–595. DOI: 10.1038/ng1362.

Rea, Sarah L.; Majcher, Veronika; Searle, Mark S.; Layfield, Rob (2014): SQSTM1 mutations--bridging Paget disease of bone and ALS/FTLD. In *Experimental cell research* 325 (1), pp. 27–37. DOI: 10.1016/j.yexcr.2014.01.020.

Reimers, Jeremy M.; Milovanovic, Michael; Wolf, Marina E. (2011): Quantitative analysis of AMPA receptor subunit composition in addiction-related brain regions. In *Brain research* 1367, pp. 223–233. DOI: 10.1016/j.brainres.2010.10.016.

Riederer, Franz; Luborzewski, Alexander; God, Ralf; Bringmann, Gerhard; Scholz, Joachim; Feineis, Doris; Moser, Andreas (2002): Modification of tyrosine hydroxylase activity by chloral derived beta-carbolines in vitro. In *Journal of neurochemistry* 81 (4), pp. 814–819. DOI: 10.1046/j.1471-4159.2002.00875.x.

Robinson-Steiner, A. M.; Beebe, S. J.; Rannels, S. R.; Corbin, J. D. (1984): Microheterogeneity of type II cAMP-dependent protein kinase in various mammalian species and tissues. In *Journal of Biological Chemistry* 259 (16), pp. 10596–10605. DOI: 10.1016/S0021-9258(18)91004-5.

Rocchi, Altea; Yamamoto, Soh; Ting, Tabitha; Fan, Yuying; Sadleir, Katherine; Wang, Yigang et al. (2017): A Becn1 mutation mediates hyperactive autophagic sequestration of amyloid oligomers and improved cognition in Alzheimer's disease. In *PLoS genetics* 13 (8), e1006962. DOI: 10.1371/journal.pgen.1006962.

Roche, K. W.; O'Brien, R. J.; Mammen, A. L.; Bernhardt, J.; Huganir, R. L. (1996): Characterization of multiple phosphorylation sites on the AMPA receptor GluR1 subunit. In *Neuron* 16 (6), pp. 1179–1188. DOI: 10.1016/s0896-6273(00)80144-0.

Rogawski, M. A. (2013): AMPA receptors as a molecular target in epilepsy therapy. In *Acta neurologica Scandinavica. Supplementum* (197), pp. 9–18. DOI: 10.1111/ane.12099.

Rogers, D. C.; Fisher, E. M.; Brown, S. D.; Peters, J.; Hunter, A. J.; Martin, J. E. (1997): Behavioral and functional analysis of mouse phenotype: SHIRPA, a proposed protocol for comprehensive phenotype assessment. In *Mammalian genome : official journal of the International Mammalian Genome Society* 8 (10), pp. 711–713. DOI: 10.1007/s003359900551.

Rohn, Troy T.; Wirawan, Ellen; Brown, Raquel J.; Harris, Jordan R.; Masliah, Eliezer; Vandenabeele, Peter (2011): Depletion of Beclin-1 due to proteolytic cleavage by caspases in the Alzheimer's disease brain. In *Neurobiology of disease* 43 (1), pp. 68–78. DOI: 10.1016/j.nbd.2010.11.003.

Rosenmund, C.; Carr, D. W.; Bergeson, S. E.; Nilaver, G.; Scott, J. D.; Westbrook, G. L. (1994): Anchoring of protein kinase A is required for modulation of AMPA/kainate receptors on hippocampal neurons. In *Nature* 368 (6474), pp. 853–856. DOI: 10.1038/368853a0.

Rowland, Aaron M.; Richmond, Janet E.; Olsen, Jason G.; Hall, David H.; Bamber, Bruce A. (2006): Presynaptic terminals independently regulate synaptic clustering and autophagy of GABAA receptors in Caenorhabditis elegans. In *J. Neurosci.* 26 (6), pp. 1711–1720. DOI: 10.1523/JNEUROSCI.2279-05.2006.

Rui, Yanfang; Tiwari, Priyanka; Xie, Zuoping; Zheng, James Q. (2006): Acute impairment of mitochondrial trafficking by beta-amyloid peptides in hippocampal neurons. In *J. Neurosci.* 26 (41), pp. 10480–10487. DOI: 10.1523/JNEUROSCI.3231-06.2006.

Saitsu, Hirotomo; Nishimura, Taki; Muramatsu, Kazuhiro; Kodera, Hirofumi; Kumada, Satoko; Sugai, Kenji et al. (2013): De novo mutations in the autophagy gene WDR45 cause static encephalopathy of childhood with neurodegeneration in adulthood. In *Nature genetics* 45 (4), 445-9, 449e1. DOI: 10.1038/ng.2562.

Sarkar, Sovan (2013): Regulation of autophagy by mTOR-dependent and mTOR-independent pathways: autophagy dysfunction in neurodegenerative diseases and therapeutic application of autophagy enhancers. In *Biochemical Society transactions* 41 (5), pp. 1103–1130. DOI: 10.1042/BST20130134.

Sarkar, Sovan; Korolchuk, Viktor I.; Renna, Maurizio; Imarisio, Sara; Fleming, Angeleen; Williams, Andrea et al. (2011): Complex inhibitory effects of nitric oxide on autophagy. In *Molecular cell* 43 (1), pp. 19–32. DOI: 10.1016/j.molcel.2011.04.029.

Sasaki, Hajime; Hashimoto, Kenji; Maeda, Yohko; Inada, Toshiya; Kitao, Yoshie; Fukui, Susumu; Iyo, Masaomi (1995): Rolipram, a selective c-AMP phosphodiesterase inhibitor suppresses oro-facial dyskinetic movements in rats. In *Life sciences* 56 (25), PL443-PL447. DOI: 10.1016/0024-3205(95)00218-u.

Scarmeas, Nikolaos; Luchsinger, Jose A.; Schupf, Nicole; Brickman, Adam M.; Cosentino, Stephanie; Tang, Ming X.; Stern, Yaakov (2009): Physical activity, diet, and risk of Alzheimer disease. In *JAMA* 302 (6), pp. 627–637. DOI: 10.1001/jama.2009.1144.

Schreyer, S. A.; Cummings, D. E.; McKnight, G. S.; LeBoeuf, R. C. (2001): Mutation of the RIIbeta subunit of protein kinase A prevents diet-induced insulin resistance and dyslipidemia in mice. In *Diabetes* 50 (11), pp. 2555–2562. DOI: 10.2337/diabetes.50.11.2555.

Scott, A. I.; Perini, A. F.; Shering, P. A.; Whalley, L. J. (1991): In-patient major depression: is rolipram as effective as amitriptyline? In *European journal of clinical pharmacology* 40 (2), pp. 127–129. DOI: 10.1007/BF00280065.

Searle, Brian C.; Pino, Lindsay K.; Egertson, Jarrett D.; Ting, Ying S.; Lawrence, Robert T.; MacLean, Brendan X. et al. (2018): Chromatogram libraries improve peptide detection and quantification by data independent acquisition mass spectrometry. In *Nature communications* 9 (1), p. 5128. DOI: 10.1038/s41467-018-07454-w.

Searle, Brian C.; Swearingen, Kristian E.; Barnes, Christopher A.; Schmidt, Tobias; Gessulat, Siegfried; Küster, Bernhard; Wilhelm, Mathias (2020): Generating high quality libraries for DIA MS with empirically corrected peptide predictions. In *Nature communications* 11 (1), p. 1548. DOI: 10.1038/s41467-020-15346-1.

Sekine, Shiori; Youle, Richard J. (2018): PINK1 import regulation; a fine system to convey mitochondrial stress to the cytosol. In *BMC biology* 16 (1), p. 2. DOI: 10.1186/s12915-017-0470-7.

Sengupta, A.; Kabat, J.; Novak, M.; Wu, Q.; Grundke-Iqbal, I.; Iqbal, K. (1998): Phosphorylation of tau at both Thr 231 and Ser 262 is required for maximal inhibition of its binding to microtubules. In *Archives of biochemistry and biophysics* 357 (2), pp. 299–309. DOI: 10.1006/abbi.1998.0813.

Shabb, J. B. (2001): Physiological substrates of cAMP-dependent protein kinase. In *Chemical reviews* 101 (8), pp. 2381–2411. DOI: 10.1021/cr000236l.

Sharifzadeh, Mohammad; Sharifzadeh, Kurdistan; Naghdi, Nasser; Ghahremani, Mohammad H.; Roghani, Ali (2005): Posttraining intrahippocampal infusion of a protein kinase AII inhibitor impairs spatial memory retention in rats. In *Journal of neuroscience research* 79 (3), pp. 392–400. DOI: 10.1002/jnr.20358.

Shehata, Mohammad; Matsumura, Hiroyuki; Okubo-Suzuki, Reiko; Ohkawa, Noriaki; Inokuchi, Kaoru (2012): Neuronal stimulation induces autophagy in hippocampal neurons that is involved in AMPA receptor degradation after chemical long-term depression. In *J. Neurosci.* 32 (30), pp. 10413–10422. DOI: 10.1523/JNEUROSCI.4533-11.2012.

Shelton, R. C.; Mainer, D. H.; Sulser, F. (1996): cAMP-dependent protein kinase activity in major depression. In *The American journal of psychiatry* 153 (8), pp. 1037–1042. DOI: 10.1176/ajp.153.8.1037.

Shen, Lei; Liang, Feng; Walensky, Loren D.; Huganir, Richard L. (2000): Regulation of AMPA Receptor GluR1 Subunit Surface Expression by a 4.1N-Linked Actin Cytoskeletal Association. In *J. Neurosci.* 20 (21), pp. 7932–7940. DOI: 10.1523/JNEUROSCI.20-21-07932.2000.

Shen, Wei; Ganetzky, Barry (2009): Autophagy promotes synapse development in Drosophila. In *Journal of Cell Biology* 187 (1), pp. 71–79. DOI: 10.1083/jcb.200907109.

Shen, Wenjuan; Kilander, Michaela B. C.; Bridi, Morgan S.; Frei, Jeannine A.; Niescier, Robert F.; Huang, Shiyong; Lin, Yu-Chih (2020): Tomosyn regulates the small RhoA GTPase to control the dendritic stability of neurons and the surface expression of AMPA receptors. In *Journal of neuroscience research* 98 (6), pp. 1213–1231. DOI: 10.1002/jnr.24608.

Shi, S.; Hayashi, Y.; Esteban, J. A.; Malinow, R. (2001): Subunit-specific rules governing AMPA receptor trafficking to synapses in hippocampal pyramidal neurons. In *Cell* 105 (3), pp. 331–343. DOI: 10.1016/s0092-8674(01)00321-x.

Shibata, Mamoru; Lu, Tao; Furuya, Tsuyoshi; Degterev, Alexei; Mizushima, Noboru; Yoshimori, Tamotsu et al. (2006): Regulation of intracellular accumulation of mutant Huntingtin by Beclin 1. In *The Journal of biological chemistry* 281 (20), pp. 14474–14485. DOI: 10.1074/jbc.M600364200.

Siddoway, Benjamin; Hou, Hailong; Xia, Houhui (2014): Molecular mechanisms of homeostatic synaptic downscaling. In *Neuropharmacology* 78, pp. 38–44. DOI: 10.1016/j.neuropharm.2013.07.009.

Silva, A. J.; Kogan, J. H.; Frankland, P. W.; Kida, S. (1998): CREB and memory. In *Annual review of neuroscience* 21, pp. 127–148. DOI: 10.1146/annurev.neuro.21.1.127.

Singh, Balwinder; Parsaik, Ajay K.; Mielke, Michelle M.; Erwin, Patricia J.; Knopman, David S.; Petersen, Ronald C.; Roberts, Rosebud O. (2014): Association of mediterranean diet with mild cognitive impairment and Alzheimer's disease: a systematic review and meta-analysis. In *Journal of Alzheimer's disease : JAD* 39 (2), pp. 271–282. DOI: 10.3233/JAD-130830.

Singleton, A. B.; Farrer, M.; Johnson, J.; Singleton, A.; Hague, S.; Kachergus, J. et al. (2003): alpha-Synuclein locus triplication causes Parkinson's disease. In *Science (New York, N.Y.)* 302 (5646), p. 841. DOI: 10.1126/science.1090278.

Skålhegg, Bjørn S.; Huang, Yongzhao; Su, Thomas; Idzerda, Rejean L.; McKnight, G. Stanley; Burton, Kimberly A. (2002): Mutation of the Calpha subunit of PKA leads to growth retardation and sperm dysfunction. In *Molecular Endocrinology* 16 (3), pp. 630–639. DOI: 10.1210/mend.16.3.0793.

Skeberdis, V. Arvydas; Chevaleyre, Vivien; Lau, C. Geoffrey; Goldberg, Jesse H.; Pettit, Diana L.; Suadicani, Sylvia O. et al. (2006): Protein kinase A regulates calcium permeability of NMDA receptors. In *Nature neuroscience* 9 (4), pp. 501–510. DOI: 10.1038/nn1664.

Slot, Jan W.; Geuze, Hans J. (2007): Cryosectioning and immunolabeling. In *Nat Protoc* 2 (10), pp. 2480–2491. DOI: 10.1038/nprot.2007.365.

Small, Scott A.; Kent, Kelly; Pierce, Aimee; Leung, Conrad; Kang, Min Suk; Okada, Hirokazu et al. (2005): Model-guided microarray implicates the retromer complex in Alzheimer's disease. In *Annals of neurology* 58 (6), pp. 909–919. DOI: 10.1002/ana.20667.

Smith, Katharine R.; Kopeikina, Katherine J.; Fawcett-Patel, Jessica M.; Leaderbrand, Katherine; Gao, Ruoqi; Schürmann, Britta et al. (2014): Psychiatric risk factor ANK3/ankyrin-G nanodomains regulate the structure and function of glutamatergic synapses. In *Neuron* 84 (2), pp. 399–415. DOI: 10.1016/j.neuron.2014.10.010.

Smith, Matthew D.; Harley, Margaret E.; Kemp, Alain J.; Wills, Jimi; Lee, Martin; Arends, Mark et al. (2018): CCPG1 Is a Non-canonical Autophagy Cargo Receptor Essential for ER-Phagy and Pancreatic ER Proteostasis. In *Developmental cell* 44 (2), 217-232.e11. DOI: 10.1016/j.devcel.2017.11.024.

Son, Jin H.; Shim, Jung Hee; Kim, Kyung Hee; Ha, Ji Young; Han, Ji Young (2012): Neuronal autophagy and neurodegenerative diseases. In *Experimental & molecular medicine* 44 (2), pp. 89–98. DOI: 10.3858/emm.2012.44.2.031.

Soukup, Sandra-Fausia; Kuenen, Sabine; Vanhauwaert, Roeland; Manetsberger, Julia; Hernández-Díaz, Sergio; Swerts, Jef et al. (2016): A LRRK2-Dependent EndophilinA Phosphoswitch Is Critical for Macroautophagy at Presynaptic Terminals. In *Neuron* 92 (4), pp. 829–844. DOI: 10.1016/j.neuron.2016.09.037.

Stavoe, Andrea K. H.; Hill, Sarah E.; Hall, David H.; Colón-Ramos, Daniel A. (2016): KIF1A/UNC-104 Transports ATG-9 to Regulate Neurodevelopment and Autophagy at Synapses. In *Developmental cell* 38 (2), pp. 171–185. DOI: 10.1016/j.devcel.2016.06.012.

Stavoe, Andrea K. H.; Holzbaur, Erika L. F. (2019): Autophagy in Neurons. In *Annual review of cell and developmental biology* 35, pp. 477–500. DOI: 10.1146/annurev-cellbio-100818-125242.

Stavoe, Andrea Kh; Gopal, Pallavi P.; Gubas, Andrea; Tooze, Sharon A.; Holzbaur, Erika Lf (2019): Expression of WIPI2B counteracts age-related decline in autophagosome biogenesis in neurons. In *eLife* 8. DOI: 10.7554/eLife.44219.

Stephan, Joseph S.; Yeh, Yuh-Ying; Ramachandran, Vidhya; Deminoff, Stephen J.; Herman, Paul K. (2009): The Tor and PKA signaling pathways independently target the Atg1/Atg13 protein kinase complex to control autophagy. In *Proceedings of the National Academy of Sciences of the United States of America* 106 (40), pp. 17049–17054. DOI: 10.1073/pnas.0903316106.

Steven, André; Friedrich, Michael; Jank, Paul; Heimer, Nadine; Budczies, Jan; Denkert, Carsten; Seliger, Barbara (2020): What turns CREB on? And off? And why does it matter? In *Cellular and molecular life sciences : CMLS* 77 (20), pp. 4049–4067. DOI: 10.1007/s00018-020-03525-8.

Stolz, Alexandra; Ernst, Andreas; Dikic, Ivan (2014): Cargo recognition and trafficking in selective autophagy. In *Nature cell biology* 16 (6), pp. 495–501. DOI: 10.1038/ncb2979.

Storm, Daniel R.; Hansel, Christian; Hacker, Beth; Parent, Angèle; Linden, David J. (1998): Impaired Cerebellar Long-Term Potentiation in Type I Adenylyl Cyclase Mutant Mice. In *Neuron* 20 (6), pp. 1199–1210. DOI: 10.1016/S0896-6273(00)80500-0.

Subhan, Z.; Hindmarch, I. (1985): Psychopharmacological effects of vinpocetine in normal healthy volunteers. In *European journal of clinical pharmacology* 28 (5), pp. 567–571. DOI: 10.1007/BF00544068.

Sudhof, Thomas C. (2004): The synaptic vesicle cycle. In *Annual review of neuroscience* 27, pp. 509–547. DOI: 10.1146/annurev.neuro.26.041002.131412.

Suzuki, K.; Kirisako, T.; Kamada, Y.; Mizushima, N.; Noda, T.; Ohsumi, Y. (2001): The pre-autophagosomal structure organized by concerted functions of APG genes is essential for autophagosome formation. In *The EMBO journal* 20 (21), pp. 5971–5981. DOI: 10.1093/emboj/20.21.5971.

Szatmari, S. Z.; Whitehouse, P. J. (2003): Vinpocetine for cognitive impairment and dementia. In *The Cochrane database of systematic reviews* (1), CD003119. DOI: 10.1002/14651858.CD003119.

Tai, Shu-Yu; Chen, Chun-Hung; Chien, Chen-Yu; Yang, Yuan-Han (2017): Cilostazol as an add-on therapy for patients with Alzheimer's disease in Taiwan: a case control study. In *BMC neurology* 17 (1), p. 40. DOI: 10.1186/s12883-017-0800-y.

Takumi, Y.; Ramírez-León, V.; Laake, P.; Rinvik, E.; Ottersen, O. P. (1999): Different modes of expression of AMPA and NMDA receptors in hippocampal synapses. In *Nature neuroscience* 2 (7), pp. 618–624. DOI: 10.1038/10172.

Tang, Guomei; Gudsnuk, Kathryn; Kuo, Sheng-Han; Cotrina, Marisa L.; Rosoklija, Gorazd; Sosunov, Alexander et al. (2014): Loss of mTOR-dependent macroautophagy causes autistic-like synaptic pruning deficits. In *Neuron* 83 (5), pp. 1131–1143. DOI: 10.1016/j.neuron.2014.07.040.

Tang, Shao Jun; Reis, Gerald; Kang, Hyejin; Gingras, Anne-Claude; Sonenberg, Nahum; Schuman, Erin M. (2002): A rapamycin-sensitive signaling pathway contributes to long-term synaptic plasticity in the hippocampus. In *Proceedings of the National Academy of Sciences of the United States of America* 99 (1), pp. 467–472. DOI: 10.1073/pnas.012605299.

Tao-Cheng, Jung-Hwa (2019): Stimulation induces gradual increases in the thickness and curvature of postsynaptic density of hippocampal CA1 neurons in slice cultures. In *Molecular brain* 12 (1), p. 44. DOI: 10.1186/s13041-019-0468-x.

Tavalin, Steven J.; Colledge, Marcie; Hell, Johannes W.; Langeberg, Lorene K.; Huganir, Richard L.; Scott, John D. (2002): Regulation of GluR1 by the A-Kinase Anchoring Protein 79 (AKAP79) Signaling Complex Shares Properties with Long-Term Depression. In *J. Neurosci.* 22 (8), pp. 3044–3051. DOI: 10.1523/JNEUROSCI.22-08-03044.2002.

Taylor, Susan S.; Ilouz, Ronit; Zhang, Ping; Kornev, Alexandr P. (2012): Assembly of allosteric macromolecular switches: lessons from PKA. In *Nature reviews. Molecular cell biology* 13 (10), pp. 646–658. DOI: 10.1038/nrm3432.

Teng, Henry K.; Teng, Kenneth K.; Lee, Ramee; Wright, Saundrene; Tevar, Seema; Almeida, Ramiro D. et al. (2005): ProBDNF induces neuronal apoptosis via activation of a receptor complex of p75NTR and sortilin. In *J. Neurosci.* 25 (22), pp. 5455–5463. DOI: 10.1523/JNEUROSCI.5123-04.2005.

Thal, L. J.; Salmon, D. P.; Lasker, B.; Bower, D.; Klauber, M. R. (1989): The safety and lack of efficacy of vinpocetine in Alzheimer's disease. In *Journal of the American Geriatrics Society* 37 (6), pp. 515–520. DOI: 10.1111/j.1532-5415.1989.tb05682.x.

Tien, Nai-Wen; Kerschensteiner, Daniel (2018): Homeostatic plasticity in neural development. In *Neural development* 13 (1), p. 9. DOI: 10.1186/s13064-018-0105-x.

Tong, L.; Thornton, P. L.; Balazs, R.; Cotman, C. W. (2001): Beta -amyloid-(1-42) impairs activity-dependent cAMP-response element-binding protein signaling in neurons at concentrations in which cell survival Is not compromised. In *Journal of Biological Chemistry* 276 (20), pp. 17301–17306. DOI: 10.1074/jbc.M010450200.

Torres-Quiroz, Francisco; Filteau, Marie; Landry, Christian R. (2015): Feedback regulation between autophagy and PKA. In *Autophagy* 11 (7), pp. 1181–1183. DOI: 10.1080/15548627.2015.1055440.

Traub, R. D.; Miles, R.; Jefferys, J. G. (1993): Synaptic and intrinsic conductances shape picrotoxin-induced synchronized after-discharges in the guinea-pig hippocampal slice. In *The Journal of Physiology* 461, pp. 525–547. DOI: 10.1113/jphysiol.1993.sp019527.

Tsukada, M.; Ohsumi, Y. (1993): Isolation and characterization of autophagy-defective mutants of Saccharomyces cerevisiae. In *FEBS letters* 333 (1-2), pp. 169–174. DOI: 10.1016/0014-5793(93)80398-e.

Turrigiano, G. G.; Leslie, K. R.; Desai, N. S.; Rutherford, L. C.; Nelson, S. B. (1998): Activity-dependent scaling of quantal amplitude in neocortical neurons. In *Nature* 391 (6670), pp. 892–896. DOI: 10.1038/36103.

Turrigiano, Gina G. (2008): The self-tuning neuron: synaptic scaling of excitatory synapses. In *Cell* 135 (3), pp. 422–435. DOI: 10.1016/j.cell.2008.10.008.

Tyanova, Stefka; Temu, Tikira; Carlson, Arthur; Sinitcyn, Pavel; Mann, Matthias; Cox, Juergen (2015): Visualization of LC-MS/MS proteomics data in MaxQuant. In *Proteomics* 15 (8), pp. 1453–1456. DOI: 10.1002/pmic.201400449.

Tyanova, Stefka; Temu, Tikira; Sinitcyn, Pavel; Carlson, Arthur; Hein, Marco Y.; Geiger, Tamar et al. (2016): The Perseus computational platform for comprehensive analysis of (prote)omics data. In *Nature methods* 13 (9), pp. 731–740. DOI: 10.1038/nmeth.3901.

Uchino, Shigeo; Wada, Hidenori; Honda, Shizuyo; Nakamura, Yasuko; Ondo, Yumiko; Uchiyama, Takayoshi et al. (2006): Direct interaction of post-synaptic density-95/Dlg/ZO-1 domain-containing synaptic molecule Shank3

with GluR1 alpha-amino-3-hydroxy-5-methyl-4-isoxazole propionic acid receptor. In *Journal of neurochemistry* 97 (4), pp. 1203–1214. DOI: 10.1111/j.1471-4159.2006.03831.x.

Uematsu, Ken; Heiman, Myriam; Zelenina, Marina; Padovan, Júlio; Chait, Brian T.; Aperia, Anita et al. (2015): Protein kinase A directly phosphorylates metabotropic glutamate receptor 5 to modulate its function. In *Journal of neurochemistry* 132 (6), pp. 677–686. DOI: 10.1111/jnc.13038.

Uhler, M. D.; McKnight, G. S. (1987): Expression of cDNAs for two isoforms of the catalytic subunit of cAMP-dependent protein kinase. In *Journal of Biological Chemistry* 262 (31), pp. 15202–15207.

Valente, Enza Maria; Abou-Sleiman, Patrick M.; Caputo, Viviana; Muqit, Miratul M. K.; Harvey, Kirsten; Gispert, Suzana et al. (2004): Hereditary early-onset Parkinson's disease caused by mutations in PINK1. In *Science (New York, N.Y.)* 304 (5674), pp. 1158–1160. DOI: 10.1126/science.1096284.

Vanhauwaert, Roeland; Kuenen, Sabine; Masius, Roy; Bademosi, Adekunle; Manetsberger, Julia; Schoovaerts, Nils et al. (2017): The SAC1 domain in synaptojanin is required for autophagosome maturation at presynaptic terminals. In *EMBO J* 36 (10), pp. 1392–1411. DOI: 10.15252/embj.201695773.

Vassar, R.; Bennett, B. D.; Babu-Khan, S.; Kahn, S.; Mendiaz, E. A.; Denis, P. et al. (1999): Beta-secretase cleavage of Alzheimer's amyloid precursor protein by the transmembrane aspartic protease BACE. In *Science (New York, N.Y.)* 286 (5440), pp. 735–741. DOI: 10.1126/science.286.5440.735.

Vijayan, Vinoy; Verstreken, Patrik (2017): Autophagy in the presynaptic compartment in health and disease. In *The Journal of cell biology* 216 (7), pp. 1895–1906. DOI: 10.1083/jcb.201611113.

Vingtdeux, Valérie; Giliberto, Luca; Zhao, Haitian; Chandakkar, Pallavi; Wu, Qingli; Simon, James E. et al. (2010): AMP-activated protein kinase signaling activation by resveratrol modulates amyloid-beta peptide metabolism. In *The Journal of biological chemistry* 285 (12), pp. 9100–9113. DOI: 10.1074/jbc.M109.060061.

Vitolo, Ottavio V.; Sant'Angelo, Antonino; Costanzo, Vincenzo; Battaglia, Fortunato; Arancio, Ottavio; Shelanski, Michael (2002): Amyloid beta -peptide inhibition of the PKA/CREB pathway and long-term potentiation: reversibility by drugs that enhance cAMP signaling. In *Proceedings of the National Academy of Sciences of the United States of America* 99 (20), pp. 13217–13221. DOI: 10.1073/pnas.172504199.

Walker-Gray, Ryan; Stengel, Florian; Gold, Matthew G. (2017): Mechanisms for restraining cAMP-dependent protein kinase revealed by subunit quantitation and cross-linking approaches. In *Proceedings of the National Academy of Sciences of the United States of America* 114 (39), pp. 10414–10419. DOI: 10.1073/pnas.1701782114.

Walsh, D. A.; Perkins, J. P.; Krebs, E. G. (1968): An adenosine 3',5'-monophosphate-dependant protein kinase from rabbit skeletal muscle. In *Journal of Biological Chemistry* 243 (13), pp. 3763–3765.

Wan, Huida; Wang, Qi; Chen, Xiuting; Zeng, Qiufang; Shao, Yanjiao; Fang, Houqin et al. (2020): WDR45 contributes to neurodegeneration through regulation of ER homeostasis and neuronal death. In *Autophagy* 16 (3), pp. 531–547. DOI: 10.1080/15548627.2019.1630224.

Wang, Bao-Hui; Hou, Qun; Lu, Yu-Qiang; Jia, Meng-Meng; Qiu, Tao; Wang, Xiao-Hang et al. (2018): Ketogenic diet attenuates neuronal injury via autophagy and mitochondrial pathways in pentylenetetrazol-kindled seizures. In *Brain research* 1678, pp. 106–115. DOI: 10.1016/j.brainres.2017.10.009.

Wang, Dayong; Yuen, Eunice Y.; Zhou, Yuan; Yan, Zhen; Xiang, Yang K. (2011): Amyloid beta peptide-(1-42) induces internalization and degradation of beta2 adrenergic receptors in prefrontal cortical neurons. In *The Journal of biological chemistry* 286 (36), pp. 31852–31863. DOI: 10.1074/jbc.M111.244335.

Wang, L. Y.; Salter, M. W.; MacDonald, J. F. (1991): Regulation of kainate receptors by cAMP-dependent protein kinase and phosphatases. In *Science (New York, N.Y.)* 253 (5024), pp. 1132–1135. DOI: 10.1126/science.1653455.

Wang, Simon Ji Hau; Tsai, Amy; Wang, Mannan; Yoo, SooHyun; Kim, Hae-Yoon; Yoo, Byoungjoo et al. (2014): Phospho-regulated Drosophila adducin is a determinant of synaptic plasticity in a complex with Dlg and PIP2 at the larval neuromuscular junction. In *Biology open* 3 (12), pp. 1196–1206. DOI: 10.1242/bio.20148342.

Wang, Tong; Martin, Sally; Papadopulos, Andreas; Harper, Callista B.; Mavlyutov, Timur A.; Niranjan, Dhevahi et al. (2015): Control of autophagosome axonal retrograde flux by presynaptic activity unveiled using botulinum neurotoxin type a. In *J. Neurosci.* 35 (15), pp. 6179–6194. DOI: 10.1523/JNEUROSCI.3757-14.2015.

Webb, Julie L.; Ravikumar, Brinda; Atkins, Jane; Skepper, Jeremy N.; Rubinsztein, David C. (2003): Alpha-Synuclein is degraded by both autophagy and the proteasome. In *The Journal of biological chemistry* 278 (27), pp. 25009–25013. DOI: 10.1074/jbc.M300227200.

Wei, Yongjie; Pattingre, Sophie; Sinha, Sangita; Bassik, Michael; Levine, Beth (2008): JNK1-mediated phosphorylation of Bcl-2 regulates starvation-induced autophagy. In *Molecular cell* 30 (6), pp. 678–688. DOI: 10.1016/j.molcel.2008.06.001.

Wenthold, R. J.; Petralia, R. S.; Blahos J, II; Niedzielski, A. S. (1996): Evidence for multiple AMPA receptor complexes in hippocampal CA1/CA2 neurons. In *J. Neurosci.* 16 (6), pp. 1982–1989. DOI: 10.1523/jneurosci.16-06-01982.1996.

Westphal, R. S.; Tavalin, S. J.; Lin, J. W.; Alto, N. M.; Fraser, I. D.; Langeberg, L. K. et al. (1999): Regulation of NMDA receptors by an associated phosphatase-kinase signaling complex. In *Science (New York, N.Y.)* 285 (5424), pp. 93–96. DOI: 10.1126/science.285.5424.93.

Wheless, James W. (2008): History of the ketogenic diet. In *Epilepsia* 49 Suppl 8, pp. 3–5. DOI: 10.1111/j.1528-1167.2008.01821.x.

Wijdeven, Ruud H.; Janssen, Hans; Nahidiazar, Leila; Janssen, Lennert; Jalink, Kees; Berlin, Ilana; Neefjes, Jacques (2016): Cholesterol and ORP1L-mediated ER contact sites control autophagosome transport and fusion with the endocytic pathway. In *Nature communications* 7 (1), p. 11808. DOI: 10.1038/ncomms11808.

Wild, Angela R.; Dell'Acqua, Mark L. (2018): Potential for therapeutic targeting of AKAP signaling complexes in nervous system disorders. In *Pharmacology & therapeutics* 185, pp. 99–121. DOI: 10.1016/j.pharmthera.2017.12.004.

Wild, Philipp; Farhan, Hesso; McEwan, David G.; Wagner, Sebastian; Rogov, Vladimir V.; Brady, Nathan R. et al. (2011): Phosphorylation of the autophagy receptor optineurin restricts Salmonella growth. In *Science (New York, N.Y.)* 333 (6039), pp. 228–233. DOI: 10.1126/science.1205405.

Wilhelm, Benjamin G.; Mandad, Sunit; Truckenbrodt, Sven; Kröhnert, Katharina; Schäfer, Christina; Rammner, Burkhard et al. (2014): Composition of isolated synaptic boutons reveals the amounts of vesicle trafficking proteins. In *Science (New York, N.Y.)* 344 (6187), pp. 1023–1028. DOI: 10.1126/science.1252884.

Winslow, Ashley R.; Chen, Chien-Wen; Corrochano, Silvia; Acevedo-Arozena, Abraham; Gordon, David E.; Peden, Andrew A. et al. (2010): α-Synuclein impairs macroautophagy: implications for Parkinson's disease. In *The Journal of cell biology* 190 (6), pp. 1023–1037. DOI: 10.1083/jcb.201003122.

Wong, Michael (2010): Mammalian target of rapamycin (mTOR) inhibition as a potential antiepileptogenic therapy: From tuberous sclerosis to common acquired epilepsies. In *Epilepsia* 51 (1), pp. 27–36. DOI: 10.1111/j.1528-1167.2009.02341.x.

Woodford, T. A.; Correll, L. A.; McKnight, G. S.; Corbin, J. D. (1989): Expression and characterization of mutant forms of the type I regulatory subunit of cAMP-dependent protein kinase. The effect of defective cAMP binding on holoenzyme activation. In *Journal of Biological Chemistry* 264 (22), pp. 13321–13328.

Wu, Chi-Hong; Ramos, Raul; Katz, Donald B.; Turrigiano, Gina G. (2021): Homeostatic synaptic scaling establishes the specificity of an associative memory. In *Current biology : CB* 31 (11), 2274-2285.e5. DOI: 10.1016/j.cub.2021.03.024.

Wu, Long-Jun; Ren, Ming; Wang, Hansen; Kim, Susan S.; Cao, Xiaoyan; Zhuo, Min (2008): Neurabin contributes to hippocampal long-term potentiation and contextual fear memory. In *PloS one* 3 (1), e1407. DOI: 10.1371/journal.pone.0001407.

Wu, Qian; Sun, Miao; Bernard, Laura P.; Zhang, Huaye (2017a): Postsynaptic density 95 (PSD-95) serine 561 phosphorylation regulates a conformational switch and bidirectional dendritic spine structural plasticity. In *The Journal of biological chemistry* 292 (39), pp. 16150–16160. DOI: 10.1074/jbc.M117.782490.

Wu, Shunquan; Ding, Yingying; Wu, Fuquan; Li, Ruisheng; Hou, Jun; Mao, Panyong (2015): Omega-3 fatty acids intake and risks of dementia and Alzheimer's disease: a meta-analysis. In *Neuroscience and biobehavioral reviews* 48, pp. 1–9. DOI: 10.1016/j.neubiorev.2014.11.008.

Wu, Yumei; Whiteus, Christina; Xu, C. Shan; Hayworth, Kenneth J.; Weinberg, Richard J.; Hess, Harald F.; Camilli, Pietro de (2017b): Contacts between the endoplasmic reticulum and other membranes in neurons. In

Proceedings of the National Academy of Sciences of the United States of America 114 (24), E4859-E4867. DOI: 10.1073/pnas.1701078114.

Wu, Z. L.; Thomas, S. A.; Villacres, E. C.; Xia, Z.; Simmons, M. L.; Chavkin, C. et al. (1995): Altered behavior and long-term potentiation in type I adenylyl cyclase mutant mice. In *Proceedings of the National Academy of Sciences of the United States of America* 92 (1), pp. 220–224. DOI: 10.1073/pnas.92.1.220.

Yamaguchi, Junji; Suzuki, Chigure; Nanao, Tomohisa; Kakuta, Soichirou; Ozawa, Kentarou; Tanida, Isei et al. (2018): Atg9a deficiency causes axon-specific lesions including neuronal circuit dysgenesis. In *Autophagy* 14 (5), pp. 764–777. DOI: 10.1080/15548627.2017.1314897.

Yan, Jingqi; Porch, Morgan W.; Court-Vazquez, Brenda; Bennett, Michael V. L.; Zukin, R. Suzanne (2018): Activation of autophagy rescues synaptic and cognitive deficits in fragile X mice. In *Proceedings of the National Academy of Sciences of the United States of America* 115 (41), E9707-E9716. DOI: 10.1073/pnas.1808247115.

Yang, Lichuan; Calingasan, Noel Y.; Lorenzo, Beverly J.; Beal, M. Flint (2008): Attenuation of MPTP neurotoxicity by rolipram, a specific inhibitor of phosphodiesterase IV. In *Experimental neurology* 211 (1), pp. 311–314. DOI: 10.1016/j.expneurol.2007.02.010.

Yang, Zhifen; Klionsky, Daniel J. (2009): An overview of the molecular mechanism of autophagy. In *Current topics in microbiology and immunology* 335, pp. 1–32. DOI: 10.1007/978-3-642-00302-8_1.

Yin, Jerry C. P.; Tully, Timothy (1996): CREB and the formation of long-term memory. In *Current opinion in neurobiology* 6 (2), pp. 264–268. DOI: 10.1016/s0959-4388(96)80082-1.

Ying, Shui-Wang; Futter, Marie; Rosenblum, Kobi; Webber, Mark J.; Hunt, Stephen P.; Bliss, Timothy V. P.; Bramham, Clive R. (2002): Brain-Derived Neurotrophic Factor Induces Long-Term Potentiation in Intact Adult Hippocampus: Requirement for ERK Activation Coupled to CREB and Upregulation of Arc Synthesis. In *J. Neurosci.* 22 (5), pp. 1532–1540. DOI: 10.1523/JNEUROSCI.22-05-01532.2002.

Yorimitsu, T.; Klionsky, D. J. (2005): Autophagy: molecular machinery for self-eating. In *Cell death and differentiation* 12 Suppl 2, pp. 1542–1552. DOI: 10.1038/sj.cdd.4401765.

Young, Jessica E.; Martinez, Refugio A.; La Spada, Albert R. (2009): Nutrient deprivation induces neuronal autophagy and implicates reduced insulin signaling in neuroprotective autophagy activation. In *Journal of Biological Chemistry* 284 (4), pp. 2363–2373. DOI: 10.1074/jbc.M806088200.

Yu, W. Haung; Cuervo, Ana Maria; Kumar, Asok; Peterhoff, Corrinne M.; Schmidt, Stephen D.; Lee, Ju-Hyun et al. (2005): Macroautophagy--a novel Beta-amyloid peptide-generating pathway activated in Alzheimer's disease. In *The Journal of cell biology* 171 (1), pp. 87–98. DOI: 10.1083/jcb.200505082.

Zarranz, Juan J.; Alegre, Javier; Gómez-Esteban, Juan C.; Lezcano, Elena; Ros, Raquel; Ampuero, Israel et al. (2004): The new mutation, E46K, of alpha-synuclein causes Parkinson and Lewy body dementia. In *Annals of neurology* 55 (2), pp. 164–173. DOI: 10.1002/ana.10795.

Zavodszky, Eszter; Seaman, Matthew N. J.; Moreau, Kevin; Jimenez-Sanchez, Maria; Breusegem, Sophia Y.; Harbour, Michael E.; Rubinsztein, David C. (2014): Mutation in VPS35 associated with Parkinson's disease impairs WASH complex association and inhibits autophagy. In *Nature communications* 5, p. 3828. DOI: 10.1038/ncomms4828.

Zeller, E.; Stief, H. J.; Pflug, B.; Sastre-y-Hernández, M. (1984): Results of a phase II study of the antidepressant effect of rolipram. In *Pharmacopsychiatry* 17 (6), pp. 188–190. DOI: 10.1055/s-2007-1017435.

Zeng, Ling-Hui; Rensing, Nicholas R.; Wong, Michael (2009): The mammalian target of rapamycin signaling pathway mediates epileptogenesis in a model of temporal lobe epilepsy. In *J. Neurosci.* 29 (21), pp. 6964–6972. DOI: 10.1523/JNEUROSCI.0066-09.2009.

Zhai, Baohui; Shang, Xueliang; Fu, Jingxuan; Li, Fangjuan; Zhang, Tao (2018): Rapamycin relieves anxious emotion and synaptic plasticity deficits induced by hindlimb unloading in mice. In *Neuroscience letters* 677, pp. 44–48. DOI: 10.1016/j.neulet.2018.04.033.

Zhang, Jifeng; Li, Jiong; Yin, Yichen; Li, Xueling; Jiang, Yuxin; Wang, Yong et al. (2020): Collapsin Response Mediator Protein 2 and Endophilin2 Coordinate Regulation of AMPA Receptor GluA1 Subunit Recycling. In *Frontiers in molecular neuroscience* 13, p. 128. DOI: 10.3389/fnmol.2020.00128.

Zhang, Tian; Shen, Shichen; Qu, Jun; Ghaemmaghami, Sina (2016): Global Analysis of Cellular Protein Flux Quantifies the Selectivity of Basal Autophagy. In *Cell reports* 14 (10), pp. 2426–2439. DOI: 10.1016/j.celrep.2016.02.040.

Zhao, Yan G.; Le Sun; Miao, Guangyan; Ji, Cuicui; Zhao, Hongyu; Sun, Huayu et al. (2015): The autophagy gene Wdr45/Wipi4 regulates learning and memory function and axonal homeostasis. In *Autophagy* 11 (6), pp. 881–890. DOI: 10.1080/15548627.2015.1047127.

Zimprich, Alexander; Biskup, Saskia; Leitner, Petra; Lichtner, Peter; Farrer, Matthew; Lincoln, Sarah et al. (2004): Mutations in LRRK2 cause autosomal-dominant parkinsonism with pleomorphic pathology. In *Neuron* 44 (4), pp. 601–607. DOI: 10.1016/j.neuron.2004.11.005.

12.Acknowledgement

Many people have accompanied me in the last few years, and I would like to thank them for their support. First and foremost, I would like to thank Prof. Natalia Kononenko, who gave me the opportunity to pursue my scientific interests in her lab and who has always been a supportive and encouraging mentor over the past years.

I would also like to thank Prof. Dirk Isbrandt and Prof. Brunhilde Wirth, who scientifically accompanied my work as TAC committee members and allowed me to conduct experiments in their laboratories. In line with that, I would also like to thank Prof. Matthias Hammerschmidt and Prof. Ansgar Büschges, who agreed to be part of my thesis committee.

Furthermore, I would like to thank my cooperation partners who have supported me in one way or another with experiments, including Dr Emmanouela Kallergi, Andrea Dell Vedove, Prof. Vassiliki Nikoletopoulou, Prof. Tim Hucho, Dr Dmytro Puchkov, Prof. Marcus Krüger, Dr Weiyi Chen, Prof. Jens Brüning and Dr Frederik Tellkamp. I would especially like to mention the support of Dr Frederik Tellkamp, without whom the collection and analysis of the phosphoproteome data would not have taken place in this way.

I would also like to thank all lab members of the kononenko lab, past and present ones, for a pleasant, productive and supportive working environment. I have also found a supportive network of interdisciplinary neuroscientists in the RTG-NCA community, for which I am very grateful.

Special thanks go to my family and friends who accompanied and supported me through my studies and always had an open ear for me.